# PRINCIPLES AND APPLICATIONS OF MICROEARTHQUAKE NETWORKS

# ADVANCES IN GEOPHYSICS

EDITED BY

BARRY SALTZMAN

DEPARTMENT OF GEOLOGY AND GEOPHYSICS

YALE UNIVERSITY

NEW HAVEN, CONNECTICUT

*Supplement* 1

Descriptive Micrometeorology

R. E. MUNN

*Supplement* 2

Principles and Applications of Microearthquake Networks

W. H. K. LEE AND S. W. STEWART

# PRINCIPLES AND APPLICATIONS OF MICROEARTHQUAKE NETWORKS

*W. H. K. Lee and S. W. Stewart*

OFFICE OF EARTHQUAKE STUDIES
U. S. GEOLOGICAL SURVEY
MENLO PARK, CALIFORNIA

1981

**ACADEMIC PRESS**

*A Subsidiary of Harcourt Brace Jovanovich, Publishers*

**New York London Toronto Sydney San Francisco**

COPYRIGHT © 1981, BY ACADEMIC PRESS, INC.
ALL RIGHTS RESERVED.
NO PART OF THIS PUBLICATION MAY BE REPRODUCED OR TRANSMITTED IN ANY FORM OR BY ANY MEANS, ELECTRONIC OR MECHANICAL, INCLUDING PHOTOCOPY, RECORDING, OR ANY INFORMATION STORAGE AND RETRIEVAL SYSTEM, WITHOUT PERMISSION IN WRITING FROM THE PUBLISHER.

ACADEMIC PRESS, INC.
111 Fifth Avenue, New York, New York 10003

*United Kingdom Edition published by*
ACADEMIC PRESS, INC. (LONDON) LTD.
24/28 Oval Road, London NW1 7DX

LIBRARY OF CONGRESS CATALOG CARD NUMBER: 65-26406

ISBN 0-12-018862-7

PRINTED IN THE UNITED STATES OF AMERICA

81 82 83 84 9 8 7 6 5 4 3 2 1

# Contents

FOREWORD vii
PREFACE ix

## 1. Introduction

1.1. Historical Development 1
1.2. Overview and Scope 9

## 2. Instrumentation Systems

2.1. General Considerations 15
2.2. The USGS Central California Microearthquake Network 23
2.3. Other Land-Based Microearthquake Systems 39
2.4. Ocean-Based Microearthquake Systems 41

## 3. Data Processing Procedures

3.1. Nature of Data Processing 46
3.2. Record Keeping 49
3.3. Event Detection 50
3.4. Event Processing 60
3.5. Computing Hypocenter Parameters 70

## 4. Seismic Ray Tracing for Minimum Time Path

4.1. Elastic Wave Propagation in Homogeneous and Heterogeneous Media 76
4.2. Derivation of the Ray Equation 78
4.3. Numerical Solutions of the Ray Equation 82
4.4. Computing Travel Time, Derivatives, and Take-Off Angle 89

## 5. Generalized Inversion and Nonlinear Optimization

5.1. Mathematical Treatment of Linear Systems 106
5.2. Physical Consideration of Inverse Problems 115
5.3. Computational Aspects of Solving Inverse Problems 116
5.4. Nonlinear Optimization 122

## 6. Methods of Data Analysis

6.1. Determination of Origin Time and Hypocenter 130
6.2. Fault-Plane Solution 139
6.3. Simultaneous Inversion for Hypocenter Parameters and Velocity Structure 148
6.4. Estimation of Earthquake Magnitude 153
6.5. Quantification of Earthquakes 158

## 7. General Applications

7.1. Permanent Networks for Basic Research 164
7.2. Temporary Networks for Reconnaissance Surveys 165
7.3. Aftershock Studies 166
7.4. Induced Seismicity Studies 166
7.5. Geothermal Exploration 168
7.6. Crustal and Mantle Structure 168
7.7. Other Applications 170

## 8. Applications for Earthquake Prediction

8.1. Seismicity Patterns 199
8.2. Temporal Variations of Seismic Velocity 208
8.3. Temporal Variations of Other Seismic Parameters 215

## 9. Discussion

Text 223

**Appendix: Glossary of Abbreviations and Unusual Terms** 226

**References** 231

AUTHOR INDEX 267
SUBJECT INDEX 278

# Foreword

Earthquakes occur over a continuous energy spectrum, ranging from high-magnitude, but rare, earthquakes to those of relatively low magnitude but high frequency of occurrence (i.e., microearthquakes). This review is concerned primarily with the underlying physical principles, techniques, and methods of analysis used in studying the low-magnitude end of the spectrum. As a consequence of advancing technological capabilities that are being applied in many diverse regional networks, this subject has grown so rapidly that the need for a coherent overview describing the present state of affairs seems clear.

One of the main reasons for the growth of interest in microearthquakes is a newly accepted concern of seismologists for *prediction* that goes along with the more traditional concerns for description and physical understanding including the use of earthquake records as probes of internal constitution of the Earth. It is now recognized that these low-amplitude microearthquakes are important signals of continuous tectonic processes in the Earth, the future evolution of which is to be forecast. In this predictive respect seismology has moved closer in its goals to meteorology, inheriting the awesome difficulties of predicting the output of an essentially aperiodic, nonlinear, stochastic, dynamic system that can only be modeled and observed in a very crude way far short of the continuum requirements in space and time.

The observational difficulties in seismology are, in fact, even more acute than those in meteorology. As we have indicated, however, there have already been substantial advances in this aspect of the problem, and this Supplement 2 volume of *Advances in Geophysics*, by Lee and Stewart, will provide a benchmark for the progress made to date.

BARRY SALTZMAN

# Preface

In the fall of 1976, Professor Stewart W. Smith invited us to contribute an article on "Network Seismology as Applied to Earthquake Prediction" for a volume in the *Advances in Geophysics* serial publication. We felt that a review of microearthquake networks and their applications would be more appropriate with respect to our experience. The manuscript grew in size beyond the usual length of a review article. We are grateful that Professor Barry Saltzman, the Editor of *Advances in Geophysics*, accepted the manuscript for publication as a supplemental volume in this series.

Seismology is the study of earthquakes and the Earth's internal structure using seismic waves generated by earthquakes and artificial sources. Individual earthquakes vary greatly in the amounts of energy released. In 1935, C. F. Richter introduced the concept of earthquake magnitude—a single number that quantifies the "size" of an earthquake based on the logarithm of the maximum amplitude of the recorded ground motion. Earthquakes of magnitude less than 3 usually are called microearthquakes. They are felt over a relatively small area, if at all. The great earthquakes, those of magnitude 8 or larger, cause severe damage if they occur in populated areas. In 1941, B. Gutenberg and C. F. Richter discovered that the logarithm of the number of earthquakes in a given magnitude interval varies inversely with the magnitude. In general, the number of earthquakes increases tenfold for each decrease of one unit of magnitude. Thus, microearthquakes of magnitude 1 are several million times more frequent than earthquakes of magnitude 8.

The principal tool in seismology is the seismograph, which detects, amplifies, and records seismic waves. Because the seismic energy released by microearthquakes is small, seismographs with high amplification must be used. With the advances in electronics in the 1950s, sensitive seismographs were developed. Thus, it became practical by the 1960s to operate an array of closely spaced and highly sensitive seismographs to study the more numerous microearthquakes. Such an array is called a microearthquake network.

Microearthquake networks are especially well suited for intensively studying seismically active areas and are a powerful tool for investigating the earthquake process in great detail and in relatively short time intervals. Their applications are numerous, such as monitoring seismicity for earthquake prediction purposes, mapping active faults for hazard evaluation, exploring for geothermal resources, and investigating the Earth's crust and mantle structure.

As far as we are aware, this book is the first attempt to present a review of the fundamentals of microearthquake networks: instrumentation systems, data processing procedures, methods of data analysis, and examples of applications. Because microearthquake networks have been developed by many independent groups in several countries, it is difficult for us to present a comprehensive review. Rather, we have relied heavily upon our experience with the USGS Central California Microearthquake Network. In this book, we have emphasized methods and techniques used in microearthquake networks. Results from applications of microearthquake networks are tabulated and referenced, but not described in any detail. We believe that interested persons should read the original articles. Due to space and time limitations, we have not treated several relevant topics, such as the principles of seismometry, and some recently developed techniques in digital instrumentation and data analysis. However, some references to these and related topics are provided.

A considerable amount of practical material relevant to earthquake seismology has been brought together here. We believe that this volume will be useful especially to those who wish to operate a microearthquake network or to interpret data from it. Each chapter has been written to be reasonably self-contained. Two preparatory chapters on seismic ray tracing, generalized inversion, and nonlinear optimization are given so that basic techniques in microearthquake data analysis can be developed systematically. In addition to author and subject indexes, a glossary of abbreviations and unusual terms has been prepared to help the reader. This work is intended for seismologists in general, and for those geologists, geophysicists, and engineers who wish to learn more about microearthquake networks and their applications.

We thank many of our colleagues for sending us preprints and reprints of their work in microearthquake studies, and for answering questions. It is a pleasure to acknowledge suggestions and comments on the manuscript by K. Aki, D. J. Andrews, R. Archuleta, U. Ascher, W. H. Bakun, M. Bath, B. A. Bolt, M. G. Bonilla, D. M. Boore, C. G. Bufe, R. Buland, P. T. Burghardt, U. Casten, R. P. Comer, C. H. Cramer, S. Crampin, R. Daniel, J. P. Eaton, N. Gould, T. C. Hanks, D. H. Harlow, T. L. Henyey, R. B. Herrmann, D. P. Hill, J. Holt, R. Jensen, J. C. Lahr, J. Langbein,

J. Lawson, F. Luk, T. V. McEvilly, W. D. Mooney, S. T. Morrissey, R. D. Nason, M. E. O'Neill, R. A. Page, N. Pavoni, R. Pelzing, V. Pereyra, L. Peselnick, G. Poupinet, C. Prodehl, M. R. Raugh, P. A. Reasenberg, I. Reid, A. Rite, J. C. Savage, R. B. Smith, P. Spudich, D. W. Steeples, C. D. Stephens, Z. Suzuki, J. Taggart, P. Talwani, C. Thurber, R. F. Yerkes, and Z. H. Zhao.

We are grateful to I. Williams for typing the manuscript, to R. Buszka and R. Eis for drafting some of the figures, to W. Hall, W. Sanders, and J. Van Schaack for technical information, and to B. D. Brown, S. Caplan, K. Champneys, D. Hrabik, M. Kauffmann-Gunn, K. Meagher, A. Rapport, and J. York for assistance in preparing and proofreading the manuscript.

The responsibility for the content of this book rests solely with the authors. We welcome communications from readers, especially concerning errors that they have found. We plan to prepare a Corrigenda, which will be available later for those who are interested.

W. H. K. LEE
S. W. STEWART

# PRINCIPLES AND APPLICATIONS OF MICROEARTHQUAKE NETWORKS

# 1. Introduction

Earthquakes of magnitudes less than 3 are generally referred to as microearthquakes. In order to extend seismological studies to the microearthquake range, it is necessary to have a network of closely spaced and highly sensitive seismographic stations. Such a network is usually called a microearthquake network. It may be operated by telemetering seismic signals to a central recording site or by recording at individual stations. Depending on the application, a microearthquake network may consist of several stations to a few hundred stations and may cover an area of a few square kilometers to $10^5$ km$^2$. Microearthquake networks became operative in the 1960s; today, there are about 100 permanent networks all over the world (see Section 7.1). These networks can generate large quantities of seismic data because of the high occurrence rate of microearthquakes and the large number of recording stations.

By probing in seismically active areas, microearthquake networks are powerful tools in studying the nature and state of tectonic processes. Their applications are numerous: monitoring seismicity for earthquake prediction purposes, mapping active faults for hazard evaluation, exploring for geothermal resources, investigating the structure of the crust and upper mantle, to name a few. Microearthquake studies are an important component of seismological research. Results from these studies are usually integrated with other field and theoretical investigations in order to understand the earthquake-generating process.

In the following sections, we present a brief historical account of the development of microearthquake studies and give an overview of the contents and scope of the present work.

## 1.1. Historical Development

Microearthquake studies were stimulated by the introduction of the earthquake magnitude scale by C. F. Richter in 1935, and by the discovery

of the earthquake frequency–magnitude relation by B. Gutenberg and C. F. Richter in 1941 (a similar relation between maximum trace amplitude and frequency of earthquake occurrence was found by M. Ishimoto and K. Iida in 1939). Implementation of microearthquake networks in the 1960s was made possible by technological advances in instrumentation, data transmission, and data processing.

In order to implement a nuclear test ban treaty in the late 1950s, extensive seismological research in detecting nuclear explosions and in discriminating them from earthquakes at teleseismic distances was carried out with support from various governments. Several arrays of seismometers in specific geometrical patterns were deployed in the 1960s. The largest and best known of these is the Large Aperture Seismic Array (LASA) in Montana. It consisted of 21 subarrays, each with 25 short-period, vertical-component seismometers (arranged in a circular pattern) and a set of long-period, three-component seismometers at the subarray center (Capon, 1973). Four smaller arrays were sponsored by the United Kingdom Atomic Energy Authority (Corbishley, 1970): these were located at Eskdalemuir, Scotland (Truscott, 1964); Yellowknife, Canada (Weichert and Henger, 1976); Gauribidanur, India (Varghese *et al.*, 1979); and Warramunga, Australia (Cleary *et al.*, 1968). Four smaller arrays were also established in Scandinavian countries: the NORSAR array in Norway (Bungum and Husebye, 1974), the Hagfors array in Sweden, and the Helsinki and Jyväskylä arrays in Finland (Pirhonen *et al.*, 1979).

Some of these arrays were among the first ever to combine digital computer methods for on-line event detection and off-line event processing. They pioneered the way for automating the processing of seismic data. However, these earlier seismic arrays were concerned almost exclusively with studying teleseismic events. It is beyond our scope to discuss them further.

In terms of historical development, microearthquake networks evolved from regional and local seismic networks rather than from seismic arrays for nuclear detection. Microearthquake networks also evolved from temporary expeditions that studied aftershocks of large earthquakes to reconnaissance surveys, and finally to permanent telemetered networks or highly mobile arrays of stations. Methods and techniques to study microearthquakes have been developed (more or less independently) by various groups in several countries, notably in Japan, South Africa, the United States, and the USSR.

Although historical development of microearthquake studies in the countries mentioned above will be discussed in Sections 1.1.4–1.1.7, many pioneering investigations have been carried out in other countries as well. For example, Quervain (1924) appeared to be the first to use a

portable seismograph to record aftershocks. By deploying an instrument near the epicenter of a strong local earthquake in Switzerland and by recording in Zurich also, he was able to use the aftershocks to estimate P and S velocities in the earth's crust.

### *1.1.1. Magnitude Scale*

Richter (1935) developed the local magnitude scale using data from the Southern California Seismic Network operated by the California Institute of Technology. At that time, this network consisted of about 10 stations spaced at distances of about 100 km. The principal equipment was the Wood–Anderson torsion seismograph (Anderson and Wood, 1925) of 2800 static magnification and 0.8 sec natural period. Richter defined the local magnitude of an earthquake at a station to be

$$M_L = \log A - \log A_0 \tag{1.1}$$

where $A$ is the maximum trace amplitude in millimeters recorded by the station's Wood–Anderson seismograph, and the term $-\log A_0$ is used to account for amplitude attenuation with epicentral distance. The concept of magnitude introduced by Richter was a turning point in seismology because it is important to be able to quantify the size of earthquakes on an instrumental basis. Furthermore, Richter's magnitude scale is widely accepted because of the simplicity in its computational procedure. Subsequently, Gutenberg (1945a,b,c) generalized the magnitude concept to include teleseismic events on a global scale.

Richter realized that the zero mark of the local magnitude scale is arbitrary. Since he did not wish to deal with negative magnitudes in the Southern California Seismic Network, he chose the term $-\log A_0$ equal to 3 at an epicentral distance of 100 km. Hence earthquakes recorded by a Wood–Anderson seismograph network are defined to be mainly of magnitude greater than 3, because the smallest maximum amplitude readable is about 1 mm. In addition, the amplitude attenuation is such that the term $-\log A_0$ equals 1.4 at zero epicentral distance. Therefore, the Wood–Anderson seismograph is capable of recording earthquakes to magnitude of about 2, provided that the earthquakes occur very near the station (Richter and Nordquist, 1948).

### *1.1.2. Frequency–Magnitude Relation*

In the course of detailed analysis of earthquakes recorded in Tokyo, Ishimoto and Iida (1939) discovered that the maximum trace amplitude $A$ of earthquakes at approximately equal focal distances is related to their

frequency of occurrence $N$ by

$$NA^m = k \quad \text{(const)} \tag{1.2}$$

where $m$ is found empirically to be 1.74. At about the same time, Gutenberg and Richter (1941) found that the magnitude $M$ of earthquakes is related to their frequency of occurrence by

$$\log N = a - bM \tag{1.3}$$

where $a$ and $b$ are constants. The Ishimoto–Iida relation does not lead directly to the frequency–magnitude formula [Eq. (1.3)] because the maximum trace amplitude recorded at a station depends on both the magnitude of the earthquake and its distance from the station. However, under general assumptions, the frequency–magnitude formula can be deduced from the Ishimoto–Iida relation as shown by Suzuki (1953).

Many studies of earthquake statistics have shown that Eq. (1.3) holds and that the value of $b$ is approximately 1. This means that the number of earthquakes increases tenfold for each decrease of one magnitude unit. Therefore, the smaller the magnitude of earthquakes one can record, the greater the amount of seismic data one collects. Microearthquake networks are designed to take advantage of this frequency–magnitude relation.

### *1.1.3. Classification of Earthquakes by Magnitude*

Seismologists have used words such as "small" or "large" to describe earthquake size. After the introduction of Richter's magnitude scale, it was convenient to classify earthquakes more definitely to avoid ambiguity. The usual classification of earthquakes according to magnitude is as follows (Hagiwara, 1964):

| Magnitude ($M$) | Classification |
|---|---|
| $M \geq 7$ | Major earthquake ("great" for $M \geq 8$) |
| $5 \leq M < 7$ | Moderate earthquake |
| $3 \leq M < 5$ | Small earthquake |
| $1 \leq M < 3$ | Microearthquake |
| $M < 1$ | Ultra-microearthquake |

There is now a tendency to denote as microearthquakes all earthquakes of magnitude less than 3, and the term ultra-microearthquake is seldom used. However, in the existing literature, terms like "small," "very small," "minimal," "weak," and "local" are often used to describe earthquakes of microearthquake size.

Because the dynamic range of seismic recordings is only of the order of $10^2 - 10^3$, different seismic networks are designed to study earthquakes of different magnitude ranges. For example, the World-Wide Standardized Seismograph Network (Oliver and Murphy, 1971) is designed to study earthquakes of magnitude between 5.5 and 7.5; regional networks (such as the Southern California Seismic Network used by C. F. Richter to develop the local magnitude scale) are designed to study small and moderate earthquakes ($3 \leq M < 6$); and microearthquake networks are designed to study micro- and ultra-microearthquakes ($M < 3$). If an earthquake of magnitude larger than the designed magnitude range of a network occurred within the network, instrumental saturation would not allow a complete study of the seismograms, but the first P-arrival times and first P-motion readings would permit precise locations and fault-plane solutions of the earthquakes.

### *1.1.4. Development in South Africa*

Earth tremors related to deep gold mining operations were first noticed in the Witwatersrand region of South Africa in 1908 (Gane *et al.*, 1946). In 1910 a 200-kg Wiechert horizontal seismograph was installed about 6.5 km north of the mining area. The records showed that many more tremors occurred than were felt. Later, it became apparent that the average tremor intensity and rate of occurrence were increasing, along with the rate of tonnage mined and the depth of mining.

In the late 1930s a group at the Bernard Price Institute of Geophysical Research began a detailed study of these tremors. Although the tremors were assumed to be related directly to the mining activity (an early example of man-made earthquakes), their exact location was the first question to be answered. In 1939 five mechanical seismographs were constructed and deployed in an array specifically to locate the tremors [Gane *et al.* (1946)]. They recognized that a frequency response up to 20 Hz and a timing resolution of 0.1 sec or better would be necessary. By establishing a seismic network for high-quality hypocenter determination, they showed that the tremors were indeed originating from within the mining area, and more specifically, from within those areas mined during the preceding 10 years.

More detailed studies of a larger number of tremors, with greater timing resolution, were needed. Gane *et al.* (1949) described a six-station radiotelemetry seismic network that they designed and applied to this problem. At the central recording site there was a multichannel photographic recorder with an automatic trigger to start recording when an earthquake was sensed. A 6-sec magnetic tape-loop delay line to preserve

the initial P-onsets was devised. The early foresight of this research group in specifying the requirements of instrumental networks to study microearthquakes and their ingenuity in the design, construction, and operation of this particular network deserve to be recognized.

### *1.1.5. Development in Japan*

Because of frequent damaging earthquakes occurring in and near Japan, Japanese seismologists pioneered in many aspects of earthquake research. In order to observe earthquakes in epicentral areas, Japanese seismologists (notably A. Imamura and M. Ishimoto) developed portable seismographs to study aftershocks and to monitor seismicity. The works by Imamura (1929), Imamura *et al.* (1932), Nasu (1929a,b, 1935a,b, 1936), Iida (1939, 1940), Omote (1944, 1950a,b, 1955), and many others greatly contributed to our knowledge of aftershocks. The paper that first introduced the word "microearthquake" was by Asada and Suzuki (1949). They chose this word to be equivalent to the Japanese word *bisho zisin*, which means very small or smaller than small earthquake (Z. Suzuki, written communication, 1979).

Asada (1957) reported the first detailed study of microearthquakes. He demonstrated that many microearthquakes could be detected in and near Kanto district by ultrasensitive seismographs having a magnification of $10^7$ at 20 Hz. Asada understood the technical requirements of recording microearthquakes and the advantages of studying microearthquakes because of their higher rate of occurrence. He investigated the frequency–magnitude relationship for microearthquakes, and tried to determine whether microearthquakes also occur in seismic regions where larger earthquakes occur. He foresaw the potential of using microearthquakes to predict larger earthquakes.

Detailed studies of microearthquakes in the Kii Peninsula, central Japan, using temporary arrays of short-period instruments and radiotelemetry seismograph systems were carried out by Miyamura and his colleagues in the 1950s and early 1960s (1966, with references therein to earlier works). Timing accuracy was stressed in order to obtain precise locations for the microearthquakes. Miyamura (1960) achieved an accuracy of $\pm 0.05$ sec by using a recording paper speed of 4 mm/sec. Miyamura *et al.* (1964) also used triggered magnetic tape recorders with a small four-station array in Gifu Prefecture, central Japan. An endless tape loop with a 20-sec delay time allowed recording of the initial P-onsets. An automatic gain control system was used to allow better readings of the S-phases.

The well-known Matsushiro earthquake swarm was first observed at

the Matsushiro Seismological Observatory in August 1965. The swarm activity increased remarkably, with more than 6000 microearthquakes recorded daily by March 1966. By mid-April slightly more than 600 earthquakes were felt in one day (Rikitake, 1976). Many special studies, including seismic and geodetic observations, were conducted. The papers are too numerous to review here, but readers may consult, for example, the *Bulletin of the Earthquake Research Institute, University of Tokyo*.

In the 1960s many microearthquake networks were established in Japan. These networks consisted of about 5–15 stations each and were operated by many groups (Suzuki *et al.*, 1979). More recently, an effort was made to combine microearthquake data from several groups into a central data processing center (T. Usami, personal communication, 1979). This should mark a new era in microearthquake studies in Japan.

### *1.1.6. Development in USSR*

The study of microearthquakes in the Soviet Union was initiated by G. A. Gamburtsev and his colleagues. The early history was documented by Riznichenko (1975). In the late 1940s Gamburtsev applied the experience gained in seismic prospecting to the study of local weak earthquakes (Soviet seismologists often used the term "weak" earthquakes to denote microearthquakes). In 1949 and 1953 Complex Seismological Expeditions were conducted in Turkmenia to map the focal region of the 1948 Ashkhabad earthquake. Networks of temporary stations were installed to make detailed studies of the seismicity (Rustanovich, 1957; Gamburtsev and Gal'perin, 1960a). In 1953 detailed studies of microearthquake distribution were carried out in the epicentral region of the 1946 Khait earthquake in the Tadzhik Republic (Gamburtsev and Gal'perin, 1960b).

A major contribution by Gamburtsev was to organize the Tadzhik Joint Seismological Expedition in the Garm and Khait regions beginning in 1954. Gamburtsev and his colleagues realized that microearthquakes could provide large quantities of data to establish relations between microearthquakes and large events and to obtain knowledge of the earthquake-generating process. The first stage of this expedition in 1955–1957 resulted in the publication of the monograph *Methods of Detailed Investigations of Seismicity* edited by Riznichenko (1960).

I. L. Nersesov became head of the Tadzhik Joint Seismological Expedition when Gamburtsev died in 1955. The expedition had a major role in the development of a new generation of seismologists in the USSR, and in the quantification of seismicity and seismic risk (Riznichenko, 1975). Nersesov and his colleagues at Garm generally are credited with providing a worldwide stimulus for earthquake prediction. In the 1960s they reported

that changes in the travel time ratio $t_s/t_p$ preceded earthquakes of moderate size (Kondratenko and Nersesov, 1962; Semenov, 1969).

Fedotov and his colleagues at the Institute of Volcanology, Petropavlovsk-Kamchatsky, USSR, made detailed studies of seismicity in the Kamchatka–Kuriles region. They developed the concept of seismic gaps and seismic cycles for the prediction of large earthquakes (Fedotov, 1965, 1968; Fedotov *et al.*, 1969).

Telemetered microearthquake networks were developed only recently in the Soviet Union, in cooperation with American seismologists (Wallace and Sadovskiy, 1976).

### *1.1.7. Development in the United States*

Systematic studies of local earthquakes in southern California began in the 1920s through the effort of H. O. Wood. Anderson and Wood (1925) developed the Wood–Anderson seismograph, a remarkably simple and sensitive instrument at that time. From the 1920s to the 1950s Wood–Anderson seismographs formed the backbone of the Southern California Seismic Network, which was first operated by the Carnegie Institution of Washington and later by the California Institute of Technology. Similar studies of local earthquakes in northern California were carried out by the Seismographic Stations of the University of California. Even though microearthquakes occurring near a station could be recorded, these regional networks were not adequate to investigate microearthquakes, because station spacing was sparse and instrument sensitivity was not high enough. The first reported microearthquake study in the United States was made by Sanford and Holmes (1962) near Socorro, New Mexico, in a manner similar to that used by Asada (1957).

In the 1950s, J. P. Eaton developed a telemetered seismograph system (peak magnification of 40,000 at 5 Hz) for the Hawaii Seismic Network. The stations were deployed densely enough to permit precise location of microearthquakes on a routine basis (Eaton, 1962). From 1961 to 1963, Don Tocher upgraded the Seismographic Stations of the University of California by telemetering seismic signals from individual stations via telephone lines to a central recording center at Berkeley (Bolt, 1977a). Thus by the early 1960s the key elements for a telemetered seismic network were known.

At about the same time, portable seismographs of high sensitivity were also developed (e.g., Lehner and Press, 1966). Several groups in the United States began microearthquake surveys. Notable among these were J. Oliver and his colleagues at the Lamont–Doherty Geological Observatory (e.g., Oliver *et al.*, 1966), and J. N. Brune and his colleagues at the

Caltech Seismological Laboratory (e.g., Brune and Allen, 1967). A detailed study of the aftershocks of the 1966 Parkfield earthquake by Eaton *et al.* (1970b) demonstrated that microearthquakes were useful in delineating the slip surface of the Parkfield earthquake in three dimensions. This experience led Eaton and his colleagues of the U.S. Geological Survey (USGS) to develop the Central California Microearthquake Network on a large scale (Eaton *et al.*, 1970a). Beginning with three local clusters of stations in 1967, this network has grown to include 250 stations covering central California in 1980.

Figures 1 and 2 illustrate one of the capabilities of a dense microearthquake network (such as the USGS Central California Microearthquake Network). Figure 1a shows numerous faults mapped in the network region. Figure 1b shows earthquake epicenters determined by a good regional network operated by the Seismographic Stations of the University of California at Berkeley for a nine-year period. With a dense network of stations, as shown in Fig. 2a, the spatial distribution of earthquake epicenters delineates their relationship to active faults in only one year's observation, as shown in Fig. 2b.

In addition to several microearthquake networks developed and operated by the U.S. Geological Survey, others have been implemented by various universities, for example, University of Washington (Crosson, 1972), St. Louis University (Stauder *et al.*, 1976), and the Lamont–Doherty Geological Observatory of Columbia University (Sykes, 1977). In the 1970s, various agencies of the United States government became concerned about earthquake hazards and supported the development and operation of many microearthquake networks. Today, about 50 permanent networks are operating in the United States (see Section 7.1).

Aggarwal *et al.* (1973) were the first to establish a network of portable seismographs in the United States specifically to search for precursory velocity anomalies similar to those reported from the Garm region, USSR. They studied a swarm of microearthquakes in the Blue Mountain Lake area of New York State. Detailed analysis of $V_p/V_s$ ratios showed the same type of behavior as in the Garm region, and changes preceding earthquakes as small as magnitude 2.5 and 3.3 were observed (Aggarwal *et al.*, 1973, 1975). Using stations from the Southern California Seismic Network, Whitcomb *et al.* (1973) reported similar precursory behavior preceding the destructive San Fernando earthquake of February 9, 1971.

## 1.2. Overview and Scope

This work reviews some principles and applications of microearthquake networks. In summarizing the present status, we emphasize methods and

**Fig. 1a.** Schematic map showing fault traces in central California. The heavy lines delineate major active faults.

techniques instead of results. Our review draws heavily on our experience with the Central California Microearthquake Network of the U.S. Geological Survey.

In Chapter 2 we describe mainly the instrumentation system employed in the USGS Central California Microearthquake Network. We emphasize the data processing systems of the same network in Chapter 3. Chapters 4 and 5 contain mathematical and computational preliminaries required in modern analyses of microearthquake data. Although numerous papers

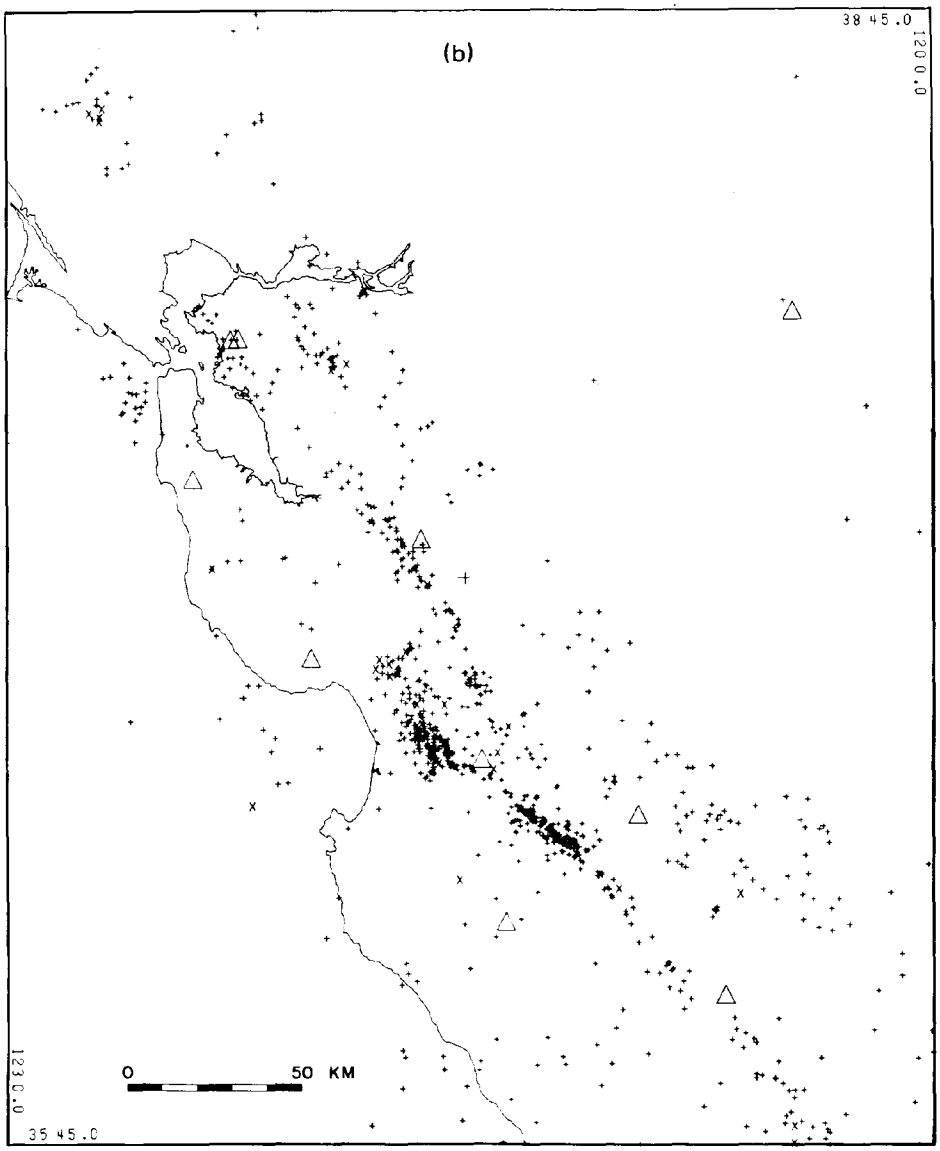


**Fig. 1b.** Map showing earthquake epicenters (for the period 1962–1970) as determined by the Seismographic Stations of the University of California at Berkeley. Station sites are shown as triangles.

have been published on generalized inversion, nonlinear optimization, and seismic ray tracing, uniformly developed and readable accounts of these topics for seismologists seem to be lacking. Therefore, we attempt to present these topics in an introductory manner. Chapter 6 deals with methods of locating microearthquakes, of fault-plane solutions, and of magnitude estimation. Simultaneous inversion of hypocenter parameters and velocity structure is also discussed.

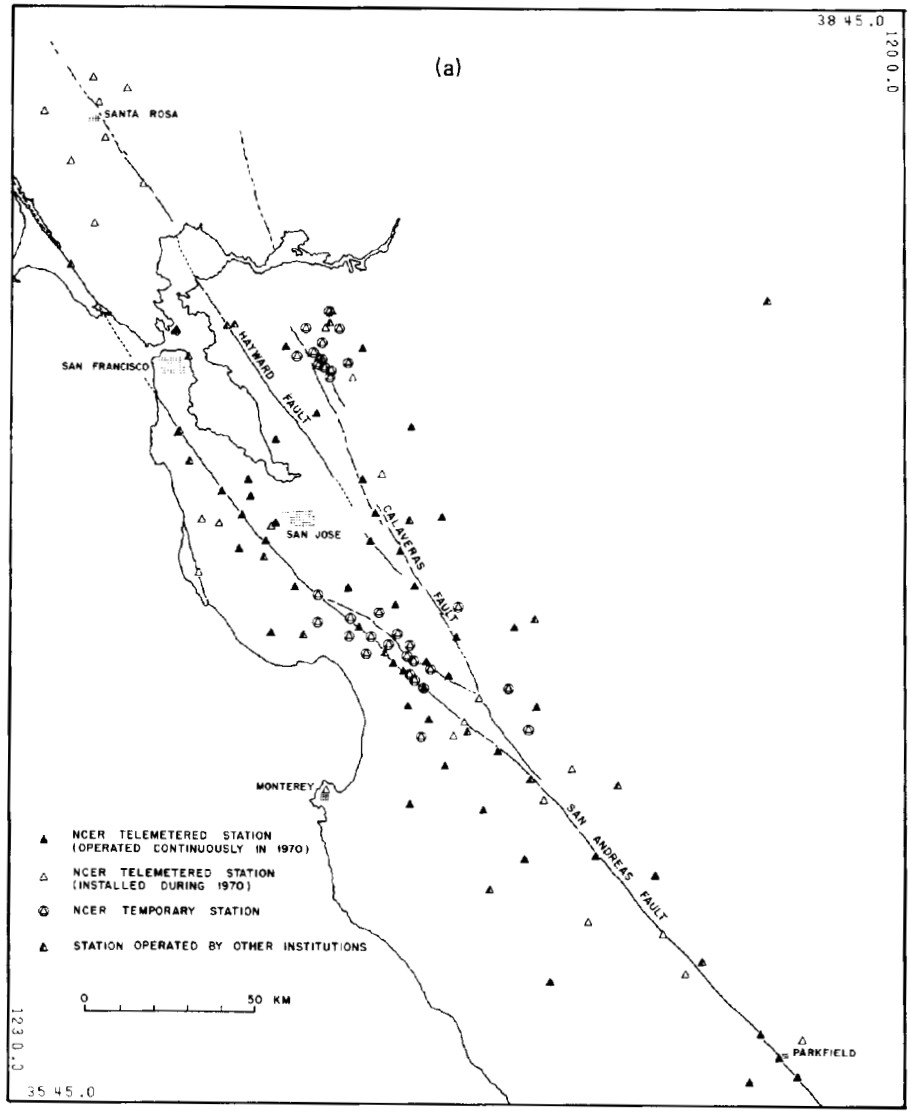


**Fig. 2a.** Map showing seismographic stations in central California for 1970.

Chapters 7 and 8 review various applications of microearthquake networks in earthquake prediction, hazard evaluation, exploration for geothermal energy, and studies of crustal and upper mantle structure. Chapter 9 is a brief summary of our personal views on microearthquake studies and a few comments on the future development of microearthquake networks. We have tried to keep mathematical notation consistent within each chapter, but it may vary from one chapter to another. This is due in part to differences in notation between the mathematical and seismological literature.

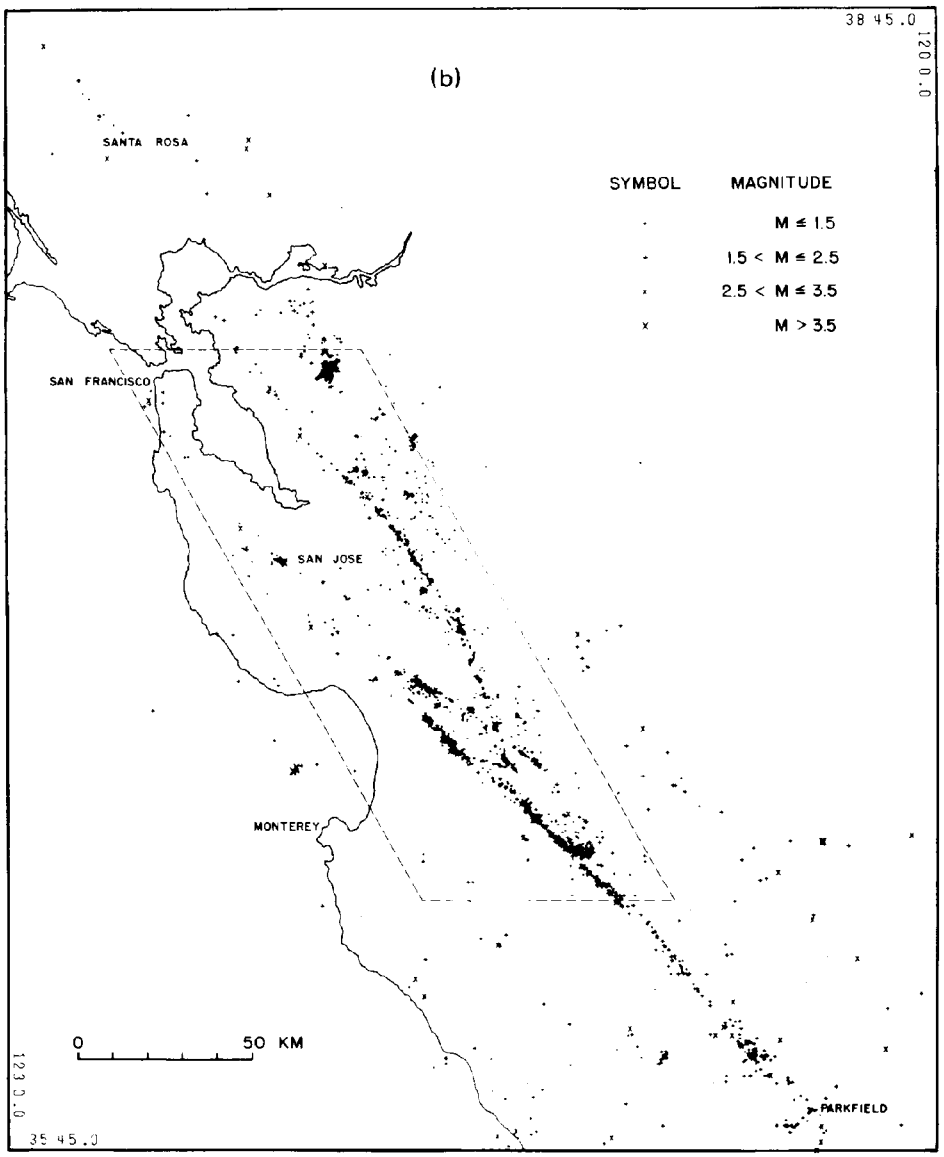


**Fig. 2b.** Map showing earthquake epicenters (for 1970) as determined by the USGS Central California Microearthquake Network using stations shown in part (a).

Microearthquake studies have been published in a wide variety of journals and reports. They also appear in languages other than English, such as Japanese, Russian, Chinese, German, and French. In the course of preparing this work, we have collected more than 2000 articles related to this subject. It is clearly beyond our abilities to treat every article equally and fairly, especially the non-English papers. Nevertheless, we have selected about 700 papers and books for references. The reference list is arranged alphabetically by authors. If the paper is not in English, we have

indicated the language in which it is written. We have cited many USGS Open-File Reports, which are on file at the libraries of the U.S. Geological Survey in Reston, Virginia; Denver, Colorado; and Menlo Park, California.

We hope that this work will provide some guidance for scientists beginning this field of research and will serve as a general reference on microearthquake studies. In an attempt to make this book more useful to readers, we have prepared a Glossary, an Author Index, and a Subject Index. If a certain term is not familiar to the reader, the following steps are recommended: (1) consult the Subject Index and refer to the pages where the term in question may be defined or discussed, (2) consult the Glossary, or (3) consult the standard references given in the Glossary.

The Author Index lists all the names that appear explicitly in the text. A paper with three or more authors is referred to in the text by the name of the first author followed by *et al.* Because the names of the other authors in this case do not appear explicitly, they are not indexed. However, all authors in the References section are included in the Author Index.

# 2. Instrumentation Systems

## 2.1. General Considerations

Some microearthquake networks are intended to study seismicity and active tectonic processes in relatively large regions. Others are set up for a single objective (e.g., to evaluate particular sites for emplacement of critical structures such as dams or nuclear power plants). In any case, the expected function of a microearthquake network should be the primary concern in its design and operation. It is not our intent to discuss in detail the design principles of all types of microearthquake networks. Rather, we will review some factors that should be considered in laying out a microearthquake network. These include: the merits of a centralized recording, timing, and processing system; some considerations for station location; and an approach to the selection of an optimal frequency response for the system. In all cases we assume that the first function of a network is to locate earthquakes that occur within the network and to compute their magnitudes. We and our colleagues in Menlo Park have been developing the large USGS network in central California (Fig. 3) for many years. We will describe our techniques in some detail because many of them could be applied to other networks. Finally, we will briefly summarize some features of other microearthquake networks.

### *2.1.1. Centralized Recording Systems*

Telemetry transmission and centralized timing and recording systems are commonly used for operating microearthquake networks. In this method the output signal from a seismometer is conditioned and amplified at the field station, and converted for telemetry transmission to a central location. At this location signals from many stations and a common time base are recorded. Recordings may be on magnetic tape, paper, or photographic film. Recent advances in digital computer technology allow seismic signals to be processed directly on-line as well.

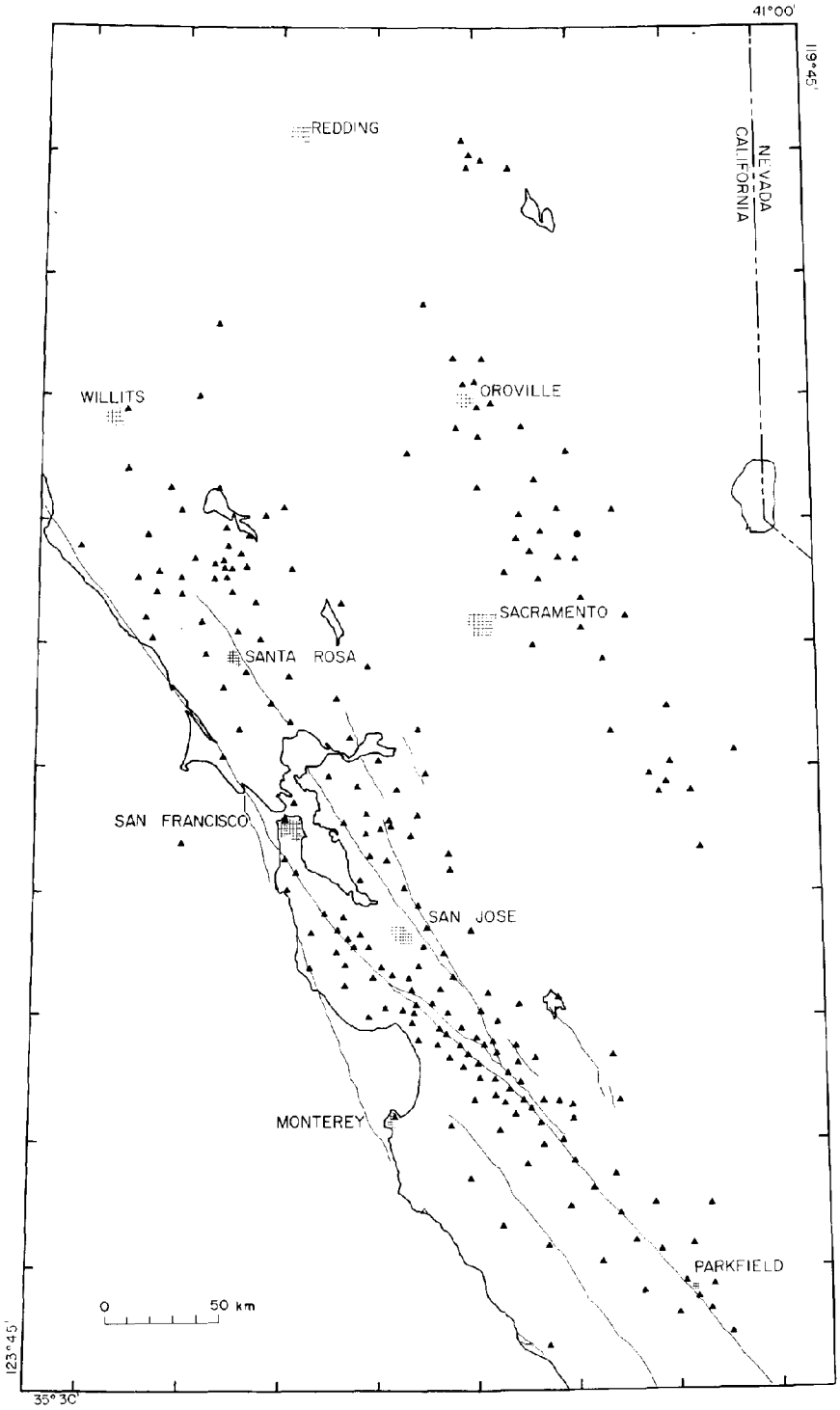


**Fig. 3.** Distribution of seismic stations (solid triangles) in the USGS Central California Microearthquake Network.

The principal advantage in using a centralized recording system is that a common time base can be established for the entire network. Since only one time base is needed, greater effort can be put into maintaining a dependable and precise time standard. The common time base eliminates the need for separate clock corrections for each station. Keeping separate clock corrections has been a principal headache for seismologists, and errors in clock corrections limit the precision in locating earthquakes.

Another advantage is that many seismic signals can be recorded on a common film or magnetic tape medium. Mass recording on film makes it easier to identify seismic events and to read records. The labor involved in reading multichannel film records is typically several times less than that for reading single-channel records. Mass recording on magnetic tape makes it possible to use a computer for more sophisticated analysis. Compared with the 1-mm/sec recording speed used by the standard 24-hr drum recorder, greatly improved time resolution is available with centralized film or tape recording systems. For example, time bases ranging from 10 to 100 mm/sec are used routinely for multichannel oscillographic playbacks from tape-recorded data.

Finally, having seismic signals from the entire network available at one location permits rapid correction of instrumental malfunctions and permits real-time monitoring and analysis of seismic activity within the network.

### *2.1.2. Station Distribution and Site Location*

Previous studies (e.g., Bolt, 1960; Lee *et al.*, 1971) suggested that if the crustal structure is homogeneous, stations in a seismic network should be evenly distributed by azimuth and distance. In particular, to obtain a reliable epicenter, the maximum azimuthal gap between stations should be less than 180°; to obtain a reliable focal depth, the distance from the epicenter to the nearest station should be less than the focal depth. For example, focal depths of central California earthquakes are typically 5–10 km. It follows that an average station spacing $\xi$ not greater than 10–20 km is needed. If earthquakes are uniformly distributed over a region of area $A$, then a network of approximately $A/\xi^2$ stations (which are evenly distributed over the region) is required. If earthquakes are concentrated along fault zones, then the minimum spacing applies only for stations near the fault zones, and the total number of stations required could be less. Optimal distribution of stations has been studied by many authors [e.g., Sato and Skoko (1965), Peters and Crosson (1972), Kijko (1978), Lilwall and Francis (1978), and Uhrhammer (1980b)].

In practice, however, we are faced with physical constraints such as accessibility and sources of cultural and natural noise. For example, Raleigh *et al.* (1976) used a 13-station network to study microearthquakes from a specific source area within a producing oil field near Rangely, Colorado. Seismicity of primary interest was confined to an area about 2 km wide by 6 km long. Focal depths were in the range 1–5 km. The purpose of the network was to determine if fluid injection and withdrawal would be effective in controlling seismic activity. Seismometers were concentrated around the area of interest and distributed more sparsely at greater distances. This arrangement provided good hypocentral control in the experimental area and still allowed seismicity in the surrounding area to be monitored.

By contrast, a 16-station microearthquake network in southeast Missouri has a relatively uniform distribution of stations (Stauder *et al.*, 1976). The primary purpose of the network is to delineate the features of the New Madrid seismic zone—the site of the major earthquakes of 1811–1812. In this case the entire area is under investigation, and it is important to establish the regional seismicity unbiased by station distribution.

Certain physical constraints will also affect station distribution. For example, Quaternary alluvium should be avoided if possible, as it usually has higher background noise than more competent rock. In some places in the USGS Central California Microearthquake Network, station distribution is relatively sparse (Fig. 3). Sometimes this is due to inaccessible terrain or to large bodies of water, where the cost of station operation outweighs the expected benefits. Other places are not instrumented because of their proximity to large cities that generate too much cultural noise.

One way to reduce cultural noise is to place seismometers at some depth. For example, Steeples (1979) placed 10-Hz geophones in steel-cased boreholes 50–58 m deep for a 12-station telemetered network in eastern Kansas. This was effective in reducing cultural noise (such as that from nearby vehicles and livestock) by as much as 10 dB. However, it was less effective in reducing train and other noise in the range of 2–3 Hz. Takahashi and Hamada (1975) described the results of placing seismometers in deep boreholes in the vicinity of Tokyo. Velocity seismometers with a natural frequency of 1 Hz were placed in a hole 3500 m deep, along with sets of accelerometers, tiltmeters, and thermometers. Within the frequency range of 1–15 Hz, the spectral amplitude of the background noise was about 1/300 to 1/1000 of that observed at the surface. This noise level was small even when compared with that from other Japanese stations located in quieter areas.

### *2.1.3. Instrumental Response*

The frequency response of a seismic system describes the relative amplitude and phase at which the system responds to ground motions as a function of frequency. The dynamic range is the ratio of the largest to the smallest input signal that the system can measure without distortion. In general, both of these parameters are functions of frequency and describe the expected performance of a system. Earthquakes ranging in magnitude from 0 to 6 may be expected to occur within a typical microearthquake network. Because the magnitude scale is logarithmic, this corresponds to ground amplitude ratios of $10^6$: 1. Achieving such a dynamic range is a challenge in instrument design. Specifying the appropriate frequency response involves seismological considerations, and this is discussed next.

The frequency content of earthquake waveforms varies with magnitude—from 200 to 1000 Hz for small, very local events (Armstrong, 1969; Bacon, 1975) to periods of 50 min or more for the normal modes of oscillation generated by great earthquakes. Within this wide spectrum, earthquakes as recorded by typical microearthquake networks show predominant spectral content between 1 and 20 Hz.

Generally one cannot arbitrarily choose a broadband instrument for a large network because of various trade-offs. At the low-frequency end ($<1$ Hz, say) microseismic noise (Peterson and Orsini, 1976) may limit the number of earthquakes recorded. At the high-frequency end ($>50$ Hz, say) faster recording speeds and increased bandwidth for the telemetry transmission system are needed. Frequency-dependent absorption within the earth would limit the registration of high-frequency events to very local ones. High-frequency cultural noise also contaminates seismic signals. All these factors work against using a broadband system for routine microearthquake studies. However, broadband systems are valuable in special topical studies of microearthquakes (e.g., Tucker and Brune, 1973).

One way to find the appropriate frequency range for a microearthquake network is first to compute spectra from a suite of earthquakes of varying magnitude and epicentral distance, and then select the frequency band corresponding to the dominant spectral levels. On the other hand, Eaton (1977) attacked the problem from an opposite point of view. He computed theoretical ground displacement spectra in the magnitude range 0–6 and then examined how these spectra would be modified by a particular instrumental system. His discussion dealt with the instrumentation presently used in the Central California Microearthquake Network of the U.S. Geological Survey. Because his method is applicable to other sys-

tems with appropriate substitution for certain parameters, it is discussed here in some detail.

From seismic source theory one can calculate spectral amplitudes of ground motion for certain source models. These calculations illustrate the variation in frequency content that would be expected for earthquakes of varying magnitude and source characteristics. The output of a particular instrumental system may then be ascertained by combining the spectrum of the expected ground motion with the frequency response of the instrumental system.

More specifically, Eaton (1977) used Brune's (1970) model of the seismic source as presented by Hanks and Thatcher (1972). It models an earthquake dislocation as a tangential stress pulse applied equally, but in opposite directions, to the two inner surfaces of a fault block. In this model the far-field shear displacement spectrum can be represented by three parameters: the long-period spectral level $\Omega_0$, the corner frequency $f_0$, and a parameter $\varepsilon$, which controls the rate of fall-off of the displacement spectrum at frequencies above $f_0$. If $\varepsilon = 1$, the stress drop associated with the earthquake is complete, that is, the effective shear stress equals the shear stress drop (Hanks and Thatcher, 1972, p. 4395). With $\varepsilon = 1$, the long-period spectral level $\Omega_0$ is constant for frequencies of less than about $f_0$ and decreases as $f^{-2}$ for frequencies greater than $f_0$.

For $\varepsilon = 1$, seismic moment $M_0$, local magnitude $M_L$, long-period spectral level $\Omega_0$, corner frequency $f_0$, stress drop $\Delta\sigma$, epicentral distance $R$, density $\rho$, and shear velocity $\beta$ are related as follows (Thatcher and Hanks, 1973):

$$M_0 = 4\pi\rho\beta^3\Omega_0 R/0.85 \tag{2.1}$$

$$\Delta\sigma = 106\ \rho R\Omega_0 f_0^3/0.85 \tag{2.2}$$

$$\log M_0 = 16 + 1.5M_L \qquad (M_0 \text{ in dyne-cm}) \tag{2.3}$$

To reduce these equations to variables only in $\Omega_0$ and $f_0$ as a function of $M_L$, Eaton (1977) followed Thatcher and Hanks (1973) and set $\rho = 2.7$ gm/cm$^3$, $\beta = 3.2$ km/sec, and $R = 100$ km. Setting the stress drop $\Delta\sigma$ to 5 bars, Eaton obtained

$$\log \Omega_0 = 1.5M_L - 9.1 \qquad (\Omega_0 \text{ in cm-sec}) \tag{2.4}$$

$$\log f_0 = 2.1 - 0.5M_L \tag{2.5}$$

The theoretical spectral amplitudes of ground displacement for earthquakes from magnitude 0 to 6 are shown in Fig. 4. These theoretical spectra were computed from Eqs. (2.4)–(2.5). The instrumental response of the short-period seismic system used in the USGS Central California Microearthquake Network is shown in Fig. 5. The set of combined dis-

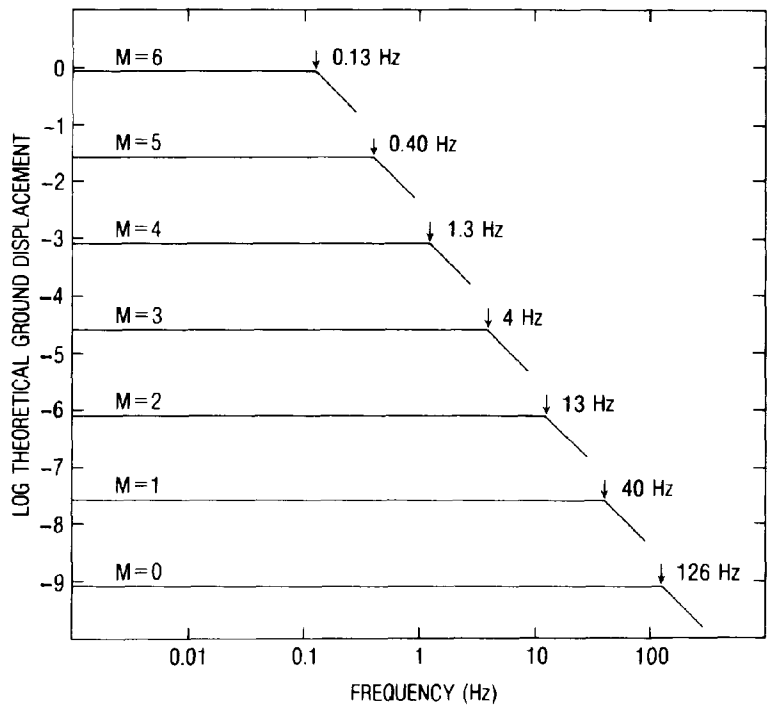


**Fig. 4.** Theoretical spectral amplitude of ground displacement as a function of frequency for earthquakes ranging in magnitude ($M$) from 0 to 6. Corner frequencies of these earthquakes are shown by arrows. Label for the ordinate has been shortened.

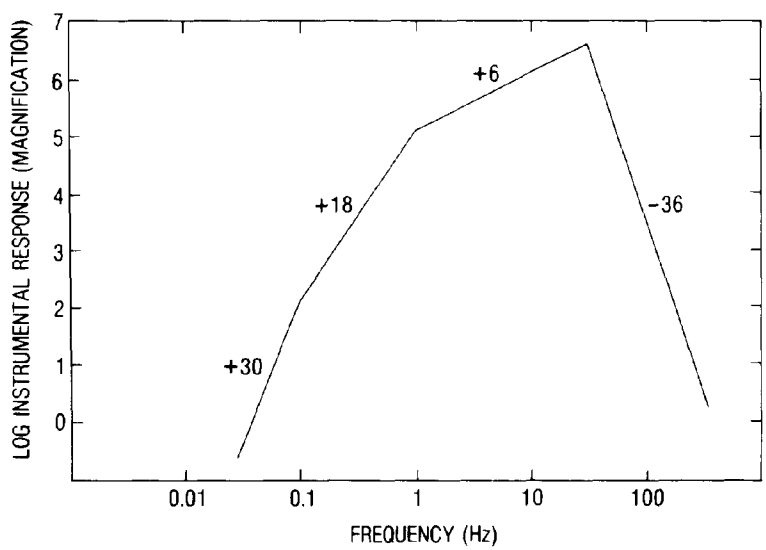


**Fig. 5.** Stylized diagram of displacement amplitude response for the USGS short-period microearthquake system (modified from Eaton, 1977). The numbers along each segment of the curve are in units of decibels per octave.

placement spectra that would be recorded by the instrumental system is shown in Fig. 6. These are obtained by adding the logarithmic instrumental response curve to each of the logarithmic theoretical ground displacement curves. The locations of the theoretical corner frequencies for earthquakes from magnitude 0 to 6 are shown by arrows in this figure. All the response curves are stylized; each is represented by a small number of linear segments. This is sufficient for the present discussion and is an accepted way to diagram frequency response (Willmore, 1961). The theoretical ground displacement curves in Fig. 4 do not include the effects of the radiation pattern at the source, absorption and scattering along the transmission path, and conditions at the recording site. These effects are discussed in Thatcher and Hanks (1973).

Some interesting relations can be inferred from the combined displacement response curves (Fig. 6). For earthquakes in the magnitude range slightly greater than 1 to about 4, the peak of the combined displacement response curve or, equivalently, the frequency of the maximum amplitude that would be seen on the seismogram, varies with the magnitude of the earthquake. For the assumed source model this frequency corresponds to the corner frequency $f_0$.

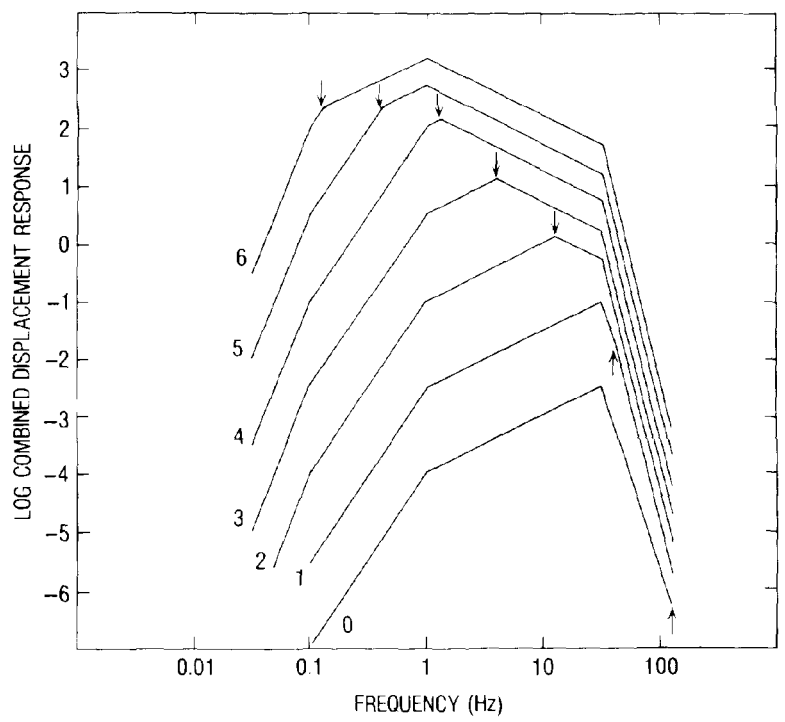


**Fig. 6.** Theoretical combined displacement response as a function of frequency for earthquakes ranging in magnitude from 0 to 6. Corner frequencies of these earthquakes are shown by arrows, and magnitude of each earthquake is indicated by an integer to the left of each curve.

Outside of this magnitude range the frequency of the maximum amplitude that would be seen on the seismogram does not change. For earthquakes greater than magnitude 4, the frequency of the maximum amplitude will always be 1 Hz. This is caused by (1) the rapid roll-off of the seismometer displacement response below its natural frequency of 1 Hz, and (2) the corner frequency being less than 1 Hz. For earthquakes less than magnitude 1 (assuming that they can be recorded at the 100-km distance assumed here), the frequency of the maximum amplitude will always be 30 Hz. This is caused by (1) the rapid roll-off of the response of the seismic amplifier and discriminators above 30 Hz, and (2) the corner frequency being greater than 30 Hz.

## 2.2. The USGS Central California Microearthquake Network

In 1966 the U.S. Geological Survey began to install a microearthquake network along the San Andreas fault system in central California. The main objective was to develop techniques for mapping microearthquakes in order to study the mechanics of earthquake generation (Eaton *et al.*, 1970a). The network was designed to telemeter seismic signals from field stations to a recording and processing center in Menlo Park, California. By early 1980 the network had grown to 250 stations.

Although the basic idea of telemetry transmission and recording has not changed, the instrumentation has been modified since 1966. Major effort has gone into (1) making the field package low power, compact, long-lived, and weather resistant; (2) increasing signal-to-noise ratio throughout the system; (3) understanding the frequency response of the entire system and its primary components; and (4) improving timing resolution and precision. In cooperative programs with other institutions, equipment similar to that in the USGS Central California Microearthquake Network has been used widely in the United States and some other countries as well. For these reasons we believe that a review of the instrumentation of this network would be instructive.

### *2.2.1. System Overview*

Figure 7 illustrates the major elements of the instrumentation system as currently used. The field package includes a seismometer, amplifier, voltage-controlled oscillator (VCO), frequency stabilizer, automatic daily calibration system, power supply, and telemetry interface. Output from one field package normally is connected to a nearby telephone line drop and transmitted continuously to Menlo Park. A standard voice-grade tele-

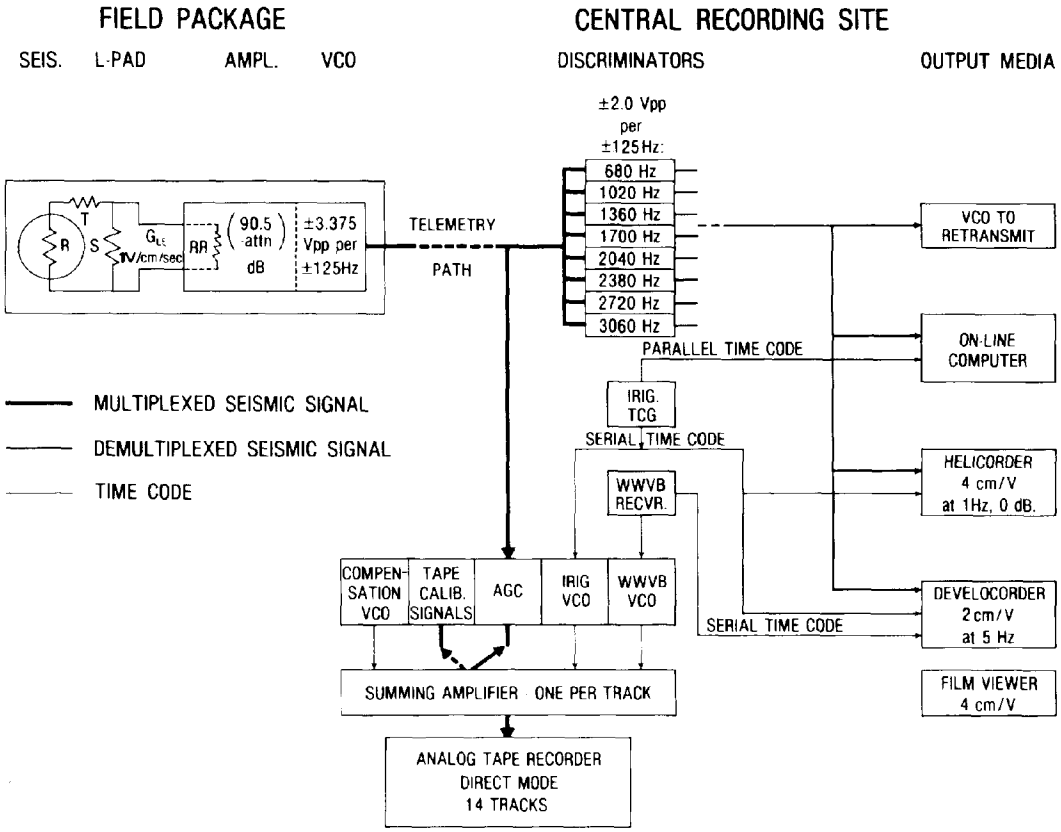


**Fig. 7.** Major elements of seismic instrumentation of the USGS Central California Microearthquake Network.

phone circuit with no special conditioning is used. If the field package output cannot be connected to a drop, it is transmitted via line-of-sight vhf radio to a convenient drop and transmitted from there using the telephone system.

As many as eight seismic signals are carried along one voice-grade circuit. This is accomplished by frequency division multiplexing (FDM), as follows. Voice-grade lines transmit audio signals in the frequency range of 300–3300 Hz. In our system of FDM the usable bandwidth is divided into eight FM subcarriers, each with a uniquely specified center frequency. A voltage-controlled oscillator in the field package converts the analog signal from the seismometer into a frequency-modulated signal for transmission. Figure 8 shows the eight subcarrier center frequencies used. The frequencies denoted as T1, T2, and C are not transmitted, and are discussed later. The maximum deviation allowed from each center frequency is ±125 Hz, which corresponds to ±3.375 V peak output from the amplifier. A spectrum analyzer monitoring a well-adjusted telemetry line

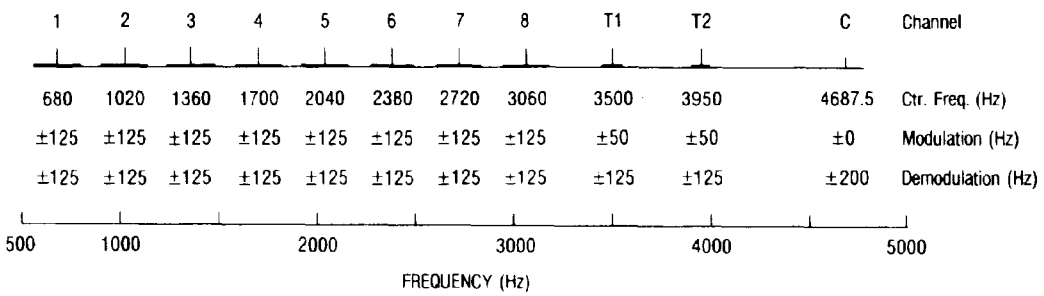


**Fig. 8.** Format of frequency division multiplexing (FDM) used for telemetry transmission and recording by the USGS Central California Microearthquake Network (modified from Eaton, 1976).

would show eight spectral peaks, spaced at intervals of 340 Hz and of approximately the same height. The reason for using FDM is to reduce the cost of data transmission.

When the telemetered FDM signal reaches the central recording site, it is divided and sent to two places (Fig. 7). First, it is sent through an automatic gain control (AGC) system, time code and other signals are added to it, and the combined signal is recorded in direct mode on an analog magnetic tape recorder. Second, it is sent through a bank of eight frequency discriminators (matching the eight FDM subcarriers), and the original analog signals are restored. The analog signals may be recorded on paper or photographic film. They may also be sent to an on-line computer system or retransmitted to other recording centers.

Eaton (1977) summarized the amplitude–frequency response of each of the major components of the USGS telemetry system (Fig. 9). Before proceeding with a summary of the instrumentation, it is instructive to consider how each system component contributes to the response of the entire system. The response curves in Fig. 9 are determined from design and manufacturers' specifications and from simple tests with a function generator. Each response curve is stylized, with emphasis given to the frequency at which various slopes change and to the rate of attenuation.

Figure 9A–C shows the essential features of the amplitude–frequency response for the major electronic units—the amplifier and VCO in the field package, and the discriminator at the central recording site. The combined response of these three units is shown in Fig. 9D and is referred to as the electronics response. The low-frequency roll-off starting at 0.1 Hz for the electronics response is due solely to the amplifier in the field package, whereas the high-frequency roll-off starting at 30 Hz has contributions from both the amplifier in the field and the discriminator at the central site. Figure 9E–G shows the response of the recording devices—the Oscillomink (a multichannel ink-jet oscillograph), the Develocorder,

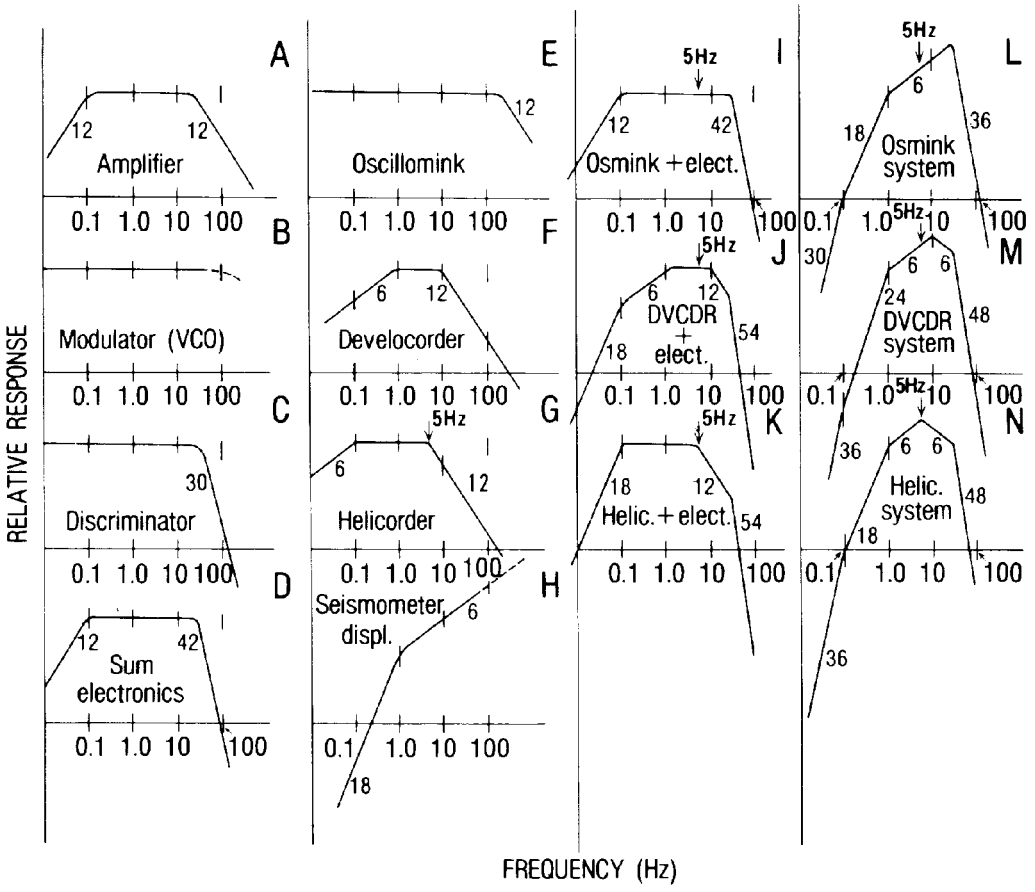


**Fig. 9.** Stylized amplitude response of individual components and combinations of components used in the USGS Central California Microearthquake Network (modified from Eaton, 1977). Amplitude attenuation is shown as an integer in dB/octave.

and the Helicorder. The Oscillomink is used for making high-speed playbacks of earthquakes originally recorded on magnetic tape. It has a flat frequency response from dc to well over 100 Hz. The Develocorder is the primary on-line film recording device. In order to suppress low-frequency microseismic noise and to prevent trace wandering caused by VCO drift, a 0.5-Hz low-cut filter has been added to each input terminal of the Develocorder. The 15.5-Hz galvanometer accounts for the high-frequency roll-off in the Develocorder response. Because the Helicorder uses recording speeds as low as 30 and 60 mm/min, its frequency response roll-off points are set at 0.1 and 5 Hz.

Figure 9I–K shows the combined response of the electronics and recording media—in other words, of everything but the seismometer. Because the Oscillomink response (Fig. 9E) is flat to well beyond 100 Hz, the

combined response (Fig. 9I) may be considered to represent that of the analog tape recorder as well. Figure 9I–K shows that the tape recorder has the broadest frequency response of the three recording media. The stylized frequency response of the complete system (Fig. 9L–N) is obtained by adding the logarithm of the seismometer response (Fig. 9H) to that of the three recording media and electronics (Fig. 9I–K). Although Fig. 9L shows that the peak response of the tape recorder is at 30 Hz, the measured peak response is at 22 Hz. The measured peak response of the Develocorder and Helicorder systems is at 14 and 5 Hz, respectively.

### *2.2.2. Field Package*

The field package (Fig. 10) contains a seismometer, amplifier, voltage-controlled oscillator (VCO), center-frequency stabilizer, automatic calibration unit, power supply, and telemetry interface.

The seismometer is a Mark Products Model L-4C, with a natural frequency of 1 Hz and a suspended mass of 1 kg. A resistive L-pad between the seismometer and the input to the amplifier results in a damping factor of 0.8 critical value and an effective motor constant of 1.0 V $cm^{-1}$ sec. The resistor values for the L-pad are calculated individually for each seismometer–amplifier pair because of measurable variations in the coil resistance, motor constant, natural frequency, and open circuit damping of the seismometers (Healy and O'Neill, 1977).

The USGS amplifier accepts signals in the microvolt to millivolt range and has a frequency passband (−3 dB points) of 0.1–30 Hz with a 12 dB/octave roll-off. System noise, referred to the input, is 1.0 $\mu$V (peak to peak) with a source impedance of 10,000 ohms. Maximum voltage gain of the unit is about 90 dB; attenuation is adjustable in 6-dB steps to 42 dB. The output from the amplifier modulates the center frequency of the USGS voltage-controlled oscillator unit for transmission.

Earlier versions of the field package consisted only of the components just described. Later, remarkable reductions in package size and power requirements were achieved by using integrated circuits. This made it practical to add two important functions to the field package—automatic calibration for the entire system and center frequency stabilization for the VCO unit.

A daily calibration sequence initiated by the field package interrupts the seismic data transmission and is recorded at the central site (Van Schaack, 1975). The sequence is about 40 sec long. It begins with a pulse-height-modulated code that provides a unique serial number for the field package. This is followed by a seismometer release test and an amplifier step

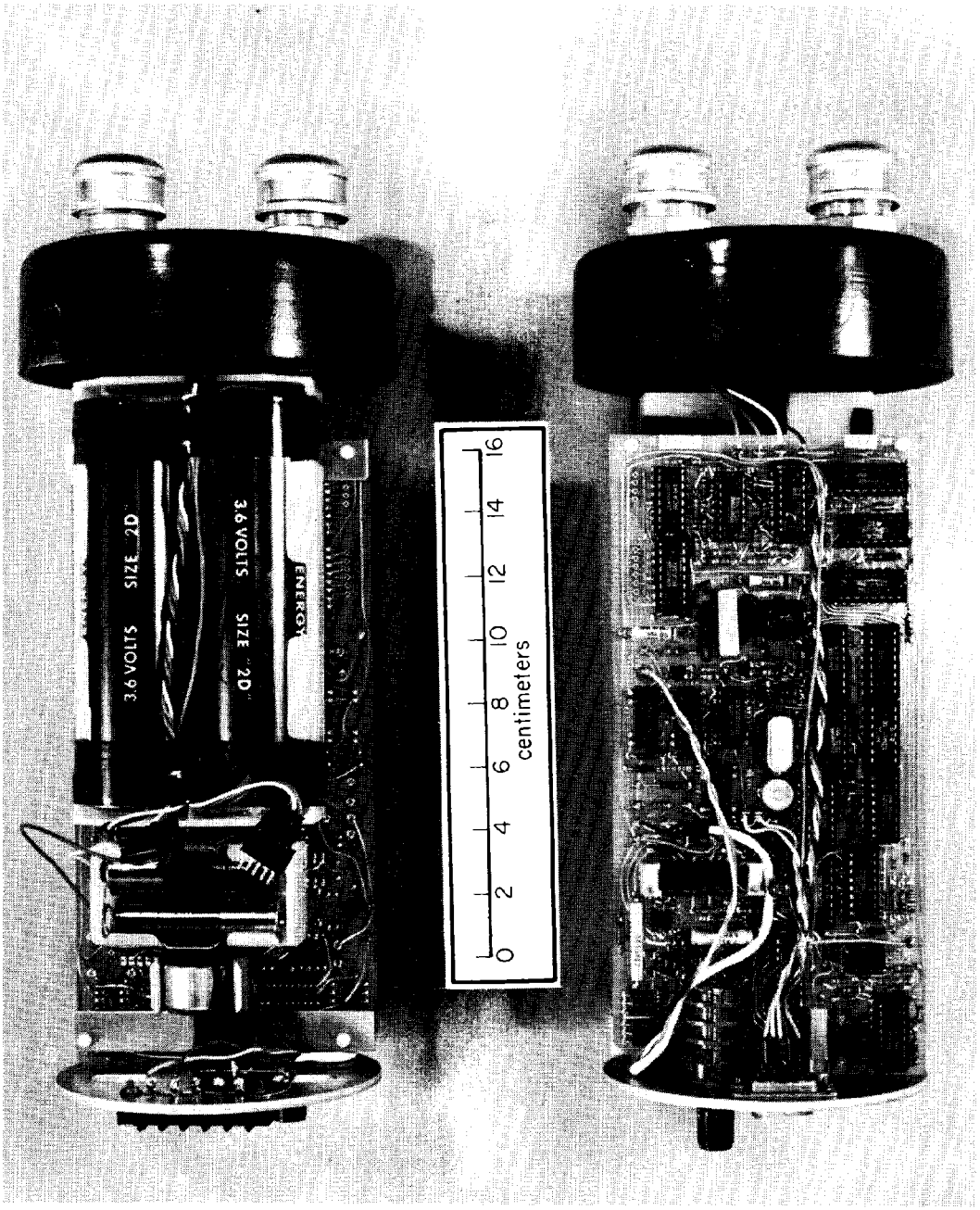


**Fig. 10.** Field package used in the USGS Central California Microearthquake Network. The back side which contains the power supply is shown on the left, and the front side which contains the electronic components is shown on the right. The seismometer is not shown.

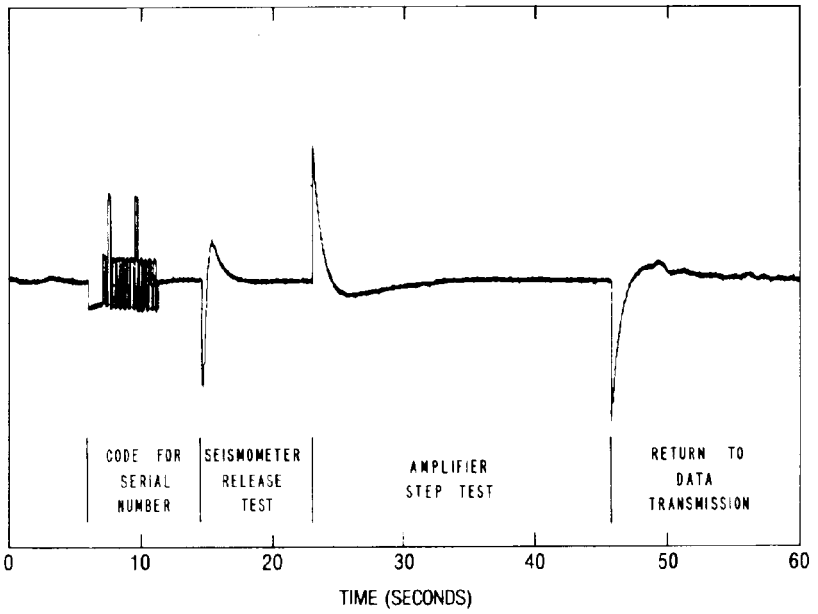


**Fig. 11.** Calibration signal generated by the automatic daily calibration system of the USGS Central California Microearthquake Network. The vertical scale is arbitrary.

test (Fig. 11). In the release test a fixed dc current is applied to the seismometer coil for a few seconds to offset the seismometer mass. The current is switched off and the seismometer mass is free to return to an equilibrium position. This motion of the seismometer mass corresponds to a step in ground acceleration. In the step test the seismometer is electrically disconnected from the amplifier and a fixed voltage step is applied to the amplifier input. The result is a second transient containing information about the frequency response of the entire system excluding the seismometer.

Center-frequency drift of the VCO unit can be caused by many factors. Among these are changes in ambient temperature and battery voltage, and aging of components. It is not unusual for the center frequency to change as much as 25% of full deviation (30 Hz out of 125 Hz maximum). A change in the center frequency introduces a dc offset in the recorded signal that degrades the signal-to-noise ratio. To combat this problem a center-frequency stabilizer was designed by Jensen (1977) and installed in the field package. The stabilizer averages the VCO output frequency over an interval of about 10 sec. A small dc correction voltage (−54 dB) is applied to shift the averaged frequency toward its nominal value. Each correction voltage is so small that it is within the system noise. However, the cumulative effect of many small corrections produces the compensation required to stabilize the center frequency.

The output impedance and signal level for the single component field package is compatible with the requirements of the telephone system. If more than one field package is used at one site, then seismic signals at different center frequencies are combined by a summing amplifier. For example, this happens when a two- or three-component system is used or when radiotelemetry signals are brought together from remote points.

Except for some components of the automatic daily calibration unit, the entire field package is powered by two 3.65-V lithium cells. The lithium cells are rated at 30 A · hr each and are the size of standard D cells. The field package continuously draws about 600 $\mu$A from these cells. To provide power for the automatic daily calibration, additional battery cells are used. Four alkaline-type AA cells provide a total of 6 V to close the relays for the 40-sec duration of the daily calibration test. A 1.35-V mercury cell is used as the voltage standard for the seismometer release test and the amplifier step test. Battery life under field operation conditions is 2 years.

### *2.2.3. Central Recording Site*

Although the field package usually provides a well-conditioned signal to the telephone system for transmission, the amplitude of the multiplexed seismic signals received at the central recording site may have large variations. These variations pose a serious problem for the analog tape recorders. To achieve adequate signal-to-noise ratio in playbacks of earthquakes from the analog tapes, the multiplexed seismic signals must be recorded within narrow amplitude limits. An automatic gain control (AGC) unit was designed and installed by Jensen (1976b) to accomplish this. The AGC unit is used only on multiplexed signals that are sent to the tape recorders. The multiplexed signals sent to the discriminators do not go through any signal conditioning circuits (Fig. 7).

Before the multiplexed seismic signals are recorded on analog tapes, each has three additional signals combined with it (Jensen, 1976a). One of these is a reference frequency for tape-speed compensation, set at 4687.5 Hz. It is used in a subtractive compensation mode on playback. The other two signals are serial time codes, set at center frequencies of 3500 and 3950 Hz, with deviation of $\pm 50$ Hz. These signals are recorded on each track in order to eliminate some sources of timing error and to increase signal-to-noise ratio upon playback of the tape. It is possible to combine these three signals with the eight from the telemetry system because their frequency range of 3450–4687.5 Hz is well above the highest frequency (3185 Hz) associated with the telemetry system, and yet is still below the 5000 Hz limit of the tape recorders running at 15/16 in./sec (Fig. 8). To obtain the desired rise times and noise reduction, Eaton and Van Schaack

(1977) showed that the frequency spacing between the timing and compensation subcarriers must be greater than that for the seismic data subcarriers.

The combined signals are recorded on Bell and Howell Model 3700B tape recorders, in direct-record mode. Fourteen tracks are recorded on the 1-in.- (25.4-mm) wide tape. The tape recorder speed of 15/16 in./sec (23.8 mm/sec) requires that the standard 7200-ft- (2195-m) length tape be changed daily. Because each multiplexed signal can have eight seismic signals within it, each 14-track tape recorder can accommodate 112 seismic signals. At present four such recorders are used for the USGS Central California Microearthquake Network.

### *2.2.4. Timing Systems*

Radio signal WWVB of the National Bureau of Standards (broadcasting at 60 kHz) is taken as the primary time base. The time signal is a serial binary code at 1 pulse/sec. The binary code is synchronized to the 60 kHz carrier and is referenced to UTC—universal time coordinated (Blair, 1974). Because radio reception of WWVB is of variable quality, a Time Code Generator made by Datum Products Co. is maintained at the central recording site as a secondary time base. It is driven by a rubidium frequency standard, with a rated precision of one part in $10^{12}$ per second. In addition, it generates a 30-bit parallel time code and two serial time codes, in IRIG-C and IRIG-E formats.

All three serial time codes (WWVB, IRIG-C, and IRIG-E) provide time of day in units of Julian day, hour, minute, and seconds. Because WWVB time code consists of 1-pulse/sec markers, time resolution less than 1 sec must be obtained by interpolation. Similarly, IRIG-C and IRIG-E consist of 2-pulse/sec and 10-pulse/sec markers, respectively, and time resolution less than 0.5 or 0.1 sec requires interpolation. The 30-bit parallel time code generated by the time code generator has a resolution of 1 sec. Serial time codes are sent to the linear recording devices (Fig. 7): Helicorder, Develocorder, and magnetic tape recorders. The parallel time code is sent to digital devices: the on-line computer and other digital data acquisition devices (not shown in Fig. 7).

The time code generator is kept within ±0.005 sec of universal time by daily comparison of the IRIG-C serial time code with the WWVB radio signal. Corrections are not made for radio propagation delay. Power failure or fluctuation at the central recording site does not affect the time code generator, as it is supplied by a float-charged battery system.

In addition to WWV and WWVB time services (Howe, 1976), which can suffer from limited range or variable propagation quality, there are

other sources of timing signals available or under development. These include the Omega navigation system (Kasper and Hutchinson, 1979) operating in the 10 kHz band, and the GOES satellite time system (Anonymous, 1978) operating in the uhf band. Furthermore, many nations broadcast their own time signals.

### *2.2.5. System Amplitude–Frequency Response*

The automatic daily calibration unit in the field package generates a sequence of transient calibration signals every day. Two different theoretical approaches to calculate system response from the signals have been developed—a Fourier transform technique (Espinosa *et al.,* 1962; Bakun and Dratler, 1976) and a least-squares technique (Mitchell and Landisman, 1969; Healy and O'Neill, 1977). In addition, Stewart and O'Neill (1980) implemented a method that combined simple analytic expressions for the response of individual components into the response function for the entire system.

In the Fourier transform method the complete seismic system is modeled as a black box which transforms a given input signal to an output signal. The complex ratio of the Fourier transform of the output signal to that of the input signal is defined as the response function of the black box. If the system is linear, causal, and time invariant, then this complex ratio completely describes the properties of the system. The Fourier transform method is purely empirical; no assumption is made about the shape of the system response.

In the Fourier transform method as applied by Bakun and Dratler (1976) the recorded transient signal generated by the seismometer mass release test or the amplifier step test (Fig. 11) is taken as the output signal for the black box. This signal is digitized and its Fourier transform is computed by the fast Fourier transform technique. The Fourier transform of the input signal is determined by theoretical considerations as follows. The input signal generated by the seismometer mass release test is equivalent to a step in ground acceleration $h(t)$, where $t$ is time. The Fourier transform of $h(t)$ is given by

$$H(f) = (GI/2\pi fM)\exp(i3\pi/2) \tag{2.6}$$

where $G$ is the seismometer motor constant, $M$ is the seismometer mass, $I$ is the current that displaces the seismometer mass, $i$ is $\sqrt{-1}$, and $f$ is the frequency in hertz. Similarly, the Fourier transform of the input signal generated by the amplifier step test is

$$S(f) = (E/2\pi f)\exp(i3\pi/2) \tag{2.7}$$

where $E$ is the voltage step applied to the amplifier.

Using the seismometer mass release test and the amplifier step test, Bakun and Dratler (1976) developed an interactive computer program to calculate complex response functions for the complete seismic system, for the electronics and recording subsystem, and for the seismometer. To avoid spectral contamination by aliasing, they recommend a digitization rate of 200 samples/sec. Figure 12 shows the amplitude response of the complete system, as computed by Bakun and Dratler (1976). The amplitude response is badly contaminated by noise at frequencies above 20 Hz.

Bakun and Dratler (1976) also developed a method to compute a smoothed system response. The method retains the same response curve as originally computed in Fig. 12 for frequencies lower than 2 or 3 Hz, and it extends an interpolated curve through the noisy portions of the response at frequencies above 10 Hz. The smoothed system amplitude response is shown in Fig. 13.

Using these same daily calibration signals, Healy and O'Neill (1977) applied a least-squares technique to compute the amplitude response. This technique assumes an analytic form for the input and output calibration transients. In deriving their analytical model Healy and O'Neill (1977) assumed that the frequency response for the seismic system (and its indi-

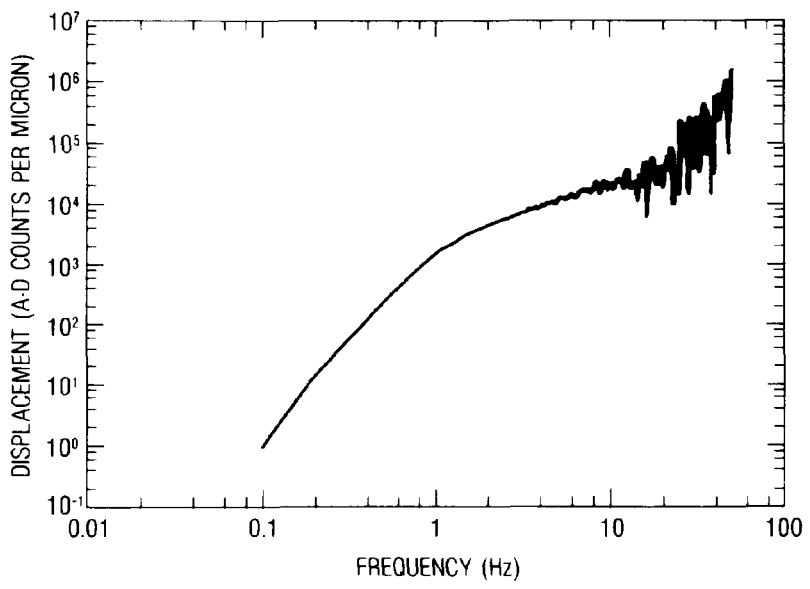


**Fig. 12.** Amplitude response of the seismic system used in the USGS Central California Microearthquake Network as determined by Bakun and Dratler (1976) using a Fourier transform technique.

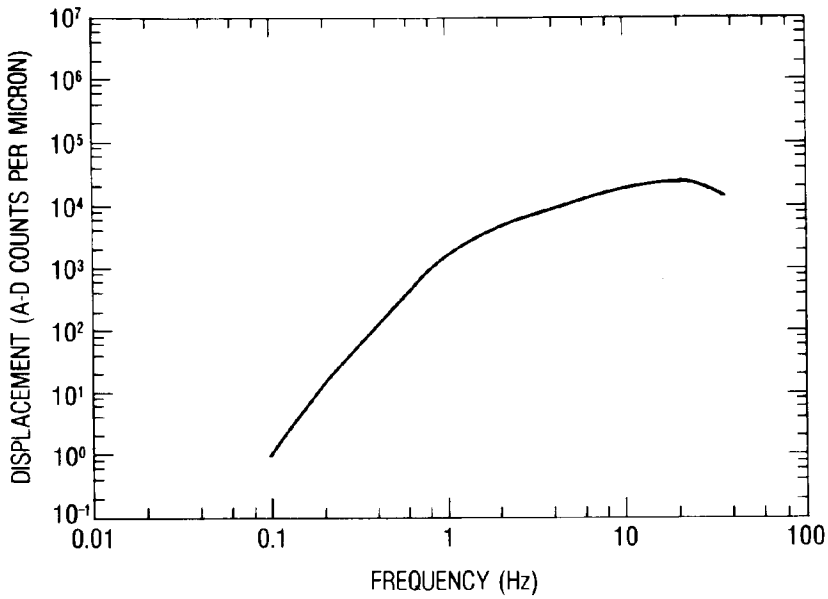


**Fig. 13.** Smoothed amplitude response of the seismic system used in the USGS Central California Microearthquake Network as determined by Bakun and Dratler (1976) using a Fourier transform technique.

vidual components as well) could be adequately approximated by

$$(2.8) \qquad F(\omega) = \frac{i^{l-n}\omega^l(C_1C_2 \cdots C_n)}{(\omega - \alpha_1)(\omega - \alpha_2) \cdots (\omega - \alpha_n)} \cdot A_1 \cdot A_2 \cdots A_m$$

$$m \leq n$$

where $\omega$ is the frequency in radians per second, $\alpha_j$ are the poles of the function $F(\omega)$, $C_j$ are real constants associated with each pole, $l$ is the power of the low-frequency roll-off, $n - l$ is the power of the high-frequency roll-off in the amplitude response, and $A_j$ are amplitude factors representing the sensitivity or gain of individual components within the system.

Because the physical system represented by $F(\omega)$ is real and causal, all the poles lie in the upper half of the complex plane. They are located either on the imaginary axis or off the axis as matched pairs (i.e., mirror images through the imaginary axis). Those that lie on the imaginary axis are single poles and have the form $-\alpha_j/(\omega - \alpha_j)$, or the form $\omega/(\omega - \alpha_j)$, where $\alpha_j = i\omega_0$, and $\omega_0$ is the frequency in radians per second. Those poles that occur as matched pairs are double poles and have the form $\alpha_j\alpha_k/(\omega - \alpha_j)(\omega - \alpha_k)$ or $\omega^2/(\omega - \alpha_j)(\omega - \alpha_k)$, where

$$(2.9) \qquad \alpha_j = \omega_0[i\beta + (1 - \beta^2)^{1/2}], \qquad \alpha_k = \omega_0[i\beta - (1 - \beta^2)^{1/2}]$$

$$\omega_0 = 2\pi f_0$$

and $\beta$ can be interpreted as a damping coefficient.

For example, if Eq. (2.8) is taken as the frequency response of the complete seismic system, then the impulse response in the time domain is

$$(2.10) \qquad f(t) = (2\pi)^{-1} \int_{-\infty}^{\infty} F(\omega) \exp(i\omega t)\, d\omega$$

When this integral is evaluated, the residue at the $j$th pole is found to be $b_j(\alpha_j) \exp(i\alpha_j t)$, where

$$(2.11) \qquad b_j(\omega) = (\omega - \alpha_j)F(\omega) = \frac{(\omega - \alpha_j)i^{l-n}\omega^l(C_1C_2 \cdots C_n)}{(\omega - \alpha_1)(\omega - \alpha_2) \cdots (\omega - \alpha_n)}$$

$b_j(\alpha_j)$ means $b_j$ evaluated at $\omega = \alpha_j$, and the factors $A_i$ have been ignored. The impulse response for the complete seismic system is written as

$$(2.12) \qquad f(t) = \sum_{j=1}^{n} ib_j(\alpha_j) \exp(i\alpha_j t)$$

Expressions similar in form to Eq. (2.12) were derived by Healy and O'Neill (1977) for the time domain representation of the amplifier step test and the seismometer release test.

Starting with the expression for the time domain form of the amplifier step test, Healy and O'Neill (1977) applied a least-squares method to calculate the locations of the poles $\alpha_i$. Trial values of the $\alpha_i$ and fixed values of $l$ and $n$ were determined from calibration of various components of the system—for the step test this is the amplifier, VCO, and the discriminator. Refined values for the poles $\alpha_i$ were computed by least squares, and these were substituted into Eq. (2.9) to compute $f_0$ and $\beta$. The refined values also were substituted into Eq. (2.8), and a theoretical response was computed for the amplifier–VCO–discriminator combination. The agreement between the calculated response and that determined by calibration in the laboratory was very good.

Stewart and O'Neill (1980) used Eq. (2.8) to calculate the frequency response for various combinations of units used in the USGS Central California Microearthquake Network. We shall illustrate their method by calculating the response of the complete seismic system from seismometer to the viewing screen used for the 16-mm Develocorder films.

Before the system response can be calculated from Eq. (2.8), the constants $l$, $n$, $C_i$, $\alpha_i$, and $A_i$ must be determined. It is convenient to divide the complete system into four units and to determine these constants sepa-

TABLE I

**Seismic System Response Parameters for USGS Central California Microearthquake Network[a]**

| Unit | $f_0$ (Hz) | $\beta$ | $n$ | $l$ | $C$-factor $C_j$ | $C$-factor $C_k$ | Response element | Standard amplitude factors $A_i$ specified by USGS |
|---|---|---|---|---|---|---|---|---|
| Seismometer and L-pad | 1.0 | 0.8 | 2 | 3 | 1 | 1 | $i\omega^3/(\omega - \alpha_j)(\omega - \alpha_k)$ | 1.0 V cm$^{-1}$ sec |
| Seismic amplifier and voltage-controlled oscillator (VCO) | 0.095 | 1.0 | 2 | 2 | 1 | 1 | $\omega^2/(\omega - \alpha_j)(\omega - \alpha_k)$ | 8318× (amplifier) |
| | 44.0 | 1.0 | 2 | 0 | $\omega_0$ | $\omega_0$ | $-1/(\omega - \alpha_j)(\omega - \alpha_k)$ | 37.04 Hz/V (VCO) |
| Discriminator | 60.0 | 1.0 | 2 | 0 | $\omega_0$ | $\omega_0$ | $-1/(\omega - \alpha_j)(\omega - \alpha_k)$ | 0.0160 V/Hz |
| | 130.0 | 0.7 | 2 | 0 | $\omega_0$ | $\omega_0$ | $-1/(\omega - \alpha_j)(\omega - \alpha_k)$ | |
| 16-mm film recorder and film viewer | 0.53 | [b] | 1 | 1 | 1 | [b] | $\omega/(\omega - \alpha_j)$ | 4 cm/V |
| | 15.5 | 0.7 | 2 | 0 | $\omega_0$ | $\omega_0$ | $-1/(\omega - \alpha_j)(\omega - \alpha_k)$ | |

[a] Stewart and O'Neill (1980).

[b] The response element is a single pole and is defined only by $f_0$.

rately for each unit (Table I). These units are (1) the seismometer and L-pad, (2) the seismic amplifier and voltage-controlled oscillator, (3) the discriminator at the central recording site, and (4) the 16-mm film recorder and film viewer.

For the seismometer and L-pad, the constants $l = 3$, $n = 2$, and $C_i = C_j = 1$ are determined by comparing Eq. (2.8) with the Fourier transform of the response of an electromagnetic seismometer to a delta function (Healy and O'Neill, 1977)

$$V(\omega) = Gi\omega^3/(\omega - \alpha_j)(\omega - \alpha_k) \tag{2.13}$$

where $V(\omega)$ is the Fourier transform of the output voltage $v(t)$, $G$ is the effective motor constant of the seismometer and L-pad combination, and $\omega$, $\alpha_j$, and $\alpha_k$ have the same meaning as in Eq. (2.8). The constants $\alpha_j$ and $\alpha_k$ are computed from Eq. (2.9) using the USGS standard values $f_0 = 1.0$ Hz, and $\beta = 0.8$. The constant $A_j = G = 1.0$ V cm$^{-1}$ sec is the USGS standard value for the effective motor constant (Fig. 7). These values are all given in the first line of Table I.

For the remaining three units, the amplitude factors $A_j$ are standard values specified by the USGS (Table I), and other response parameters are determined by calibration in the laboratory. For each of the three units the measured frequency response curves were compared to sets of master response curves calculated for certain values of $l$, $n$, $C_j$ and, where appropriate, $\beta$. A visual fit of the laboratory calibration curves to the master curves provided the values of $f_0$ and $\beta$ for each instrumental unit. From these values $\alpha_j$ and $\alpha_k$ were determined from Eq. (2.9).

Table I contains all the data required by Eq. (2.8) to calculate the system amplitude response. If complex arithmetic is used to calculate $F(\omega)$, then the system amplitude response is the absolute value of the complex expression Eq. (2.8). The amplitude response for the system specified by Table I is shown in Fig. 14.

Bakun and Dratler (1976) summarized the relative merits of the Fourier transform and least-squares techniques. They pointed out that these two approaches are complementary, and each has its applications in calibrating microearthquake networks. The Fourier transform technique may be used routinely to verify that the system is operating within specifications with no unexpected sources of noise. It may also be used to correct seismic data for system response at lower frequencies, as required by some seismological studies. The least-squares approach may be used in studies that require an analytical expression for the response function. It may also be used to extend the system response to higher frequencies than those computed from the Fourier transform technique.

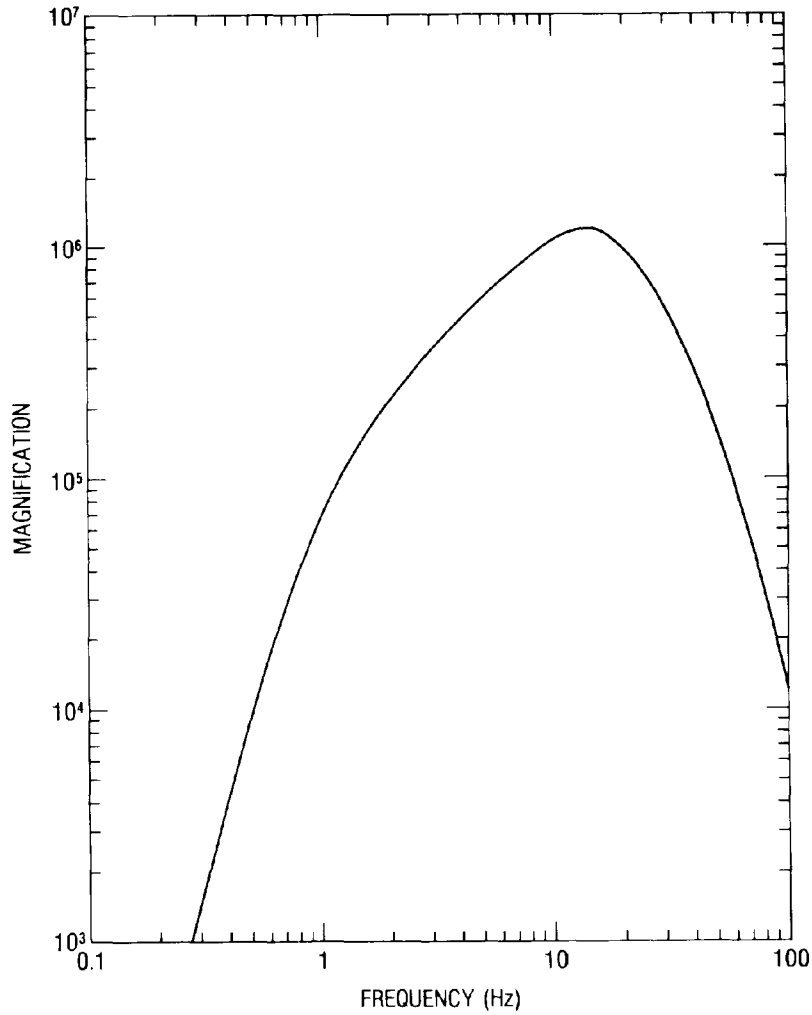


**Fig. 14.** Response of the seismic system used in the USGS Central California Microearthquake Network as determined by Stewart and O'Neill (1980).

### *2.2.6. System Dynamic Range*

The internal noise generated by the seismic amplifier sets an upper limit on the dynamic range that can be achieved by the instrumentation system. This limit is the ratio of the maximum undistorted amplitude attainable by the amplifier to its internal noise level as measured at the output of the amplifier. For the USGS system, the maximum amplifier output at a gain of 18 dB is approximately 8 V (peak to peak), and the corresponding internal noise level is about 4 $\mu$V, in the frequency range of 0.1–30 Hz. Thus the theoretical upper limit of the dynamic range for the USGS system is about 126 dB (Eaton and Van Schaack, 1977).

The practical limit on the dynamic range is determined by the tape record–reproduce unit. Tests made with the voltage-controlled oscillators, multiplexers, and discriminators all coupled together, but without the tape recorder–reproduce unit, show a dynamic range of about 60 dB. When the tape recorder–reproduce unit is added, dynamic range varies from 34 to 46 dB, decreasing with increasing center frequency of the FM carrier. The drop in dynamic range is caused primarily by tape speed variations in the record and reproduce equipment. When a subtractive compensation signal is applied to the analog output from the discriminators, the dynamic range is increased to approximately 50 dB (Eaton and Van Schaack, 1977).

The achievable dynamic range can be estimated by comparing the average noise amplitude of a low-gain seismic system to the maximum amplitude of an earthquake signal that can pass through the same system without electronic distortion. This will be the lower bound of the dynamic range because the noise measured from the low-gain system is greater than the system electronic noise. To estimate this lower bound, a few earthquakes with amplitude large enough to distort slightly a low-gain seismic system were selected. The seismic signal and its preceding noise were digitized. The ratio of the peak amplitude of the undistorted signal to the peak amplitude of the noise varies from 43 to 49 dB. This is in good agreement with the 50-dB dynamic range cited in the preceding paragraph.

## 2.3. Other Land-Based Microearthquake Systems

The principal components of a microearthquake network are easily categorized: a seismometer, signal conditioning device, signal transmission circuitry, recording media, time base, and power supply. The details of the instrumentation in microearthquake networks are highly variable, but technical descriptions of the instrumentation are seldom reported in the published literature. In the previous section we described the instrumentation for the USGS Central California Microearthquake Network. With few exceptions all permanent microearthquake networks now in operation use a similar technique, but the instrument components may come from different manufacturers. In the United States there are at least three commercial manufacturers of complete systems for microearthquake networks—Kinemetrics, Inc. (222 Vista Ave., Pasadena, CA 91107), W. F. Sprengnether Instrument Co., Inc. (4567 Swan Ave., St. Louis, MO 63110), and Teledyne Geotech (3401 Shiloh Rd., Garland, TX 75041).

Although the preceding manufacturers offer several types of seis-

mometers, many microearthquake networks in the United States use Model L-4C seismometers from Mark Products, Inc. (10507 Kinghurst Dr., Houston, TX 77099) because they are small, light weight, and inexpensive. The principles of seismometry are not discussed here, but readers may refer to some standard seismology texts, e.g., Bath (1973, pp. 27–58) and Aki and Richards (1980, pp. 477–524). Operating characteristics of seismometers are available from the manufacturers.

Many microearthquake networks record seismic data continuously in analog form. Since earthquake signals constitute only a small part of the continuous records, a few networks have employed triggered recording of earthquakes (e.g., Teng *et al.*, 1973; Johnson, 1979). Digital transmission and recording of seismic data has been utilized, for example, by Harjes and Seidl (1978) in Germany and by Hayman and Shannon (1979) in Canada. The advantages of an all digital system are increased dynamic range and easier data processing by computers. Presently, it is more expensive and less efficient in data density to transmit and record seismic data continuously in digital form than in analog form.

So far we have discussed instrumentation for telemetered microearthquake networks that are intended to operate for an indefinite time. To reduce operating cost, field instrument packages must not require frequent maintenance, and efficient data transmission and recording must be established. Thus months of planning and installation are often necessary. However, in many applications, rapid deployment of a temporary microearthquake network is essential and a permanent network is not required.

For temporary microearthquake networks, the instrument system must be highly portable and self-contained. Seismic data are usually recorded at the station site or may be transmitted by cable or radio to a nearby recording point. And it is seldom possible to use the telephone system for data transmission. In general, the portable instrument systems do not differ greatly from those used for the permanent networks. The crucial difference is that seismic data from a temporary network are recorded in the field and often at many individual sites or a central field site rather than in a permanent laboratory. Thus temporary networks require more intensive labor in both field operation and data processing.

The standard portable seismograph for microearthquake studies usually has a visual recorder and is completely self-contained in a carrying case, except perhaps for the seismometer. The unit also has an amplifier, filters, timing system, and power supply. Record size for the seismogram is approximately 30 by 60 cm. Recording is made by an ink pen or by a stylus on smoked paper. Daily change of records is generally required in order to achieve a timing resolution of better than 0.1 sec. Early versions

of such portable seismographs have been described, for example, by Oliver *et al.* (1966) and Prothero and Brune (1971). At present standard portable seismographs are commercially available through the three manufacturers mentioned above and others.

There have been several attempts to use analog magnetic tape recorders in portable seismic systems. Readers are referred to, for example, Eaton *et al.* (1970b), Muirhead and Simpson (1972), Green (1973), Long (1974), and Stevenson (1976). More recently, portable digital recording and event detection systems have been developed (e.g., Prothero, 1976, 1980) and are now available, for example, through the three manufacturers mentioned above as well as from Argosystems, Inc. (884 Hermosa Court, Sunnyvale, CA 94086) and Terra Technology Corp. (3860 148th Ave. N.E., Redmond, WA 98052). Analysis of seismic signals is easier by recording on digital magnetic tape. The use of digital event detection and triggered recording systems has begun recently (e.g., Prothero *et al.*, 1976; Brune *et al.*, 1980; Fletcher, 1980) and may soon become the standard recording instrument for microearthquake studies.

## 2.4. Ocean-Based Microearthquake Systems

On a global scale most earthquakes occur near the ocean–continent boundaries. Because of the difficulties in carrying out experiments at sea, ocean-based microearthquake studies have been less extensive than those on land. Typically the ocean-based studies are reconnaissance in nature and involve only a few temporary stations. At present there are no permanent oceanic microearthquake networks, although a shallow-water microearthquake network is operating off the coast of southern California (Henyey *et al.*, 1979).

Two basic types of instrumentation are used to study earthquakes in an ocean environment: (1) a sonobuoy–hydrophone system in which the seismic transducer is suspended in the water, and (2) an ocean bottom seismograph (OBS) system in which the seismic transducer is placed on the sea floor. The sonobuoy system usually is free floating; its transducer is a hydrophone sensitive to pressure variations transmitted through the water. The OBS system is coupled to the sea floor and uses standard seismometers to detect seismic waves arriving through the oceanic crust.

Phillips and McCowan (1978) reviewed the current state of ocean bottom seismograph systems. They believed that signal-to-noise ratios comparable to the best land stations could be achieved by emplacing OBS systems in shallow boreholes in the sea floor. Recent advances in ocean technology, particularly in deep sea drilling, acoustic telemetry, and tech-

niques to emplace and recover instrument packages, will facilitate microearthquake observations at sea.

In the following subsections we summarize the shallow-water microearthquake network described by Henyey *et al.* (1979) and then give examples of sonobuoy–hydrophone systems and OBS systems commonly used in deeper water.

### *2.4.1. A Shallow-Water Microearthquake Network*

Since the summer of 1978 a microearthquake network of eight vertical-component stations has been monitoring seismic activity around the offshore Dos Cuadras oil field near Santa Barbara, California (Henyey *et al.*, 1979). Three of the stations are onshore; five are in shallow water (20–100-m depth) and surround the offshore oil platforms. The seismometers have a 1-Hz natural frequency. The ocean bottom seismometers are emplaced in a steel pipe driven 2–5 m into the sea floor in order to obtain better coupling to the sediments and thus to improve the signal-to-noise ratio. Output from each of the five ocean bottom seismometers is transmitted by cable to a central collection point on one of the platforms. The instrument package does not require power because amplifiers are not needed for signal transmission between the seismometer and the platform. Thus the package is very simple and its lifetime is not limited by power requirements. The analog seismic signals are multiplexed at the platform and transmitted by cable to a collection point on land. Here the three signals from the land stations are added, and the bundle of eight signals is transmitted by telephone line to a central recording site.

Comparisons of the recordings from the onshore and offshore sites have been made for regional earthquakes of moderate size. Those recordings from the offshore sites show good signal quality for the first arrivals, and the waveforms are similar to those recorded on land. Henyey *et al.* (1979) attribute this in part to their method of coupling the instrument package to the material below the sediment–sea water interface.

### *2.4.2. Sonobuoy–Hydrophone Systems*

Reid *et al.* (1973) summarized the principles and practice of using sonobuoy–hydrophone systems. Typically a small number of these systems (say, 3–6) is deployed by ship or airplane in the area of interest. The sonobuoy itself floats on the surface, while the hydrophone is suspended below at a depth of 20–100 m. Pressure variations in the water are detected by a piezoelectric crystal, amplified, and transmitted by cable to the sonobuoy. Here the signal is conditioned and transmitted by FM telem-

etry to a central recording site. Typically the central site is a nearby ship, but for short-lived systems aircraft can be used. A land-based recording site can be used if the sonobuoy array is sufficiently close to land.

A major problem with sonobuoy arrays is determining the location of each unit so that precise hypocenters can be calculated. The drift of the sonobuoy units relative to each other further complicates the problem. Reid *et al.* (1973) used an air gun aboard the recording ship to determine the relative sonobuoy position. The time delay between firing the air gun and the arrival of the direct water wave at the hydrophone gives the distance between the ship and the hydrophone. If the air gun shots are recorded with the ship at different positions, and if the sonobuoy has not drifted too far in the meantime, then the position of each sonobuoy relative to the ship can be determined by triangulation. Absolute position of the ship can be determined by standard navigational methods.

Reid *et al.* (1973) found that predominant frequencies of oceanic microearthquakes were largely in the 20-Hz range. This required no modification of the frequency response characteristics of most hydrophones. They stated that their system could detect magnitude zero earthquakes at a distance of about 10 km.

If the sonobuoy has a life of a few days, and if the array is close to land, then the expense of a ship standing by just to record the data may be avoided by anchoring sonobuoys to the ocean bottom and recording on land. However, moored systems are much noisier, and special anchors, cables, and other devices must be used.

### *2.4.3. Anchored Buoy OBS Systems*

In the anchored buoy system, the instrument package that rests on the sea floor contains everything necessary to detect and record the seismic data. The package is lowered to the sea floor by means of a cable. The cable usually is attached to an anchored buoy, although it may be attached to a ship. The instrument package must be isolated from the buoy and the cable to avoid vibrational noise. Rykunov and Sedov (1967) and Nagumo and Kasahara (1976) described cable systems in which the buoy was held in place by an anchor and ballast weights on the sea floor. The instrument package was 150–250 m from the anchor and was connected to it by a series of shackles and rope. The package was recovered by pulling it up with the rope. The anchored buoy method allows the instrument package to be self-contained, but operation in deep ocean is difficult (Francis, 1977).

Rykunov and Sedov (1967) used a vertical-component seismometer with 3.5-Hz natural frequency. Seismic data were recorded on analog

magnetic tape at 1.2 mm/sec speed; tape cartridges with 180 m of tape allowed continuous recording up to 41 hr. Nagumo and Kasahara (1976) used a vertical-component seismometer with 1-Hz natural frequency and a horizontal-component seismometer with a 4.5-Hz natural frequency. Seismic data were recorded on analog magnetic tape at 0.15 mm/sec speed, and a 548-m tape allowed continuous recording of 1000 hr.

### *2.4.4. Telemetered Buoy OBS Systems*

In the telemetered buoy system, seismic data from the instrument package are transmitted by an acoustic link or a cable to a buoy or a surface ship for recording. Latham and Nowroozi (1968) developed a system in which the telemetry link was an underwater cable leading to a recording site on land. The cable was used to transmit command and control functions and 60 Hz power to the OBS. It was also used to transmit seismic data to the recording site by an amplitude-modulated 8-kHz carrier. The instrument package contained a three-component seismometer set with 15-sec natural period, a three-component set with 1-sec natural period, and other sensors such as hydrophones, pressure transducers, and a water temperature device. In 1966 this system was emplaced about 130 km offshore from Point Arena in northern California, at a water depth of 3.9 km (Nowroozi, 1973). It recorded many earthquakes occurring near the junction of the San Andreas fault and the Mendocino fracture zone. This OBS station provided critical azimuthal coverage for studying these earthquakes. It operated until September 1972 when the cable was broken and could not be repaired (Roy Miller, personal communication, 1979).

### *2.4.5. Pop-Up OBS Systems*

In the pop-up system, the instrument package with a base plate is emplaced by a free fall to the ocean floor. The buoyant instrument package is recovered by separating it from the heavier base plate using a time release or an acoustic command mechanism. Descriptions of pop-up OBS systems may be found, for example, in Carmichael *et al.* (1973), Francis *et al.* (1975), Mattaboni and Solomon (1977), and Prothero (1979).

Carmichael *et al.* (1973) used one vertical- and one horizontal-component seismometer, each with a 2-Hz natural frequency. Seismic data were recorded on a modified four-channel entertainment-type tape recorder, operating at 23.8 mm/sec. Logarithmic amplifiers were used to extend the dynamic range of the recording system to about 50 dB. Their system weighed about 200 kg and had an operating life of about 15 hr.

Francis *et al.* (1975) used a three-component seismometer, each having a 2-Hz natural frequency. Seismic data were recorded in FM mode, at a tape speed of 1.9 mm/sec. This allowed a bandwidth of 0–20 Hz and 9 days of continuous recording. Dynamic range of the recording system is about 40 dB. Their system weighed about 570 kg on launching and 413 kg on recovery.

More recently, digital event detection and recording schemes have been incorporated into pop-up OBS systems [e.g., Mattaboni and Solomon, (1977), Solomon *et al.* (1977), and Prothero (1979)]. By recording only detected events, magnetic tape and power to drive the tape recorder are conserved. Thus the operational life of these pop-up OBS systems can be extended to a few months. In addition, digital recording permits greater dynamic range.

Mattaboni and Solomon (1977) used a three-component seismometer set, with 4.5-Hz natural frequency. Effective bandwidth of the system was 2–50 Hz. By using a 12-bit analog-to-digital converter and 8 bits of automatic gain control, they obtained a dynamic range of 102 dB for their system. Although the system had only enough magnetic tape for about 7 hr of continuous recording, the triggering technique for event recording allowed the system to operate on the sea floor for one month or more. Typically, several hundred earthquakes could be recorded in a single drop of the instrument.

Prothero (1979) developed a pop-up OBS system which he stated was versatile, low cost, and easy to deploy. The instrument package contained a set of three-component geophones (4.5-Hz natural frequency), gain-ranging amplifiers, a 12-bit analog-to-digital converter, a microprocessor controller, a digital cassette recorder, and an acoustic release unit. The dynamic range of the system was 128 dB. Approximately $10^6$ data samples could be recorded on one digital cassette tape. Thus several hundred earthquakes with an average recording time of 20 sec per earthquake could be stored. Prothero stated that this capacity was sufficient for deployments of up to one month in fairly active seismic areas.

# 3. Data Processing Procedures

Microearthquake networks are designed to record as many earthquakes as nature and instruments permit, and they can produce an immense volume of data. For small microearthquake networks in areas of relatively low seismicity, data processing should not be a problem. But for small networks in areas of high seismicity, or for large microearthquake networks, processing voluminous data can be a serious problem. For example, the USGS Central California Microearthquake Network generates about $10^{13}$ bits of raw observational data per year. This annual amount is equivalent to a few million books, or the holdings of a very large library. Compared with a traditional seismological observatory, a microearthquake network can generate orders of magnitude more data. The general aspects of the data processing procedures do not differ greatly between these two types of operations. However, the larger volume of microearthquake data requires careful planning and application of modern data processing techniques.

For traditional seismological observatories, a manual of practice containing much useful information is available (Willmore, 1979). Some of this information can be applied to the operation of microearthquake networks. A comparable manual of practice for microearthquake networks is not known to us at present. In this chapter, we are not writing a manual of practice for microearthquake networks, but rather discussing some of the problems and possible solutions in processing microearthquake data. In the following sections, we discuss first the nature of data processing and then some of the procedures for record keeping, event detection, event processing, and basic calculations.

## 3.1. Nature of Data Processing

Many scientific advances are based on accurate and long-term observations. For example, planetary motion was not understood until the seven-

teenth century despite the fact that observations were made for thousands of years. We owe this understanding to several pioneers. In particular, Tycho Brahe recognized the need for and made accurate, continuous observations for 21 years; and Johannes Kepler spent 25 years deriving the three laws of planetary motion from Brahe's data (Berry, 1898). The period of sidereal revolution for the terrestrial planets is of the order of 1 year, but observational data an order of magnitude greater in duration were required to derive the laws of planetary motion. Because disastrous earthquakes in a given region recur in tens or hundreds of years, it could be argued by analogy that many years of accurate observations might be needed before reliable earthquake predictions could be made.

A present strategy in earthquake prediction is to carry out intensive monitoring of seismically active areas with microearthquake networks and other geophysical instruments. By studying microearthquakes, which occur more frequently than the larger events, we hope to understand the earthquake generating process in a shorter time. Intensive monitoring produces vast amounts of data which make processing tedious and difficult to keep up with. Therefore, we must consider the nature of these data in order to devise an effective data processing scheme.

In a manner similar to that of Anonymous (1979), data associated with microearthquake networks may be classified as follows:

(1) Level 0: Instrument location, characteristics, and operational details.
(2) Level 1: Raw observational data, i.e., continuous signals from seismometers.
(3) Level 2: Earthquake waveform data, i.e., observational data containing seismic events.
(4) Level 3: Earthquake phase data, such as P- and S-arrival times, maximum amplitude and period, first motion, signal duration, etc.
(5) Level 4: Event lists containing origin time, epicenter coordinates, focal depth, magnitude, etc.
(6) Level 5: Scientific reports describing seismicity, focal mechanism, etc.

In order to discuss the amounts of data in levels 0–4, we use the USGS Central California Microearthquake Network as an example. Level 0 data for this network consists of the locations, characteristics, and operational details for about 250 stations; this information is about $2 \times 10^6$ bits/year. Level 1 data consists of about $10^{13}$ bits/year of continuous signals from the seismometers at the stations. These data are recorded on analog magnetic tapes (4 tapes/day), and most of them are also recorded on 16-mm mi-

crofilms (13 rolls/day). The analog magnetic tapes are used because each can record roughly 300 times more data than a standard 800 BPI digital magnetic tape. But even four analog magnetic tapes per day are too many to keep on a permanent basis, so we save only the earthquake waveform data by dubbing to another analog tape. The dubbed waveform data for this network (level 2) consists of approximately $5 \times 10^{11}$ bits/year in analog form (about 75 analog tapes per year). These analog waveform data can be further condensed if we digitize only the relevant portions of the analog waveforms from the stations that recorded the earthquakes adequately. That amount of digital data is about $5 \times 10^{10}$ bits/year and requires some 500 reels of 800 BPI tapes. Earthquake phase data (level 3) are prepared from the dubbed waveform data and/or from the 16-mm microfilms, and consist of about $10^8$ bits/year. Finally at level 4, the event lists consist of about $5 \times 10^6$ bits/year and are derived from the phase data using an earthquake location program.

Since data processing is not an end in itself, any effective procedures must be considered with respect to the users. Because of the volume of microearthquake data, a considerable amount of processing and interpretation are required before the data become useful for research. In the following discussion, we consider the human and technological factors that limit our ability to process and comprehend large amounts of data. Although some readers may not agree with our order-of-magnitude approach, we believe that practical limits do exist and that in some instances we are close to reaching or exceeding them.

The basic unit of information is 1 bit (either 0 or 1). A letter in the English alphabet is commonly represented by 8 bits or 1 byte. A number usually takes from 10 to 60 bits depending on the precision required. A page of a scientific paper contains about $2 \times 10^4$ bits of information, whereas a color picture can require up to $10^8$ bits/frame to display. Thus a picture is generally much higher in information density than a page of words or numbers. For a human being or a data processing device, the limiting factors are data capacity, data rate or execution time, and access delay time. Although human beings may have a large data capacity and quick recall time, they are limited to a reading speed of less than 1000 words/min or $10^3$ bits/sec, and a computing speed of less than one arithmetic operation per second. On the other hand, a large computer may have a data capacity of $10^{12}$ bits, a data rate of $10^7$ bits/sec, and an execution speed of $10^7$ instructions per second.

Data processing requires at least several computer instructions for each data sample, and there are about $3 \times 10^7$ seconds in a year. Hence, it is clear that a large computer cannot process more than $10^{13}$ bits/year of data at present, nor can a human being read more than $10^{10}$ bits/year of infor-

mation. In fact, since most people have a short memory span, we cannot assimilate more than about $10^6$ bits (or 50 pages) of new information at any given time. This simple analysis suggests that for any given scientific observation, we should collect less than $10^{13}$ bits/year of raw data in order not to exceed the capabilities of our present computers. We must also reduce our results to units of the order of $10^6$ bits each so that we can comprehend them. For the USGS Central California Microearthquake Network, we have reached the present computer capabilities in processing the raw data. However, advances in computer technology are rapid, and we should be able to process the volume of our raw data by using, for example, microprocessors in parallel operation. On the other hand, our human limitations make it difficult for us to assimilate any order of magnitude increase of new results. Even if the relevant information is present in the raw data, it is not clear whether we are able to extract it concisely in order to understand the earthquake-generating process. The problem is human limitations and not the computers.

## 3.2. Record Keeping

Record keeping is a procedure to implement data processing goals. It includes collecting, storing, and cataloging all the information associated with the operation of a microearthquake network. By "all information" we mean level 0–level 5 data, which were described in Section 3.1. Although the need for record keeping is self-evident, many microearthquake network operators fail to pay enough attention to this task and ultimately suffer the consequences. It is very tempting to believe that one will remember the necessary information and to take shortcuts in record keeping. However, experience shows that unless the information is entered carefully and immediately on a permanent record, it will soon be forgotten or lost. For temporary microearthquake networks, it is critical to keep good records because these networks are often deployed and operated under unfavorable conditions. For permanent microearthquake networks, it is not too difficult to devise a record keeping procedure. However, it is more difficult to maintain it over a long period of time, especially with turnover of staff. Rather than describe all the details, we will mention a few typical problems that are often overlooked.

One should begin record keeping as soon as the first station of a microearthquake network is installed in the field. The station location should be marked on a large-scale map, such as a 1 : 24,000 topographic sheet. The position of the station should be surveyed or at least be fixed with respect to several known landmarks using a compass. One test for the

correctness of the station location on the map is to let another person find the station using the map alone. The station coordinates should be carefully read from the map, usually to ±0.01 minute in latitude and longitude, and to a few meters in elevation. These coordinates should be checked by at least one other person. A chronological record should be kept on instrument characteristics and maintenance services performed. At the central recording site, it is necessary to have a record keeping procedure for the raw seismic data and a place to store the data safely. If absolute time such as WWVB radio signal is not recorded, then clock correction information must be saved. The one-to-one correspondence between the station and its seismic signal should be directly identifiable from the recorded media, such as analog magnetic tapes and 16-mm microfilms. If it is not, then assignment of recording position for each station must be kept. For example, Houck *et al.* (1976) compiled a handbook of station coordinates, polarity, and recording position on the analog magnetic tapes and 16-mm microfilms for the USGS Central California Microearthquake Network.

Many steps are involved in processing the raw seismic data into event lists of hypocenter parameters, magnitude, etc. It is important to keep records of processing procedures, selection criteria, intermediate data, and final results. It is also important to publish regularly the basic information and results of a microearthquake network. Data from a microearthquake network can quickly fill up a room. Therefore, the data must be organized, cataloged, and filed properly. The data should not be taken from the storage room unless it is absolutely necessary; otherwise, they have a tendency to be lost.

In summary, the goals of record keeping are to make all information from a microearthquake network easily accessible and to maintain the long-term continuity of the data.

### 3.3. Event Detection

Event detection is the procedure for recording the approximate time of occurrence of an earthquake within a microearthquake network. A scan list is a tabulation, in chronological order, of the times of the detected earthquakes. If regional or teleseismic earthquakes are to be detected and processed, then they are also included in the scan list. Scan lists generated by visual or semiautomatic methods may be annotated, for instance, with a remark as to the type of event (local, regional or teleseismic earthquake, or explosion) and with an estimate of its signal duration. Scan lists are used to guide the processing of a set of events and to ensure that all events

selected are processed. Events detected by automatic systems either are recorded immediately (as in triggered recording systems) or are processed and located right away (as in on-line location systems). The output from the triggered system or the on-line system serves as the scan list. Regardless of how the scan list is prepared, it is important to document the criteria used for event detection and to include this in the record keeping described previously.

### *3.3.1. Visual Methods*

The most direct method of event detection is simply to examine the paper or film seismograms. In permanent microearthquake networks the seismograms from slow-speed drum recorders frequently are used for event detection, while the seismic data recorded on 16-mm microfilms or on playbacks from magnetic tape are used for event processing. Alternatively, the microfilms themselves are scanned, as a first pass, to detect the earthquakes and record their approximate times of occurrence. The earthquakes are timed and processed in more detail during subsequent passes at the microfilms or from the magnetic tape playbacks.

For some temporary microearthquake networks, it is common to use a few drum recorders for event detection and portable tape recorders to collect seismic data for event processing. If the tape systems are triggered, then the continuous seismograms from the drum recorders can be used to verify that the triggered systems are functioning properly. Some temporary networks have used only magnetic tape recorders, without a visible recording monitor. In one instance, a 14-channel FM system was used to record 11 channels of seismic data, 1 channel of tape speed compensation signal, and 2 channels of time code (e.g., Stevenson, 1976). The tape was played back at a time compression of 80× and the output from all tape channels was recorded continuously on a high-speed multichannel oscillograph. The effective playback speed was 75 mm/min—fast enough to read the time code and identify the earthquakes, but slow enough to conserve paper. The scan list was prepared by examining the playback visually.

Other temporary networks have used a number of multichannel tape recorders, each recording seismic data and radio time code at one station site. In one example, the output of one seismic channel from selected recorders was played back and recorded on a drum seismograph modified to record at a high speed (e.g., Eaton *et al.*, 1970b). By matching the time compression of the tape playback system to the increased drum speed, a 24-hr seismogram with recording speed of 60 mm/min was obtained. The

scan list was prepared by visually examining the standard seismograms made in this way. Absolute time was determined by recording a few minutes of radio time code at the beginning and end of each seismogram.

### *3.3.2. Semiautomated Methods*

Several semiautomated methods to detect seismic events have been tried, but the results have not been satisfactory. Nevertheless, we will give two examples here.

Seismic data recorded on analog magnetic tapes can be played back fast enough to be audible. Earthquakes can then be detected by hearing changes in the level and pitch of the sound. With a little practice, it is not difficult to detect the onset of earthquakes. For smaller events the changes in the level and pitch of the sound may be subtle. The detected earthquakes can be verified by displaying the events on an oscilloscope.

When 16-mm microfilms are scanned, earthquakes are often noted to pass across the viewing screen as a whited-out blur for the large events, or as a darkened blur for the smaller events. In either case, a change in the light intensity transmitted through the microfilm is observed. An experimental detector has been constructed by E. G. Jensen and W. H. K. Lee of the USGS to take advantage of this property. The light intensity of a 16-mm microfilm as seen on a viewing screen is measured by a phototransducer along a narrow, vertical portion of the screen. As the microfilm moves across the detector, the film transport of the viewer is automatically stopped if the light intensity deviates substantially from an average value. The presence of an earthquake can be visually verified, its onset time recorded, and the scanning process resumed by restarting the film transport. This type of semiautomated scanning of 16-mm microfilms is about three times faster than visual scanning and is less tiring for the scanner. However, high-quality recording of the microfilm is required.

### *3.3.3. Automated Methods: Principles of Event Detectors*

Except for aftershock sequences and swarm activities, signals containing seismic events are typically a few percent or less of the total incoming signals from a microearthquake network. Because of this property, event detectors have been developed and applied for triggered recording of seismic signals in order to reduce the volume of recorded data and to generate simultaneously a scan list of earthquakes. In addition, some event detectors can produce fairly accurate onset times and have been applied to on-line data processing and real-time earthquake location.

To detect microearthquakes in the incoming signals, we must exploit

their signal characteristics. In Fig. 15, examples of various types of incoming signals are shown. The background signals typically have a low amplitude and a low frequency; their appearance can be either quite periodic (Fig. 15a) or quite random (Fig. 15b). Because of instrumental noise and cultural activities, transient signals over a broad range of amplitudes and periods are often present. For example, a short-lived and impulsive transient noise from a telephone line is shown in Fig. 15c. A more emergent type of noise is shown in Fig. 15d. Its envelope, indicated by the dashed line, is roughly elliptical in shape.

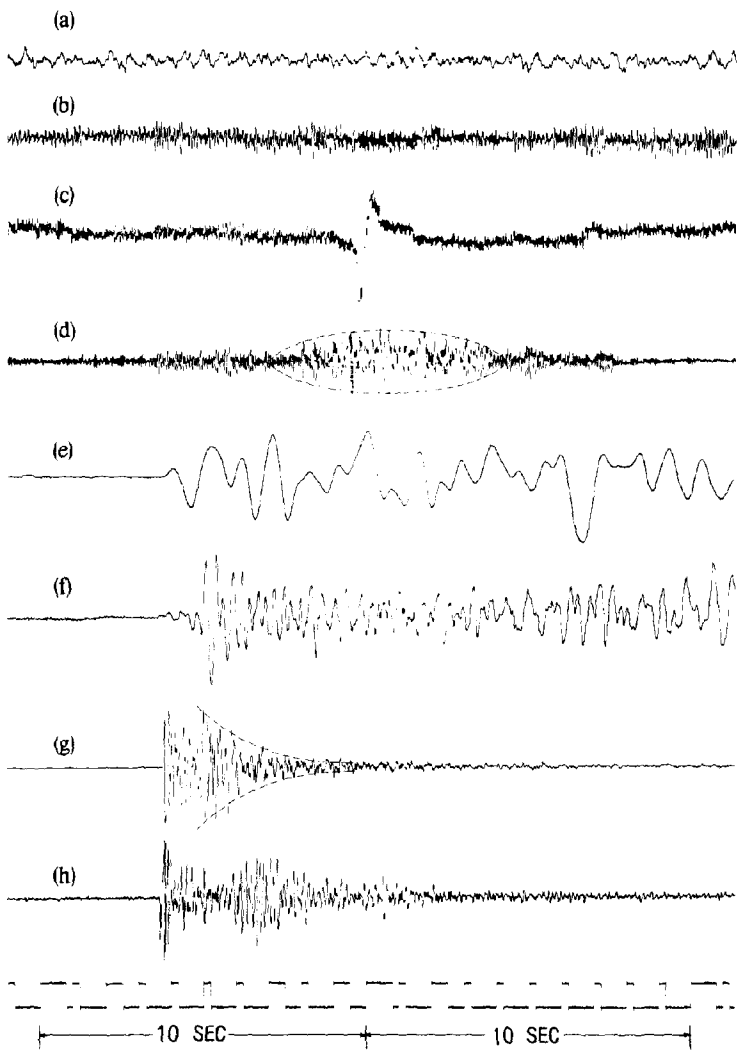


**Fig. 15.** Examples of signals recorded on the short-period, vertical-component seismographs of the USGS Central California Microearthquake Network. The time scale is shown by the last trace. See text for explanation.

Seismic signals are generally classified into three types depending on the distance from the source to the station. Earthquakes occurring more than 2000 km from a seismic network usually are called teleseismic events. An example of a teleseismic event as recorded by a microearthquake network station is shown in Fig. 15e. Depending on the size of the event, teleseismic amplitudes can range from barely perceptible to those that saturate the instrument. Their predominant periods are typically a few seconds. Earthquakes occurring, say, a few hundred kilometers to 2000 km outside the network are called regional events. An example of a regional earthquake as recorded by a microearthquake network station is shown in Fig. 15f. As with the teleseismic event, amplitudes of regional earthquakes can range from barely perceptible to large, but their predominant periods are less than those of the teleseismic events. Earthquakes occurring within a few hundred kilometers of a seismic network are called local events. Local earthquakes often are characterized by impulsive onsets and high-frequency waves as shown in Fig. 15g and h. The envelope of local earthquake signals typically has an exponentially decreasing tail as also shown by the dashed line in Fig. 15g. Another characteristic of all (teleseismic, regional, or local) earthquake signals is that the predominant period generally increases with time from the onset of the first arrival. On the other hand, a given transient signal of instrumental or cultural origin often has the same predominant period throughout its duration.

In summary, the incoming signals from a microearthquake network can have a wide range of amplitudes, but local earthquakes are characterized generally by their impulsive onsets, high-frequency content, exponential envelope, and decreasing signal frequency with time.

To exploit these characteristics of microearthquakes, the concept of short-term and long-term time averages of incoming signal amplitude has been introduced by a number of authors (e.g., Stewart *et al.*, 1971; Ambuter and Solomon, 1974). If the amplitude of the incoming signal is denoted by $A(\tau)$, where $\tau$ is time, then the short-term average at time $t$, $\alpha(t)$, can be defined by

$$\alpha(t) = (\tau_1)^{-1} \int_{t-\tau_1}^{t} |A(\tau)| \, d\tau \tag{3.1}$$

where $\tau_1$ is the length of the time window for the short-term average, typically 1 sec or less. This permits a quick response to changes in the signal level that characterize the onset of an earthquake. Similarly, the long-term average at time $t$, $\beta(t)$, can be defined by

$$\beta(t) = (\tau_2)^{-1} \int_{t-\tau_2}^{t} |A(\tau)| \, d\tau \tag{3.2}$$

where $\tau_2$ is the length of the time window for the long-term average, which depending on the application, may range from a few seconds to a few minutes. Because $\tau_2$ is usually much longer than the predominant period of the incoming signal, $\beta(t)$ represents the long-term average of the signal level as detected by the seismometer. It is useful to denote the ratio of the short-term average to the long-term average at time $t$ by $\gamma(t)$, i.e.,

$$\gamma(t) = \alpha(t)/\beta(t) \tag{3.3}$$

An event is said to be detected when

$$\gamma(t) > \gamma_d \tag{3.4}$$

where $\gamma_d$ is the threshold level for event detection. There is a trade-off between the threshold level $\gamma_d$ and the number of detections. If the threshold level is set too low, noise bursts will cause too many false detections. If the threshold level is set too high, the number of false detections will decrease, and so will the number of detected earthquakes.

There are two major applications of event detectors. They have been implemented with analog or with digital components. In the following two subsections, we describe applications for triggered recording and applications for on-line data processing.

### *3.3.4. Automated Methods: Applications of Event Detectors for Triggered Recording*

Triggered recording involves two automated tasks. The first task is to detect an earthquake event and to initiate recording. The second task is to determine when to stop recording and to return to the detection mode. In addition, a delay-line memory is required so that at least a few seconds of the signal preceding the earthquake will be recorded, and recording directly on computer-compatible media is preferred so that further data processing can be easily carried out. The simplest method to stop recording is to record the seismic data for some preset duration. This will assure that recording for each detection does not use up the storage medium quickly. For a given amount of storage medium, the maximum number of detected events that will be recorded can be determined beforehand. However, for any given choice of recording duration, some larger earthquakes will not be completely recorded, and some smaller earthquakes will use up too much storage medium. A variable cutoff criterion will avoid these difficulties, but will need some protection against recording indefinitely after an event is detected.

Until digital electronic components became widely available, event detectors were based on analog technology and were not very satisfactory. For example, a continuous loop of analog magnetic tape on a recorder

with both record and playback heads was often used as a delay-line memory. In this system, the playback head was placed a few centimeters beyond the record head, and the amount of time delay depended on the tape speed and the distance between the heads. When an earthquake was detected, the event detector turned on another tape recorder which would record the seismic signals from the playback head. Because of the continuous wear of the tape and heads in the tape-loop recorder, the signal-to-noise ratio of the recorded seismic signals became increasingly poor. Therefore, such analog event detector and recording units were impractical.

Although an effective event detector can be built using analog components, the digital approach is more advantageous for the following reasons. The problems encountered with the analog delay-line memory and rerecording can be avoided. If the analog seismic signal can be digitized immediately after amplification and signal conditioning, its dynamic range and signal-to-noise ratio can be preserved without further degradation. The digital detection algorithm can be complex and flexible if programmed in a microprocessor. The digitized seismic signal is most suitable for recording and processing by other computers. A reasonable amount of data preceding an earthquake can be stored by using digital memory. For example, assume that 4000 words of digital memory are used as a delay line for a three-component event detector and recording system. If each component is digitized at a rate of 100 samples/sec, then about 13 sec of data can be in the delay line at any time for each of the three components.

We now give a few recent examples of applying event detectors for triggered recording systems.

Teng *et al.* (1973) described an on-line event detection and recording system for a telemetered microearthquake network in the Los Angeles Basin, California. Each telemetered signal was sent to an analog event detector and was also recorded continuously on an analog magnetic tape unit. When a signal level exceeded twice its background level, a detection pulse was produced. To avoid most false detections, two or more event detectors had to be triggered simultaneously and the weighted sum of the detection pulses had to reach some predetermined voltage. When these conditions were met, a second analog tape unit and two chart recorders were activated to record the data from the first tape unit. The playback head of the first tape unit lagged behind the recording head by about 5 sec so that the entire earthquake signal could be subsequently recorded. Teng *et al.* (1973) stated that the number of false detections was less than 5% of the number of detected seismic events. In late 1973, the analog tape delay memory was replaced by shift registers to avoid signal degradation introduced by analog rerecording (T. L. Teng, personal communication, 1980).

Ambuter and Solomon (1974) described a system using analog components for event detection logic and digital components for the delay-line memory and tape recording unit. Their cutoff criterion for recording was to stop recording 30 sec after the ratio of the short-term average to the long-term average, $\gamma(t)$, dropped below the threshold level $\gamma_d$. They accomplished this by adding a feedback amplifier to the circuit that determined the long-term average. When an event was detected, the feedback amplifier was switched on and produced a slightly positive gain so that the long-term average would increase. Thus, $\gamma(t)$ eventually would drop below the threshold level, and the recorder would be turned off 30 sec later.

Eterno *et al.* (1974) suggested an alternative technique to cut off the recording after an event was detected. A cutoff level $\gamma_c$ can be defined by

$$\gamma_c = \gamma(t_d + 1) \tag{3.5}$$

where $\gamma(t_d + 1)$ is the value of $\gamma(t)$ at 1 sec after the event is detected at time $t_d$. The recording is terminated at some preset time after $\gamma(t)$ drops below the cutoff level $\gamma_c$. If $\gamma(t)$ drops below the detection threshold level $\gamma_d$ within 1 sec after the time $t_d$, then the event is considered to be false and the detection is canceled.

Johnson (1979) used a modification of the short-term and long-term averages technique (as described in Section 3.3.3) in an on-line detection and recording system for a large microearthquake network in southern California. The incoming analog seismic signals were digitized continuously, and the detected events were written on digital magnetic tapes for subsequent off-line processing.

Prothero (1979) has designed an ocean bottom seismograph system in which an event detector triggered a digital recording unit. The event detector was programmed in a microprocessor and could be changed readily if necessary.

Other variations in methods of event detection and recording cutoff are possible. With rapid advances in microprocessor and related technology, these methods can become increasingly complex. Techniques for automatic detection of an event may become indistinguishable from those for automatic determination of the arrival times of an event.

### *3.3.5. Automated Methods: Applications of Event Detectors for On-Line Data Processing*

On-line processing of the incoming signals from a microearthquake network is required if real-time earthquake location is desired for earthquake prediction purposes. As discussed in the previous subsection, it

is more advantageous to implement an event detector using digital technology rather than analog components. In the digital approach, the event detector is implemented as an algorithm for an on-line computer. Stewart *et al.* (1971) noted that the algorithm must be simple and must not require much analysis of the past data so that the computer can keep up with the incoming flow of new data. For example, if the incoming analog signals are digitized at 100 samples/sec, and if 100 seismic stations are monitored by one central processing unit in real time, then the time available for processing each data sample is only 100 $\mu$sec. Many existing computers can perform such a data processing task with ease. However, most microearthquake networks can only afford a modest computer system at a cost of about $100,000. Under such a monetary constraint, a computer suitable for on-line data processing has a cycle time of the order of 1 $\mu$sec and an addressable random access memory of approximately 64 kbytes. Therefore, to monitor 100 stations digitized at 100 samples/sec, the computer cannot perform more than a few tens of basic instructions on each data sample, nor can it store more than about 1 sec of the incoming digitized data in its main memory.

Although event detection based on waveform correlation has been applied successfully for teleseismic events recorded by large seismic arrays (e.g., Capon, 1973), this technique does not seem to be practical for microearthquake networks. The reason is that the waveforms of microearthquakes recorded at neighboring stations are remarkably dissimilar in general. Moreover, the processing times for correlation methods are rather excessive.

Stewart *et al.* (1971) used a small digital computer to implement a real-time detection and processing system for the USGS Central California Microearthquake Network. Their detection technique is summarized in Fig. 16. In this figure, $X_k$ is the raw input signal to the computer at time $t_k$, where $k$ is an index for counting the digitized samples. In order to filter out the lower frequency noise in the input signal, a difference operation is performed, i.e.,

$$DX_k = |X_k - X_{k-1}| \tag{3.6}$$

where $DX_k$ is the conditioned input signal. This difference operation is analogous to the filtering and rectifying operations usually performed by analog event detectors. The conditioned input signal $DX_k$ is used in the same manner as the $|A(\tau)|$ in Eq. (3.1). $W_k$ is a recursive approximation to a 10 point moving time average of $DX_k$. Because in this example the input signal is digitized at a rate of 50 samples/sec, a 10 point time average is equivalent to a time window of 0.2 sec. $W_k$ is intended to approximate the short-term average $\alpha(t)$ as given in Eq. (3.1) with $\tau_1 = 0.2$ sec. Similarly,

$Z_k$ is a recursive approximation to a 250 point moving time average of $W_k$. $Z_k$ is intended to approximate the long-term average $\beta(t)$ as given in Eq. (3.2) with $\tau_2 = 5$ sec. The recursive approximations are used to save computer time and storage space.

The parameters $\xi_k$ and $\eta_k$ in Fig. 16 are used to detect and to confirm the onset of an earthquake, respectively. These parameters are compared with the predetermined threshold levels as shown by dashed lines in Fig. 16. When the current value of $\xi_k$ exceeds its threshold level, then the time

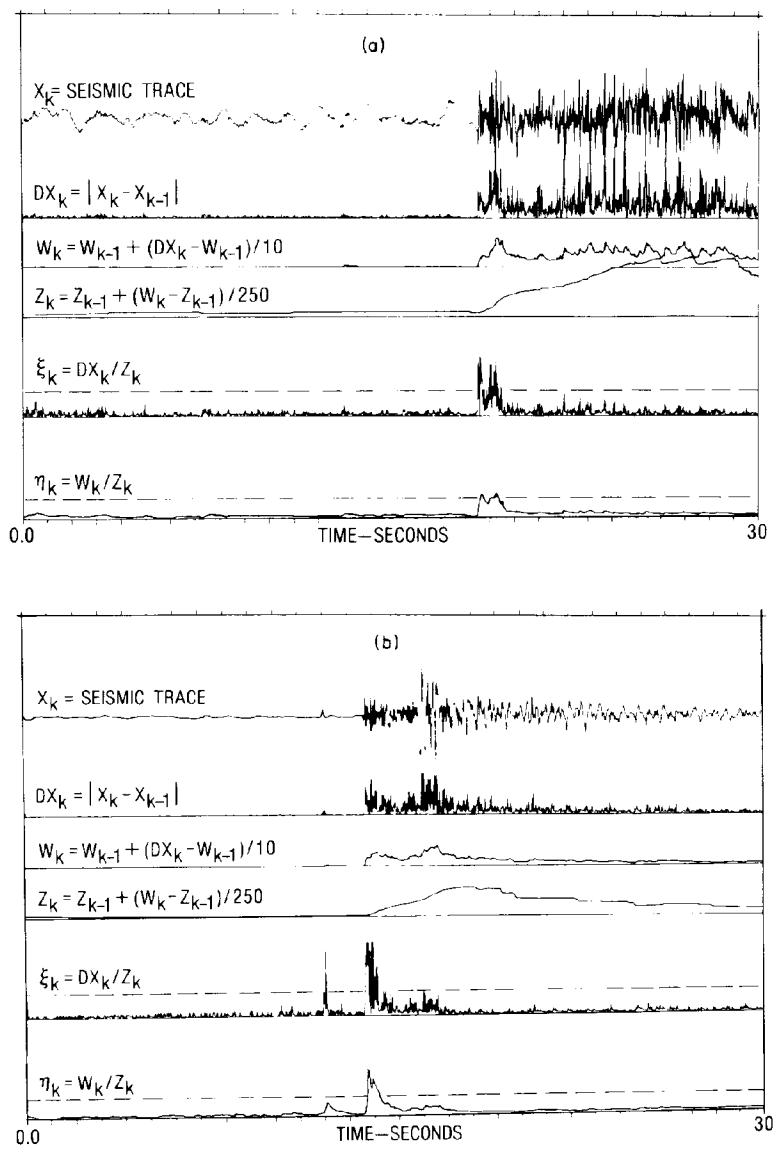


**Fig. 16.** Variation of the parameters as a function of time calculated in the real-time detection process described by Stewart *et al.* (1971). See text for explanation. (a) Example with long-period noise preceding the earthquake. (b) Example with a small transient preceding the earthquake.

$t_k$ is taken to be the onset time of an event for this input signal. If $\eta_k$ exceeds its threshold level within 1 sec after time $t_k$, then the event is confirmed to be an earthquake. Otherwise, the onset time $t_k$ is discarded, and no earthquake is confirmed for this input signal. So far, the detection and confirmation tests are performed on individual input signals, and it is common for nonseismic events to be confirmed as earthquakes. To minimize this difficulty, Stewart *et al.* (1971) utilized simple properties of the arrival time pattern in a microearthquake network. In other words, the event must be confirmed on some minimum number of seismic stations within some small interval of time. This time interval must be consistent with the station spacing and the velocity of seismic waves in the earth's crust. The system measured onset times and maximum amplitudes for up to 32 incoming seismic signals, but hypocentral locations and magnitudes were not computed.

Massinon and Plantet (1976) summarized an on-line earthquake detection and location system for a telemetered seismic network in France. Their method of event detection is similar to that described in Section 3.3.3. The signals from each of 20 short-period seismic stations were transmitted to a central site where they were monitored by event detectors as well as recorded directly for subsequent off-line processing. If more than five stations reported a detection, then the detection times were taken as the first arrival times and an epicenter was calculated automatically. Massinon and Plantet (1976) were interested primarily in regional or teleseismic earthquakes.

Kuroiso and Watanabe (1977) used the short-term average [Eq. (3.1)] to detect local earthquakes in an 11-station telemetered network in Japan. They computed the short-term average by first bandpass filtering and rectifying the incoming seismic signal. The detected event was written to a disk. If subsequent analysis of the data on the disk confirmed that the event was a local earthquake, then its onset time and other parameters were determined automatically. The hypocenter and magnitude were then computed.

## 3.4. Event Processing

Event processing is the procedure for measuring some basic parameters from the recorded seismic traces that describe the earthquake ground motion. These parameters are generally known as phase data and include: (1) the onset time and the direction of motion of the first P-arrival; (2) the onset time of later arrivals, such as the S-arrival (if possible); (3) the maximum trace amplitude and its associated period; and (4) the signal

duration of the earthquake. Precise measurement of the phase data is essential because they are used to compute the origin time, hypocenter, and magnitude of the earthquake, and to deduce its focal mechanism. In the following subsection, we give some general methods of measuring the phase data.

The goals of event processing are to measure the phase data as uniformly and precisely as possible and to prepare the so-called phase list containing these data for each earthquake. In this section, we discuss processing the individual seismic traces, while in Section 3.5 we discuss processing the phase lists.

### *3.4.1. Visual Methods*

The traditional way of measuring phase data is to read visually the phase time, amplitudes and periods, etc., from the seismograms using rulers or scales (see, e.g., Willmore, 1979). The phase data are usually recorded on a printed form to facilitate punching cards or otherwise entering the data into a computer. The visual method has the advantage that it is straightforward. It is also a simple matter to read and merge data from a variety of visual recording media. For a small microearthquake network operating in an area of moderate seismicity, this may be the most cost-effective method to use. However, the visual method has the following disadvantages: (1) different analysts may read the seismograms differently; (2) errors may be introduced in measuring, writing, or keypunching the data; and (3) it may be difficult to carry out such a tedious task over a long period of time. Also, visual recording media have a limited dynamic range and a limited recording speed, so that some of the phase data (such as first P-motion, S-arrival, and maximum trace amplitude) cannot be read precisely, if at all.

For a large microearthquake network where the data volume is large, the visual method of measuring phase data requires a considerable amount of checking to minimize errors in data handling. This includes systematic checking of measured phase data by another analyst before keypunching, and systematic verifying of the phase data after keypunching. Our experience shows that analysts or keypunch operators occasionally enter the data in the wrong place or transpose digits in the data. For example, a P-arrival time of 13.55 sec may be written or keypunched as 31.55 sec.

### *3.4.2. Semiautomated Methods*

Semiautomated methods usually are designed to eliminate the tasks of recording and keypunching data that are required in the visual methods.

The analyst is still required to examine each seismic trace on the film or paper seismograms and to make decisions about what should be measured. Instead of a ruler or scale, however, the analyst uses a digitizing cursor to indicate where each measurement should be made and a keyboard to enter additional information. In the simplest case, the output from the digitizing cursor and the keyboard is written automatically on punched cards by a standard keypunch machine. In the more elaborate case, a small computer is used to provide the analyst with an interactive mode of measuring phase data. We now give an example of each case.

A noninteractive semiautomatic system to measure phase data from the 16-mm microfilms recorded by the USGS Central California Microearthquake Network has been in use since 1973. It has replaced the routine visual method of measuring phase data discussed in the previous subsection. This system consists of an overhead projector, an electronic digitizer, a keyboard, and a standard keypunch machine. The electronic digitizer has a digitizing table about 90 by 130 cm in size and a digitizing cursor; its digitizing resolution is about 0.025 mm. About 60 sec of one 16-mm microfilm is projected onto the digitizing table from the overhead projector. The optical magnification is about 30× so that 1 sec in time is equivalent to 1.5 cm in length on the digitizing table. For each earthquake, the analyst uses the keyboard to enter the data and time of the event and the microfilm identification. The digitizing cursor is used to enter the coordinates of (1) time fiducials, (2) seismic trace levels, (3) P-phase onsets, and (4) other measurements. The output from the keyboard and the digitizing cursor is punched on cards automatically as an unformatted string of alphanumeric characters.

Using the scan list, phase data for all earthquakes recorded on one roll of microfilm are processed sequentially. Because several rolls of microfilms per day are recorded by the USGS Central California Microearthquake Network, this procedure is repeated for each roll of microfilm. The resulting deck of punched cards is processed off-line by a computer. The processing program translates the unformatted string of alphanumeric characters into the intended phase data, organizes the phase data by earthquakes, and outputs a phase list for earthquake location. Routine processing of phase data using this system is about two to three times faster than the visual method described in the previous subsection because reading off a scale, writing down the data, and keypunching the data are eliminated.

A major drawback of this processing system is that it is a two-step procedure, and errors often are not detected until the punched cards are processed off-line. To remedy this difficulty, W. H. K. Lee and colleagues introduced a low-priced microcomputer to control the data processing of

16-mm microfilms. The microcomputer prompts the analyst to perform the measuring tasks. If an error is detected, the analyst is asked to repeat the measurement. The microcomputer processes the measurements of each earthquake into a phase list and calculates the hypocenter parameters for the earthquake. This system will be further discussed in Section 3.5.2.

### *3.4.3. Automated Methods: Determining First P-Arrival Times*

Because most microearthquake networks are designed for precise determination of earthquake hypocenters, it is crucial that any automated system be able to determine the first P-arrival times accurately. Otherwise, the automated system is no better than an event detection system. In this subsection, we discuss some published techniques for automated determination of first P-arrival times. Very little discussion will be given to the simpler procedures for determining the directions of first motion, amplitudes, and periods.

The waveforms of microearthquakes recorded at neighboring stations have been observed to be remarkably dissimilar in general. This has led to computer algorithms that process each incoming digital signal as an independent time series. Before processing the signal, most investigators apply bandpass filtering to reduce noise that is outside the frequency range of interest and to eliminate the dc bias level.

The concept of characteristic functions is useful in designing computer algorithms for determining first P-arrival times. The incoming signal in digital form is seldom used directly in the algorithms. It is usually transformed into one or more time series that are more suitable for determining first P-arrival times. The transformed time series is referred to here as the characteristic function $f(k)$, where $k$ is a time index.

One of the simplest characteristic functions is obtained by performing a difference operation on the incoming digital signal. Stewart *et al.* (1971) and Crampin and Fyfe (1974) defined their characteristic function as the absolute value of the difference between adjacent data points, i.e.,

$$f_1(k) = |X_k - X_{k-1}|, \qquad k = 2, 3, \ldots \tag{3.7}$$

where $X_k$ is the amplitude of the incoming signal at time $t_k$, and $k$ is an index for counting the data points. This operation filters out the low-frequency portions of the incoming signal as shown in Fig. 16a. This characteristic function works well in conditioning the incoming signal that contains impulsive high-frequency seismic waves.

Crampin and Fyfe (1974) referred to Eq. (3.7) as the one-sample mechanism. They also computed a four-sample mechanism and an eight-sample

mechanism according to

$$f_4(k) = |X_k - X_{k-4}|, \qquad k = 5, 6, \ldots \tag{3.8}$$

$$f_8(k) = |X_k - X_{k-8}|, \qquad k = 9, 10, \ldots \tag{3.9}$$

respectively. For a digitizing interval of 0.04 sec, Crampin and Fyfe (1974) showed that $f_1(k)$, $f_4(k)$, and $f_8(k)$ were filters with peak responses at frequencies of 12.5, 3.1, and 1.56 Hz, respectively. For each channel of incoming signal, mechanisms $f_1(k)$, $f_4(k)$, and $f_8(k)$ are checked in sequence against their preset threshold levels. If any one of these mechanisms exceeds its threshold level, this channel is said to be triggered. Because $f_1(k)$ is sensitive to transients, additional testing is performed if any channel is triggered by the $f_1(k)$ mechanism. An event is declared if at least three channels are triggered within a short time window. For each channel, the time of its first trigger within this window is taken as the first P-arrival time at its corresponding station.

Recognizing the limitation of $f_1(k)$ defined by Eq. (3.7) as a characteristic function, Stewart (1977) devised the following characteristic function $f(k)$ instead. If $d_k$ denotes the difference between adjacent data points, i.e., $d_k = X_k - X_{k-1}$, then

$$f(k) = \begin{cases} d_k, & \text{if } g(k) \neq g(k-1) \\ d_k, & \text{if } g(k) = g(k-1) \text{ and } h(k) = 8 \\ d_k + d_{k-1}, & \text{if } g(k) = g(k-1) \text{ and } h(k) \neq 8 \end{cases} \tag{3.10}$$

where

$$g(k) = \begin{cases} +1, & \text{if } d_k \text{ is positive or zero} \\ -1, & \text{if } d_k \text{ is negative} \end{cases} \tag{3.11}$$

and

$$h(k) = \left| \sum_{k-7}^{k} g(k) \right| \tag{3.12}$$

This characteristic function $f(k)$ extends the response of $f_1(k)$ to lower frequencies, and is more suitable to detect less impulsive P-wave arrivals. It can also be easily computed in a real-time environment because Eq. (3.10) involves only addition, subtraction, and comparison operations. Figure 17 shows the effect of this characteristic function on a sinusoidal signal. Using $f(k)$ defined by Eq. (3.10), a moving time average $\overline{f(k)} = \Sigma|f(k)|$ is computed. If $|f(k)/\overline{f(k)}|$ exceeds 2.9 at time index $k = j$, then a tentative detection is declared to have occurred at time $t_j$. Within the next

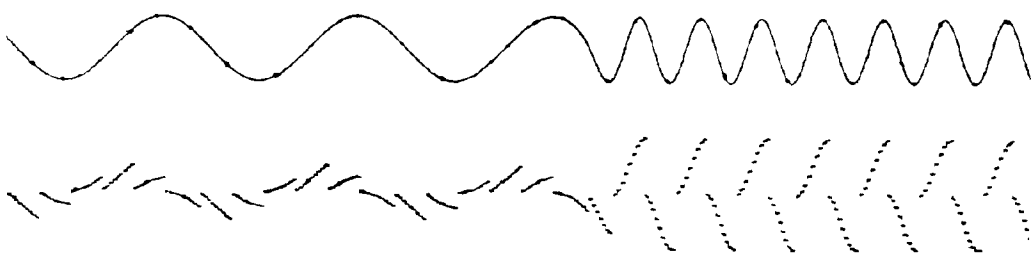

**Fig. 17.** Effect of the characteristic function $f(k)$ used by Stewart (1977) on a sinusoidal signal. The upper signal is the input function, and the lower signal is the computed characteristic function. The horizontal scale is time (approximately 5 sec shown here), and the vertical scale is arbitrary.

0.5 sec, four additional tests are performed to see if this tentative detection can be confirmed as an event. If so, the first P-arrival time is computed according to $t_j - h(j) \cdot \Delta t$, where $\Delta t$ is the digitizing time interval, and $h(j)$ is defined by Eq. (3.12).

Allen (1978) devised a characteristic function sensitive to variations in signal amplitude and its first derivative. If the amplitude of the incoming signal is $X_k$ at time $t_k$, then the modified signal amplitude (filtered to remove the dc offset) is defined by

$$R_k = C_1 R_{k-1} + (X_k - X_{k-1}) \tag{3.13}$$

where $C_1$ is a weighting constant. Allen's characteristic function is defined by

$$f(k) = R_k^2 + C_2(X_k - X_{k-1})^2 \tag{3.14}$$

where $C_2$ is also a weighting constant. Using this characteristic function, a short-term and a long-term time average are computed by

$$\alpha(k) = \alpha(k-1) + C_3[f(k) - \alpha(k-1)] \tag{3.15}$$

$$\beta(k) = \beta(k-1) + C_4[f(k) - \beta(k-1)] \tag{3.16}$$

where $C_3$ and $C_4$ are constants with values ranging from 0.2 to 0.8 and from 0.005 to 0.05, respectively. If $\alpha(k)/\beta(k)$ exceeds 5 at time index $k = j$, then an event is declared to have occurred at time $t_j$. The first P-arrival time is determined by the intersection of the slope of the modified signal amplitude at time $t_j$ with the zero level of the modified signal.

So far, all the characteristic functions discussed depend on calculating the first difference of the incoming signal and examining each digitized data point. Anderson (1978) proposed a different method to compute the

characteristic function. If the amplitude of the incoming signal is $X_k$ at time $t_k$, then the modified signal amplitude (filtered to remove the dc bias) is defined by

$$Y(k) = X_k - \bar{X}_k \tag{3.17}$$

where $\bar{X}_k$ is a moving time average of $X_k$ and is used to estimate the dc offset in the incoming signal. A moving time average of the absolute values of the modified signal amplitude is defined by

$$Z(k) = (n + 1)^{-1} \sum_{i=k-n}^{k} |Y(i)| \tag{3.18}$$

where the length of the time window is $n \cdot \Delta t$, and $\Delta t$ is the digitizing interval. This moving time average $Z(k)$ is used to compute the threshold level.

In Fig. 18a, the modified incoming signal $Y(k)$ may be represented as a set of points $\{t_k, Y_k\}$, $k = 1, 2, \ldots, K$. Anderson (1978) introduced a characteristic function that is obtained from the $\{t_k, Y_k\}$ by saving only the zero crossing points and those points corresponding to the maximum amplitude (either positive or negative) between two successive zero crossings, as shown in Fig. 18b. Thus the $K$ elements of the modified incoming signal are condensed into a sawtooth function with $M$ elements $\{\tau_i, b_i\}$, $i = 1, 2, \ldots, M$, where $M < K$. This characteristic function removes the higher frequency components of the signal, but preserves the oscillatory character of the signal. It consists of a series of serrations, each of which is referred to as a blip.

To detect the first P-arrivals, the characteristic function $f(k)$ as shown in Fig. 18b is examined blip by blip. A blip at time $\tau_j$ is defined by three points $\{\tau_j, b_j\}$, $\{\tau_{j+1}, b_{j+1}\}$, $\{\tau_{j+2}, b_{j+2}\}$. If the duration of a blip, i.e., $\tau_{j+2} - \tau_j$, exceeds 0.06 sec and $b_{j+1}/Z(\tau_{j+1})$ exceeds 6, then a P-arrival is declared to have occurred at time $\tau_j$. The direction of first motion is the sign of $b_{j+1}$. To confirm this tentative P-arrival, the next 1 sec of the characteristic function is examined. Within this time window, if there are at least three blips with $b/Z$ greater than 6 and if the dominant frequency lies between 1 and 10 Hz, then the tentative P-arrival is confirmed. The dominant frequency is determined by one-half the number of blips divided by the total time duration of the blips. If the tentative P-arrival is not confirmed, then the next blip will be examined.

It is customary to describe the first P-onset as either impulsive (iP), or emergent (eP), or questionable (P?). Therefore, a relative weight is frequently assigned to the first P-arrival time to take into account the quality

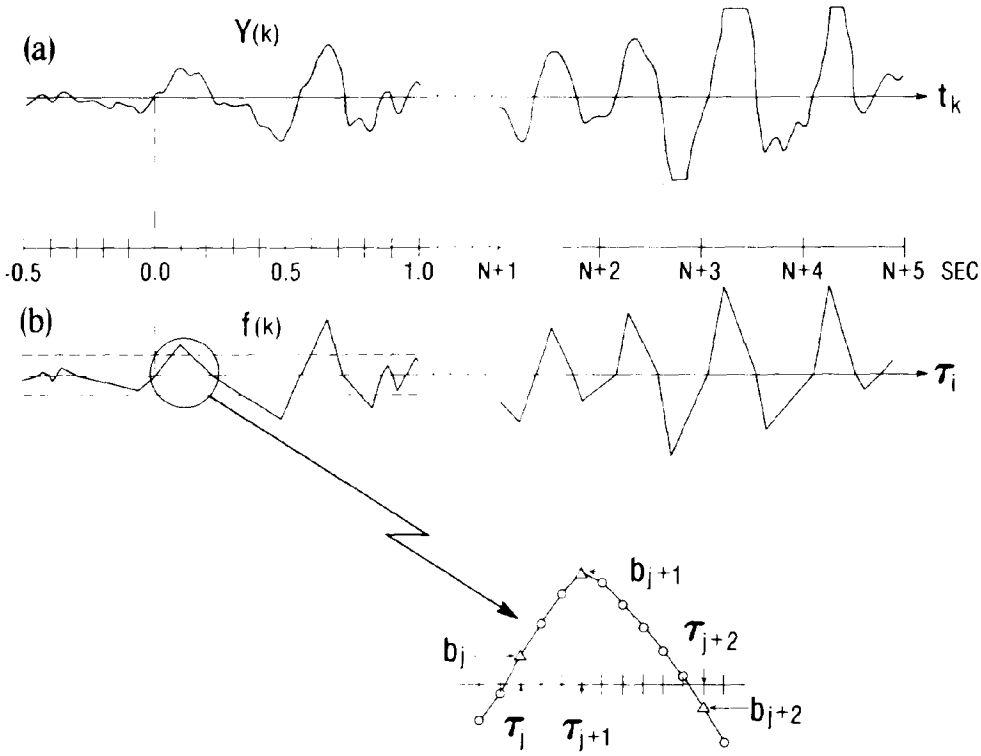


**Fig. 18.** (a) Schematic graph showing a P-wave onset and a portion of the coda of an earthquake. The modified signal amplitude $Y(k)$ is plotted against time $t$, where $k$ is a counting index. (b) The characteristic function $f(k)$ described by Anderson (1978) in which $Y(k)$ is transformed to a set of blips. See text for explanation.

of the onset. But assigning a relative weight is subjective and often ambiguous. Crampin and Fyfe (1974) and Stewart (1977) assigned equal weights to all the first P-arrival times regardless of their onset quality. Allen (1978) assigned relative weights to the first P-arrival times empirically by using (1) the background level just before the onsets, (2) the first difference in signal amplitude at the onset times, and (3) the peak amplitudes of the first three peaks after the onsets. Anderson (1978) did not assign relative weights to the first P-arrival times, but discussed an objective method to estimate the accuracy of first P-arrival times. The standard deviation of the arrival time $\sigma_t$ was computed by

$$\sigma_t = \sigma_n / g \tag{3.19}$$

where $\sigma_n$ is the standard deviation of the noise, and $g$ is the slope of the line between the threshold crossing and the first maximum amplitude. Although Anderson cited some problems with this approach, the theoretical foundation exists and could be developed further (see, e.g., Torrieri, 1972).

Shirai and Tokuhiro (1979) used a log-likelihood ratio function to time P-

and S-onsets of local earthquakes. Their method utilized both amplitude and frequency information, and allowed backtracking over the data to improve the reliability of the timing to a few hundredths of a second.

### *3.4.4. Automated Methods: Cutoff Criteria and Signal Duration*

In order to estimate earthquake magnitude, real-time processing of a detected seismic event may be carried out well into its coda portion. Since earthquakes may occur within the coda portion of another earthquake, especially during an aftershock sequence or a swarm, the event detection algorithm must be able to handle such cases. The steps that lead to a decision to stop processing a detected event and return to the search mode for the next earthquake will be referred to as the cutoff criterion.

Stewart (1977) computed the magnitude of local earthquakes from an estimate of the signal duration according to the method developed by Lee *et al.* (1972). In order to be consistent with the manual processing method, Stewart's real-time processing algorithm for determining the signal duration depended on setting a cutoff threshold level empirically. Successive peaks and troughs of the detected seismic signal were examined. The end of an earthquake was defined as that time when the signal last crossed the cutoff threshold level and remained within it for at least 2 sec. Signal duration was defined as the time interval between the end time and the first P-arrival time of an earthquake. This procedure was automatically terminated if the signal duration exceeded 60 sec in order to return to the detection mode. The 60 sec cutoff was chosen so that the magnitude of microearthquakes (i.e., magnitude less than 3) could be computed by the real-time processing system.

Allen (1978) developed cutoff criteria to terminate the signal processing well before the end of the earthquake coda. After an event was detected, a continuation criteria level $G(k)$ was computed. $G(k)$ depended on (1) the long-term average $\beta(k)$ of the characteristic function (Eq. 3.16), and (2) the current count $M$ of the number of observed peaks in the event, and increased during an event to ensure termination. At each zero crossing of $R_k$ (Eq. 3.13), the current value of $G(k)$ was compared with the short-term average $\alpha(k)$ (Eq. 3.15). A counter $S$ is increased by 1 if $G > \alpha$. The counter $S$ always contained the number of consecutive zero crossings that had occurred in which $G > \alpha$. A termination parameter $L$ was defined to be $(3 + M/3)$. The event was declared to be over when the counter $S$ reached the value of the parameter $L$. The manner in which $L$ was defined ensured that large events were not terminated too soon even if they had relatively low amplitudes between different phase arrivals. For events of short signal durations, the parameter $L$ was small so that events could be

terminated quickly. In Allen's approach, peak amplitudes and zero-crossing times were saved. Thus earthquake magnitudes could be computed afterward.

In the off-line processing system described by Crampin and Fyfe (1974), the detected event was saved by writing the digitized data onto a digital tape for further processing. Each detected event was saved for at least 80 sec, beyond which the data were saved in blocks of 20 sec in length until the total number of triggers fell below some preset minimum.

### *3.4.5. Automated Methods: Event Association*

An automated processing system generates a phase list, i.e., a list of chronologically ordered first P-arrival times and other parameters measured from the incoming seismic signals. In the event association process, the phase list is divided into sets of first P-arrival times, each of which is intended to be associated with an earthquake event. Each set of first P-arrival times may contain some incorrect data because (1) some nonseismic transients may have been picked as first P-arrivals, (2) some later arrivals may be mistaken as first P-arrivals, and (3) some first P-arrival times may belong to a different event with a similar origin time.

The automated processing systems described so far have some abilities to discriminate against nonseismic transients, especially if their signal durations are short. Nonseismic transients can also be recognized if they occur at the same time or if only one or two of them occur within a small time interval. Later seismic phases are sometimes difficult to distinguish from the first P-phase. However, if only a few arrival times of later phases are included in a set of first P-arrival times, some location programs (e.g., Lee and Lahr, 1975) can often identify them by statistical tests. Readers may refer, for example, to Lee *et al.* (1981) for further details.

In order to associate a set of first P-arrival times with an earthquake event, we make use of the fact that it takes a finite time interval for seismic waves from a given earthquake to reach a set of stations within a microearthquake network. This time interval can be estimated from the network station geometry and the P-velocity structure beneath the network. Thus an earthquake event is considered to be valid for further data processing if some minimum number of stations report a first P-arrival time within a given time interval or window. For example, starting from a given first P-arrival time, Stewart (1977) required that at least four stations report first P-arrivals within an 8-sec time window. If this condition was met, then an earthquake was declared to have occurred and all additional first P-arrival times within the next 1 min were associated with this earthquake. If this condition was not met, then this first P-arrival time was

ignored and the same procedure was repeated for the next first P-arrival time detected. For a small microearthquake network in which the first P-arrivals of the desired earthquakes can be expected to reach all the stations, the time window may be set to be the maximum propagation time across the network. For example, Crampin and Fyfe (1974) used a 16-sec time window for the 100-km aperture LOWNET array in Scotland. They required that a valid earthquake must have at least three stations reporting first P-arrival times within this time window.

Because more than one earthquake may occur within one minute in a large microearthquake network, Stewart (1977) carried out additional tests on the first P-arrival time data to separate earthquakes with similar origin times. His approach considers first the time relationship and then the spatial relationship of the first P-arrival time data. If a gap of 8 sec or more is found between successive arrival times, then the arrival times before that gap are separated out as one subset of time-coherent data to be examined further for spatial coherence. The 8-sec gap is chosen for the USGS Central California Microearthquake Network from considerations of the station spacing and the P-velocity structure beneath this network. In order to consider the spatial relationship of the first P-arrival time data, the network is subdivided into eight distinct geographic zones and each station is assigned to only one zone. For a given subset of time-coherent data, the number of first P-arrivals in pairs of adjacent zones is counted. If this number is greater than 3, then the first P-arrival time data in such zones are considered to belong to one earthquake event. If this is not the case, then those data that fail the test are discarded and the remaining data in this time-coherent subset are examined in a similar manner. The details of this approach are described in Stewart (1977).

### 3.5. Computing Hypocenter Parameters

The hypocenter parameters calculated routinely for microearthquakes include the origin time, epicenter coordinates, focal depth, magnitude, and estimates of their errors. If enough first-motion data are available, a plot of the first P-motions on the focal sphere is also made. In this section, we describe some of the practical aspects of computing these parameters with examples taken from two large microearthquake networks in California. The mathematical aspects of hypocenter calculation, fault-plane solution, and magnitude estimation will be treated in Chapter 6.

Because hypocenter parameters are usually calculated by digital computers, there are three basic approaches in obtaining the results. Each approach is iterative in nature since errors in the input data are unavoid-

able. The first approach is the batch method, in which the analyst and the computer perform their tasks separately. The second approach is the interactive method, in which the analyst and the computer interact directly in performing their tasks. The third approach is the automated method, in which the hypocenter parameters are calculated by the computer without any intervention from the analyst.

### *3.5.1. Batch Method*

In the batch method, the analyst first sets up the input data (these include station coordinates, velocity structure parameters, and phase data) required by an earthquake location program. The analyst then submits the program and the input data as a batch job to be run by a computer. After the output from the computer is obtained, the analyst examines the results and makes corrections to the input data if necessary. The corrected input data are run on the computer again, and the procedure is repeated until the analyst is satisfied with the results. In some earthquake location programs (e.g., Lee and Lahr, 1975), statistical tests are performed to identify some commonly occurring errors. These errors are flagged in the computer output to aid the analyst.

It is common for the analyst to assign relative weights to the first P-arrival times because the quality of the first P-onset varies from station to station. For example, five levels of quality designation ($Q$) are used in the routine work of the USGS Central California Microearthquake Network. The relative weight $W$ assigned to a first P-arrival time is related to the quality designation $Q$ by

$$W = 1 - Q/4 \tag{3.20}$$

In other words, a full weight of 100% corresponds to $Q = 0$, and 75, 50, 25, and 0% weights correspond to $Q = 1, 2, 3$, and 4, respectively. This reverse relationship between weight and quality designation was first applied by the USGS Central California Microearthquake Network and is now widely used. Because the weight most commonly assigned to the first P-arrival times in this network is 100%, the analyst can leave the value of $Q$ blank for data entry to the computer.

The direction of the first P-motion at a vertical-component station is often designated by a single character as either $U$ (for up) or $D$ (for down). Unless the first P-motion is clear, the analyst usually ignores it. However, the notation of either + or − may be used to substitute for $U$ or $D$ to indicate a low-amplitude first P-onset. This practice increases the number of first P-motion data available for a given earthquake and may help identify the nodal planes on the first P-motion plot. If the station polarity is

correct, then the up direction on the seismogram of a vertical-component station corresponds to a compression in ground motion, whereas the down direction corresponds to a dilatation. Since station polarity may be accidentally reversed, it should be checked periodically by examining the directions of first P-motions of large teleseismic events. For example, Houck *et al.* (1976) carried out this check for the USGS Central California Microearthquake Network. About 15% of the stations were found to be reversed.

Magnitudes of microearthquakes are frequently estimated from signal durations because of the difficulties in calibrating large numbers of stations in a microearthquake network, and in measuring maximum amplitudes and periods from recordings with limited dynamic range. Signal duration of microearthquakes has been defined in several ways as is discussed in Section 6.4. Recently, the Commission on Practice of the International Association of Seismology and Physics of Earth's Interior has recommended that the signal duration be defined as "the time in seconds between the first onset and the time the trace never again exceeds twice the noise level which existed immediately prior to the first onset."

### *3.5.2. Interactive Method*

The batch method just described has a serious drawback in that it is time consuming to go back to the seismic records for correcting errors and to enter the corrections into a computer. If one or a small group of earthquakes is processed at a time, then errors can be corrected more efficiently. Furthermore, if the data processing procedure is under computer control, then an interactive dialogue between the analyst and the computer can speed the entire process. Basically, a computer can perform bookkeeping chores well, but it is more difficult to program the computer to make intelligent decisions. There are two approaches in the interactive method. In the first approach, the seismic traces are digitized and stored in a computer for further processing. In the second approach, the seismic traces are available only as visual records.

For the first approach, several interactive systems for processing microearthquake data have been developed. For example, Johnson (1979) described the CEDAR (Caltech Earthquake Detection and Recording) system for processing seismic data from the Southern California Seismic Network. This system consists of four stages of data processing. In the first stage, an on-line computer detects events and records them on digital magnetic tapes. The remaining stages of data processing are performed on an off-line computer using the digital tapes. In the second stage, the detected events are plotted, and the analyst separates the seismic events

from the noise events by visual examination. In the third stage, the seismic data are displayed on a graphics terminal, and the analyst identifies and picks each arriving phase using an adjustable cross-hair cursor. The computer then calculates the arrival times and stores the phase data. After a small group of earthquakes is processed, the computer works out preliminary locations. In the fourth stage, retiming and final analysis are performed. The phase data can be corrected by reexamining the digital seismic data, and data from other sources can be added. A final hypocenter location and magnitude estimation can then be calculated.

In another example, staff members of the USGS Central California Microearthquake Network have developed an interactive processing system. The input data for this system are derived from the four analog magnetic tapes recorded daily from this network. A daily event list is prepared by examining the monitor and microfilm recordings of the seismic data. Events in this list are dubbed under computer control from the four daily analog tapes onto a library tape. Earthquakes on the library tape are digitized and processed by the Interactive Seismic Display System (ISDS) written by Stevenson (1978). The algorithm developed by Allen (1978) is used to automatically pick first P-arrival times. The seismic traces and the corresponding automatic picks are displayed on a graphics terminal. The analyst can use a cross-hair cursor to correct the picks if necessary. An earthquake location program (Lee *et al.*, 1981) is executed, and the output is examined for errors. This procedure can be repeated until the analyst is satisfied with the results.

Ichikawa (1980) and Ichikawa *et al.* (1980) described an interactive system for processing seismic data from a telemetered network operated by the Japan Meteorological Agency. This system was installed in 1975 and monitors more than 70 stations. Its operation is similar to that described in the preceding paragraph.

For the second approach, an interactive data processing system for earthquakes recorded on 16-mm microfilms has been developed by W. H. K. Lee and his colleagues. This system consists of three components: (1) an optical–electromechanical unit that advances and projects four rolls of 16-mm microfilm onto a digitizing table; (2) a digitizing unit with a cursor that allows the analyst to pick seismic phases; and (3) a microcomputer that controls the bookkeeping and processing tasks, reduces the digitized data to phase data, and computes hypocenter location and magnitude from the phase data. Usually, one earthquake is processed at a time until the analyst is satisfied with the results. Because all processing steps for one earthquake are carried out while the seismic traces are displayed, errors can be easily identified and corrected by the analyst. This method can process 16-mm microfilms about twice as fast as a noninteractive

semiautomated method, and is ideally suited for a microearthquake network of about 70 stations, which are recorded on four rolls of microfilms.

### *3.5.3. Automated Method*

In the automated method, digitized seismic data are first set up in a computer, the first P-arrival times and other phase data are determined by some algorithm, and the hypocenter parameters are then calculated by the computer. The complete processing procedure is performed automatically without the analyst's intervention. At present, several automated data processing systems for microearthquake networks have been reported (e.g., Crampin and Fyfe, 1974; Watanabe and Kuroiso, 1977; Stewart, 1977).

In theory, the automated method looks very attractive because it frees the analyst from doing tedious work. In practice, however, the automated method is limited by two factors: (1) the complexity of incoming signals generated by a microearthquake network; and (2) the difficulty in designing a computer system that can handle this complexity. The most serious problem is distinguishing between seismic onsets and nonseismic transients. An analyst can rely on past experience, whereas it would be difficult to program a computer to handle every conceivable case.

Some simple schemes have been devised to minimize or eliminate the effect of erroneous arrival times on the computed hypocenter parameters. For example, the signal-to-noise ratio at a station generally decreases with increasing distance from the earthquake hypocenter. Therefore, the P-arrival times from stations at greater distances should be given less weight. This weighting can be applied either according to the chronological order of first P-arrival times (Crampin and Fyfe, 1974) or according to epicentral distances to stations (Stewart, 1977). Large arrival time residuals calculated in a hypocenter location program are often caused by a large error in one or more first P-arrival times. Therefore, arrival times with large residuals should be given less weight or discarded. For instance, Stewart (1977) was able to improve the quality of the hypocenter solution by discarding the arrival time with the largest residual and relocating the event.

Several studies have been reported that compare the performance of automated data processing techniques with that of an analyst. For example, Stewart (1977) compared the results from his real-time processing system with those obtained by a routine manual processing method. His system monitored 91 stations of the USGS Central California Microearthquake Network. For the period of October 1975 the routine processing method located 260 earthquakes using data from 150 stations. Stewart's

system detected 86% of these events, but missed 4%. The remaining 10% of the earthquakes occurred in a sparsely monitored portion of the network and would not be expected to be detected. About half of the detected earthquakes had computed hypocenter parameters that agreed favorably with those obtained routinely.

Anderson (1978) compared 44 first P-arrival times obtained by his algorithm with those determined by an analyst. The data were taken from a magnitude 3.5 earthquake with epicentral distances to stations in the range of 4.5–115 km. The comparison showed that 77% of Anderson's first P-arrival times were within $\pm 0.01$ sec, and 89% were within $\pm 0.05$ sec. Similarly, Allen (1978) reported that his algorithm timed about 70% of the first P-arrivals within $\pm 0.05$ sec of the times determined by an analyst in several test runs.

So far, the analyst does a better job in identifying poor first P-onsets and in deciding which stations to ignore in calculating hypocenter parameters. Nevertheless, automated methods are useful in obtaining rapid earthquake locations and in processing large quantities of data. The quality of the results is often good enough for a preliminary reporting of a main shock and its aftershocks (e.g., see Lester *et al.*, 1975). We expect that improved automated methods will soon take over most of the routine data processing tasks now performed by analysts.

# 4. Seismic Ray Tracing for Minimum Time Path

The earth is continuously being deformed by internal and external stresses. If the stresses are not too large, elastic and/or plastic deformation will occur. But if the stresses accumulate over a period of time, fracture will eventually take place. Fracture involves a sudden release of stress and generates elastic waves that travel through the earth. A seismic network at the earth's surface may record the ground motion caused by the passage of elastic waves. The major problem is to deduce the earthquake source parameters and seismic properties of the earth from a set of surface observations. Before we attempt to solve this inverse problem, we need to understand the forward problem, namely, how elastic waves travel in the earth. We will now present an outline of the forward problem in order to provide a background for seismological applications.

## 4.1 Elastic Wave Propagation in Homogeneous and Heterogeneous Media

Karal and Keller (1959) presented a modern treatment of elastic wave propagation in homogeneous and heterogeneous media, and our outline here follows their approach. The equation of motion for a homogeneous, isotropic, and initially unstressed elastic body may be obtained using the conservation principles of continuum mechanics (e.g., Fung, 1969, p. 261) as

$$\rho \frac{\partial^2 u_i}{\partial t^2} = (\lambda + \mu) \frac{\partial \theta}{\partial x_i} + \mu \nabla^2 u_i, \qquad i = 1, 2, 3 \tag{4.1}$$

where $\theta \equiv \sum_j \partial u_j / \partial x_j$ is the dilatation, $\rho$ is the density, $u_i$ is the $i$th component of the displacement vector $\mathbf{u}$, $t$ is the time, $x_i$ is the $i$th component of the coordinate system, and $\lambda$ and $\mu$ are elastic constants. Equation (4.1)

may be rewritten in vector form as

$$\rho(\partial^2\mathbf{u}/\partial t^2) = (\lambda + \mu)\,\nabla(\nabla \cdot \mathbf{u}) + \mu\nabla^2\mathbf{u} \tag{4.2}$$

If we differentiate both sides of Eq. (4.1) with respect to $x_i$, sum over the three components, and bring $\rho$ to the right-hand side, we obtain

$$\partial^2\theta/\partial t^2 = [(\lambda + 2\mu)/\rho]\nabla^2\theta \tag{4.3}$$

If we apply the curl operator ($\nabla\times$) to both sides of Eq. (4.2), bring $\rho$ to the right-hand side, and note that $\nabla \cdot (\nabla \times \mathbf{u}) = 0$, we have

$$\partial^2(\nabla \times \mathbf{u})/\partial t^2 = (\mu/\rho)\nabla^2(\nabla \times \mathbf{u}) \tag{4.4}$$

Now Eqs. (4.3)–(4.4) are in the form of the classical wave equation

$$\partial^2\psi/\partial t^2 = v^2\,\nabla^2\psi \tag{4.5}$$

where $\psi$ is the wave potential, and $v$ is the velocity of propagation. Thus a dilatational disturbance $\theta$ (or a compressional wave) may be transmitted through a homogeneous elastic body with a velocity $V_p$ where

$$V_p = [(\lambda + 2\mu)/\rho]^{1/2} \tag{4.6}$$

according to Eq. (4.3), and a rotational disturbance $\nabla \times \mathbf{u}$ (or a shear wave) may be transmitted with a velocity $V_s$ where

$$V_s = (\mu/\rho)^{1/2} \tag{4.7}$$

according to Eq. (4.4). In seismology, these two types of waves are called the primary (P) and the secondary (S) waves, respectively.

For a heterogeneous, isotropic, and elastic medium, the equation of motion is more complex than Eq. (4.2), and is given by (Karal and Keller, 1959, p. 699)

$$\begin{aligned}\rho(\partial^2\mathbf{u}/\partial t^2) = {} & (\lambda + \mu)\,\nabla(\nabla \cdot \mathbf{u}) + \mu\nabla^2\mathbf{u} + \nabla\lambda(\nabla \cdot \mathbf{u}) \\ & + \nabla\mu \times (\nabla \times \mathbf{u}) + 2(\nabla\mu \cdot \nabla)\mathbf{u}\end{aligned} \tag{4.8}$$

where $\mathbf{u}$ is the displacement vector. Furthermore, the compressional wave motion is no longer purely longitudinal, and the shear wave motion is no longer purely transverse.

A significant portion of seismological research is based on the solution of the elastic wave equations with the appropriate initial and boundary conditions. However, explicit and unique solutions are rare, except for a few simple problems. One approach is to develop through specific boundary conditions a solution in terms of normal modes (e.g., Officer, 1958, Chapter 2). Another approach is to transform the wave equation to the eikonal equation and seek solutions in terms of wave fronts and rays that are valid at high frequencies (e.g., Cerveny *et al.*, 1977).

## 4.2. Derivation of the Ray Equation

The seismic ray approach is particularly relevant to the problem of inverting arrival times observed in a microearthquake network. To carry out the inversion, the travel time and ray path between the source and the receiving stations must be known. This information may be obtained by solving the ray equation between two end points for a given earth model. Two independent derivations of the ray equation are given next in order to provide some insight into its solution and applications.

### *4.2.1. Derivation from the Wave Equation*

The wave equation may be transformed to a first-order partial differential equation known as the eikonal equation whose solutions can be interpreted in terms of wave fronts and rays (e.g., Officer, 1958, pp. 36–42). In brief, the general three-dimensional wave equation [Eq. (4.5)] has associated with it the equation of characteristics (Officer, 1958, p. 37) given by

$$(\partial\psi/\partial x)^2 + (\partial\psi/\partial y)^2 + (\partial\psi/\partial z)^2 = (1/v^2)(\partial\psi/\partial t)^2 \tag{4.9}$$

A particularly simple solution for the wave potential $\psi$ in Eq. (4.5) or Eq. (4.9) is

$$\psi = \psi(ax + by + cz - vt) \tag{4.10}$$

where $a$, $b$, and $c$ are the three direction cosines. A more general solution takes the form

$$\psi = \psi[W(x, y, z) - v_0 t] \tag{4.11}$$

where $W$ describes the wave front and $v_0$ is a constant reference velocity. If we substitute the solution for $\psi$ [Eq. (4.11)] into the equation of characteristics [Eq. (4.9)], we obtain the time-independent equation known as the eikonal equation

$$(\partial W/\partial x)^2 + (\partial W/\partial y)^2 + (\partial W/\partial z)^2 = v_0^2/v^2 = n^2 \tag{4.12}$$

where we have defined the index of refraction $n = v_0/v$. The eikonal equation leads directly to the concept of rays. It is especially useful in the solution of problems in a heterogeneous medium where the velocity is a function of the spatial coordinates.

The eikonal equation [Eq. (4.12)] is a first-order partial differential equation, and its solutions,

$$W(x, y, z) = \text{const} \tag{4.13}$$

represent surfaces in three-dimensional space. For a given value of $W$ and a given instant of time $t_1$, all points along the surface will be in phase although not necessarily of the same amplitude. Because of the one-to-one correspondence of the motion along this surface, such a surface is called a wave front. At a later time $t_2$, the motion along the surface will be in a different phase of motion. Wave propagation may thus be described by successive wave fronts. The normals to the wave front define the direction of propagation and are called rays.

The equation for the normals to the wave front is (Officer, 1958, p. 41)

$$\frac{dx}{\partial W/\partial x} = \frac{dy}{\partial W/\partial y} = \frac{dz}{\partial W/\partial z} \tag{4.14}$$

where the denominators are the direction numbers of the normal. Because the direction cosines are proportional to the direction numbers, we may write

$$\begin{gathered} dx/ds = k(\partial W/\partial x), \qquad dy/ds = k(\partial W/\partial y) \\ dz/ds = k(\partial W/\partial z) \end{gathered} \tag{4.15}$$

where $k$ is a constant and $ds$ is an element of the ray path. The sum of the squares of direction cosines is unity, i.e.,

$$(dx/ds)^2 + (dy/ds)^2 + (dz/ds)^2 = 1 \tag{4.16}$$

By squaring and adding the three equations in Eq. (4.15), and using the eikonal equation [Eq. (4.12)]

$$1 = k^2[(\partial W/\partial x)^2 + (\partial W/\partial y)^2 + (\partial W/\partial z)^2] = k^2n^2 \tag{4.17}$$

Thus,

$$k = 1/n \tag{4.18}$$

and Eq. (4.15) becomes

$$\begin{gathered} n(dx/ds) = \partial W/\partial x, \qquad n(dy/ds) = \partial W/\partial y \\ n(dz/ds) = \partial W/\partial z \end{gathered} \tag{4.19}$$

Taking a derivative $d/ds$ along the ray path of any one member of Eq. (4.19), we obtain an equation of the form

$$\frac{d}{ds}\left(n\frac{dx}{ds}\right) = \frac{d}{ds}\left(\frac{\partial W}{\partial x}\right) = \frac{\partial}{\partial x}\left(\frac{\partial W}{\partial x}\frac{dx}{ds} + \frac{\partial W}{\partial y}\frac{dy}{ds} + \frac{\partial W}{\partial z}\frac{dz}{ds}\right) \tag{4.20}$$

By using Eq. (4.19) and then Eq. (4.16), the right-hand side of Eq. (4.20) reduces to $\partial n/\partial x$. By repeating the same procedure, we obtain the

following set of equations from Eq. (4.19):

$$\frac{d}{ds}\left(n\frac{dx}{ds}\right) = \frac{\partial n}{\partial x}, \qquad \frac{d}{ds}\left(n\frac{dy}{ds}\right) = \frac{\partial n}{\partial y}, \qquad \frac{d}{ds}\left(n\frac{dz}{ds}\right) = \frac{\partial n}{\partial z} \tag{4.21}$$

These are three members of the ray equation in which the index of refraction $n$ characterizes the medium.

### *4.2.2. Derivation from Fermat's Principle*

The ray equation may also be derived from Fermat's principle. This approach is most appealing when one investigates the ray path and travel time between two end points as required in several seismological applications. The derivation is well known in optics (e.g., Synge, 1937, pp. 99–107) and is shown in detail by Yang and Lee (1976, pp. 6–15). Our treatment here is brief.

One basic assumption in the mathematical derivation concerns the functional properties of the velocity $v$ in a heterogeneous and isotropic medium. We assume that the velocity (1) is a function only of the spatial coordinates, and (2) is continuous and has continuous first partial derivatives. The time $T$ required to travel from point $A$ to point $B$ is given by

$$T = \int_A^B ds/v(x, y, z) \tag{4.22}$$

where $ds$ is an element along a ray path. For a minimum time path, Fermat's principle states that the time $T$ has a stationary value.

Let us introduce a new parameter, $q$, to characterize a ray path, and write

$$x = x(q), \qquad y = y(q), \qquad z = z(q) \tag{4.23}$$

An element of the ray path may then be written as

$$ds = (\dot{x}^2 + \dot{y}^2 + \dot{z}^2)^{1/2}\, dq \tag{4.24}$$

where the dot symbol indicates differentiation with respect to the parameter $q$. Equation (4.22) now becomes

$$T = \int_{q_1}^{q_2} w\, dq \tag{4.25}$$

where

$$w \equiv (\dot{x}^2 + \dot{y}^2 + \dot{z}^2)^{1/2}/v \tag{4.26}$$

and $q = q_1$ at $A$, and $q = q_2$ at $B$.

Consider a set of adjacent curves joining $A$ and $B$, each described by equations of the form of Eq. (4.23). Then the variation of $T$ on passing from one of these curves to its neighbor is

$$\begin{aligned}\delta T &= \int_{q_1}^{q_2} \delta w \, dq \\ &= \int_{q_1}^{q_2} \left( \frac{\partial w}{\partial x} \delta x + \frac{\partial w}{\partial y} \delta y + \frac{\partial w}{\partial z} \delta z \right. \\ &\quad \left. + \frac{\partial w}{\partial \dot{x}} \delta \dot{x} + \frac{\partial w}{\partial \dot{y}} \delta \dot{y} + \frac{\partial w}{\partial \dot{z}} \delta \dot{z} \right) dq\end{aligned} \tag{4.27}$$

because from Eq. (4.26) $w$ is a function of $x$, $y$, $z$, $\dot{x}$, $\dot{y}$, and $\dot{z}$, and $\delta x$, $\delta y$, $\delta z$, $\delta \dot{x}$, $\delta \dot{y}$, and $\delta \dot{z}$ are infinitesimal increments obtained in passing from a point on one curve to the point on its neighbor with the same value of $q$. If we perform integration by parts for the last three terms of Eq. (4.27), we have

$$\begin{aligned}\delta T &= \left[ \frac{\partial w}{\partial \dot{x}} \delta x + \frac{\partial w}{\partial \dot{y}} \delta y + \frac{\partial w}{\partial \dot{z}} \delta z \right]_{q_1}^{q_2} \\ &\quad - \int_{q_1}^{q_2} \left( \frac{d}{dq} \frac{\partial w}{\partial \dot{x}} - \frac{\partial w}{\partial x} \right) \delta x \, dq \\ &\quad - \int_{q_1}^{q_2} \left( \frac{d}{dq} \frac{\partial w}{\partial \dot{y}} - \frac{\partial w}{\partial y} \right) \delta y \, dq \\ &\quad - \int_{q_1}^{q_2} \left( \frac{d}{dq} \frac{\partial w}{\partial \dot{z}} - \frac{\partial w}{\partial z} \right) \delta z \, dq\end{aligned} \tag{4.28}$$

Since the curves have fixed end points $A$ and $B$, $\delta x = \delta y = \delta z = 0$ at these points. Therefore, the first term in the right-hand side of Eq. (4.28) vanishes. If one of the curves, say $\Gamma$, is the minimum time path from point $A$ to point $B$, then the remaining integrals of Eq. (4.28) must also vanish. Hence the following conditions must hold:

$$\begin{gathered}\frac{d}{dq}\left(\frac{\partial w}{\partial \dot{x}}\right) - \frac{\partial w}{\partial x} = 0, \qquad \frac{d}{dq}\left(\frac{\partial w}{\partial \dot{y}}\right) - \frac{\partial w}{\partial y} = 0 \\ \frac{d}{dq}\left(\frac{\partial w}{\partial \dot{z}}\right) - \frac{\partial w}{\partial z} = 0\end{gathered} \tag{4.29}$$

Equation (4.29) is known as Euler's equation for the extremals of $\int w \, dq$ in the calculus of variations (e.g., Courant and John, 1974, p. 755; Gelfand and Fomin, 1963, p. 15).

Using the definition of $w$ from Eq. (4.26), we may rewrite Eq. (4.29) as

$$
\begin{aligned}
&\frac{d}{dq}\left[\frac{\dot{x}}{v(\dot{x}^2+\dot{y}^2+\dot{z}^2)^{1/2}}\right] - (\dot{x}^2+\dot{y}^2+\dot{z}^2)^{1/2}\frac{\partial}{\partial x}\left(\frac{1}{v}\right) = 0\\
(4.30)\qquad &\frac{d}{dq}\left[\frac{\dot{y}}{v(\dot{x}^2+\dot{y}^2+\dot{z}^2)^{1/2}}\right] - (\dot{x}^2+\dot{y}^2+\dot{z}^2)^{1/2}\frac{\partial}{\partial y}\left(\frac{1}{v}\right) = 0\\
&\frac{d}{dq}\left[\frac{\dot{z}}{v(\dot{x}^2+\dot{y}^2+\dot{z}^2)^{1/2}}\right] - (\dot{x}^2+\dot{y}^2+\dot{z}^2)^{1/2}\frac{\partial}{\partial z}\left(\frac{1}{v}\right) = 0
\end{aligned}
$$

The parameter $q$ along the minimum time path $\Gamma$ is still arbitrary. If we choose $q = s$, the arc length along $\Gamma$, then in order to satisfy Eq. (4.24), we must have

$$(\dot{x}^2+\dot{y}^2+\dot{z}^2)^{1/2} = 1 \tag{4.31}$$

along $\Gamma$. Hence, Eq. (4.30) reduces to

$$
\begin{aligned}
&\frac{d}{ds}\left(\frac{1}{v}\frac{dx}{ds}\right) - \frac{\partial}{\partial x}\left(\frac{1}{v}\right) = 0, \qquad \frac{d}{ds}\left(\frac{1}{v}\frac{dy}{ds}\right) - \frac{\partial}{\partial y}\left(\frac{1}{v}\right) = 0\\
(4.32)\qquad &\frac{d}{ds}\left(\frac{1}{v}\frac{dz}{ds}\right) - \frac{\partial}{\partial z}\left(\frac{1}{v}\right) = 0
\end{aligned}
$$

When multiplied by a reference velocity $v_0$, Eq. (4.32) is exactly the same as the ray equation given by Eq. (4.21).

## 4.3. Numerical Solutions of the Ray Equation

In order to study the heterogeneous structure of the earth, several different techniques to trace seismic rays in three dimensions have been developed; for example, see Jackson (1970), Jacob (1970), Julian (1970), Wesson (1971), Yang and Lee (1976), Julian and Gubbins (1977), Pereyra *et al.* (1980), Lee *et al.* (1982b), and Luk *et al.* (1982). Some authors formulated seismic ray tracing as an initial value problem, whereas others formulated it as a two-point boundary value problem. These two approaches and a unified formulation are described in the following subsections.

As pointed out by Wesson (1971), tracing seismic rays between two end points is required in many seismological applications, such as earthquake location (e.g., Engdahl, 1973; Engdahl and Lee, 1976) and determining three-dimensional velocity structure under a seismic array (e.g., Aki and Lee, 1976; Lee *et al.*, 1982a). However, computer programs to trace seismic rays are complex and time consuming, so they have not been widely applied in microearthquake studies.

### 4.3.1. Initial Value Formulation

The ray equation can be solved numerically as an initial value problem. Eliseevnin (1965) presented an initial value formulation for the propagation of acoustic waves in a heterogeneous medium. Since the ray equation for seismic waves is the same as that for acoustic waves, Eliseevnin's formulation can be applied directly to seismological problems. For the two-dimensional case, Eliseevnin derived a set of three first-order differential equations from the eikonal equation. For the three-dimensional case, he gave a set of six first-order equations derived in a manner analogous to the two-dimensional case. These equations are

$$
\begin{aligned}
&dx/dt = v\cos\alpha, \qquad dy/dt = v\cos\beta, \qquad dz/dt = v\cos\gamma \\
&\frac{d\alpha}{dt} = \frac{\partial v}{\partial x}\sin\alpha - \frac{\partial v}{\partial y}\cot\alpha\cos\beta - \frac{\partial v}{\partial z}\cot\alpha\cos\gamma \\
&\frac{d\beta}{dt} = -\frac{\partial v}{\partial x}\cos\alpha\cot\beta + \frac{\partial v}{\partial y}\sin\beta - \frac{\partial v}{\partial z}\cot\beta\cos\gamma \\
&\frac{d\gamma}{dt} = -\frac{\partial v}{\partial x}\cos\alpha\cot\gamma - \frac{\partial v}{\partial y}\cos\beta\cot\gamma + \frac{\partial v}{\partial z}\sin\gamma
\end{aligned}
\tag{4.33}
$$

where $\alpha$, $\beta$, and $\gamma$ are the instantaneous direction angles of the ray at point $(x, y, z)$ in a heterogeneous and isotropic medium in which the velocity is specified by $v = v(x, y, z)$, and $t$ is time. The direction cosines are defined by

$$\cos\alpha = dx/ds, \qquad \cos\beta = dy/ds, \qquad \cos\gamma = dz/ds \tag{4.34}$$

where $ds$ is an element of the ray path. The first three members of Eq. (4.33) specify the change of ray position with respect to time, and the last three members specify the change of ray direction with respect to time. The six initial conditions for Eq. (4.33) are provided by the three spatial coordinates of the source and the three direction angles of the ray at the source. If they are specified, then Eq. (4.33) can be solved numerically by integration as described in many texts (e.g., Acton, 1970; Gear, 1971; Shampine and Gordon, 1975).

Equation (4.33) is given in the Cartesian coordinate system. In microearthquake studies, this coordinate system is appropriate because the space under consideration is small. However, the spherical coordinate system should be used for global problems. For example, Jacob (1970) and Julian (1970) have derived equivalent sets of equations for this case.

The initial value formulation has been applied to a number of seismological problems. For example, Jacob (1970) and Julian (1970) developed numerical techniques to trace seismic rays in a heterogeneous medium in

order to study the propagation of seismic waves in island arc structures. Engdahl (1973) and Engdahl and Lee (1976) applied the ray tracing technique as developed by Julian (1970) to relocate earthquakes in the central Aleutians and in central California, respectively.

### *4.3.2. Boundary Value Formulation*

In many seismological applications, tracing seismic rays between two end points is required. It is therefore natural to seek a solution of the ray equation with the spatial coordinates of the two end points as boundary conditions. For example, Wesson (1971) presented a boundary value formulation for two-point seismic ray tracing in a heterogeneous and isotropic medium. He noted that the three second-order members of the ray equation [Eq. (4.32)] are not independent, because the direction cosines [Eq. (4.34)] are related by Eq. (4.16). If the ray path is parameterized by

$$y = y(x), \qquad z = z(x) \tag{4.35}$$

and the coordinate system is transformed such that the two end points lie in the $xz$ plane, then Eq. (4.32) reduces to two second-order equations

$$\begin{aligned} &\frac{d}{dx}\left[\frac{y'}{v(1 + y'^2 + z'^2)^{1/2}}\right] + \frac{(1 + y'^2 + z'^2)^{1/2}}{v^2}\frac{\partial v}{\partial y} = 0 \\ &\frac{d}{dx}\left[\frac{z'}{v(1 + y'^2 + z'^2)^{1/2}}\right] + \frac{(1 + y'^2 + z'^2)^{1/2}}{v^2}\frac{\partial v}{\partial z} = 0 \end{aligned} \tag{4.36}$$

where $y' = dy/dx$, and $z' = dz/dx$.

By using central finite differences to approximate the derivatives in Eq. (4.36), Wesson (1971) derived a set of nonlinear algebraic equations which he solved by an iterative procedure. For two selected areas in California, he was able to construct theoretical velocity models that are consistent with travel time data from explosions and with the known geological structure.

Chander (1975) used a method due originally to L. Euler that applied a sum to approximate the integral for the travel time and solved for the minimum time path directly. Yang and Lee (1976) showed that this formulation was equivalent to the central finite-difference approximation used by Wesson (1971).

Yang and Lee (1976) introduced a different technique for solving the two-point seismic ray tracing problem. In order to reduce the ray equation to a set of first-order equations they recast Eq. (4.36) into

$$\begin{aligned} y'' &= F_1(y', z', z'', v, v_x, v_y, v_z) \\ z'' &= F_2(z', y', y'', v, v_x, v_y, v_z) \end{aligned} \tag{4.37}$$

where

$$F_1 \equiv (1 + z'^2)^{-1}\{(\xi^2/v)[v_x y' - v_y(1 + z'^2) + v_z z' y'] + z' z'' y'\}$$
$$F_2 \equiv (1 + y'^2)^{-1}\{(\xi^2/v)[v_x z' - v_z(1 + y'^2) + v_y y' z'] + y' y'' z'\} \tag{4.38}$$

$$\xi = (1 + y'^2 + z'^2)^{1/2} \tag{4.39}$$

$$v_x = \partial v/\partial x, \qquad v_y = \partial v/\partial y, \qquad v_z = \partial v/\partial z \tag{4.40}$$

They noted that second- or higher-order systems of ordinary differential equations could be reduced to first-order systems by introducing auxiliary variables. They defined

$$y_1 \equiv y, \quad y_2 \equiv y_1' = y'; \qquad z_1 \equiv z, \quad z_2 \equiv z_1' = z' \tag{4.41}$$

as new variables and reduced Eq. (4.37) to a system of four first-order equations:

$$y_1' = y_2, \qquad y_2' = F_1, \qquad z_1' = z_2, \qquad z_2' = F_2 \tag{4.42}$$

This system of equations was solved by using an adaptive finite-difference program later published by Lentini and Pereyra (1977). For two-dimensional linear velocity models with known analytic solutions for the minimum time paths, Yang and Lee (1976) showed that their approach was more accurate and used less computer time than the central finite-difference technique used by Wesson (1971).

Although the parameterization method adopted by Wesson (1971) and Yang and Lee (1976) had two instead of three second-order equations to be solved, Julian and Gubbins (1977) pointed out its inherent difficulty. If the ray path is defined by functions $y(x)$ and $z(x)$ as in Eq. (4.35), these functions can be multiple valued and can have infinite derivatives at turning points. Therefore, it is better to solve the ray equations parameterized in arc length such as that given in Eq. (4.32). Starting from Euler's equation [Eq. (4.29)], Julian and Gubbins (1977) chose the parameter $q$ to be:

$$q = s/S \tag{4.43}$$

and derived the following set of second-order equations:

$$\begin{aligned} -u_x(\dot{y}^2 + \dot{z}^2) + u_y\dot{x}\dot{y} + u_z\dot{x}\dot{z} + u\ddot{x} &= 0 \\ -u_y(\dot{x}^2 + \dot{z}^2) + u_x\dot{x}\dot{y} + u_z\dot{y}\dot{z} + u\ddot{y} &= 0 \\ \dot{x}\ddot{x} + \dot{y}\ddot{y} + \dot{z}\ddot{z} &= 0 \end{aligned} \tag{4.44}$$

where $s$ is an element of arc length, $S$ is the total length of the ray path between the two end points, $u$ is the slowness or the reciprocal of the velocity, the dot symbol indicates differentiation with respect to $q$, and $u_x$,

$u_y$, and $u_z$ denote partial derivatives of $u$ with respect to $x$, $y$, and $z$, respectively. By using central finite differences to approximate the derivatives, Eq. (4.44) was reduced to a set of nonlinear algebraic equations which was solved by an iterative procedure.

### *4.3.3. A Unified Formulation*

In the last decade, accurate and efficient numerical methods in solving boundary value and initial value problems have been developed by mathematicians (e.g., Gear, 1971; Keller, 1968, 1976; Lentini and Pereyra, 1977; Roberts and Shipman, 1972; Shampine and Gordon, 1975). Following the approach by Pereyra *et al.* (1980), we will describe a unified formulation for the seismic ray tracing problem. This formulation is suitable for solving the problem by either the boundary value or the initial value approach. In essence, solving the seismic ray tracing problem can be considered as an example of solving a set of first-order differential equations. In order to take advantage of recent numerical methods, the ray equation will be cast into a form suitable for general first-order system solvers.

We begin by introducing a position vector $\mathbf{r}$ defined by

$$\mathbf{r} = \begin{pmatrix} x \\ y \\ z \end{pmatrix} \tag{4.45}$$

and slowness $u$ defined as the reciprocal of the velocity $v$, i.e.,

$$u(\mathbf{r}) = 1/v(\mathbf{r}) \tag{4.46}$$

The general ray equation as given by Eq. (4.32) may then be written compactly as

$$\frac{d}{ds}\left[u\left(\frac{d\mathbf{r}}{ds}\right)\right] = \nabla u \tag{4.47}$$

where $\nabla u$ is the gradient of $u$, i.e.,

$$\nabla u = \begin{pmatrix} \partial u/\partial x \\ \partial u/\partial y \\ \partial u/\partial z \end{pmatrix} \tag{4.48}$$

By carrying out the differentiation in Eq. (4.47), we have

$$\frac{d^2\mathbf{r}}{ds^2} = \frac{1}{u}\left(\nabla u - \frac{d\mathbf{r}}{ds}\frac{du}{ds}\right) \tag{4.49}$$

Let us denote $du/ds$ by $G$, then according to the chain rule of differentiation

$$G \equiv \frac{du(\mathbf{r})}{ds} = \frac{\partial u}{\partial x}\frac{dx}{ds} + \frac{\partial u}{\partial y}\frac{dy}{ds} + \frac{\partial u}{\partial z}\frac{dz}{ds} \tag{4.50}$$
$$= u_x\dot{x} + u_y\dot{y} + u_z\dot{z}$$

where the dot symbol denotes differentiation with respect to $s$, and $u_x = \partial u/\partial x$, $u_y = \partial u/\partial y$, and $u_z = \partial u/\partial z$. Thus Eq. (4.49) may be written as three second-order differential equations

$$\ddot{x} = v(u_x - G\dot{x}), \qquad \ddot{y} = v(u_y - G\dot{y}), \qquad \ddot{z} = v(u_z - G\dot{z}) \tag{4.51}$$

If we denote the variables to be solved by a vector $\boldsymbol{\omega}$ whose components are

$$\begin{aligned} \omega_1 &= x, & \omega_2 &= \dot{x}, & \omega_3 &= y \\ \omega_4 &= \dot{y}, & \omega_5 &= z, & \omega_6 &= \dot{z} \end{aligned} \tag{4.52}$$

then Eq. (4.51) is equivalent to the following six first-order differential equations:

$$\begin{aligned} \dot{\omega}_1 &= \omega_2, & \dot{\omega}_3 &= \omega_4 \\ \dot{\omega}_2 &= v(u_x - G\omega_2), & \dot{\omega}_4 &= v(u_y - G\omega_4), \\ \dot{\omega}_5 &= \omega_6 \\ \dot{\omega}_6 &= v(u_z - G\omega_6) \end{aligned} \tag{4.53}$$

where $G$ as given by Eq. (4.50) is

$$G = u_x\omega_2 + u_y\omega_4 + u_z\omega_6 \tag{4.54}$$

Since in many seismological applications, the travel time between point $A$ and point $B$, $T = \int_A^B u\,ds$, is of utmost interest, we introduce an additional variable $\omega_7$ to represent the partial travel time $\tau$, along a segment of the ray path from point $A$. The corresponding differential equation is simply $\dot{\omega}_7 = u$. With this addendum, the total travel time is given by $T = \tau$ (at point $B$) $= \omega_7(S)$, where $S$ is the total path length, and is computed to the same precision as the coordinates describing the ray path. To determine $S$ (which is a constant for a given ray path), we introduce one more variable, $\omega_8 = S$, and its corresponding differential equation, $\dot{\omega}_8 = 0$. It is also computationally convenient to scale the arc length $s$ such that its value is between 0 and 1. We therefore introduce a new variable $t$ for $s$ such that

$$t = s/S \tag{4.55}$$

and we use the prime (′) symbol to denote differentiation with respect to $t$.

Thus the final set of eight first-order differential equations to be solved is

$$
\begin{aligned}
\omega_1' &= \omega_8\omega_2, & \omega_5' &= \omega_8\omega_6 \\
\omega_2' &= \omega_8 v(u_x - G\omega_2), & \omega_6' &= \omega_8 v(u_z - G\omega_6) \\
\omega_3' &= \omega_8\omega_4, & \omega_7' &= \omega_8 u \\
\omega_4' &= \omega_8 v(u_y - G\omega_4), & \omega_8' &= 0
\end{aligned}
\tag{4.56}
$$

$$t \in [0, 1]$$

The variables corresponding to the solution of these equations are

$$
\begin{aligned}
&\omega_1 = x, \quad \omega_2 = dx/ds, \quad \omega_3 = y, \quad \omega_4 = dy/ds \\
&\omega_5 = z, \quad \omega_6 = dz/ds, \quad \omega_7 = \tau, \quad \omega_8 = S
\end{aligned}
\tag{4.57}
$$

The boundary conditions are

$$
\begin{aligned}
&\omega_1(0) = x_A, \quad \omega_3(0) = y_A, \quad \omega_5(0) = z_A \\
&\omega_1(1) = x_B, \quad \omega_3(1) = y_B, \quad \omega_5(1) = z_B \\
&\omega_7(0) = 0, \quad \omega_2^2(0) + \omega_4^2(0) + \omega_6^2(0) = 1
\end{aligned}
\tag{4.58}
$$

where the coordinates for point $A$ are $(x_A, y_A, z_A)$ and those for point $B$ are $(x_B, y_B, z_B)$. The boundary condition for $\omega_7$ is determined by the fact that the partial travel time at the initial point $A$ is zero. The last boundary condition in Eq. (4.58) simply states that the sum of squares of direction cosines is unity, as given by Eq. (4.16).

Equation (4.53) is a set of six first-order differential equations which are simple and exhibit a high degree of symmetry. This set of equations is equivalent to either Eq. (4.33) or Eq. (4.44) and is easier to solve using recently developed numerical methods. Equation (4.56) is an extension of Eq. (4.53) so that the travel time and the ray path can be solved together. Otherwise, the travel time would have to be computed by numerial integration after the ray path is solved.

Pereyra *et al.* (1980) described in detail how to solve a first-order system of nonlinear ordinary differential equations subject to general nonlinear two-point boundary conditions, such as Eqs. (4.56)–(4.58). In their first-order system solver, high accuracy and efficiency were achieved by using variable order finite-difference methods on nonuniform meshes which were selected automatically by the program as the computation proceeded. The method required the solution of large, sparse systems of nonlinear equations, for which a fairly elaborate iterative procedure was designed. This in turn required a special linear equation solver that took into account the structure of the resulting matrix of coefficients. The variable mesh technique allowed the program to adapt itself to the particu-

lar problem at hand, and thus it produced more detailed computations where it was necessary, as in the case of highly curved seismic rays.

Lee *et al.* (1982b) applied the numerical technique developed by Pereyra *et al.* (1980) to trace seismic rays in several two- and three-dimensional velocity models. Three different types of models were considered: continuous and piecewise continuous velocity models given in analytic form, and general models specified by velocity values at grid points of a nonuniform mesh. Results of their numerical solutions were in excellent agreement with several known analytic solutions.

Using an initial value approach for tracing seismic rays, Luk *et al.* (1982) noted that solving Eq. (4.53) was computationally more efficient than solving Eq. (4.33) because trigonometric functions were not involved. They solved Eq. (4.53) by numerical integration using the DEROOT subroutine described by Shampine and Gordon (1975). Thus starting from a given seismic source, a set of initial direction angles may be used to trace out a corresponding set of ray paths. This is very useful in studying the behavior of seismic rays in a heterogeneous medium.

For two-point seismic ray tracing, one may solve a series of initial value problems starting from one end point and design a scheme so that the ray converges to the other end point. Luk *et al.* (1982) solved Eq. (4.53) by shooting a ray from the source and adjusting the ray to hit the receiver using a nonlinear equation solver. This technique was found to be just as efficient as the method of Pereyra *et al.* (1980) which used a boundary value approach.

## 4.4. Computing Travel Time, Derivatives, and Take-Off Angle

In many seismological problems, such as earthquake location, we need to compute travel times between a source and a set of stations, and the corresponding spatial derivatives evaluated at the source. Take-off angles of the seismic rays at the source to a set of stations are also needed to determine the fault-plane solution. For a heterogeneous earth model, travel times, derivatives, and take-off angles can be computed by solving the ray equation as discussed in the previous section. But in practice, we may not have enough information to construct a realistic three-dimensional model for the velocity structure of the crust and upper mantle beneath a microearthquake network. Furthermore, it is expensive to solve the three-dimensional ray equation numerically. For instance, about 0.3 sec CPU time in a large computer (e.g., IBM 370/168) is required to find the minimum time path between a source and a station in a typical three-dimensional heterogeneous model. Because we may need to trace thou-

sands of rays in a given problem, it is not economical at present to apply these numerical ray tracing techniques in routine microearthquake studies. Consequently, much simplified velocity models are used. Before we discuss these models, we will derive formulas to compute travel time derivatives and the take-off angle for the three-dimensional heterogeneous case. These formulas are readily adaptable to the simplified models.

### *4.4.1. Heterogeneous Velocity Model*

In the unified formulation (Section 4.3.3), the minimum travel time is one of the variables to be solved from Eq. (4.56). In the solution of Eq. (4.56), we also obtain the variables $dx/ds$, $dy/ds$, and $dz/ds$. These variables are the direction cosines of the ray as given by Eq. (4.34). Using a variational technique due to R. Comer (written communication, 1979), we now derive formulas for the spatial derivatives of the travel time in terms of the direction cosines of the ray at the source. The formula for the take-off angle at the source follows readily from these derivatives.

Let us consider the minimum time path $\Gamma_1$ between a source at point $A$ and a station at point $B$. Let the spatial position of point $A$ be $\mathbf{r}_1 = (x_1, y_1, z_1)$, and that for point $B$ be $\mathbf{r}_2 = (x_2, y_2, z_2)$. Let us also consider a neighboring minimum time path $\Gamma_2$ between points $C$ and $B$, where $C$ is a neighboring point of $A$ and its spatial position is given by $\mathbf{r}_1 + \delta\mathbf{r}_1$. Let the position along each path be parameterized by an arbitrary parameter $q$ as discussed in Section 4.2.2, such that $q = q_1$ at point $A$ and point $C$, and $q = q_2$ at point $B$.

The variation of travel time $T$ on passing from $\Gamma_1$ to $\Gamma_2$ is given by Eq. (4.28). Because $\Gamma_1$ and $\Gamma_2$ are minimum time paths, they satisfy Euler's equation as given by Eq. (4.29). Thus, the three integrals on the right-hand side of Eq. (4.28) vanish, and Eq. (4.28) reduces to

$$\delta T = \left[\frac{\partial w}{\partial \dot{x}}\,\delta x + \frac{\partial w}{\partial \dot{y}}\,\delta y + \frac{\partial w}{\partial \dot{z}}\,\delta z\right]_{q_1}^{q_2} \tag{4.59}$$

Because the second end point $B$ is the same for $\Gamma_1$ and $\Gamma_2$, the right-hand side of Eq. (4.59) evaluated at $q = q_2$ is zero. Therefore, the variation of travel time is

$$\begin{aligned}\delta T &= -\left(\frac{\partial w}{\partial \dot{x}}\,\delta x + \frac{\partial w}{\partial \dot{y}}\,\delta y + \frac{\partial w}{\partial \dot{z}}\,\delta z\right)\bigg|_{q=q_1 \text{ at } A} \\ &= -\frac{\partial w}{\partial \dot{x}}\bigg|_A \delta x_1 - \frac{\partial w}{\partial \dot{y}}\bigg|_A \delta y_1 - \frac{\partial w}{\partial \dot{z}}\bigg|_A \delta z_1\end{aligned} \tag{4.60}$$

where $|_A$ denotes functional evaluation at point $A$. If we introduce slowness $u$ as defined by Eq. (4.46), then Eq. (4.26) which defines $w$ becomes

$$w = u(\dot{x}^2 + \dot{y}^2 + \dot{z}^2)^{1/2} \tag{4.61}$$

By differentiating Eq. (4.61) with respect to $\dot{x}$, $\dot{y}$ and $\dot{z}$, respectively, and using Eq. (4.31), we have

$$\begin{gathered} \partial w/\partial \dot{x} = u\, dx/ds, \qquad \partial w/\partial \dot{y} = u\, dy/ds \\ \partial w/\partial \dot{z} = u\, dz/ds \end{gathered} \tag{4.62}$$

Using these relationships, Eq. (4.60) further reduces to

$$\delta T = -\left(u\,\frac{dx}{ds}\right)\bigg|_A \delta x_1 - \left(u\,\frac{dy}{ds}\right)\bigg|_A \delta y_1 - \left(u\,\frac{dz}{ds}\right)\bigg|_A \delta z_1 \tag{4.63}$$

Noting that $T$ is a function of the six end-point coordinates, the variation $\delta T$ can be written by the chain rule of differentiation as

$$\begin{aligned} \delta T = {} & (\partial T/\partial x_1)\,\delta x_1 + (\partial T/\partial y_1)\,\delta y_1 + (\partial T/\partial z_1)\,\delta z_1 \\ & + (\partial T/\partial x_2)\,\delta x_2 + (\partial T/\partial y_2)\,\delta y_2 + (\partial T/\partial z_2)\,\delta z_2 \end{aligned} \tag{4.64}$$

Because the second end point $B$ is fixed, $\delta x_2 = \delta y_2 = \delta z_2 = 0$, and Eq. (4.64) reduces to

$$\delta T = (\partial T/\partial x)|_A\,\delta x_1 + (\partial T/\partial y)|_A\,\delta y_1 + (\partial T/\partial z)|_A\,\delta z_1 \tag{4.65}$$

By comparing Eq. (4.63) with Eq. (4.65), we have

$$\begin{gathered} \frac{\partial T}{\partial x}\bigg|_A = -\left(u\,\frac{dx}{ds}\right)\bigg|_A, \qquad \frac{\partial T}{\partial y}\bigg|_A = -\left(u\,\frac{dy}{ds}\right)\bigg|_A \\ \frac{\partial T}{\partial z}\bigg|_A = -\left(u\,\frac{dz}{ds}\right)\bigg|_A \end{gathered} \tag{4.66}$$

If we solve the ray equation in the form of Eq. (4.56), then Eq. (4.66) becomes

$$\begin{gathered} \partial T/\partial x|_A = -u(0)\,\omega_2(0), \qquad \partial T/\partial y|_A = -u(0)\,\omega_4(0) \\ \partial T/\partial z|_A = -u(0)\omega_6(0) \end{gathered} \tag{4.67}$$

where $\omega_2$, $\omega_4$, and $\omega_6$ are the second, fourth, and sixth components of the solution vector $\boldsymbol{\omega}$ to Eq. (4.56). Since our normalized parameter $t$ for Eq. (4.56) is zero at point $A$, we write (0) to denote functional value at point $A$. According to Eq. (4.57), $\omega_2(0)$, $\omega_4(0)$, and $\omega_6(0)$ are the direction cosines of the ray at the source.

The direction cosines of the seismic ray are the cosines of the direction angles which are defined with respect to the positive direction of the coordinate axes. By Eq. (4.34) these direction angles are

$$\alpha = \arccos(dx/ds), \qquad \beta = \arccos(dy/ds) \qquad \gamma = \arccos(dz/ds) \tag{4.68}$$

In the usual Cartesian coordinate system, the positive $z$ axis is pointing upward. However, in seismological applications, it is more convenient to let the positive $z$ axis point downward. The take-off angle $\psi$ at the source (with respect to the downward vertical) is just the direction angle $\gamma$ at the source, i.e., $\psi = \gamma|_A$, or

$$\psi = \arccos(dz/ds)|_A \tag{4.69}$$

If we solve the ray equation in the form of Eq. (4.56), then $\omega_6(0)$ is the value of $dz/ds$ at the source. Therefore, Eq. (4.69) may be written as

$$\psi = \arccos[\omega_6(0)] \tag{4.70}$$

Equation (4.66) is very important because it relates the spatial derivatives of the travel time to the direction cosines of the seismic ray and the slowness (i.e., the reciprocal of the velocity) of the medium at the earthquake source. We will use this equation frequently in the following subsections.

### *4.4.2. Constant Velocity Model*

This is the simplest velocity model; the velocity $v$ is a constant and is independent of the spatial coordinates. The minimum time path between any two points $A$ and $B$ is a straight line (i.e., $\overline{AB}$). If the earthquake source is at point $A$ with coordinates $(x_A, y_A, z_A)$, and the receiving station is at point $B$ with coordinates $(x_B, y_B, z_B)$, then the path length $S$ between $A$ and $B$ is $[(x_B - x_A)^2 + (y_B - y_A)^2 + (z_B - z_A)^2]^{1/2}$. The travel time $T$ is simply given by

$$T = S/v \tag{4.71}$$

The direction cosines for the ray $\overline{AB}$ are constant and are given by $(x_B - x_A)/S$, $(y_B - y_A)/S$, and $(z_B - z_A)/S$. Using Eq. (4.66), the spatial derivatives of the travel time at the source for this case are

$$\partial T/\partial x|_A = -(x_B - x_A)/(vS), \qquad \partial T/\partial y|_A = -(y_B - y_A)/(vS) \qquad \partial T/\partial z|_A = -(z_B - z_A)/(vS) \tag{4.72}$$

Using Eq. (4.69), the take-off angle at the source is

$$\psi = \arccos[(z_B - z_A)/S] \tag{4.73}$$

In this simple model, we do not really need to apply the formulas for the general three-dimensional case. Eq. (4.72) for the spatial derivatives can

be obtained by differentiating Eq. (4.71). Equation (4.73) for the take-off angle follows from geometrical consideration of the ray path $\overline{AB}$ with respect to the positive $z$ direction.

### *4.4.3. One-Dimensional Continuous Velocity Model*

The next simplest class of velocity models is that in which the velocity is a function of only one of the spatial coordinates. Because seismic velocity generally increases with depth in the earth's crust, it is very common to consider the velocity to be a continuous function of depth, i.e., $v = v(z)$. Let us now consider the two-point seismic ray tracing problem in the $xz$ plane for this case (Fig. 19). The ray equation, Eq. (4.32), reduces to

$$\frac{1}{v(z)}\frac{dx}{ds} = \text{const}, \qquad \frac{d}{ds}\left(\frac{1}{v(z)}\frac{dz}{ds}\right) = -\frac{1}{v^2}\frac{dv}{dz} \tag{4.74}$$

From Fig. 19, the direction cosines are

$$\cos\alpha = dx/ds = \sin\theta, \qquad \cos\gamma = dz/ds = \cos\theta \tag{4.75}$$

where $\theta$ is the angle the ray makes with the positive $z$ direction. The first

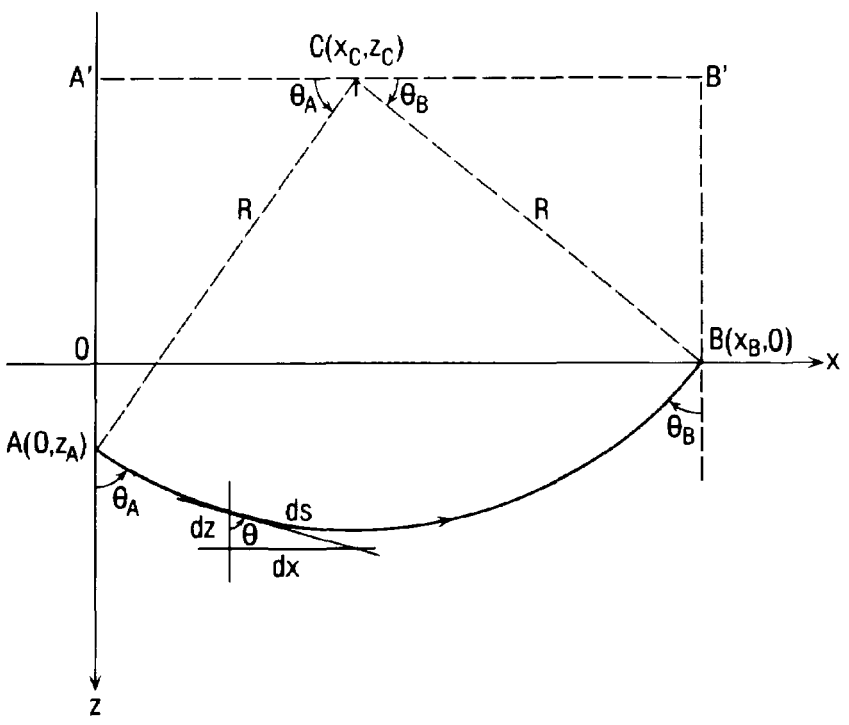


**Fig. 19.** Geometry of seismic ray tracing in the $xz$ plane where the velocity $v = v(z)$. The example shown here is for the case where $v$ is a linear function of $z$.

member of Eq. (4.74) is then

$$\sin\theta/v(z) = \text{const} \equiv p \tag{4.76}$$

This equation is Snell's law, and $p$ is called the ray parameter. Thus the ratio of the sine of the inclination angle of a ray to the velocity is a constant along any given ray path. The second member of Eq. (4.74) reduces to (Officer, 1958, p. 48)

$$d\theta/ds = p\, dv/dz \tag{4.77}$$

This equation states that the curvature of a ray, $d\theta/ds$, is directly proportional to the velocity gradient, $dv/dz$. For a region where the velocity increases with depth, $dv/dz$ is positive. Equation (4.77) implies that $d\theta/ds$ is also positive, and thus the ray will curve upward. Similarly, for a region where the velocity decreases with depth, the ray will curve downward.

Referring to Fig. 19 and using Eqs. (4.75)–(4.77), the travel time $T$ from point $A$ to point $B$ is

$$T = \int_A^B \frac{ds}{v(z)} = \int_A^B \frac{dz}{v(z)\cos\theta} = \int_{\theta_A}^{\theta_B} \frac{d\theta}{(dv/dz)\sin\theta} \tag{4.78}$$

where $\theta = \theta_A$ at point $A$ and $\theta = \theta_B$ at point $B$.

Now let us consider the simplest case in which the velocity is linear with depth, i.e.,

$$v(z) = g_0 + gz \tag{4.79}$$

where $g_0$ and $g$ are constants. From Eq. (4.77), we have

$$d\theta/ds = pg = \text{const} \tag{4.80}$$

This equation states that the curvature along any given ray is a constant. Therefore, the ray path is an arc of a circle with radius $R$ given by

$$R = (d\theta/ds)^{-1} = v/(g\sin\theta) \tag{4.81}$$

using Eqs. (4.80) and (4.76). Let us denote the center of this circle by the point $C$ at $(x_C, z_C)$, as shown in Fig. 19. We now proceed to determine $x_C$ and $z_C$ in terms of the velocity model parameters, $g_0$ and $g$, and the coordinates of the two end points $A$ and $B$. In our example shown in Fig. 19, we choose a coordinate system such that point $A$ is at $(0, z_A)$ and point $B$ is at $(x_B, 0)$. We observe that $\overline{AC}^2 = \overline{A'C}^2 + \overline{A'A}^2 = \overline{R}^2 = \overline{BC}^2 = \overline{B'C}^2 + \overline{B'B}^2$ or

$$x_C^2 + (z_A - z_C)^2 = (x_B - x_C)^2 + z_C^2 \tag{4.82}$$

From Fig. 19, we observe that $\sin\theta_B = \overline{BB'}/\overline{BC} = -z_C/R$, and $R = g_0/(g\sin\theta_B)$ at point $B$ using Eqs. (4.81) and (4.79). Thus, $z_C = -g_0/g$.

Substituting this result into Eq. (4.82), we can solve for $x_C$. Hence, the center of the circular ray path, point $C$, is given by

$$x_C = \frac{(x_B^2 - 2(g_0/g)z_A - z_A^2)}{2x_B}, \qquad z_C = \frac{-g_0}{g} \tag{4.83}$$

From Eqs. (4.78)–(4.79), the travel time $T$ from point $A$ to point $B$ is given by

$$T = \int_{\theta_A}^{\theta_B} \frac{d\theta}{g \sin \theta} = \frac{1}{g} \ln \left[ \frac{\tan(\theta_B/2)}{\tan(\theta_A/2)} \right] \tag{4.84}$$

where

$$\theta_A = \arctan[(z_A - z_C)/x_C], \qquad \theta_B = \arctan[-z_C/(x_B - x_C)] \tag{4.85}$$

According to Eqs. (4.66) and (4.75), the spatial derivatives of $T$ at the source are

$$\begin{aligned} \partial T/\partial x|_A &= -\sin \theta_A/(g_0 + gz_A) \\ \partial T/\partial z|_A &= -\cos \theta_A/(g_0 + gz_A) \end{aligned} \tag{4.86}$$

The take-off angle at the source with respect to the downward vertical $\psi$ is just the angle $\theta_A$, i.e.,

$$\psi = \theta_A \tag{4.87}$$

For treating the more general case in which the velocity is an arbitrary function of depth, there have been some recent advances. An important concept is $\tau(p)$, the intercept or delay time function introduced by Gerver and Markushevich (1966, 1967). It is defined by $\tau(p) = T(p) - pX(p)$, where $T$ is the travel time, $X$ is the epicentral distance, and $p$ is the ray parameter defined by Eq. (4.76). The expression for $\tau(p)$ is analogous to the more familiar equation $T_i = T - X/v$ for a refracted wave along a layer of velocity $v$, and $T_i$ is the intercept time. The delay time function $\tau(p)$ has several convenient properties. Whereas travel time $T$ may be a multiple-valued function of $X$ due to triplications, the corresponding $\tau(p)$ function is always single valued and monotonically decreasing. Calculations based on the $\tau(p)$ function have the advantages that low-velocity regions can be treated in a straightforward way, and that considerable geometric and physical interpretation can be applied to the mathematical formalism. This approach has been useful in calculating travel times for synthetic seismograms (e.g., Dey-Sarkar and Chapman, 1978), and for inversion of travel-time data for the velocity function $v(z)$ (e.g., Garmany *et al.*, 1979). For further details, readers are referred to the above-mentioned works and references therein.

### *4.4.4. One-Dimensional Multilayer Velocity Models*

The most commonly used velocity model in microearthquake studies consists of a sequence of horizontal layers of constant velocity, each layer having a higher velocity than the layer above it. For the source and the station at the same elevation, the ray paths and travel times are well known (e.g., Officer, 1958, pp. 239–242). For an earthquake source at depth, the specific formulas involved have been given by Eaton (1969, pp. 26–38). We now derive an equivalent set of formulas by a systematic approach using results from Section 4.4.1.

Let us first consider the simple case of a single layer of thickness $h_1$ and velocity $v_1$ over a half-space of velocity $v_2$ (Fig. 20). For a surface source at point $A$, we consider two possible ray paths to a surface station at point $B$. The travel time of the direct wave, $T_d$, along path $\overline{AB}$ is

$$T_d = \Delta/v_1 \tag{4.88}$$

where $\Delta$ is the epicentral distance between the source and the station, i.e., $\Delta = \overline{AB}$. The travel time of the refracted wave, $T_r$, along path $\overline{ACDB}$ is

$$T_r = (\overline{AC}/v_1) + (\overline{CD}/v_2) + (\overline{DB}/v_1) \tag{4.89}$$

Using Snell's law, we have

$$\sin\theta/v_1 = \sin 90°/v_2 = \sin\phi/v_1 \tag{4.90}$$

so that $\theta = \phi$ (Fig. 20), and $\overline{AC} = \overline{DB}$. Consequently, Eq. (4.89) can be written in terms of $\theta$, $h_1$, and $\Delta$ as (see Officer, 1958, p. 240),

$$T_r = \frac{\Delta}{v_2} + \frac{2h_1}{v_1}\cos\theta \tag{4.91}$$

Using Eqs. (4.88) and (4.91), we can plot travel time versus epicentral

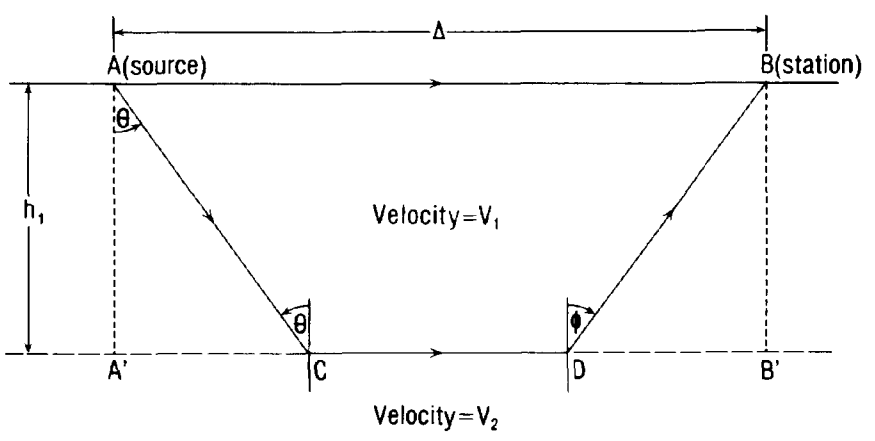


**Fig. 20.** Diagram of direct and refracted paths in a velocity model of one layer over a half-space.

distance as shown in Fig. 21. The travel time versus distance curve for the direct wave is a straight line through the origin with slope of $1/v_1$. The corresponding curve for the refracted wave is also a straight line, but with slope of $1/v_2$ and time intercept at $\Delta = 0$ equal to the second term on the right-hand side of Eq. (4.91). These two straight lines intersect at $\Delta = \Delta_c$, the crossover distance. For $\Delta < \Delta_c$, the first arrival will be a direct wave, whereas the first arrival at $\Delta > \Delta_c$ will be a refracted wave. In our case, it is more useful to consider the critical distance for refraction, i.e., the distance beyond which there is a refracted arrival. With reference to Fig. 20, the minimum refracted path is such that $\overline{CD} = 0$. Thus the critical distance $\xi$ is given by

$$\xi = 2h_1 \tan \theta \tag{4.92}$$

If the velocity of the first layer is greater than the velocity of the underlying half-space, there will be no refracted arrival. The reason is that by Snell's law [Eq. (4.90)], $\sin \phi = v_1/v_2$, and $\phi$ does not exist for the case where $v_1 > v_2$.

Results from a single layer over a half-space can be generalized into the case of $N$ multiple horizontal layers over a half-space. With reference to Fig. 22, the travel times along different paths may be written as

$$\begin{aligned} T_1 &= \frac{\Delta}{v_1}, \qquad T_2 = \frac{\Delta}{v_2} + \frac{2h_1}{v_1} \cos \theta_{12} \\ T_3 &= \frac{\Delta}{v_3} + \frac{2h_1}{v_1} \cos \theta_{13} + \frac{2h_2}{v_2} \cos \theta_{23} \end{aligned} \tag{4.93}$$

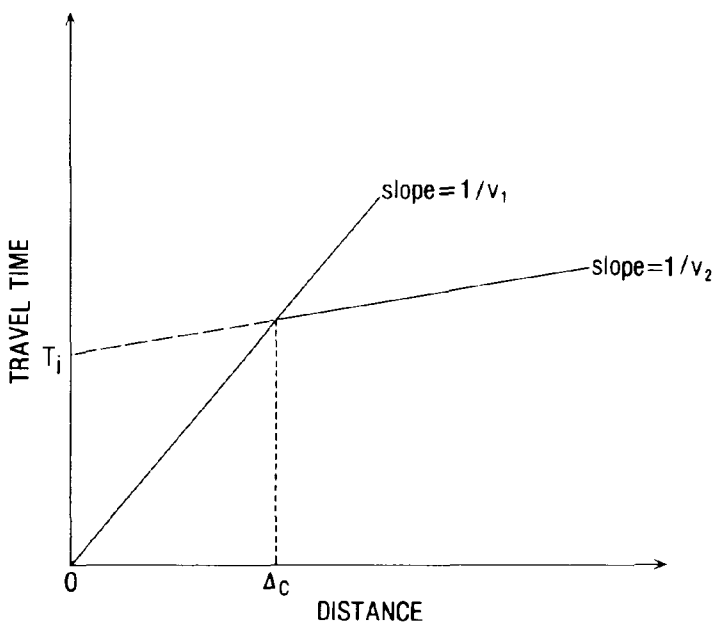


**Fig. 21.** Travel time versus distance for the model illustrated in Fig. 20.

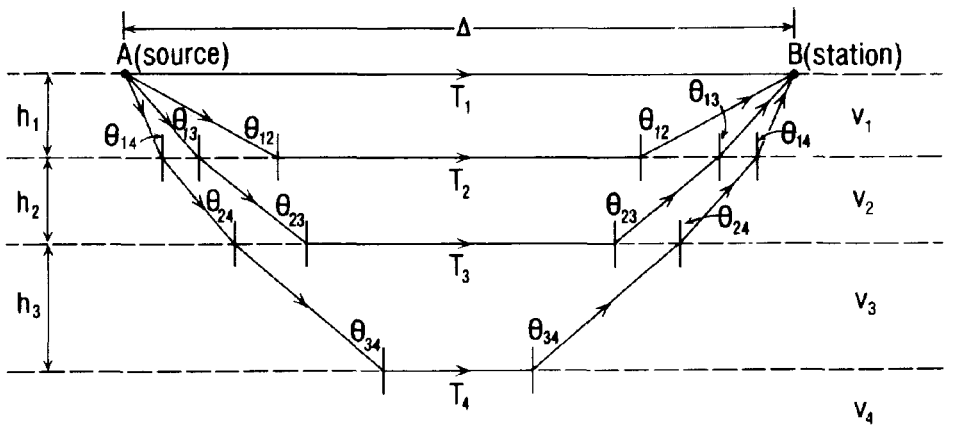


**Fig. 22.** Diagram of travel paths in a velocity model of multiple layers with a source at the surface.

and so on, or in general,

$$T_k = \frac{\Delta}{v_k} + 2\sum_{i=1}^{k-1} \frac{h_i}{v_i} \cos\theta_{ik}, \qquad k = 2, 3, \ldots, N \tag{4.94}$$

The corresponding critical distances may be written in general as

$$\xi_k = 2\sum_{i=1}^{k-1} h_i \tan\theta_{ik}, \qquad k = 2, 3, \ldots, N \tag{4.95}$$

The relations between the angles $\theta_{ik}$ are given by Snell's law and are written in general as

$$\sin\theta_{ik} = v_i/v_k \qquad \text{for} \quad i = 1, 2, \ldots, N-1, \quad k = 2, 3, \ldots, N \tag{4.96}$$

Using Eq. (4.96) and trigonometric relations between sine, cosine, and tangent, we may express Eqs. (4.94)–(4.95) directly in terms of layer velocities

$$\begin{aligned} T_k &= \frac{\Delta}{v_k} + 2\sum_{i=1}^{k-1} \frac{h_i(v_k^2 - v_i^2)^{1/2}}{v_i v_k} \\ \xi_k &= 2\sum_{i=1}^{k-1} \frac{h_i v_i}{(v_k^2 - v_i^2)^{1/2}} \qquad \text{for} \quad k = 2, 3, \ldots, N \end{aligned} \tag{4.97}$$

The first member of Eq. (4.97) shows that the time versus distance relation for a wave refracted along the top of the $k$th layer has a linear form: the slope of the line is $1/v_k$, and the intercept on the time axis is the sum of the down-going and up-going intercept times (with respect to the $k$th layer) through the layers overlying the $k$th layer.

We can now proceed to the general case where the source is at any

arbitrary depth in a model consisting of $N$ multiple horizontal layers over a half-space as shown in Fig. 23. Let the earthquake source be at point $A$ with coordinates $(x_A, y_A, z_A)$, and the station be at point $B$ with coordinates $(x_B, y_B, z_B)$. We construct our model such that the station is at the top of the first layer, and we use $v_i$ and $h_i$ to denote the velocity and the thickness of the $i$th layer, respectively. In Fig. 23, we let the source be inside the $j$th layer at depth $\zeta$ from the top of the $j$th layer. The difference between this case and the surface-source case is that the down-going travel path of the refracted wave starts at depth $z_A$ instead of at the surface. This means that the down-going seismic wave has the following less layers to travel: the first $(j-1)$ layers from the surface, and an imaginary layer within the $j$th layer of thickness $\zeta$. We can therefore write down a set of equations for this case in a manner similar to Eq. (4.97)

$$
\begin{aligned}
T_{jk} &= \frac{\Delta}{v_k} - \frac{\zeta\Omega_{kj}}{v_j v_k} + \sum_{i=1}^{j-1} \frac{h_i\Omega_{ki}}{v_i v_k} + 2\sum_{i=j}^{k-1} \frac{h_i\Omega_{ki}}{v_i v_k} \\
\xi_{jk} &= -\frac{\zeta v_j}{\Omega_{kj}} + \sum_{i=1}^{j-1} \frac{h_i v_i}{\Omega_{ki}} + 2\sum_{i=j}^{k-1} \frac{h_i v_i}{\Omega_{ki}}
\end{aligned}
\tag{4.98}
$$

for $j = 1, 2, \ldots, N-1$ and $k = 2, 3, \ldots, N$, where $T_{jk}$ is the travel time for the ray that is refracted along the top of the $k$th layer from a source at the

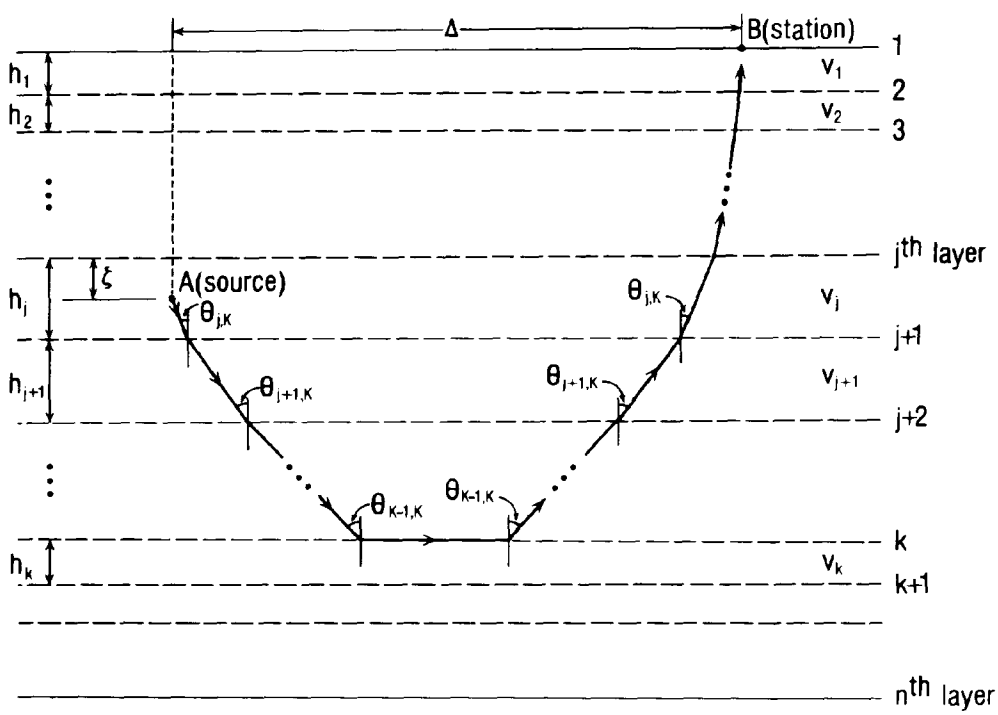


**Fig. 23.** Diagram of the refracted path along the $k$th layer for a source located in the $j$th layer.

$j$th layer, $\xi_{jk}$ is the corresponding critical distance, $\Delta$ is the epicentral distance given by $\Delta = [(x_B - x_A)^2 + (y_B - y_A)^2]^{1/2}$, the thickness $\zeta$ is given by $\zeta = z_A - (h_1 + h_2 + \cdots + h_{j-1})$, the symbol $\Omega_{ki} = (v_k^2 - v_i^2)^{1/2}$, and the symbol $\Omega_{kj} = (v_k^2 - v_j^2)^{1/2}$.

These equations allow us to calculate the travel times for various refracted paths and the corresponding critical distances beyond which refracted waves will exist. In many instances, one of the refracted paths is the minimum time path sought. However, there are cases in which the direct path is the minimum time path. This is considered next.

If the earthquake source is in the first layer (with velocity $v_1$), then the travel time for the direct wave is the same as that in the constant velocity model (see Section 4.4.2), i.e.,

$$T_d = [(x_B - x_A)^2 + (y_B - y_A)^2 + (z_B - z_A)^2]^{1/2}/v_1 \tag{4.99}$$

However, if the earthquake source is in the second or deeper layer, there is no explicit formula for computing the travel time of the direct path. In this case, we must use an iterative procedure to find an angle $\phi$ such that its associated ray will reach the receiving station along a direct path. Let us consider a model where the earthquake source is in the second layer, as shown in Fig. 24. Let the first layer have a thickness $h_1$, and let $v_1$ and $v_2$ be the velocity of the first and the second layer, respectively. In our model the layer velocity increases with depth so that $v_2 > v_1$. We choose a coordinate system such that the $z$ axis passes through the source at point $A$, and the $\eta$ axis passes through the station at point $B$. Let the coordinates

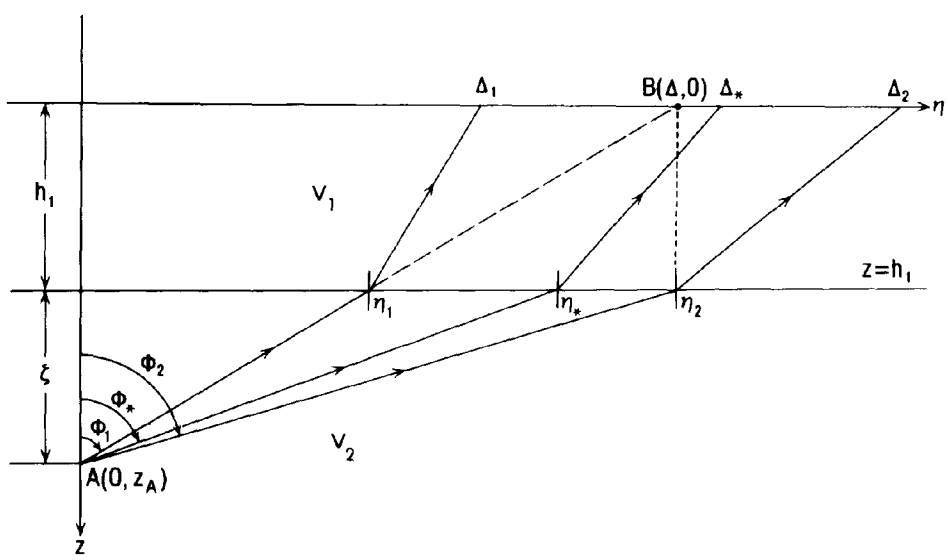


**Fig. 24.** Diagram to illustrate the computation of the travel path of a direct wave for a layered velocity model.

of point $A$ be $(0, z_A)$, and that for point $B$ be $(\Delta, 0)$. For simplicity, we will label the points along the $\eta$ axis by their $\eta$ coordinates; for example, point $\Delta_1$ has the coordinates $(\Delta_1, 0)$. We will also label the points along the line $z = h_1$ by their $\eta$ coordinates; for example, point $\eta_1$ has the coordinates $(\eta_1, h_1)$. We define $\zeta = z_A - h_1$. Let the $\phi$'s be the angles measured from the negative $z$ direction to the lines joining point $A$ with the appropriate points along the line $z = h_1$ (see Fig. 24).

To find by an iterative procedure an angle $\phi$ whose associated ray path will reach the station, we first consider lower and upper bounds ($\phi_1$ and $\phi_2$) for the angle $\phi$. If we join points $A$ and $B$ by a straight line, then $\overline{AB}$ intersects the line $z = h_1$ at point $\eta_1$ such that its $\eta$ coordinate is given by $\eta_1 = \Delta(\zeta/z_A)$. By Snell's law and the fact that $v_2 > v_1$, this ray $\overline{A\eta_1}$ will emerge to the surface at a point with $\eta$ coordinate of $\Delta_1$, which is always less than $\Delta$. Thus the angle $\phi_1$ associated with the ray $\overline{A\eta_1}$ can be selected as the lower bound of $\phi$. To find the upper bound of $\phi$, we let $\eta_2$ be the point directly below the station and on the line $z = h_1$, i.e., $\eta_2 = \Delta$. Again by Snell's law and $v_2 > v_1$, the ray $\overline{A\eta_2}$ will emerge to the surface at a point with $\eta$ coordinate of $\Delta_2$, which is always greater than $\Delta$. Thus the angle $\phi_2$ associated with the ray $\overline{A\eta_2}$ can be selected as the upper bound of $\phi$.

To start the iterative procedure, we consider a trial ray $\overline{A\eta_*}$ and its associated trial angle $\phi_*$ (see Fig. 24) such that $\eta_*$ is approximated by

$$(\eta_* - \eta_1)/(\eta_2 - \eta_1) = (\Delta - \Delta_1)/(\Delta_2 - \Delta_1) \tag{4.100}$$

and

$$\phi_* = \arctan(\eta_*/\zeta) \tag{4.101}$$

By Snell's law and knowing $\eta_*$, we can determine the $\eta$ coordinate, $\Delta_*$, of the point where the ray $\overline{A\eta_*}$ emerges to the surface. In order for the trial angle $\phi_*$ to be acceptable, the ray $\overline{A\eta_*}$ must emerge to the surface very close to the station, i.e., $|\Delta - \Delta_*| < \varepsilon$, where the error limit $\varepsilon$ is typically a few tens of meters. If $|\Delta - \Delta_*| > \varepsilon$, we select a new $\phi_*$ and repeat the same procedure until the trial ray emerges close to the station. To perform the iteration, we must consider the following two cases:

(1) If $\Delta_* > \Delta$, the new $\phi_*$ is chosen between the two rays $\overline{A\eta_1}$ and $\overline{A\eta_*}$. To do this, in Eq. (4.100), the current values for $\Delta_*$ and $\eta_*$ replace $\Delta_2$ and $\eta_2$ respectively, and a new value for $\eta_*$ is computed.

(2) If $\Delta_* < \Delta$, the new $\phi_*$ is chosen between the rays $\overline{A\eta_*}$ and $\overline{A\eta_2}$. To do this, in Eq. (4.100), the current values of $\Delta_*$ and $\eta_*$ replace $\Delta_1$ and $\eta_1$, respectively, and a new value for $\eta_*$ is computed. In both cases, a new value for $\phi_*$ can be obtained from Eq. (4.101).

The preceding procedure for a source in the second layer can be generalized to a source in a deeper layer, say, the $j$th layer. Once a trial angle $\phi_*$ is chosen, we may use Snell's law to compute successive incident angles to each overlying layer until the trial ray reaches the surface at point $\Delta_*$ with the $\eta$ coordinate given by

$$\Delta_* = \eta_* + \sum_{i=j-1}^{1} h_i \tan \theta_i \tag{4.102}$$

where $\theta_j = \phi_*$. The incident angles are related by

$$\frac{\sin \theta_i}{v_i} = \frac{\sin \theta_{i+1}}{v_{i+1}} \qquad \text{for} \quad 1 \le i < j \tag{4.103}$$

where $\theta_i$ is the incident angle for the $i$th layer with velocity $v_i$ and thickness $h_i$. With the proper substitutions, Eq. (4.102) can also be used to calculate $\Delta_1$ and $\Delta_2$.

In this iterative procedure, the trial angle $\phi_*$ converges rapidly to the angle $\phi$ whose associated ray path reaches the station within the error limit $\varepsilon$. Since this ray path consists of $j$ segments of a straight line in each of the $j$ layers, we can sum up the travel time in each layer to obtain the travel time from the source to the station.

Knowing how to compute travel time for both the direct and the refracted paths, we can then select the minimum travel time path. The spatial derivatives and the take-off angle can be computed from the direction cosines using results from Section 4.4.1 as follows.

Let us consider an earthquake source at point $A$ with spatial coordinates $(x_A, y_A, z_A)$, and a station with spatial coordinates $(x_B, y_B, z_B)$. Let us choose a coordinate system such that points $A$ and $B$ lie on the $\eta z$ plane, and $A'$ is the projection of $A$ on $z = z_B$. In Fig. 25, let us consider an element of ray path $ds$ with direction angles $\alpha$, $\beta$, and $\gamma$, and components $dx$, $dy$, and $dz$ (with respect to the $x$, $y$, and $z$ axes, respectively). In Fig. 25a, the projection of $ds$ on the $\eta$ axis is $\sin \gamma \, ds$. In Fig. 25b, this projected element can be related to the components $dx$ and $dy$ of $ds$ by

$$dx = \cos \alpha' \sin \gamma \, ds, \qquad dy = \cos \beta' \sin \gamma \, ds \tag{4.104}$$

where $\alpha'$ and $\beta'$ are the angles between the $\eta$ axis and the $x$ and $y$ axes, respectively. Consequently, from Eq. (4.104) and the definition of direction cosine for $\gamma$, we have

$$\begin{gathered} dx/ds = \cos \alpha' \sin \gamma, \qquad dy/ds = \cos \beta' \sin \gamma \\ dz/ds = \cos \gamma \end{gathered} \tag{4.105}$$

The angles $\alpha'$ and $\beta'$ can be determined from Fig. 25b as

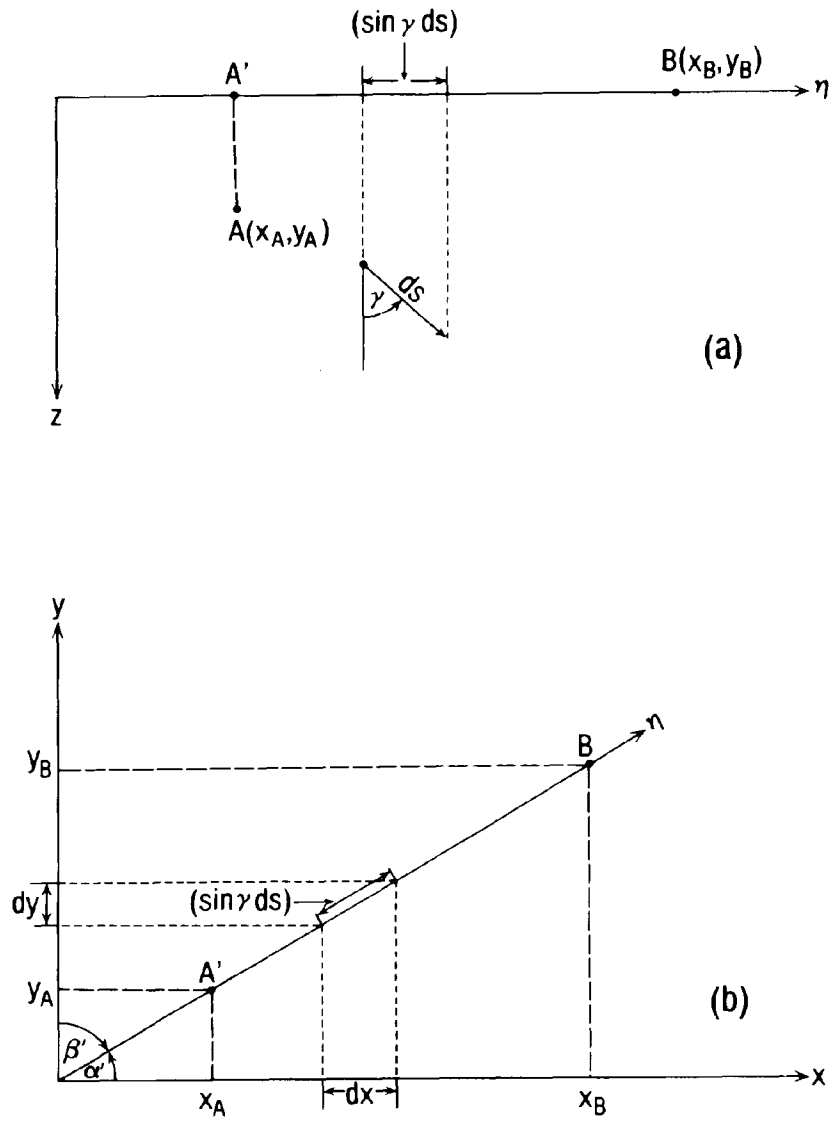


**Fig. 25.** Diagram of the projections of an element of ray path $ds$ on the $\eta z$ plane (a) and on the $xy$ plane (b).

(4.106) $$\cos\alpha' = (x_B - x_A)/\Delta, \qquad \cos\beta' = (y_B - y_A)/\Delta$$

where $\Delta$ is the epicentral distance between points $A'$ and $B$ and is given by

(4.107) $$\Delta = [(x_B - x_A)^2 + (y_B - y_A)^2]^{1/2}$$

For the refracted waves in a multilayer model (see Fig. 23), the direction angle $\gamma$ at the source is the take-off angle for the refracted path. If the earthquake source is in the $j$th layer and the ray is refracted along the top of the $k$th layer, then by Eq. (4.96)

$$\gamma|_A = \theta_{jk} = \arcsin(v_j/v_k) \tag{4.108}$$

Therefore Eq. (4.105) becomes

$$\begin{aligned} dx/ds &= [(x_B - x_A)/\Delta](v_j/v_k) \\ dy/ds &= [(y_B - y_A)/\Delta](v_j/v_k) \\ dz/ds &= [1 - (v_j/v_k)^2]^{1/2} \end{aligned} \tag{4.109}$$

Using Eq. (4.66), the spatial derivatives of the travel time evaluated at the source for this case are

$$\begin{aligned} \partial T_{jk}/\partial x|_A &= -(x_B - x_A)/(\Delta \cdot v_k) \\ \partial T_{jk}/\partial y|_A &= -(y_B - y_A)/(\Delta \cdot v_k) \\ \partial T_{jk}/\partial z|_A &= -(v_k^2 - v_j^2)^{1/2}/(v_j \cdot v_k) \end{aligned} \tag{4.110}$$

and the take-off angle [according to Eq. (4.108)] is

$$\psi_{jk} = \arcsin(v_j/v_k) \tag{4.111}$$

where the limits for $j$ and $k$ are given in Eq. (4.98).

For the direct wave with earthquake source in the first layer, the spatial derivatives of the travel time and the take-off angle are the same as those given in Section 4.4.2 for a constant velocity model.

For the direct wave with earthquake source in the $j$th layer (with velocity $v_j$), we find the direct ray path and its associated angle $\phi$ by an iterative procedure as described previously. The direction angle $\gamma$ at the source is the take-off angle $\psi$ for the direct path. Since the take-off angle is measured from the positive $z$ direction whereas the angle $\phi$ is measured from the negative $z$ direction (see Fig. 24), we have

$$\gamma|_A = \psi = 180° - \phi \tag{4.112}$$

Thus, using Eqs. (4.105), (4.106), and (4.66), and noting that $\sin(180° - \phi) = \sin\phi$, and $\cos(180° - \phi) = -\cos\phi$, the spatial derivatives of the travel time evaluated at the source for this case are

$$\begin{aligned} \partial T/\partial x|_A &= -[(x_B - x_A)/(\Delta \cdot v_j)] \sin\phi \\ \partial T/\partial y|_A &= -[(y_B - y_A)/(\Delta \cdot v_j)] \sin\phi \\ \partial T/\partial z|_A &= \cos\phi/v_j \end{aligned} \tag{4.113}$$

# 5. Generalized Inversion and Nonlinear Optimization

Many scientific problems involve estimating parameters from nonlinear models or solving nonlinear differential equations that describe the physical processes. In the previous chapter, the problem of finding the minimum-time ray path between the earthquake source and a receiving station involves solving a set of first-order differential equations. These equations are approximated by a set of nonlinear algebraic equations, which are then solved by an iterative procedure involving the solution of a set of linear equations. In the next chapter, calculation of earthquake hypocenters will be treated as a nonlinear optimization problem which also involves solving a set of linear equations. Therefore, solving linear equations is frequently required in microearthquake research as it is for other sciences. In fact, 75% of scientific problems deal with solving a set of $m$ simultaneous linear equations for $n$ unknowns, as estimated by Dahlquist and Bjorck (1974, p. 137).

In solving linear equations, it is convenient to use matrix notation as commonly developed in linear algebra or matrix calculus. Readers are assumed to be familiar with vectors and matrices and their properties. Among numerous texts on these topics, we recommend the following: Lanczos (1956, 1961), Noble (1969), G. W. Stewart (1973), and Strang (1976). In general, components of a matrix can be either real or complex numbers. However, in most microearthquake applications, we deal with real numbers. Hence, we will be concerned here only with real matrices.

In matrix notation, the problem of solving a set of linear equations may be written as

$$\mathbf{A}\mathbf{x} = \mathbf{b} \tag{5.1}$$

where $\mathbf{A}$ is a real matrix of $m$ rows by $n$ columns, $\mathbf{x}$ is an $n$-dimensional vector, and $\mathbf{b}$ is an $m$-dimensional vector. Our problem is to solve for the

unknown vector $\mathbf{x}$, given a model matrix $\mathbf{A}$ and a set of observations $\mathbf{b}$. One is very tempted to write down

$$\mathbf{x} = \mathbf{A}^{-1}\mathbf{b} \tag{5.2}$$

where $\mathbf{A}^{-1}$ denotes the inverse of $\mathbf{A}$, and hand the problem to a programmer to solve by a computer. In due time, the programmer brings back the answers and everyone lives happily thereafter. However, it may happen that the scientist is very cautious and notices that a certain unknown that from experience should be positive turns out to be negative as given by the computer. But the programmer assures the scientist that he has used the best matrix inversion subroutine in the computer program library and has checked the program very carefully. The scientist may be at a loss about what to do next. He may look up his old high-school notes on Cramer's rule, sit down to program the problem himself, and discover many surprises. Alternatively, he may consult his colleagues in computer science, and take advantage of recent techniques in computational mathematics to solve his problem.

In order to help the reader become better acquainted with some recent advances in computational mathematics, we briefly review the mathematical, physical, and computational aspects of the inversion problem in the first part of this chapter. In the second part, we briefly discuss nonlinear optimization problems that arise in scientific research and how to reduce these problems to solving linear equations. The material in this chapter includes some fundamental mathematical tools for analyzing scientific data. We recognize that such material is not normally expected to be given in a work such as this one. However, by presenting these mathematical tools, some methods for analyzing microearthquake data may be developed more systematically.

Throughout this chapter, we will refer to many publications treating the inversion problem from the mathematical point of view. There are also numerous papers presenting the inversion problem from the geophysical point of view. Readers may refer, for example, to Backus and Gilbert (1967, 1968, 1970), Jackson (1972), Wiggins (1972), Jupp and Vozoff (1975), Parker (1977), and Aki and Richards (1980).

## 5.1. Mathematical Treatment of Linear Systems

If one is asked to solve a set of linear equations in the form of $\mathbf{Ax} = \mathbf{b}$, it is reasonable to expect that there be as many equations as unknowns. If there are fewer equations than unknowns, we know right away that we are in trouble. If there are more equations than unknowns, we may transform

the overdetermined set of equations into an even-determined one by the least-squares method. Thus on the surface, one may think that $n$ equations are sufficient to determine $n$ unknowns. Unfortunately, this is not always true, as illustrated by the following example:

$$x_1 + x_2 + x_3 = 1, \qquad x_1 - x_2 + x_3 = 3 \qquad 2x_1 + 2x_2 + 2x_3 = 2 \tag{5.3}$$

These three equations are not sufficient to determine the three unknowns because there are actually only two equations, the third equation being a mere repetition of the first. Readers may notice that the determinant for the system of equations in Eq. (5.3) is zero, and hence the system is singular and no inverse exists. However, the solvability of a linear system depends on more than the value of the determinant. For example, a small value for a determinant does not mean that the system is difficult to solve. Let us consider the following system, in which the off-diagonal elements of the matrix are zero:

$$\begin{pmatrix} 10^{-1} & & & \\ & 10^{-1} & & \\ & & \ddots & \\ & & & 10^{-1} \end{pmatrix} \begin{pmatrix} x_1 \\ x_2 \\ \vdots \\ x_{100} \end{pmatrix} = \begin{pmatrix} 1 \\ 1 \\ \vdots \\ 1 \end{pmatrix} \tag{5.4}$$

The determinant is $10^{-100}$, which is very small indeed. But the solution is simple, i.e., $x_1 = x_2 = \cdots = x_{100} = 10$. On the other hand, a reasonable determinant does not mean that the solution is stable. For example,

$$\begin{pmatrix} 2.0 & 4.0 \\ 3.8 & 8.1 \end{pmatrix} \begin{pmatrix} x_1 \\ x_2 \end{pmatrix} = \begin{pmatrix} 2.0 \\ 3.8 \end{pmatrix} \tag{5.5}$$

leads to a simple solution of $\mathbf{x} = \binom{1}{0}$, and the determinant is 1. However, if we perturb the right-hand side to $\mathbf{b} = \binom{2.1}{3.8}$, the solution becomes $\mathbf{x} = \binom{1.81}{-0.38}$. In other words, if $b_1$ is changed by 5%, the solution is entirely different.

### *5.1.1. Analysis of an Even-Determined System*

The preceding discussion clearly demonstrates that solving $n$ linear equations for $n$ unknowns is not straightforward, because we need to know some critical properties of the matrix $\mathbf{A}$. We now present an analysis of the properties of $\mathbf{A}$, and our treatment here closely follows Lanczos (1956, pp. 52–79). We first write Eq. (5.1) in reversed sequence as

$$\mathbf{b} = \mathbf{A}\mathbf{x} \tag{5.6}$$

Geometrically, we may consider both **b** and **x** as $n$-dimensional vectors in an even-determined system. Equation (5.6) says that multiplication of a vector **x** by the matrix **A** generates a new vector **b**, which can be thought of as a transformation of the original vector **x**. Let us investigate the case where the new vector **b** happens to have the same direction as the original vector **x**. In this case, **b** is simply proportional to **x** and we have the condition

$$\mathbf{A}\mathbf{x} = \lambda\mathbf{x} \tag{5.7}$$

Equation (5.7) is really a set of $n$ homogeneous linear equations, i.e., $(\mathbf{A} - \lambda\mathbf{I})\,\mathbf{x} = \mathbf{0}$, where **I** is an identity matrix. It will have a nontrivial solution only if the determinant of the system is zero, i.e.,

$$\begin{vmatrix} A_{11} - \lambda & A_{12} & \cdots & A_{1n} \\ A_{21} & A_{22} - \lambda & \cdots & A_{2n} \\ \vdots & \vdots & \vdots & \vdots \\ A_{n1} & A_{n2} & \cdots & A_{nn} - \lambda \end{vmatrix} = 0 \tag{5.8}$$

This determinant is a polynomial of order $n$ in $\lambda$, and thus Eq. (5.8) leads to the characteristic equation

$$\lambda^n + c_{n-1}\lambda^{n-1} + c_{n-2}\lambda^{n-2} + \cdots + c_0 = 0 \tag{5.9}$$

In order for $\lambda$ to satisfy this algebraic equation, $\lambda$ must be one of its roots. Since an $n$th order algebraic equation has exactly $n$ roots, there are exactly $n$ values of $\lambda$, called the eigenvalues of the matrix **A**, for which Eq. (5.7) is solvable. We assume that these eigenvalues are distinct (see Wilkinson, 1965, for the general case), and write them as

$$\lambda = \lambda_1, \lambda_2, \ldots, \lambda_n \tag{5.10}$$

To every possible $\lambda = \lambda_j$, a solution of Eq. (5.7) can be found. We may tabulate these solutions as follows

$$\begin{aligned} \lambda &= \lambda_1: & \mathbf{x} &= (x_1^{(1)}, x_2^{(1)}, \ldots, x_n^{(1)})^{\mathrm{T}} \\ \lambda &= \lambda_2: & \mathbf{x} &= (x_1^{(2)}, x_2^{(2)}, \ldots, x_n^{(2)})^{\mathrm{T}} \\ &\vdots & &\vdots \\ \lambda &= \lambda_n: & \mathbf{x} &= (x_1^{(n)}, x_2^{(n)}, \ldots, x_n^{(n)})^{\mathrm{T}} \end{aligned} \tag{5.11}$$

where the superscript $(j)$ denotes the solution corresponding to $\lambda_j$, and the superscript T denotes the transpose of a vector or a matrix. These solutions represent $n$ distinct vectors of the $n$-dimensional space, and they are

called the eigenvectors of the matrix **A**. We may denote them by $\mathbf{u}_1$, $\mathbf{u}_2$, . . . , $\mathbf{u}_n$, where

$$
\begin{aligned}
\mathbf{u}_1 &= (x_1^{(1)}, x_2^{(1)}, \ldots, x_n^{(1)})^{\mathrm{T}} \\
\mathbf{u}_2 &= (x_1^{(2)}, x_2^{(2)}, \ldots, x_n^{(2)})^{\mathrm{T}} \\
&\vdots \\
\mathbf{u}_n &= (x_1^{(n)}, x_2^{(n)}, \ldots, x_n^{(n)})^{\mathrm{T}}
\end{aligned}
\tag{5.12}
$$

Because Eq. (5.7) is valid for each $\lambda = \lambda_j$, $j = 1, \ldots, n$, we have

$$\mathbf{A}\mathbf{u}_j = \lambda_j \mathbf{u}_j, \qquad j = 1, \ldots, n \tag{5.13}$$

In order to write these $n$ equations in matrix notation, we introduce the following definitions:

$$\mathbf{\Lambda} = \begin{pmatrix} \lambda_1 & & & \\ & \lambda_2 & & \\ & & \ddots & \\ & & & \lambda_n \end{pmatrix} \tag{5.14}$$

$$\mathbf{U} = \begin{pmatrix} | & | & & | \\ \mathbf{u}_1 & \mathbf{u}_2 & \ldots & \mathbf{u}_n \\ | & | & & | \end{pmatrix} \tag{5.15}$$

In other words, $\mathbf{\Lambda}$ is a diagonal matrix with the eigenvalues of matrix **A** as diagonal elements, and **U** is an $n \times n$ matrix with the eigenvectors of matrix **A** as columns. Equation (5.13) now becomes

$$\mathbf{AU} = \mathbf{U\Lambda} \tag{5.16}$$

Let us carry out a similar analysis for the transposed matrix $\mathbf{A}^{\mathrm{T}}$ whose elements are defined by

$$A_{ij}^{\mathrm{T}} = A_{ji} \tag{5.17}$$

Because any square matrix and its transpose have the same determinant, both matrix **A** and its transpose $\mathbf{A}^{\mathrm{T}}$ satisfy the same characteristic equation (5.9). Consequently, the eigenvalues of $\mathbf{A}^{\mathrm{T}}$ are identical with the eigenvalues of **A**. If we let $\mathbf{v}_1, \mathbf{v}_2, \ldots, \mathbf{v}_n$ denote the eigenvectors of $\mathbf{A}^{\mathrm{T}}$ and define

$$\mathbf{V} = \begin{pmatrix} | & | & & | \\ \mathbf{v}_1 & \mathbf{v}_2 & \ldots & \mathbf{v}_n \\ | & | & & | \end{pmatrix} \tag{5.18}$$

then the eigenvalue problem for $\mathbf{A}^{\mathrm{T}}$ becomes

$$\mathbf{A}^{\mathrm{T}}\mathbf{V} = \mathbf{V}\boldsymbol{\Lambda} \tag{5.19}$$

Let us take the transpose on both sides of Eq. (5.19)

$$\mathbf{V}^{\mathrm{T}}\mathbf{A} = \boldsymbol{\Lambda}\mathbf{V}^{\mathrm{T}} \tag{5.20}$$

and let us postmultiply this equation by $\mathbf{U}$

$$\mathbf{V}^{\mathrm{T}}\mathbf{A}\mathbf{U} = \boldsymbol{\Lambda}\mathbf{V}^{\mathrm{T}}\mathbf{U} \tag{5.21}$$

On the other hand, let us premultiply both sides of Eq. (5.16) by $\mathbf{V}^{\mathrm{T}}$

$$\mathbf{V}^{\mathrm{T}}\mathbf{A}\mathbf{U} = \mathbf{V}^{\mathrm{T}}\mathbf{U}\boldsymbol{\Lambda} \tag{5.22}$$

Because the left-hand sides of Eq. (5.21) and Eq. (5.22) are equal, we obtain

$$\boldsymbol{\Lambda}\mathbf{V}^{\mathrm{T}}\mathbf{U} = \mathbf{V}^{\mathrm{T}}\mathbf{U}\boldsymbol{\Lambda} \tag{5.23}$$

Let us denote the product $\mathbf{V}^{\mathrm{T}}\mathbf{U}$ by $\mathbf{W}$, whose elements are $W_{ij}$ and write out Eq. (5.23)

$$\begin{pmatrix} 0 & (\lambda_1 - \lambda_2)W_{12} & \cdots & (\lambda_1 - \lambda_n)W_{1n} \\ (\lambda_2 - \lambda_1)W_{21} & 0 & \cdots & (\lambda_2 - \lambda_n)W_{2n} \\ \vdots & \vdots & \vdots & \vdots \\ (\lambda_n - \lambda_1)W_{n1} & (\lambda_n - \lambda_2)W_{n2} & \cdots & 0 \end{pmatrix} = \mathbf{0} \tag{5.24}$$

If it is assumed that the eigenvalues are distinct, we obtain $W_{ij} = 0$ for $i \neq j$. This proves that $\mathbf{V}^{\mathrm{T}}$ and $\mathbf{U}$ are orthogonal. Since the length of eigenvectors is arbitrary, we may choose $\mathbf{V}^{\mathrm{T}}\mathbf{U} = \mathbf{I}$, where $\mathbf{I}$ is the identity matrix. Thus, we have

$$\mathbf{V}^{\mathrm{T}} = \mathbf{U}^{-1}, \quad \mathbf{V} = (\mathbf{U}^{\mathrm{T}})^{-1}; \qquad \mathbf{U} = (\mathbf{V}^{\mathrm{T}})^{-1}, \quad \mathbf{U}^{\mathrm{T}} = \mathbf{V}^{-1} \tag{5.25}$$

We are now in a position to derive the fundamental decomposition theorem. If we postmultiply Eq. (5.16) by $\mathbf{V}^{\mathrm{T}}$, we have

$$\mathbf{A}\mathbf{U}\mathbf{V}^{\mathrm{T}} = \mathbf{U}\boldsymbol{\Lambda}\mathbf{V}^{\mathrm{T}} \tag{5.26}$$

In view of Eq. (5.25), $\mathbf{U}\mathbf{V}^{\mathrm{T}} = \mathbf{I}$, so that

$$\mathbf{A} = \mathbf{U}\boldsymbol{\Lambda}\mathbf{V}^{\mathrm{T}} \tag{5.27}$$

Equation (5.27) shows that any $n \times n$ matrix $\mathbf{A}$ with distinct eigenvalues is obtainable by multiplying three matrices together, namely, the matrix $\mathbf{U}$ with the eigenvectors of $\mathbf{A}$ as columns, the diagonal matrix $\boldsymbol{\Lambda}$ with the

eigenvalues of $\mathbf{A}$ as diagonal elements, and the matrix $\mathbf{V}^T$. The columns of matrix $\mathbf{V}$ are the eigenvectors of $\mathbf{A}^T$.

The solution of the eigenvalue problem $\mathbf{Ax} = \lambda\mathbf{x}$ also solves the matrix inversion problem when $\mathbf{A}$ is nonsingular. If we premultiply Eq. (5.7) by $\mathbf{A}^{-1}$, the inverse of $\mathbf{A}$, we obtain

$$\mathbf{x} = \lambda\mathbf{A}^{-1}\mathbf{x} \tag{5.28}$$

or

$$\mathbf{A}^{-1}\mathbf{x} = \lambda^{-1}\mathbf{x} \tag{5.29}$$

Equation (5.29) is just the eigenvalue problem of $\mathbf{A}^{-1}$. This means that both matrix $\mathbf{A}$ and its inverse $\mathbf{A}^{-1}$ have the same eigenvectors, but their eigenvalues are reciprocal to each other. Applying the fundamental decomposition theorem [Eq. (5.27)], we obtain

$$\mathbf{A}^{-1} = \mathbf{U}\mathbf{\Lambda}^{-1}\mathbf{V}^T \tag{5.30}$$

Hence if we decompose $\mathbf{A}$, its inverse can be easily found. We also see that if one of the eigenvalues of $\mathbf{A}$, say $\lambda_i$, is zero, we cannot compute $\lambda_i^{-1}$ and consequently $\mathbf{A}^{-1}$ does not exist.

The preceding analysis offers some insight into the solvability of an even-determined system of linear equations. But have we really solved our problem? Calculation of eigenvalues requires finding the roots of an $n$th order algebraic equation. These roots, or eigenvalues, are in general complex and difficult to determine. Fortunately, the eigenvalues of a symmetric matrix are real, and this fact can be exploited not only for solving a general nonsymmetric matrix, but also for solving the general nonsquare matrix as well.

### *5.1.2. Analysis of an Underdetermined System*

There are usually an infinity of solutions for an underdetermined system, that is, one in which the number of unknowns exceeds the number of equations. However, we must be aware that there may be no solution at all for some underdetermined systems. For instance, the following system of two equations for three unknowns:

$$x_1 - x_2 + x_3 = 1, \qquad 2x_1 - 2x_2 + 2x_3 = 3 \tag{5.31}$$

has no solution because the second equation contradicts the first one.

The high degree of nonuniqueness of solutions in an underdetermined system has been exploited in geophysical applications in a series of papers by Backus and Gilbert (1967, 1968, 1970). Since then it has been popular to model any property of the earth as an infinite continuum, i.e., the

number of unknowns is infinite. But because geophysical data are limited, the number of observations is finite. In other words, we write a finite number of equations corresponding to our observations, but our unknown vector **x** is of infinite dimension. In order to obtain a unique answer, the solution chosen is the one which maximizes or minimizes a subsidiary integral. In actual practice, we minimize a sum of squares to produce a smooth solution. A typical mathematical formulation may look like

$$\begin{pmatrix} \mathbf{A} \\ \hline \diagdown\diagdown\diagdown \end{pmatrix} \mathbf{x} \approx \begin{pmatrix} \mathbf{b} \\ \hline \mathbf{0} \end{pmatrix} \tag{5.32}$$

where the top block **A** represents the underdetermined constraint equations with the observed data vector **b**, the vector **x** contains the unknowns, and the bottom block is a band matrix which specifies that some filtered version of **x** should vanish. As pointed out by Claerbout (1976, p. 120), the choice of a filter is highly subjective, and the solution is often very sensitive to the filter chosen. The Backus–Gilbert inversion is intended for analysis of systems in which the unknowns are functions, i.e., they are infinite-dimensional, as opposed to, say, hypocenter parameters in the earthquake location problem, which are four-dimensional. For an application of the Backus–Gilbert inversion to travel time data, readers may refer, for example, to Chou and Booker (1979).

### *5.1.3. Analysis of an Overdetermined System*

Most scientists are modest in their data modeling and would have more observations than unknowns in their model. On the surface it may seem very safe, and one should not expect difficulties in obtaining a reasonable solution for an overdetermined system. However, an overdetermined system may in fact be underdetermined because some of the equations may be superfluous and do not add anything new to the system. For example, if we use only first P-arrivals to locate an earthquake which is considerably outside a microearthquake network, the problem is underdetermined no matter how many observations we have. In other words, in many physical situations we do not have sufficient information to solve our problem uniquely. Unfortunately, many scientists overlook this difficulty. Therefore, it is instructive to quote the general principle given by Lanczos (1961, p. 132) that "a lack of information cannot be remedied by any mathematical trickery."

Usually a given overdetermined system is mathematically incompatible, i.e., some equations are contradictory because of errors in the observations. This means that we cannot make all the components of the re-

sidual vector $\mathbf{r} \equiv \mathbf{Ax} - \mathbf{b}$ equal to zero. In the least squares method we seek a solution in which $\|\mathbf{r}\|^2$ is minimized, where $\|\mathbf{r}\|$ denotes the Euclidean length of $\mathbf{r}$. In matrix notation, we write $\|\mathbf{r}\|^2$ as (see Draper and Smith, 1966, p. 58)

$$\|\mathbf{r}\|^2 = (\mathbf{Ax} - \mathbf{b})^{\mathrm{T}}(\mathbf{Ax} - \mathbf{b}) = \mathbf{x}^{\mathrm{T}}\mathbf{A}^{\mathrm{T}}\mathbf{Ax} - 2\mathbf{x}^{\mathrm{T}}\mathbf{A}^{\mathrm{T}}\mathbf{b} + \mathbf{b}^{\mathrm{T}}\mathbf{b} \tag{5.33}$$

To minimize $\|\mathbf{r}\|^2$, partial differentiate Eq. (5.33) with respect to each component of $\mathbf{x}$ and equate each result to zero. The resulting set of $n$ equations may be rearranged into matrix form as

$$2\mathbf{A}^{\mathrm{T}}\mathbf{Ax} - 2\mathbf{A}^{\mathrm{T}}\mathbf{b} = \mathbf{0} \tag{5.34}$$

or

$$\mathbf{A}^{\mathrm{T}}\mathbf{Ax} = \mathbf{A}^{\mathrm{T}}\mathbf{b} \tag{5.35}$$

Equation (5.35) is called the system of normal equations and is an even-determined system. Furthermore, the matrix $\mathbf{A}^{\mathrm{T}}\mathbf{A}$ is always symmetric, and its eigenvalues are not only real but nonnegative. By applying the least squares method, we not only get rid of the incompatibility of the original equations, but also have a much nicer and smaller set of equations to solve. For these reasons, scientists tend to use exclusively the least squares approach for their problems. Unfortunately, there are two serious drawbacks. In solving the normal equations by a computer, one needs twice the computational precision of the original equations. By forming $\mathbf{A}^{\mathrm{T}}\mathbf{A}$ and $\mathbf{A}^{\mathrm{T}}\mathbf{b}$, one also destroys certain information in the original system. We shall discuss these drawbacks later.

### *5.1.4. Analysis of an Arbitrary System*

Since the determinant is defined only for a square matrix, we cannot carry out an eigenvalue analysis for a general nonsquare matrix. However, Lanczos (1961) has shown an interesting approach to analyze an arbitrary system. The fundamental problem to solve is

$$\mathbf{Ax} = \mathbf{b} \tag{5.36}$$

where the matrix $\mathbf{A}$ is $m \times n$, i.e., $\mathbf{A}$ has $m$ rows and $n$ columns. Equation (5.36) says that $\mathbf{A}$ transforms a vector $\mathbf{x}$ of $n$ components into a vector $\mathbf{b}$ of $m$ components. Therefore matrix $\mathbf{A}$ is associated with two spaces: one of $m$ dimensions and the other of $n$ dimensions. Let us enlarge Eq. (5.36) by considering also the adjoint system

$$\mathbf{A}^{\mathrm{T}}\mathbf{y} = \mathbf{c} \tag{5.37}$$

where the matrix $\mathbf{A}^{\mathrm{T}}$ is $n \times m$, $\mathbf{y}$ is an $m$-dimensional vector, and $\mathbf{c}$ is an

$n$-dimensional vector. We now combine Eq. (5.36) and Eq. (5.37) as follows:

$$\left(\begin{array}{c|c} \mathbf{0} & \mathbf{A} \\ \hline \mathbf{A}^{\mathrm{T}} & \mathbf{0} \end{array}\right)\left(\begin{array}{c} \mathbf{y} \\ \hline \mathbf{x} \end{array}\right)=\left(\begin{array}{c} \mathbf{b} \\ \hline \mathbf{c} \end{array}\right) \tag{5.38}$$

Now, this combined system has a symmetric matrix, and one can proceed to perform an eigenvalue analysis like that described before (for details, see Lanczos, 1961, pp. 115–123). Finally, one arrives at a decomposition theorem similar to Eq. (5.27) for a real $m \times n$ matrix $\mathbf{A}$ with $m \geq n$

$$\mathbf{A} = \mathbf{U}\mathbf{S}\mathbf{V}^{\mathrm{T}} \tag{5.39}$$

where

$$\mathbf{U}^{\mathrm{T}}\mathbf{U} = \mathbf{I}_m, \qquad \mathbf{V}^{\mathrm{T}}\mathbf{V} = \mathbf{I}_n \tag{5.40}$$

and

$$\mathbf{S} = \left(\begin{array}{cccc} \sigma_1 & & & \\ & \sigma_2 & & \\ & & \ddots & \\ & & & \sigma_n \\ \hline & & \mathbf{0} & \end{array}\right) \tag{5.41}$$

The $m \times m$ matrix $\mathbf{U}$ consists of $m$ orthonormalized eigenvectors of $\mathbf{A}\mathbf{A}^{\mathrm{T}}$, and the $n \times n$ matrix $\mathbf{V}$ consists of $n$ orthonormalized eigenvectors of $\mathbf{A}^{\mathrm{T}}\mathbf{A}$. Matrices $\mathbf{I}_m$ and $\mathbf{I}_n$ are $m \times m$ and $n \times n$ identity matrices, respectively. The matrix $\mathbf{S}$ is an $m \times n$ diagonal matrix with off-diagonal elements $S_{ij} = 0$ for $i \neq j$, and diagonal elements $S_{ii} = \sigma_i$, where $\sigma_i$, $i = 1, 2, \ldots, n$ are the nonnegative square roots of the eigenvalues of $\mathbf{A}^{\mathrm{T}}\mathbf{A}$. These diagonal elements are called singular values and are arranged in Eq. (5.41) such that

$$\sigma_1 \geq \sigma_2 \geq \cdots \geq \sigma_n \geq 0 \tag{5.42}$$

The above decomposition is known as singular value decomposition (SVD). It was proved by J. J. Sylvester in 1889 for square real matrices and by Eckart and Young (1939) for general matrices. Most modern texts on matrices (e.g., Ben-Israel and Greville, 1974, pp. 242–251; Forsythe and Moler, 1967, pp. 5–11; G. W. Stewart, 1973, pp. 317–326) give a derivation of the singular value decomposition. The form we give here follows that given by Forsythe *et al.* (1977, p. 203). Lanczos (1961, pp. 120–123) did not introduce the singular values explicitly, but used the term

eigenvalues rather loosely. Consequently, some works of geophysicists who use Lanczos' notation may be confusing to readers. Strictly speaking, eigenvalues and eigenvectors are not defined for an $m \times n$ rectangular matrix because eigenvalue analysis can be performed only for a square matrix.

## 5.2. Physical Consideration of Inverse Problems

In the previous section, we considered the model matrix $\mathbf{A}$ and the data vector $\mathbf{b}$ in the problem $\mathbf{Ax} = \mathbf{b}$ to be exact. In actual applications, however, our model $\mathbf{A}$ is usually an approximation, and our data contain errors and have no more than a few significant figures. Consequently, we should write our problem as

$$(\mathbf{A} \pm \Delta\mathbf{A})\mathbf{x} = \mathbf{b} \pm \Delta\mathbf{b} \tag{5.43}$$

where $\Delta\mathbf{A}$ and $\Delta\mathbf{b}$ denote uncertainties in $\mathbf{A}$ and $\mathbf{b}$, respectively. In this section we investigate what constitutes a good solution, realizing that there are uncertainties in both our model and data. The treatment here follows an approach given by Jackson (1972).

Our task is to find a good estimate to the solution of the problem

$$\mathbf{Ax} = \mathbf{b} \tag{5.44}$$

where $\mathbf{A}$ is an $m \times n$ matrix. Let us denote such an estimate by $\hat{\mathbf{x}}$; $\hat{\mathbf{x}}$ may be defined formally with the help of a matrix $\mathbf{H}$ of dimensions $n \times m$ operating on both sides of Eq. (5.44)

$$\hat{\mathbf{x}} \equiv \mathbf{Hb} = \mathbf{HAx} \tag{5.45}$$

The matrix $\mathbf{H}$ will be a good inverse if it satisfies the following criteria:

(1) $\mathbf{AH} \approx \mathbf{I}$, where $\mathbf{I}$ is an $m \times m$ identity matrix. This is a measure of how well the model fits the data, because $\hat{\mathbf{b}} \equiv \mathbf{A}\hat{\mathbf{x}} = \mathbf{A}(\mathbf{Hb}) = (\mathbf{AH})\mathbf{b} = \mathbf{b}$, if $\mathbf{AH} = \mathbf{I}$.

(2) $\mathbf{HA} \approx \mathbf{I}$, where $\mathbf{I}$ is an $n \times n$ identity matrix. This is a measure of uniqueness of the solution, because $\hat{\mathbf{x}} \equiv \mathbf{x}$, if $\mathbf{HA} = \mathbf{I}$.

(3) The uncertainties in $\hat{\mathbf{x}}$ are not too large, i.e., the variance of $\hat{\mathbf{x}}$ is small. For statistically independent data, the variance of the $k$th component of $\hat{\mathbf{x}}$ is given by

$$\operatorname{var}(\hat{x}_k) = \sum_{i=1}^{m} H_{ki}^2 \operatorname{var}(b_i) \tag{5.46}$$

where $H_{ki}$ is the $(k, i)$-element of $\mathbf{H}$, and $b_i$ is the $i$th component of $\mathbf{b}$.

Because of uncertainties in our model and data, an exact solution to Eq. (5.44) may never be obtainable. Furthermore, there may be many solutions satisfying $\mathbf{Ax} = \mathbf{b}$. By Eq. (5.45), our estimate $\hat{\mathbf{x}}$ is related to the true solution by the product $\mathbf{HA}$. Let us call this product the resolution matrix $\mathbf{R}$, i.e.,

$$\mathbf{R} \equiv \mathbf{HA} \tag{5.47}$$

and hence Eq. (5.45) becomes

$$\hat{\mathbf{x}} = \mathbf{Rx} \tag{5.48}$$

This equation tells us that the matrix $\mathbf{R}$ maps the entire set of solutions $\mathbf{x}$ into a single vector $\hat{\mathbf{x}}$. Any component of vector $\hat{\mathbf{x}}$, say $\hat{\mathbf{x}}_k$, is the product of the $k$th row of matrix $\mathbf{R}$ with any vector $\mathbf{x}$ that satisfies $\mathbf{Ax} = \mathbf{b}$. Therefore, $\mathbf{R}$ is a matrix whose rows are "windows" through which we may view the general solution $\mathbf{x}$ and obtain a definite result. If $\mathbf{R}$ is an identity matrix, each component of vector $\mathbf{x}$ is perfectly resolved and our solution $\hat{\mathbf{x}}$ is unique. If $\mathbf{R}$ is a near diagonal matrix, each component, say $\hat{x}_k$, is a weighted sum of components of $\mathbf{x}$ with subscripts near $k$. Hence, the degree to which $\mathbf{R}$ approximates the identity matrix is a measure of the resolution obtainable from the data.

In a similar manner, we may call the product $\mathbf{AH}$ the information density matrix $\mathbf{D}$ (Wiggins, 1972), i.e.,

$$\mathbf{D} \equiv \mathbf{AH} \tag{5.49}$$

It is a measure of the independence of the data. The theoretical data $\hat{\mathbf{b}}$ that satisfies exactly our solution $\hat{\mathbf{x}}$ is given by

$$\hat{\mathbf{b}} \equiv \mathbf{A}\hat{\mathbf{x}} = \mathbf{AHb} = \mathbf{Db} \tag{5.50}$$

In actual applications, the criteria (1), (2), and (3) mentioned previously are not equally important and may be weighted for a specific problem. For example, there is a trade-off between resolution and variance.

## 5.3. Computational Aspects of Solving Inverse Problems

There are many ways to solve the problem $\mathbf{Ax} = \mathbf{b}$. For example, one learns Cramer's rule and Gaussian elimination in high school. We also know that by applying the least squares method, we can reduce any over- or underdetermined system of equations to an even-determined one. With digital computers generally available, one wonders why the machines cannot simply grind out the answers and let the scientists write up the results. Unfortunately, this point of view has led many scientists astray.

As pointed out by Hamming (1962, front page), "the purpose of computing is insight, not numbers."

Using computers blindly would not lead us anywhere. Suppose we wish to solve a system of 20 linear equations. Although it is possible to program Cramer's rule to do the job on a modern computer, it would take at least 300 million years to grind out the solution (Forsythe *et al.*, 1977, p. 30). On the other hand, using Gaussian elimination would take less than 1 sec on a modern computer. However, if the matrix were ill-conditioned, Gaussian elimination would not give us a meaningful answer. Worse yet, we might not be aware of this.

In this section, we first review briefly the nature of computer computations. We then summarize some computational aspects of generalized inversion.

### *5.3.1. Nature of Computer Computations*

Although we are accustomed to real numbers in mathematical analysis, it is impossible to represent all real numbers in computers of finite word length. Thus, arithmetic operations on real numbers can only be approximated in computer computations. Nearly all computers use floating-point numbers to approximate real numbers. A set of floating-point numbers is characterized by four parameters: the number base $\beta$, the precision $t$, and the exponent range $[p_1, p_2]$ (see, e.g., Forsythe *et al.*, 1977, p. 10). Each floating-point number $x$ has the value

$$x = \pm(d_1/\beta + d_2/\beta^2 + \cdots + d_t/\beta^t)\beta^p \tag{5.51}$$

where the integers $d_1, \ldots, d_t$ satisfy $0 \le d_i \le \beta - 1$ $(i = 1, \ldots, t)$, and the integer $p$ has the range: $p_1 \le p \le p_2$.

In using a computer, it is important to know the relative accuracy of the arithmetic (which is estimated by $\beta^{1-t}$ and the upper and lower bounds of floating-point numbers (which are given approximately by $\beta^{p_2}$ and $\beta^{p_1}$, respectively). For example, the single precision floating-point numbers for IBM computers are specified by $\beta = 16$, $t = 6$, $p_1 = -65$, and $p_2 = 63$. Thus, the relative accuracy is about $10^{-6}$, the lower bound is about $10^{-78}$, and the upper bound is about $10^{75}$. The IBM double precision floating-point numbers have $t = 14$, so that the relative accuracy is about $2 \times 10^{-16}$, but they have the same exponent range as their single-precision counterparts.

The set of floating-point numbers in any computer is not a continuum, or even an infinite set. Thus, it is not possible to represent the continuum of real numbers in any detail. Consequently, arithmetic operations (such as addition, subtraction, multiplication, and division) on floating-point

numbers in computers rarely correspond to those on real numbers. Since floating-point numbers have a finite number of digits, roundoff error occurs in representing any number that has more significant digits than the computer can hold. An arithmetic operation on floating-point numbers may introduce roundoff error and can result in underflow or overflow error. For example, if we multiply two floating-point numbers $x$ and $y$, each of $t$ significant digits, the product is either $2t$ or $(2t - 1)$ significant digits, and the computer must round off the product to $t$ significant digits. If $x$ and $y$ has exponents of $p_x$ and $p_y$, it may cause an overflow if $(p_x + p_y)$ exceeds the upper exponent range allowed, and may cause an underflow if $(p_x + p_y)$ is smaller than the lower exponent range allowed.

An effective way to minimize roundoff errors is to use double precision floating-point numbers and operations whenever in doubt. Unfortunately, the exponent range for single precision and double precision floating-point numbers for most computers is the same, and one must be careful in handling overflow and underflow errors. In addition, there are many other pitfalls in computer computations. Readers are referred to textbooks on computer science, such as Dahlquist and Bjorck (1974) and Forsythe *et al.* (1977), for details.

### 5.3.2. *Computational Aspects of Generalized Inversion*

The purpose of generalized inversion is to help us understand the nature of the problem $\mathbf{Ax} = \mathbf{b}$ better. We are interested in getting not only a solution to the problem $\mathbf{Ax} = \mathbf{b}$, but also answers to the following questions: (1) Do we have sufficient information to solve the problem? (2) Is the solution unique? (3) Will the solution change a lot for small errors in $\mathbf{b}$ and/or $\mathbf{A}$? (4) How important is each individual observation to our solution?

In Section 5.2 we solved our problem $\mathbf{Ax} = \mathbf{b}$ by seeking a matrix $\mathbf{H}$ which serves as an inverse and satisfies certain criteria. The singular value decomposition described in Section 5.1 permits us to construct this inverse quite easily. Let $\mathbf{A}$ be a real $m \times n$ matrix. The $n \times m$ matrix $\mathbf{H}$ is said to be the Moore-Penrose generalized inverse of $\mathbf{A}$ if $\mathbf{H}$ satisfies the following conditions (Ben-Israel and Greville, 1974, p. 7):

$$\mathbf{AHA} = \mathbf{A}, \qquad \mathbf{HAH} = \mathbf{H}, \qquad (\mathbf{AH})^{\mathrm{T}} = \mathbf{AH} \qquad (\mathbf{HA})^{\mathrm{T}} = \mathbf{HA} \tag{5.52}$$

The unique solution of this generalized inverse of $\mathbf{A}$ is commonly denoted as $\mathbf{A}^{+}$. It can be verified that if we perform singular value decomposition

on **A** [see Eqs. (5.39)–(5.41)], i.e.,

$$\mathbf{A} = \mathbf{U}\mathbf{S}\mathbf{V}^{\mathrm{T}} \tag{5.53}$$

then by the properties of orthogonal matrices,

$$\mathbf{A}^{\dagger} = \mathbf{V}\mathbf{S}^{\dagger}\mathbf{U}^{\mathrm{T}} \tag{5.54}$$

where $\mathbf{S}^{\dagger}$ is an $n \times m$ matrix,

$$\mathbf{S}^{\dagger} = \left(\begin{array}{cccc|c} \sigma_1^{\dagger} & & & & \\ & \sigma_2^{\dagger} & & & \\ & & \ddots & & \mathbf{0} \\ & & & \sigma_n^{\dagger} & \end{array}\right) \tag{5.55}$$

and for $i = 1, \ldots, n$,

$$\sigma_i^{\dagger} = \begin{cases} 1/\sigma_i & \text{for} \quad \sigma_i > 0 \\ 0 & \text{for} \quad \sigma_i = 0 \end{cases} \tag{5.56}$$

It is straightforward to find the resolution matrix **R** and the information density matrix **D**. Since $\mathbf{R} \equiv \mathbf{H}\mathbf{A} = \mathbf{A}^{\dagger}\mathbf{A}$, we have

$$\mathbf{R} = \mathbf{V}\mathbf{S}^{\dagger}\mathbf{U}^{\mathrm{T}}\mathbf{U}\mathbf{S}\mathbf{V}^{\mathrm{T}} = \mathbf{V}\mathbf{S}^{\dagger}\mathbf{S}\mathbf{V}^{\mathrm{T}} \tag{5.57a}$$

because $\mathbf{U}^{\mathrm{T}}\mathbf{U} = \mathbf{I}$ by Eq. (5.40). Let us consider the overdetermined case where $m > n$. If the rank of matrix **A** is $r$ ($r \leq n$), then there are $r$ nonzero singular values. If we denote the $r \times r$ identity matrix by $\mathbf{I}_r$, then by Eqs. (5.41) and (5.55),

$$\mathbf{S}^{\dagger}\mathbf{S} = \begin{array}{c} \left(\begin{array}{c|c} \mathbf{I}_r & \mathbf{0} \\ \hline \mathbf{0} & \mathbf{0} \end{array}\right) \begin{array}{l} \}\, r \\ \}\, n - r \end{array} \\ \begin{array}{cc} \underbrace{\phantom{\mathbf{I}_r}}_{r} & \underbrace{\phantom{\mathbf{0}}}_{n-r} \end{array} \end{array} \tag{5.57b}$$

Hence,

$$\mathbf{R} = \mathbf{V}_r\mathbf{V}_r^{\mathrm{T}} \tag{5.57c}$$

where $\mathbf{V}_r$ is the first $r$ columns of **V** corresponding to the $r$ nonzero singular values. Similarly, from $\mathbf{D} \equiv \mathbf{A}\mathbf{H} = \mathbf{A}\mathbf{A}^{\dagger}$, we have

$$\mathbf{D} = \mathbf{U}\mathbf{S}\mathbf{V}^{\mathrm{T}}\mathbf{V}\mathbf{S}^{\dagger}\mathbf{U}^{\mathrm{T}} = \mathbf{U}_r\mathbf{U}_r^{\mathrm{T}} \tag{5.57d}$$

where $\mathbf{U}_r$ is the $m \times r$ submatrix of **U** corresponding to the $r$ nonzero singular values.

The resulting estimate of the solution

$$\hat{\mathbf{x}} = \mathbf{A}^{-}\mathbf{b} \tag{5.58}$$

is always unique. If matrix $\mathbf{A}$ is of full rank (i.e., $r = n$), then $\mathbf{R} = \mathbf{I}_n$ and $\mathbf{D} = \mathbf{I}_m$. Thus, $\hat{\mathbf{x}}$ corresponds to the usual least squares solution. If matrix $\mathbf{A}$ is rank deficient (i.e., $r < n$), then there is no unique solution to the least squares problem. In this case, we must choose a solution by some criteria. A simple criterion is that the solution $\hat{\mathbf{x}}$ has the least vector length, and Eq. (5.58) satisfies this requirement. Finally, we introduce the unscaled covariance matrix $\mathbf{C}$ (Lawson and Hanson, 1974, pp. 67–68)

$$\mathbf{C} \equiv \mathbf{V}(\mathbf{S}^{\dagger})^2\mathbf{V}^{\mathrm{T}} \tag{5.59}$$

The Moore–Penrose generalized inverse is one of many generalized inverses (Ben-Israel and Greville, 1974). In other words, there are other choices for the matrix $\mathbf{H}$, which can serve as an inverse, and thus one can obtain different approximate solutions to the problem $\mathbf{Ax} = \mathbf{b}$. For example, in the method of damped least squares (or ridge regression), the matrix $\mathbf{H}$ is chosen to be

$$\mathbf{H} = \mathbf{VFS}^{\dagger}\mathbf{U}^{\mathrm{T}} \tag{5.60a}$$

In this equation, $\mathbf{F}$ is an $n \times n$ diagonal filter matrix whose components are

$$F_{ii} = \sigma_i^2/(\sigma_i^2 + \theta^2) \qquad \text{for} \quad i = 1, 2, \ldots, n \tag{5.60b}$$

where $\theta$ is an adjustable parameter usually much less than the largest singular value $\sigma_1$.

The effect of this $\mathbf{H}$ as the inverse is to produce an estimate $\hat{\mathbf{x}}$ whose components along the singular vectors corresponding to small singular values are damped in comparison with their values obtained from the Moore–Penrose generalized inverse solution. This $\hat{\mathbf{x}}$ can be shown (Lawson and Hanson, 1974) to solve the problem

$$\text{minimize } \{\|\mathbf{Ax} - \mathbf{b}\|^2 + \theta^2\|\mathbf{x}\|^2\} \tag{5.60c}$$

and thus represents a compromise between fitting the data and limiting the size of the solution. Such an idea is also used in the context of nonlinear least squares where it is known as the Levenberg–Marquardt method (see Section 5.4.3).

Unlike the ordinary inverse, the Moore–Penrose generalized inverse always exists, even when the matrix is singular. In constructing this generalized inverse, we are careful to handle the zero singular values. In Eq. (5.56), we define $\sigma_i^{\dagger} = 1/\sigma_i$ only for $\sigma_i > 0$, and $\sigma_i^{\dagger} = 0$, for $\sigma_i = 0$. This avoids the problem of the ordinary inverse, where $\sigma_i^{-1} \equiv 1/\sigma_i$. Furthermore, singular values give insight to the rank and condition of a matrix.

The usual definition of rank of a matrix is the maximum number of

independent columns. Such a definition is very difficult to apply in practice for a general matrix. However, if the matrix is triangular, the rank is simply the number of nonzero diagonal elements. Since an orthogonal transformation, such as that in the singular value decomposition, does not affect the rank, we see right away that the rank of **A** is equal to the rank of **S** in its singular value decomposition. Hence a practical definition of the rank of a matrix is the number of its nonzero singular values. Because of finite precision in any computer, it may be difficult to distinguish a small singular value and a zero one. Therefore, we define the effective rank as the number of singular values greater than some prescribed tolerance which reflects the accuracy of the machine and the data.

Reducing the rank of a matrix has the effect of improving the variance of the solution. In Eq. (5.59), the singular value $\sigma_i$ enters into the covariance matrix as $1/\sigma_i^2$. Therefore, if $\sigma_i$ is small, the covariance, and hence the variance will be large. By discarding small singular values, we decrease the variance. However, we pay the price of poorer resolution. For a full-rank matrix, the resolution matrix **R** is simply the identity matrix and we have full resolution. Decreasing the rank makes **R** further away from being an identify matrix.

Since our model and data have uncertainties, we have to consider the condition number of the matrix **A**. In practice, we are not solving $\mathbf{Ax} = \mathbf{b}$, but $\mathbf{Ax} = \mathbf{b} \pm \mathbf{\Delta b}$, assuming **A** to be exact at this moment. It can be shown (Forsythe *et al.*, 1977, pp. 41–43) that the error $\mathbf{\Delta x}$ in **x** resulting from the error $\mathbf{\Delta b}$ in **b** is given by

$$\|\mathbf{\Delta x}\|/\|\mathbf{x}\| \leq \gamma[\|\mathbf{\Delta b}\|/\|\mathbf{b}\|] \tag{5.61}$$

where $\gamma$ is the condition number of **A**, and $\|\cdot\|$ denotes the vector norm. Forsythe *et al.* (1977, pp. 205–206) also show that we can define the condition number of **A** by

$$\gamma = \sigma_{\max}/\sigma_{\min} \tag{5.62}$$

i.e., $\gamma$ is the ratio of the largest and smallest singular values of **A**. We see from Eq. (5.61) that the condition number $\gamma$ is an upper bound in magnifying the relative error in our observations. In microearthquake studies, the relative error in observations is about $10^{-3}$. Therefore, if $\gamma$ is $10^3$, then the error in our solution may be comparable to the solution itself.

In conclusion, the singular value decomposition (SVD) approach to generalized inversion offers a powerful analysis of our problem. Numerical computation of SVD has been worked out by Golub and Reinsch (1970), and a SVD subroutine is generally available as a library subroutine in most computer centers. Although SVD analysis requires more computational time than, say, solving the normal equations by the Cholesky

method, it is well worth it. In actual count of multiplicative operations, SVD requires $2mn^2 + 4n^3$, whereas the normal equations approach requires $mn^2/2 + n^3/6$ (Van Loan, 1976, p. 8). For example, if one solves 1000 equations for 300 unknowns, SVD analysis will take about six times longer on a computer than the normal equations approach.

However, let us point out two major drawbacks of the normal equations approach. First, the condition number of the normal equations matrix is the square of that of the original matrix. Thus, we need to double the floating-point precision $t$ (see Section 5.3.1) in forming and solving the normal equations to avoid roundoff errors in computing. Second, the normal equations approach does not allow us to compute the information density matrix.

## 5.4. Nonlinear Optimization

An equation, $f(x_1, x_2, \ldots, x_n)$, is said to be linear in a set of independent variables, $x_1, x_2, \ldots, x_n$, if it has the form

$$f(x_1, x_2, \ldots, x_n) = a_0 + \sum_{i=1}^{n} a_i x_i \tag{5.63}$$

where the coefficients $a_0$ and $a_i (i = 1, 2, \ldots, n)$ are not functions of $x_i$. Any equation that is not linear is called a nonlinear equation (Bard, 1974, p. 5). The discussion we have had so far in this chapter concerns generalized inversion of linear problems, i.e., we attempted to solve a set of linear equations. If the number of equations exceeds the number of unknowns, we may use the least-squares method and we have a linear least-squares problem.

In actual practice, we often have to solve nonlinear equations because many physical problems can not be described adequately by linear models. For example, the travel time between two points in nearly all media (including the simplest case of constant velocity) is a nonlinear function of the spatial coordinates. Thus locating earthquakes in a microearthquake network is usually formulated as a nonlinear least squares problem. The sum of the squares of residuals between the observed and the calculated arrival times for a set of stations is to be minimized. This leads directly into the problem of nonlinear optimization.

Since methods of nonlinear optimization have many scientific applications, they have been extensively treated in the literature (e.g., Murray, 1972; Luenberger, 1973; Adby and Dempster, 1974; Wolfe, 1978; R.

Fletcher, 1980; Gill *et al.*, 1981). Unfortunately, no single method has been found to solve all problems effectively. The subject is being actively pursued by scientists in many disciplines. In this section, we briefly describe some elementary aspects of nonlinear optimization.

### *5.4.1. Problem Definition*

The basic mathematical problem in optimization is to minimize a scalar quantity $\psi$ which is the value of a function $F(x_1, x_2, \ldots, x_n)$ of $n$ independent variables. These independent variables, $x_1, x_2, \ldots, x_n$, must be adjusted to obtain the minimum required, i.e.,

$$\text{minimize } \{\psi = F(x_1, x_2, \ldots, x_n)\} \tag{5.64}$$

The function $F$ is referred to as the objective function because its value $\psi$ is the quantity to be minimized.

It is useful to consider the $n$ independent variables, $x_1, x_2, \ldots, x_n$, as a vector in $n$-dimensional Euclidean space,

$$\mathbf{x} = (x_1, x_2, \ldots, x_n)^{\mathrm{T}} \tag{5.65}$$

where the superscript T denotes the transpose of a vector or a matrix. During the optimization process, the coordinates of $\mathbf{x}$ will take on successive values as adjustments are made. Each set of adjustments to $\mathbf{x}$ is termed an iteration, and a number of iterations are generally required before a minimum is reached. In order to start an iterative procedure, an initial estimate of $\mathbf{x}$ must be given. After $K$ iterations, we denote the value of $\psi$ by $\psi_{(K)}$, and the value of $\mathbf{x}$ by $\mathbf{x}_{(K)}$. Changes in the value of $\mathbf{x}$ between two successive iterations are just the adjustments applied. These adjustments may also be thought of as components of an adjustment vector,

$$\boldsymbol{\delta}\mathbf{x} = (\delta x_1, \delta x_2, \ldots, \delta x_n)^{\mathrm{T}} \tag{5.66}$$

The goal of optimization is to find after $K$ iterations a $\mathbf{x}_{(K)}$ that gives a minimum value $\psi_{(K)}$ of the objective function $F$. A point $\mathbf{x}_{(K)}$ is called a global minimum if it gives the lowest possible value of $F$. In general, a global minimum need not be unique; and in practice, it is very difficult to tell if a global minimum has been reached by an iterative procedure. We may only claim that a minimum within a local area of search has been obtained. Even such a local minimum may not be unique locally.

Methods in optimization may be divided into three classes: (1) search methods which use function evaluation only; (2) methods which in addition require gradient information or first derivatives; and (3) methods which require function, gradient, and second-derivative information. The appeal of each class depends on the particular problem and the available

information about derivatives. In general, the optimization problem can be solved more effectively if more information about derivatives is provided. However, this must be traded off against the extra computing needed to compute the derivatives. Search methods usually are not effective when the function to be optimized has more than one independent variable. Methods in the third class are modifications of the classical Newton–Raphson (or Newton) method. Methods in the second and third classes may be referred to as derivative methods, and are discussed next.

### *5.4.2. Derivative Methods*

These methods for optimization are based on the Taylor expansion of the objective function. For a function of one variable, $f(x)$, which is differentiable at least $n$ times in an interval containing points $(x)$ and $(x + \delta x)$, we may expand $f(x + \delta x)$ in terms of $f(x)$ as given by Courant and John (1965, p. 446) as

$$f(x + \delta x) \simeq f(x) + \frac{df(x)}{dx}\,\delta x + \cdots + \frac{1}{n!}\,\frac{d^n f(x)}{dx^n}\,(\delta x)^n \tag{5.67}$$

For a function of $n$ variables, $F(\mathbf{x})$, where $\mathbf{x}$ is given by Eq. (5.65), we may generalize this procedure (Courant and John, 1974, pp. 68–70) and write

$$F(\mathbf{x} + \boldsymbol{\delta}\mathbf{x}) \simeq F(\mathbf{x}) + \mathbf{g}^{\mathrm{T}}\,\boldsymbol{\delta}\mathbf{x} + \tfrac{1}{2}\boldsymbol{\delta}\mathbf{x}^{\mathrm{T}}\mathbf{H}\,\boldsymbol{\delta}\mathbf{x} + \cdots \tag{5.68}$$

where $\mathbf{g}^{\mathrm{T}}$ is the transpose of the gradient vector $\mathbf{g}$ and is given by

$$\mathbf{g}^{\mathrm{T}} = \nabla F(\mathbf{x}) = (\partial F/\partial x_1,\ \partial F/\partial x_2,\ \ldots,\ \partial F/\partial x_n) \tag{5.69}$$

and $\mathbf{H}$ is the Hessian matrix given by

$$\mathbf{H} = \begin{pmatrix} \dfrac{\partial^2 F}{\partial x_1^2} & \dfrac{\partial^2 F}{\partial x_1\,\partial x_2} & \cdots & \dfrac{\partial^2 F}{\partial x_1\,\partial x_n} \\ \dfrac{\partial^2 F}{\partial x_2\,\partial x_1} & \dfrac{\partial^2 F}{\partial x_2^2} & \cdots & \dfrac{\partial^2 F}{\partial x_2\,\partial x_n} \\ & & \vdots & \\ \dfrac{\partial^2 F}{\partial x_n\,\partial x_1} & \dfrac{\partial^2 F}{\partial x_n\,\partial x_2} & \cdots & \dfrac{\partial^2 F}{\partial x_n^2} \end{pmatrix} \tag{5.70}$$

In Eq. (5.68), we have neglected terms involving third- and higher-order derivatives. The last two terms on the right-hand side of Eq. (5.68) are the first- and the second-order scalar corrections to the function value at $\mathbf{x}$

which yields an approximation to the function value at $(\mathbf{x} + \boldsymbol{\delta}\mathbf{x})$. Thus we may write

$$F(\mathbf{x} + \boldsymbol{\delta}x) \simeq \psi + \delta\psi \tag{5.71}$$

where $\delta\psi$ corresponds to the value of the scalar corrections or the change in value of the objective function.

The simplest derivative method is the method of steepest descent in which we use only the first-order correction term,

$$\delta\psi = \mathbf{g}^{\mathrm{T}}\,\boldsymbol{\delta}\mathbf{x} = \|\mathbf{g}\|\,\|\boldsymbol{\delta}\mathbf{x}\| \cos\theta \tag{5.72}$$

where $\theta$ is the angle between the vectors $\mathbf{g}$ and $\boldsymbol{\delta}\mathbf{x}$, and $\|\cdot\|$ denotes the vector norm or length. For any given $\|\mathbf{g}\|$ and $\|\boldsymbol{\delta}\mathbf{x}\|$, $\delta\psi$ depends on $\cos\theta$ and takes the maximum negative value if $\theta = \pi$. Thus the maximum reduction in $\psi$ is obtained by making an adjustment $\boldsymbol{\delta}\mathbf{x}$ along the direction of the negative gradient $-\mathbf{g}$, i.e., $\boldsymbol{\delta}\mathbf{x} = \lambda(-\mathbf{g}/\|\mathbf{g}\|)$, where $\lambda$ is a parameter to be determined by a linear search along the direction of the negative gradient for a maximum reduction in $\psi$. Because the local direction of the negative gradient is generally not toward the global minimum, an iterative procedure must be used, and convergence to a minimum point is usually very slow.

For Newton's method, we use both the first- and second-order correction terms, i.e.,

$$\begin{aligned}\delta\psi &= \mathbf{g}^{\mathrm{T}}\,\boldsymbol{\delta}\mathbf{x} + \tfrac{1}{2}\boldsymbol{\delta}\mathbf{x}^{\mathrm{T}}\mathbf{H}\,\boldsymbol{\delta}\mathbf{x} \\ &= \sum_{i=1}^{n} \frac{\partial F(\mathbf{x})}{\partial x_i}\,\delta x_i + \frac{1}{2}\sum_{i=1}^{n}\sum_{j=1}^{n} \delta x_i\,\frac{\partial^2 F(\mathbf{x})}{\partial x_i\,\partial x_j}\,\delta x_j\end{aligned} \tag{5.73}$$

To find the condition for an extremum, we carry out partial differentiation of the right-hand side of Eq. (5.73) with respect to $\delta x_k$, $k = 1, 2, \ldots, n$. Assuming $\mathbf{g}$ and $\mathbf{H}$ are fixed in differentiation with respect to $\delta x_k$, we set the results to zero and obtain

$$\frac{\partial F(\mathbf{x})}{\partial x_k} + \sum_{i=1}^{n} \delta x_i\,\frac{\partial^2 F(\mathbf{x})}{\partial x_i\,\partial x_k} = 0, \qquad k = 1, 2, \ldots, n \tag{5.74}$$

In matrix notation and using Eqs. (5.69) and (5.70), Eq. (5.74) becomes

$$\mathbf{g} + \mathbf{H}\,\boldsymbol{\delta}\mathbf{x} = \mathbf{0} \tag{5.75}$$

Because Eq. (5.75) is a set of linear equations in $\delta x_i$, $i = 1, 2, \ldots, n$, we may apply linear inversion and obtain an optimal adjustment vector given by

$$\boldsymbol{\delta}\mathbf{x} = -\mathbf{H}^{-1}\mathbf{g} \tag{5.76}$$

If the objective function is quadratic in $\mathbf{x}$, the approximation used in Newton's method is exact, and the minimum can be reached from any $\mathbf{x}$ in a single step. For more general objective functions, an iterative procedure must be used with an initial estimate of $\mathbf{x}$ sufficiently near the minimum in order for Newton's method to converge. Since this can not be guaranteed, modern computer codes for optimization usually include modifications to ensure that (1) the $\boldsymbol{\delta}\mathbf{x}$ generated at each iteration is a descent or downhill direction, and (2) an approximate minimum along this direction is found. The general form of the iteration is $\boldsymbol{\delta}\mathbf{x} = -\alpha\mathbf{G}\mathbf{g}$, where $\mathbf{G}$ is a positive-definite approximation to $\mathbf{H}^{-1}$ based on second-derivative information, and $\alpha$ represents the distance along the $-\mathbf{G}\mathbf{g}$ direction to step. Alternatively, as iterations proceed, an approximate Hessian matrix may be built up without computing second derivatives. This is known as the Quasi-Newton or variable metric method. For more details on the derivative methods and their implementations, readers may refer, for example, to R. Fletcher (1980), and Gill *et al.* (1981).

### *5.4.3. Nonlinear Least Squares*

The application of optimization techniques to model fitting by least squares may be considered as a method for minimizing errors of fit (or residuals) at a set of $m$ data points where the coordinates of the $k$th data point are $(\mathbf{x})_k$, $k = 1, 2, \ldots, m$. The objective function for the present problem is

$$F(\mathbf{x}) = \sum_{k=1}^{m} [r_k(\mathbf{x})]^2 \tag{5.77}$$

where $r_k(\mathbf{x})$ denotes the evaluation of residual $r(\mathbf{x})$ at the $k$th data point. We may consider $r_k(\mathbf{x})$, $k = 1, 2, \ldots, m$, as components of a vector in an $m$-dimensional Euclidean space and write

$$\mathbf{r} = (r_1(\mathbf{x}), \quad r_2(\mathbf{x}), \quad \ldots, \quad r_m(\mathbf{x}))^{\mathrm{T}} \tag{5.78}$$

Therefore, Eq. (5.77) becomes

$$F(\mathbf{x}) = \mathbf{r}^{\mathrm{T}}\mathbf{r} \tag{5.79}$$

To find the gradient vector $\mathbf{g}$, we perform partial differentiation on Eq. (5.77) with respect to $x_i$, $i = 1, 2, \ldots, n$, and obtain

$$\partial F(\mathbf{x})/\partial x_i = \sum_{k=1}^{m} 2r_k(\mathbf{x})[\partial r_k(\mathbf{x})/\partial x_i], \qquad i = 1, 2, \ldots, n \tag{5.80}$$

or in matrix form using Eq. (5.69)

$$\mathbf{g} = 2\mathbf{A}^{\mathrm{T}}\mathbf{r} \tag{5.81}$$

where the Jacobian matrix $\mathbf{A}$ is defined by

$$\mathbf{A} = \begin{pmatrix} \partial r_1/\partial x_1 & \partial r_1/\partial x_2 & \cdots & \partial r_1/\partial x_n \\ \partial r_2/\partial x_1 & \partial r_2/\partial x_2 & \cdots & \partial r_2/\partial x_n \\ & & \vdots & \\ \partial r_m/\partial x_1 & \partial r_m/\partial x_2 & \cdots & \partial r_m/\partial x_n \end{pmatrix} \tag{5.82}$$

To find the Hessian matrix $\mathbf{H}$, we perform partial differentiation on Eq. (5.80) with respect to $x_j$ assuming that $r_k(\mathbf{x})$, $k = 1, 2, \ldots, m$, have continuous second partial derivatives, and obtain

$$\frac{\partial^2 F(\mathbf{x})}{\partial x_i\, \partial x_j} = 2\sum_{k=1}^{m} \frac{\partial r_k(\mathbf{x})}{\partial x_i}\frac{\partial r_k(\mathbf{x})}{\partial x_j} + 2\sum_{k=1}^{m} r_k(\mathbf{x})\frac{\partial^2 r_k(\mathbf{x})}{\partial x_i\, \partial x_j} \tag{5.83}$$

for $i = 1, 2, \ldots, n$ and $j = 1, 2, \ldots, n$. In the usual least-squares method, we neglect the second term on the right-hand side of Eq. (5.83), and we have in matrix notation using Eq. (5.70)

$$\mathbf{H} \simeq 2\mathbf{A}^{\mathrm{T}}\mathbf{A} \tag{5.84}$$

This approximation to $\mathbf{H}$ requires only the first derivatives of the residuals. Now, we can apply Newton's method and find an optimal adjustment vector. Substituting Eqs. (5.81) and (5.84) into Eq. (5.76), we have

$$\boldsymbol{\delta}\mathbf{x} = -[\mathbf{A}^{\mathrm{T}}\mathbf{A}]^{-1}\mathbf{A}^{\mathrm{T}}\mathbf{r} \tag{5.85}$$

and the resulting iterative procedure is known as the Gauss–Newton method.

In actual applications, the Gauss–Newton method may fail for a wide variety of reasons. For example, if the initial estimate of $\mathbf{x}$ to start the iterative procedure is not near the minimum, then the quadratic approximation used in Eq. (5.73) may not be valid. Although we have reduced a nonlinear problem to solving a set of linear equations, we may still encounter many difficulties in linear inversion as discussed previously. Many strategies have been proposed to improve the Gauss–Newton method. For example, Levenberg (1944) suggested that Eq. (5.85) be replaced by

$$\boldsymbol{\delta}\mathbf{x} = -[\mathbf{A}^{\mathrm{T}}\mathbf{A} + \theta^2\mathbf{I}]^{-1}\mathbf{A}^{\mathrm{T}}\mathbf{r} \tag{5.86}$$

where $\mathbf{I}$ is an identity matrix, and $\theta$ may be adjusted to control the iteration step size. If $\theta \to \infty$, $\boldsymbol{\delta}\mathbf{x}$ tends to $\mathbf{A}^{\mathrm{T}}\mathbf{r}/\theta^2$ which is an adjustment in the

steepest descent direction. If $\theta \to 0$, $\boldsymbol{\delta}\mathbf{x}$ is the Gauss–Newton adjustment vector. The idea is to guarantee a decrease in the sum of squares of the residuals via steepest descent when x is far from the minimum, and to switch to the rapid convergence of Newton's method as the minimum is approached. Marquardt (1963) improved upon Levenberg's idea by devising a simple scheme for choosing $\theta$ at each iteration. The Levenberg–Marquardt method is also known as the damped least squares method and has been widely used.

In the last two decades, numerous papers have been written on nonlinear least squares. Readers may consult, for example, Chambers (1977), Gill and Murray (1978), Dennis *et al.* (1979), R. Fletcher (1980), and Gill *et al.* (1981) for more detailed information.

# 6. Methods of Data Analysis

After a microearthquake network is in operation, the first problem facing the seismologist is to determine the basic parameters of the recorded earthquakes, such as origin time, hypocenter location, magnitude, fault-plane solution, etc. In Chapter 3 we discussed various techniques of processing seismic data to obtain arrival times, first motions, amplitudes and periods, and signal durations. To determine origin time and hypocenter location, we need the coordinates of the network stations, a realistic velocity structure model that characterizes the network area, and at least four arrival times to the network stations. The principal arrival time data from a microearthquake network are first P-arrival times. Arrival times of later phases are usually difficult to determine because most microearthquake networks consist mainly of vertical-component seismometers and record with a limited dynamic range and frequency bandwidth. Locating earthquakes with P-arrivals only is not too difficult if the earthquakes occurred inside the network. However, for earthquakes outside the network, first P-arrival times may not be sufficient to determine earthquake locations.

Difficulties in identifying later phases also limit the study of focal mechanism to fault-plane solutions of first P-motions. Earthquake magnitude is usually estimated either by maximum amplitude and period or by signal duration. In this chapter, we review the basic methods for determining earthquake parameters and the velocity structure beneath a microearthquake network. Emphasis is placed on methods that utilize general-purpose digital computers. In order to avoid some mathematical details in this section, we have developed the necessary mathematical tools in Chapters 4 and 5. These two chapters are a prerequisite to understand the following material.

## 6.1. Determination of Origin Time and Hypocenter

If an earthquake occurs at origin time $t_0$ and at hypocenter location ($x_0$, $y_0$, $z_0$), a set of arrival times may be obtained from a microearthquake network. Using these data to find the origin time and hypocenter of an earthquake is referred to as the earthquake location problem. This problem has been studied extensively in seismology (see, e.g., Byerly, 1942, pp. 216–225; Richter, 1958, pp. 314–323; Bath, 1973, pp. 101–110; Buland, 1976). In this section, we discuss how to solve the earthquake location problem for microearthquake networks. We will concentrate on a single method (i.e., Geiger's method) because it is the technique most commonly implemented on a general-purpose digital computer today.

Because a computer does fail occasionally, it is useful to know a few simple techniques to determine an earthquake epicenter quickly. Origin time and focal depth are often of secondary importance and may be estimated crudely. For a dense microearthquake network, the location of the station with the earliest first P-arrival time is a good estimate of the earthquake epicenter, provided that this station is not situated near the edge of the network. If one plots the first P-arrival times on a map of the stations, one may contour the times and place the epicenter at the point with the earliest possible time.

If both P- and S-arrival times are available, one may use S–P intervals to obtain a rough estimate of the epicentral distance $D$ to the station

$$D = [V_p V_s/(V_p - V_s)](T_s - T_p) \tag{6.1}$$

where $V_p$ is the P-wave velocity, $V_s$ the S-wave velocity, $T_s$ the S-arrival time, and $T_p$ the P-arrival time. For a typical P-wave velocity of 6 km/sec, and $V_p/V_s \simeq 1.8$, the distance $D$ in kilometers is about 7.5 times the S–P interval measured in seconds. If three or more epicentral distances $D$ are available, the epicenter may be placed at the intersection of circles with the stations as centers and the appropriate $D$ as radii. The intersection will seldom be a point and its areal extent gives a rough estimate of the uncertainty of the epicenter location.

### *6.1.1. Formulation of the Earthquake Location Problem*

Because the horizontal extent of a microearthquake network seldom exceeds several hundred kilometers, curvature of the earth may be neglected, and it is adequate to use a Cartesian coordinate system ($x$, $y$, $z$) for locating local earthquakes. Usually a point near the center of a given microearthquake network is chosen as the coordinate origin. The $x$ axis is along the east–west direction, the $y$ axis is along the north–south direc-

tion, and the $z$ axis is along the vertical direction pointing downward. Any position on earth may be specified by latitude $\phi$, longitude $\lambda$, and elevation above sea level $h$. If the position is between 70°N and 70°S in latitude, it may be converted to $(x, y, z)$ with respect to the coordinate origin at latitude $\phi_0$, longitude $\lambda_0$, and elevation at sea level by a method described by Richter (1958, pp. 701–705), as

$$x = 60 \cdot A(\lambda - \lambda_0), \qquad y = 60 \cdot B(\phi - \phi_0) \qquad z = -0.001h \tag{6.2}$$

where $x$, $y$, and $z$ are in kilometers, $\lambda$, $\lambda_0$, $\phi$, and $\phi_0$ are given in degrees, and $h$ is given in meters. Values for $A$ and $B$ may be derived from Woodward (1929)

$$\begin{aligned} A &\simeq (1.8553654 + 0.0062792 \sin^2\Phi + 0.0000319 \sin^4\Phi)\cos\Phi \\ B &\simeq 1.8428071 + 0.0187098 \sin^2\Phi + 0.0001583 \sin^4\Phi \end{aligned} \tag{6.3}$$

where $\Phi = \frac{1}{2}(\phi + \phi_0)$ and is given in degrees.

In the earthquake location problem, we are concerned with a four-dimensional space: the time coordinate $t$, and the spatial coordinates $x$, $y$, and $z$. A vector in this space may be written as

$$\boldsymbol{\chi} = (t, x, y, z)^{\mathrm{T}} \tag{6.4}$$

where the superscript T denotes the transpose. In Chapter 5, we used $\mathbf{x}$ to denote a vector in an $n$-dimensional Euclidean space in which the coordinates are $x_1, x_2, \ldots, x_n$. Since it is common to denote the spatial coordinates by $x$, $y$, and $z$, we have changed our notation here. Furthermore, the subscript $k$ of the coordinates is now used to index the observation made at the $k$th station.

To locate an earthquake using a set of arrival times $\tau_k$ from stations at positions $(x_k, y_k, z_k)$, $k = 1, 2, \ldots, m$, we must first assume an earth model in which theoretical travel times $T_k$ from a trial hypocenter at position $(x^*, y^*, z^*)$ to the stations can be computed. Let us consider a given trial origin time and hypocenter as a trial vector $\boldsymbol{\chi}^*$ in a four-dimensional Euclidean space

$$\boldsymbol{\chi}^* = (t^*, x^*, y^*, z^*)^{\mathrm{T}} \tag{6.5}$$

Theoretical arrival time $t_k$ from $\boldsymbol{\chi}^*$ to the $k$th station is the theoretical travel time $T_k$ plus the trial origin time $t^*$, or

$$t_k(\boldsymbol{\chi}^*) = T_k(\boldsymbol{\chi}^*) + t^* \qquad \text{for} \quad k = 1, 2, \ldots, m \tag{6.6}$$

Strictly speaking, $T_k$ does not depend on $t^*$, but we express $T_k$ as $T_k(\boldsymbol{\chi}^*)$ for convenience in notation.

We now define the arrival time residual at the $k$th station, $r_k$, as the difference between the observed and the theoretical arrival times, or

$$(6.7) \qquad \begin{aligned} r_k(\boldsymbol{\chi}^*) &= \tau_k - t_k(\boldsymbol{\chi}^*) \\ &= \tau_k - T_k(\boldsymbol{\chi}^*) - t^* \qquad \text{for} \quad k = 1, 2, \ldots, m \end{aligned}$$

Our objective is to adjust the trial vector $\boldsymbol{\chi}^*$ such that the residuals are minimized in some sense. Generally, the least squares approach is used in which we minimize the sum of the squares of the residuals.

We have shown in Chapter 4 that the travel time between two end points is usually a nonlinear function of the spatial coordinates. Thus locating earthquakes is a problem in nonlinear optimization. In Section 5.4, we have given a brief introduction to nonlinear optimization, and we now make use of some of those results.

### *6.1.2. Derivation of Geiger's Method*

Geiger (1912) appears to be the first to apply the Gauss–Newton method (see Section 5.4.3) in solving the earthquake location problem. Although Geiger presented a method for determining the origin time and epicenter, it can be easily extended to include focal depth. Using the mathematical tools developed in Section 5.4.3, Geiger's method may be derived as follows. The objective function for the least squares minimization [Eq. (5.77)] as applied to the earthquake location problem is

$$(6.8) \qquad F(\boldsymbol{\chi}^*) = \sum_{k=1}^{m} [r_k(\boldsymbol{\chi}^*)]^2$$

where the residual $r_k(\boldsymbol{\chi}^*)$ is given by Eq. (6.7), and $m$ is the total number of observations. We may consider the residuals $r_k(\boldsymbol{\chi}^*)$, $k = 1, 2, \ldots, m$, as components of a vector in an $m$-dimensional Euclidean space and write

$$(6.9) \qquad \mathbf{r} = (r_1(\boldsymbol{\chi}^*), \quad r_2(\boldsymbol{\chi}^*), \quad \ldots, \quad r_m(\boldsymbol{\chi}^*))^{\mathrm{T}}$$

The adjustment vector [Eq. (5.66)] now becomes

$$(6.10) \qquad \boldsymbol{\delta\chi} = (\delta t, \delta x, \delta y, \delta z)^{\mathrm{T}}$$

In the Gauss–Newton method, a set of linear equations is solved for the adjustment vector at each iteration step. In our case, the set of linear equations [Eq. (5.85)] may be written as

$$(6.11) \qquad \mathbf{A}^{\mathrm{T}}\mathbf{A}\boldsymbol{\delta\chi} = -\mathbf{A}^{\mathrm{T}}\mathbf{r}$$

where the Jacobian matrix **A** as defined by Eq. (5.82) is now

$$\mathbf{A} = \begin{pmatrix} \partial r_1/\partial t & \partial r_1/\partial x & \partial r_1/\partial y & \partial r_1/\partial z \\ \partial r_2/\partial t & \partial r_2/\partial x & \partial r_2/\partial y & \partial r_2/\partial z \\ \vdots & \vdots & \vdots & \vdots \\ \partial r_m/\partial t & \partial r_m/\partial x & \partial r_m/\partial y & \partial r_m/\partial z \end{pmatrix} \tag{6.12}$$

and the partial derivatives are evaluated at the trial vector $\boldsymbol{\chi}^*$. Using arrival time residuals defined by Eq. (6.7), the Jacobian matrix **A** becomes

$$\mathbf{A} = -\begin{pmatrix} 1 & \partial T_1/\partial x & \partial T_1/\partial y & \partial T_1/\partial z \\ 1 & \partial T_2/\partial x & \partial T_2/\partial y & \partial T_2/\partial z \\ \vdots & \vdots & \vdots & \vdots \\ 1 & \partial T_m/\partial x & \partial T_m/\partial y & \partial T_m/\partial z \end{pmatrix}\Bigg|_{\chi^*} \tag{6.13}$$

The minus sign on the right-hand side of Eq. (6.13) arises from the traditional definition of arrival time residuals given by Eq. (6.7). Substituting Eq. (6.13) into Eq. (6.11), and carrying out the matrix operations, we have a set of four simultaneous linear equations in four unknowns

$$\mathbf{G}\,\boldsymbol{\delta\chi} = \boldsymbol{\rho} \tag{6.14}$$

where

$$\mathbf{G} = \begin{pmatrix} m & \sum a_i & \sum b_i & \sum c_i \\ \sum a_i & \sum a_i^2 & \sum a_i b_i & \sum a_i c_i \\ \sum b_i & \sum a_i b_i & \sum b_i^2 & \sum b_i c_i \\ \sum c_i & \sum a_i c_i & \sum b_i c_i & \sum c_i^2 \end{pmatrix} \tag{6.15}$$

$$\boldsymbol{\rho} = \left(\sum r_k, \sum a_k r_k, \sum b_k r_k, \sum c_k r_k\right)^{\mathrm{T}} \tag{6.16}$$

and the summation $\Sigma$ is for $k = 1, 2, \ldots, m$. In Eqs. (6.15) and (6.16), we have introduced

$$a_k = \partial T_k/\partial x|_{\chi^*}, \qquad b_k = \partial T_k/\partial y|_{\chi^*}, \qquad c_k = \partial T_k/\partial z|_{\chi^*} \tag{6.17}$$

in order to simplify writing the elements of **G** and $\boldsymbol{\rho}$.

Equation (6.14) is usually referred to as the system of normal equations for the earthquake location problem. Given a set of arrival times and the ability to compute travel times and derivatives from a trial vector $\boldsymbol{\chi}^*$, we may solve Eq. (6.14) for the adjustment vector $\boldsymbol{\delta\chi}$. We then replace $\boldsymbol{\chi}^*$ by

$\chi^* + \delta\chi$, and repeat the same procedure until some cutoff criteria are satisfied to stop the iteration. In other words, the nonlinear earthquake location problem is solved by an iterative procedure involving only solutions of a set of four linear equations.

Instead of solving an even-determined system of four linear equations as given by Eq. (6.14), we may derive an equivalent overdetermined system of $m$ linear equations from Eq. (6.11) as

$$\mathbf{A}\,\delta\chi = -\mathbf{r} \tag{6.18}$$

where the Jacobian matrix $\mathbf{A}$ is given by Eq. (6.13). Equation (6.18) is a set of $m$ equations written in matrix form, and by Eqs. (6.9), (6.10), and (6.13), it may be rewritten as

$$\begin{aligned} &\delta t + (\partial T_k/\partial x)|_{\chi^*}\,\delta x + (\partial T_k/\partial y)|_{\chi^*}\,\delta y + (\partial T_k/\partial z)|_{\chi^*}\,\delta z \\ &\quad = r_k(\chi^*) \qquad \text{for} \quad k = 1, 2, \ldots, m \end{aligned} \tag{6.19}$$

By using generalized inversion as discussed in Chapter 5, the system of $m$ equations as given by Eq. (6.19) may be solved directly for the adjustments $\delta t$, $\delta x$, $\delta y$, and $\delta z$. This way, we may avoid some of the computational difficulties associated with solving the normal equations as discussed in Section 5.3.2.

### *6.1.3. Implementation of Geiger's Method*

Geiger's method as derived in the previous subsection is computationally straightforward, but the method is too tedious for hand computation and hence was ignored by seismologists for nearly 50 years. In the late 1950s digital computers became generally available, and several seismologists quickly seized this opportunity to implement Geiger's method for determining origin time and hypocenter (e.g., Bolt, 1960; Flinn, 1960; Nordquist, 1962; Bolt and Turcotte, 1964; Engdahl and Gunst, 1966). Since then, many additional computer programs have been written for this problem, especially for locating local earthquakes (e.g., Eaton, 1969; Crampin, 1970; Lee and Lahr, 1975; Shapira and Bath, 1977; Klein, 1978; Herrmann, 1979; Johnson, 1979; Lahr, 1979; Lee *et al.*, 1981).

In deriving Geiger's method, we have not specified any particular seismic arrival times. Normally, the method is applied only to first P-arrival times because first P-arrivals are easier to identify on seismograms and the P-velocity structure of the earth is better known. However, if arrival times of later phases (such as S, $P_n$, etc.) are available, we can set up

additional equations [in the form of Eq. (6.19)] that are appropriate for the particular observed arrivals. Furthermore, if absolute timing is not available, we can still use S–P interval times to locate earthquakes. In this case, we modify Eq. (6.19) to read

$$(\partial T_k/\partial x)|_{\chi^*}\,\delta x + (\partial T_k/\partial y)|_{\chi^*}\,\delta y + (\partial T_k/\partial z)|_{\chi^*}\,\delta z = r_k(\chi^*) \qquad \text{for} \quad k = 1, 2, \ldots, m \tag{6.20}$$

where $r_k$ is the residual for the S–P interval time at the $k$th station, $T_k$ is the theoretical S–P interval time, and the $\delta t$ term in Eq. (6.19) drops out because S–P interval times do not depend on the origin time.

We must be cautious in using arrival times of later phases for locating local earthquakes because later phases may be misidentified on the seismograms and their corresponding theoretical arrival times may be difficult to model. If the station coverage for an earthquake is adequate azimuthally (i.e., the maximum azimuthal gap between stations is less than 90°), and if one or more stations are located with epicentral distances less than the focal depth, then later arrivals are not needed in the earthquake location procedure. On the other hand, if the station distribution is poor, then later arrivals will improve the earthquake location, as we will discuss later.

Before we examine the pitfalls of applying Geiger's method to the earthquake location problem, let us first summarize its computational procedure. Given a set of observed arrival times $\tau_k$, $k = 1, 2, \ldots, m$, at stations with coordinates $(x_k, y_k, z_k)$, $k = 1, 2, \ldots, m$, we wish to determine the origin time $t_0$, and the hypocenter $(x_0, y_0, z_0)$ of an earthquake. Geiger's method involves the following computational steps:

(1) Guess a trial origin time $t^*$, and a trial hypocenter $(x^*, y^*, z^*)$.
(2) Compute the theoretical travel time $T_k$, and its spatial partial derivatives, $\partial T_k/\partial x$, $\partial T_k/\partial y$, and $\partial T_k/\partial z$ evaluated at $(x^*, y^*, z^*)$, from the trial hypocenter to the $k$th station for $k = 1, 2, \ldots, m$.
(3) Compute matrix G as given by Eqs. (6.15) and (6.17), and vector $\boldsymbol{\rho}$ as given by Eqs. (6.16), (6.17), and (6.7).
(4) Solve the system of four linear equations as given by Eq. (6.14) for the adjustments $\delta t$, $\delta x$, $\delta y$, and $\delta z$.
(5) An improved origin time is then given by $t^* + \delta t$, and an improved hypocenter by $(x^* + \delta x, y^* + \delta y, z^* + \delta z)$. We use these as our new trial origin time and hypocenter.
(6) Repeat steps 2 to 5 until some cutoff criteria are met. At that point, we set $t_0 = t^*$, $x_0 = x^*$, $y_0 = y^*$, and $z_0 = z^*$ as our solution for the origin time and hypocenter of the earthquake.

It is obvious from step 2 that a model of the seismic velocity structure underneath the microearthquake network must be specified in order to compute theoretical travel times and derivatives. Therefore, earthquakes are located with respect to the assumed velocity model and not to the real earth. Routine earthquake locations for microearthquake networks are based mainly on a horizontally layered velocity model, and the problem of lateral velocity variations usually is ignored. Such a practice is often due to our poor knowledge of the velocity structure underneath the microearthquake network and the difficulties in tracing seismic rays in a heterogeneous medium (see Chapter 4). As a result, it is not easy to obtain accurate earthquake locations, as shown, for example, by Engdahl and Lee (1976).

Although step 3 is straightforward, we must be careful in forming the normal equations to avoid roundoff errors (see Section 5.3.1). Many numerical methods are available to solve a set of four linear equations in step 4, but few will handle ill-conditioned cases (see Section 5.3.2). The matrix **G** is often ill-conditioned if the station distribution is poor. Having data from four or more stations is not always sufficient to locate an earthquake. These stations should be distributed such that the earthquake hypocenter is surrounded by stations. Since most seismic stations are located near the earth's surface and whereas earthquakes occur at some depth, it is difficult to determine the focal depth in general. Similarly, if an earthquake occurs outside a microearthquake network, it is also difficult to determine the epicenter. To illustrate these difficulties, let us consider a simple case with only four observations. In this case, we do not need to form the normal equations, and our problem is to solve Eq. (6.18) for $m = 4$. The Jacobian matrix **A** becomes

$$\mathbf{A} = -\begin{pmatrix} 1 & \partial T_1/\partial x & \partial T_1/\partial y & \partial T_1/\partial z \\ 1 & \partial T_2/\partial x & \partial T_2/\partial y & \partial T_2/\partial z \\ 1 & \partial T_3/\partial x & \partial T_3/\partial y & \partial T_3/\partial z \\ 1 & \partial T_4/\partial x & \partial T_4/\partial y & \partial T_4/\partial z \end{pmatrix} \tag{6.21}$$

Let us recall that the determinant of a matrix is zero if any column of it is a multiple of another column (Noble, 1969, p. 204). Since the first column of **A** is all 1's, it is easy for the other columns of **A** to be a multiple of it. For example, if P-arrivals from the same refractor are observed in a layered velocity model, then all elements in the $\partial T/\partial z$ column have the same value, and the fourth column of **A** is thus a multiple of the first column. Similarly, if an earthquake occurs outside the network, it is likely that the

elements of the $\partial T/\partial x$ column and the corresponding elements of the $\partial T/\partial y$ column will be nearly proportional to each other.

The preceding argument may be generalized for the $m \times 4$ Jacobian matrix **A** given by Eq. (6.13). As discussed in Section 5.3, the rank of a matrix is defined as the maximum number of independent columns. If a matrix has a column that is nearly a multiple of another column, then we have a rank-defective matrix with a very small singular value. Consequently, the condition number of the matrix is very large, so that the linear system given by Eq. (6.18) is difficult to solve. This is usually referred to as an ill-conditioned case. Hence the properties of the Jacobian matrix **A** determine whether or not step 4 can be carried out numerically.

The elements of the Jacobian matrix **A** are the spatial partial derivatives of the travel times from the trial hypocenter to the stations, as given by Eq. (6.13). As discussed in Section 4.4.1, these derivatives depend on the velocity and the direction angles of the seismic rays at the trial hypocenter [see Eq. (4.66)]. Because the direction angles of the seismic rays depend on the geometry of the trial hypocenter with respect to the stations, station distribution relative to the earthquakes plays a critical role in whether or not the earthquakes can be located by a microearthquake network.

If the station distribution is poor, introducing arrival times of later phases in the earthquake location procedure is desirable. Because they have different values for their travel time derivatives than those for the first P-arrivals, the chance that the Jacobian matrix **A** will have nearly dependent columns may be reduced. In other words, later arrivals will reduce the condition number of matrix **A**, so that Eq. (6.18) may be solved numerically.

Lee and Lahr (1975) recognized that there may be difficulties in solving for the adjustment vector $\boldsymbol{\delta\chi}^*$ in Eq. (6.14). They introduced a stepwise multiple regression technique (e.g., Draper and Smith, 1966) in the earthquake location procedure. Basically, if the Jacobian matrix **A** is ill-conditioned, we reduce the components of $\boldsymbol{\delta\chi}^*$ to be solved. In other words, a hypocenter parameter will not be adjusted if there is not sufficient information in the observed data to determine its adjustment. Another approach is to apply generalized inversion techniques as discussed in Chapter 5. Examples of using this approach are the location programs written by Bolt (1970), Klein (1978), Johnson (1979), and Lee *et al.* (1981).

Geiger's method is an iterative procedure. Naturally, we ask if the iteration converges to the global minimum of our objective function as given by Eq. (6.8). This depends on the station distribution with respect to the earthquake, the initial guess of the trial origin time and hypocenter, the observed arrival times, and the velocity model used to compute travel-times and derivatives. At present, there is no method available to guaran-

tee reaching a global minimum by an iterative procedure, and readers are referred to Section 5.4 and the references cited therein. Iterations usually are terminated if the adjustments or the root-mean-square value of the residuals falls below some prescribed value, or if the allowed maximum number of iterations is exceeded.

There are errors and sometimes blunders in reading arrival times and station coordinates. The least squares method is appropriate if the errors are independent and random. Otherwise, it will give disproportional weight to data with large errors and distort the solution so that errors are spread among the stations. Consequently, low residuals do not necessarily imply that the earthquake location is good. It must be emphasized that the quality of an earthquake location depends on the quality of the input data. No mathematical manipulation can substitute for careful preparation of the input data. It is quite easy to write an earthquake location program for a digital computer using Geiger's method. However, it is difficult to validate the correctness of the program code. Furthermore, it is not easy to write an earthquake location program that will handle errors in the input data properly and let the users know if they are in trouble. The mechanics of locating earthquakes have been discussed, for example, by Buland (1976), and problems of implementing a general-purpose earthquake location program for microearthquake networks are discussed, for example, by Lee *et al.* (1981).

In this section, we have not treated the method for joint hypocenter determination and related techniques. These techniques are generalizations of Geiger's method to include station corrections for travel time as additional parameters to be determined from a group of earthquakes. Readers may refer to works, for example, by Douglas (1967), Dewey (1971), and Bolt *et al.* (1978). Also, we have not dealt with the problem of using more complicated velocity models for microearthquake location. In principle, seismic ray tracing in a heterogeneous medium (see Chapter 4) can be applied in a straightforward manner (e.g., Engdahl and Lee, 1976), but at present the computation is too expensive for routine work. Recently, Thurber and Ellsworth (1980) introduced a method to compute rapidly the minimum time ray path in a heterogeneous medium. They first constructed a one-dimensional, laterally average velocity model from a given three-dimensional velocity structure, and then determined the minimum time ray path by the standard technique for a horizontally layered velocity model (see Section 4.4.4.). In addition, many advances in seismic ray tracing and in inversion for velocity structure have been made in explosion seismology. Numerous publications have appeared, and readers may refer to works, for example, by McMechan (1976), Mooney and Prodehl (1978), Cerveny and Hron (1980), and McMechan and Mooney

(1980). We expect that many techniques resulting from these advances will be applied to microearthquake data in the near future.

## 6.2. Fault-Plane Solution

The elastic rebound theory of Reid (1910) is commonly accepted as an explanation of how most earthquakes are generated. This theory has been concisely described by Stauder (1962, p. 1) as follows: earthquakes occur in regions of the earth that are undergoing deformation. Energy is stored in the form of elastic strain as the region is deformed. This process continues until the accumulated strain exceeds the strength of the rock, and then fracture or faulting occurs. The opposite sides of the fault rebound to a new equilibrium position, and the energy is released in the vibrations of seismic waves and in heating and crushing of the rock. If earthquakes are caused by faulting, it is possible to deduce the nature of faulting from an adequate set of seismograms, and in turn, the nature of the stresses that deform the region.

Let us now consider a simple earthquake mechanism as suggested by the 1906 San Francisco earthquake. Figure 26 illustrates in plan view a

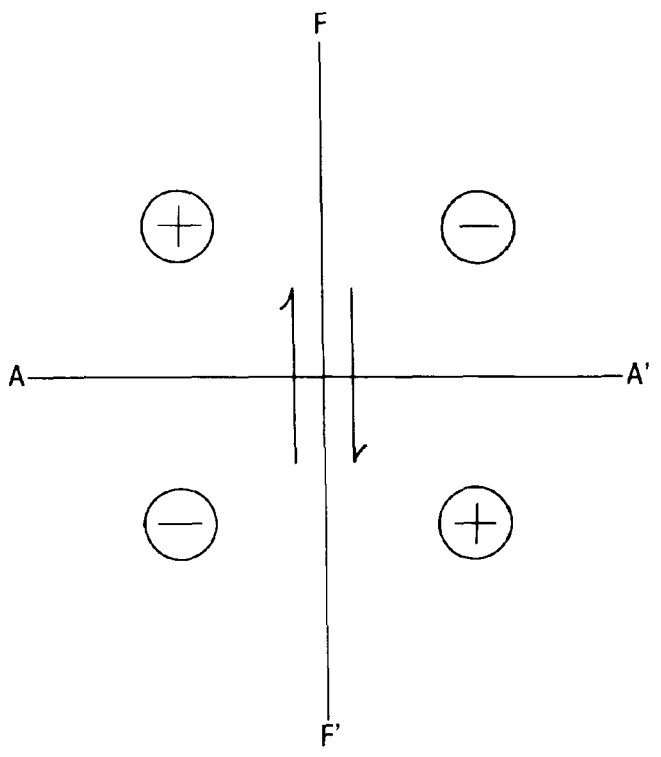


**Fig. 26.** Plan view of the distribution of compressions (+) and dilatations (−) resulting from a right lateral displacement along a vertical fault *FF'*.

purely horizontal motion on a vertical fault $FF'$, and the arrows represent the relative movement of the two sides of the fault. Intuition suggests that material ahead of the arrows is compressed or pushed away from the source, whereas material behind the arrows is dilated or pulled toward the source. Consequently, the area surrounding the earthquake focus is divided into quadrants in which the first motion of P-waves is alternately a compression or a dilatation as shown in Fig 26. These quadrants are separated by two orthogonal planes $AA'$ and $FF'$, one of which ($FF'$) is the fault plane. The other plane ($AA'$) is perpendicular to the direction of fault movement and is called the auxiliary plane.

As cited by Honda (1962), T. Shida in 1919 found that the distribution of compressions and dilatations of the initial motions of P-waves of two earthquakes in Japan showed very systematic patterns. This led H. Nakano in 1923 to investigate theoretically the propagation of seismic waves that are generated by various force systems acting at a point in an infinite homogeneous elastic medium. Nakano found that a source consisting of a single couple (i.e., two forces oppositely directed and separated by a small distance) would send alternate compressions and dilatations into quadrants separated by two orthogonal planes, just as our intuition suggests in Fig. 26. Since the P-wave motion along these planes is null, they are called nodal planes and correspond to the fault plane and the auxiliary plane described previously. Encouraged by Nakano's result, P. Byerly in 1926 recognized that if the directions of first motion of P-waves in regions around the source are known, it is possible to infer the orientation of the fault and the direction of motion on it. However, the earth is not homogeneous, and faulting may take place in any direction along a dipping fault plane. Therefore, it is necessary to trace the observed first motions of P-waves back to a hypothetical focal sphere (i.e., a small sphere enclosing the earthquake focus), and to develop techniques to find the two orthogonal nodal planes which separate quadrants of compressions and dilatations on the focal sphere.

From the 1920s to the 1950s, many methods for determining fault planes were developed by seismologists in the United States, Canada, Japan, Netherlands, and USSR. Notable among them are P. Byerly, J. H. Hodgson, H. Honda, V. Keilis-Borok, and L. P. G. Koning. Not only are first motions of P-waves used, but also data from S-waves and surface waves. Readers are referred to review articles by Stauder (1962) and by Honda (1962) for details.

### *6.2.1. P-Wave First Motion Data*

For most microearthquake networks, fault-plane solutions of earthquakes are based on first motions of P-waves. The reason is identical to

that for locating earthquakes: later phases are difficult to identify because of limited dynamic range in recording and the common use of only vertical-component seismometers. As discussed earlier, deriving a fault-plane solution amounts to finding the two orthogonal nodal planes which separate the first motions of P-waves into compressional and dilatational quadrants on the focal sphere. The actual procedure consists of three steps:

(1) First arrival times of P-waves and their corresponding directions of motion for an earthquake are read from vertical-component seismograms. Normally one uses the symbol $U$ or $C$ or $+$ for up motions, and either $D$ or $-$ for down motions.

(2a) Information for tracing the observed first motions of P-waves back to the focal sphere is available from the earthquake location procedure using Geiger's method. The position of a given seismic station on the surface of the focal sphere is determined by two angles $\alpha$ and $\beta$. $\alpha$ is the azimuthal angle (measured clockwise from the north) from the earthquake epicenter to the given station. $\beta$ is the take-off angle (with respect to the downward vertical) of the seismic ray from the earthquake hypocenter to the given station. The former is computed from the coordinates of the hypocenter and of the given station. The latter is determined in the course of computing the travel time derivatives as described in Section 4.4. Accordingly, if first motions of P-waves ($\gamma$) are observed at a set of $m$ stations, we will have a data set $(\alpha_k, \beta_k, \gamma_k)$, $k = 1, 2, \ldots, m$, describing the polarities of first motions on the focal sphere; $\gamma_k$ will be either a $C$ for compression or a $D$ for dilatation.

(2b) Since it is not convenient to plot data on a spherical surface, we need some means of projecting a three-dimensional sphere onto a piece of paper. Various projection techniques have been employed to plot the P-wave first motion data. The most commonly used are stereographic or equal-area projection. The stereographic projection has been used extensively in structural geology to describe and analyze faults and other geological features. Readers are referred to some elementary texts (e.g., Billings, 1954, pp. 482–488; Ragan, 1973, pp. 91–102) for a discussion of this technique. The equal-area projection is very similar to the stereographic projection and is preferred for fault-plane solutions because area on the focal sphere is preserved in this projection (see Fig. 27 for comparison). A point on the focal sphere may be specified by $(R, \alpha, \beta)$, where $R$ is the radius, $\alpha$ is the azimuthal angle, and $\beta$ is the take-off angle. In equal-area projection, these parameters $(R, \alpha, \beta)$ are transformed to plane polar coordinates $(r, \theta)$ by the following formulas (Maling, 1973, pp. 141–144):

$$r = 2R \sin(\beta/2), \qquad \theta = \alpha \tag{6.22}$$

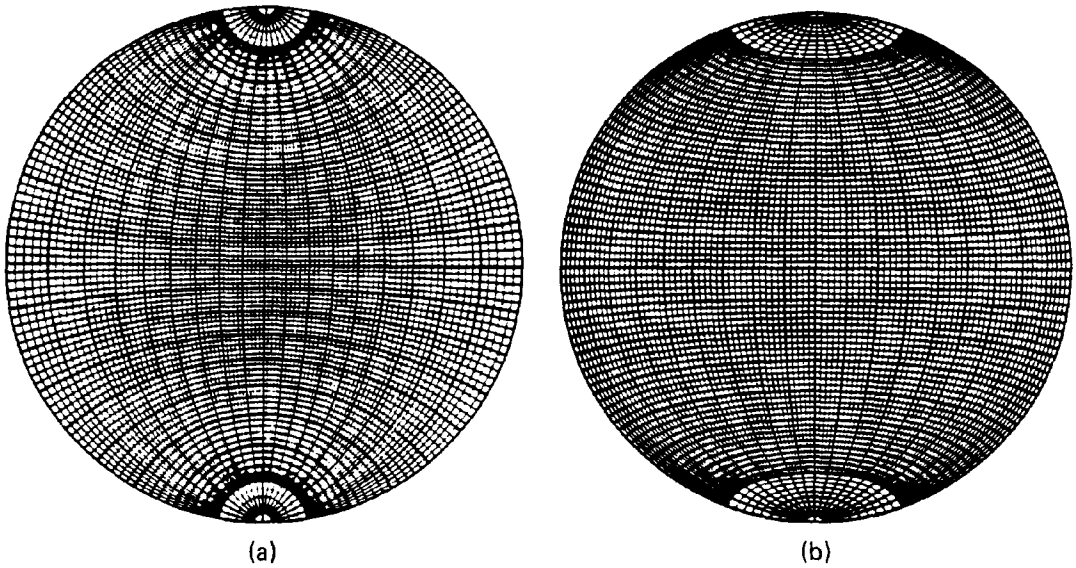


**Fig. 27.** Comparison of the stereographic (or Wulff) net (a) and the equal-area (or Schmidt) net (b). Note the areal distortion of the Wulff net compared with the Schmidt net.

Since the radius of the focal sphere ($R$) is immaterial and the maximum value of $r$ is more conveniently taken as unity, Eq. (6.22) is modified to read

$$r = \sqrt{2}\sin(\beta/2), \qquad \theta = \alpha \tag{6.23}$$

This type of equal-area projection appears to have been introduced by Honda and Emura (1958) in fault-plane solution work. The set of P-wave first motion polarities ($\alpha_k$, $\beta_k$, $\gamma_k$), $k = 1, 2, \ldots, m$, may then be represented by plotting the symbol for $\gamma_k$ at ($r_k$, $\theta_k$) using Eq. (6.23). This is usually plotted on computer printouts by an earthquake location program, such as HYPO71 (Lee and Lahr, 1975).

(2c) Because most seismic rays from a shallow earthquake recorded by a microearthquake network are down-going rays, it is convenient to use the equal-area projection of the lower focal hemisphere. In this case, we must take care of up-going rays (i.e., $\beta > 90°$) by substituting ($180° + \alpha$) for $\alpha$, and ($180° - \beta$) for $\beta$. For example, the HYPO71 location program provides P-wave first motion plots on the lower focal hemisphere. This practice is preferred over the upper focal hemisphere projection because it is more natural to visualize fault planes on the earth in the lower focal hemisphere projection. Readers are warned, however, that some authors use the upper focal hemisphere projection, and some do not specify which one they use.

(2d) Two elementary operations on the equal-area projection are required in order to carry out fault-plane solutions manually. Figure 28

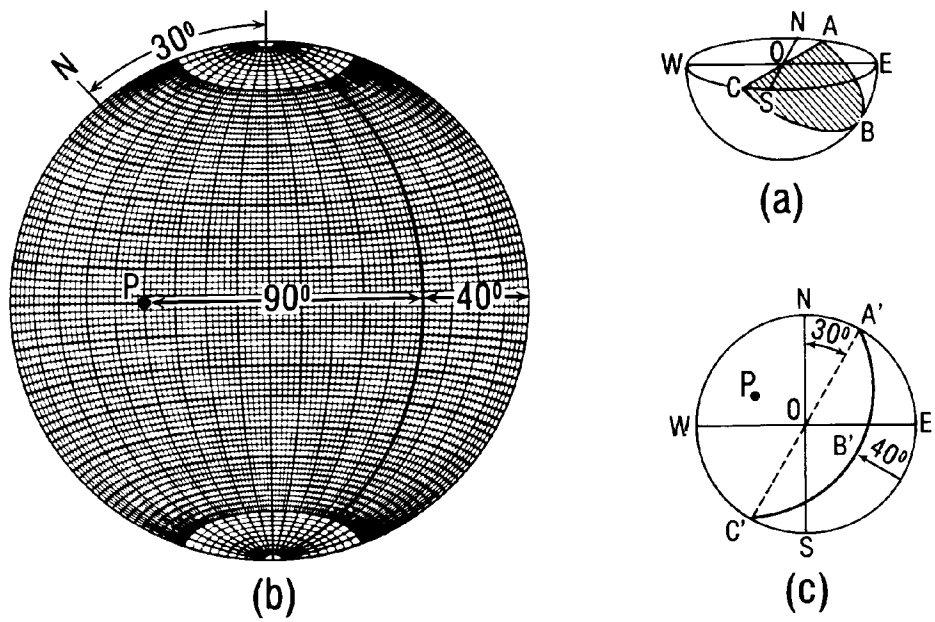


**Fig. 28.** Equal-area plot of a plane and its pole (modified from Ragan, 1973, p. 94). (a) Perspective view of the inclined plane to be plotted (shaded area). (b) The position of the overlay and net for the actual plot. (c) The overlay as it appears after the plot.

illustrates how a fault plane (strike N 30° E and dip 40° SE) may be projected. The intersection of this fault plane with the focal sphere is the great circle *ABC* (Fig. 28a). On a piece of tracing paper we draw a circle matching the outer circumference of the equal-area net (Fig. 28b) and mark *N*, *E*, *S*, and *W*. We overlay the tracing paper on the net, rotate the overlay 30° counterclockwise from the north for the strike, count 40° along the east–west axis from the circumference for the dip, and trace the great circle arc from the net as shown in Fig. 28b. The resulting plot is shown on Fig. 28c. Thus *A'B'C'* is an equal area plot of the fault plane *ABC*. On Fig. 28b, if we count 90° from the great circle arc for the fault plane, we find the point *P* which represents the pole or the normal axis to the fault plane. By reversing this procedure, we can read off the strike and dip of a fault plane on an equal-area projection with the aid of an equal-area net. Similarly, Fig. 29 illustrates how to plot an axis *OP* with strike of S 42° E, and plunge 40°. Again by reversing the procedure, we can read off the azimuth and plunge of any axis plotted.

(3a) To determine manually the nodal planes from a P-wave first motion plot, we need an equal-area net (often called a Schmidt net) as shown in Fig. 27b. If we fasten an equal-area net (normally 20 cm in diameter to match plots by the HYPO71 computer program) on a thin transparent plastic board and place a thumbtack through the center of the net, we can

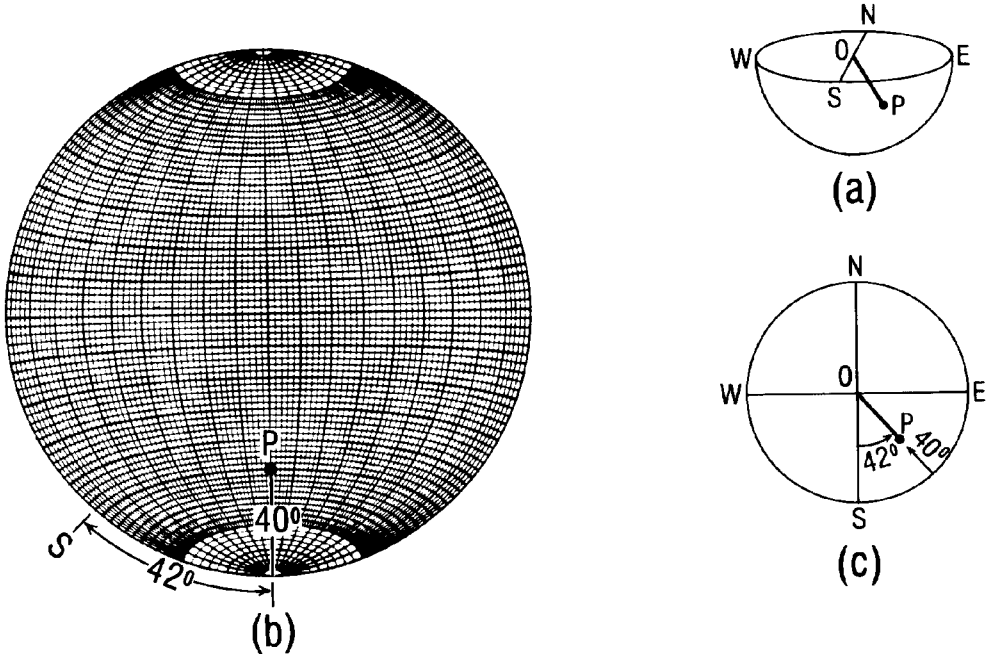


**Fig. 29.** Equal-area plot of an axis (or line or vector) *OP* (modified from Ragan, 1973, p. 95). (a) Perspective view of the inclined axis *OP*. (b) The position of the overlay and net for the actual plot. (c) The overlay as it appears after the plot.

easily superpose the computer plot on our net. The computer paper is usually not transparent enough, so it is advisable to work on top of a light table, and hence the use of a transparent board to mount the equal-area net. Figure 30 shows a P-wave first motion plot for a microearthquake recorded by the USGS Santa Barbara Network. We have redrafted the computer plot using solid dots for compressions (*C*) and open circles for dilatations (*D*) (smaller dots and circles represent poor-quality polarities) so that we may use letters for other purposes.

(3b) We attempt to separate the P-wave first motions on the focal sphere such that adjacent quadrants have opposite polarities. These quadrants are delineated by two orthogonal great circles which mark the intersection of the nodal planes with the focal sphere. Accordingly, we rotate the plot so that a great circle arc on the net separates the compressions from the dilatations as much as possible. In our example shown in Fig. 30, arc *WBCE* represents the projection of a nodal plane; it strikes east–west and dips 44° to the north. The pole or normal axis of this nodal plane is point *A* which is 90° from the great circle arc *WBCE*. Since the second nodal plane is orthogonal to the first, its great circle arc representation must pass through point *A*. To find the second nodal plane, we rotate the plot so that another great circle arc passes through point *A* and also

separates the compressions from the dilatations. This arc is *FBAG* in Fig. 30; it strikes N 54° W and dips 52° to the southwest, as measured from the equal-area net. The pole or normal axis of the second nodal plane is point *C*, which is 90° from arc *FBAG* and lies in the first nodal plane. In our example, the two nodal planes do not separate the compressional and dilatational quadrants perfectly. A small solid dot occurs in the northern dilatational field, and a small open circle in the western compressional field. Since these symbols represent poor-quality data, we ignore them here. In fact, some polarity violations are expected since there are uncertainties in actual observations and in reducing the data on the focal sphere.

(3c) The intersection of the two nodal planes is point *B* in Fig. 30, which is also called the null axis. The plane normal to the null axis is represented by the great circle arc *CTAP* in Fig. 30. This arc contains four

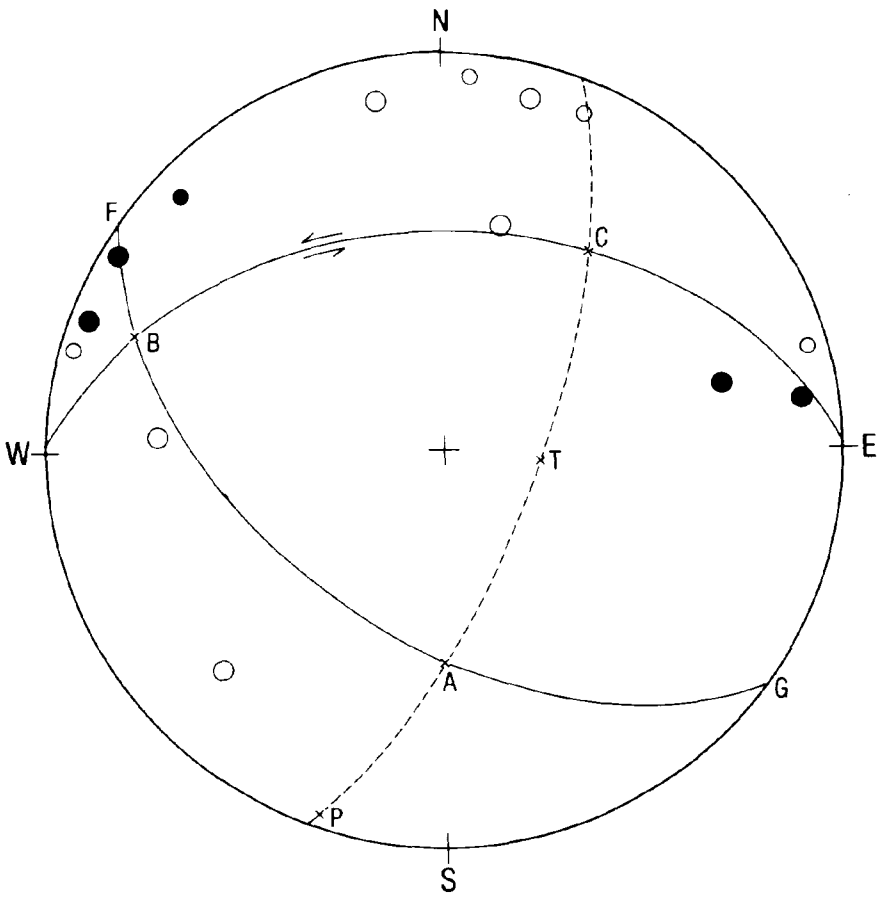


**Fig. 30.** A fault plane solution for a microearthquake in the Santa Barbara, California, region. The diagram is an equal-area projection of the lower focal hemisphere. See text for explanation.

important axes: the axes normal to the two nodal planes ($A$ and $C$), the $P$ axis, and the $T$ axis. In the general case, the $T$ axis is 45° from the $A$ and $C$ axes and lies in the compressional quadrant, and the $P$ axis is 90° from the $T$ axis. The $P$ axis is commonly assumed to represent the direction of maximum compressive stress, whereas the $T$ axis is commonly assumed to represent the direction of maximum tensile stress. If we select the first nodal plane (arc $WBCE$) as the fault plane, then point $C$ (which represents the axis normal to the auxiliary plane) is the slip vector and is commonly assumed to be parallel to the resolved shearing stress in the fault plane. This assumption is physically reasonable if earthquakes occur in homogeneous rocks. Many if not most earthquakes occur on preexisting faults in heterogeneous rocks, and thus the assumption is invalid on theoretical grounds. Readers are referred to McKenzie (1969) and Raleigh *et al.* (1972) for discussions of the relations between fault-plane solutions and directions of principal stresses. It must also be emphasized that we cannot distinguish from P-wave first motion data alone which nodal plane represents the fault plane. However, geological information on existing faults in the region of study or distribution of aftershocks will usually help in selecting the proper fault plane.

(3d) Let us now summarize our results from analyzing the P-wave first motion plot using an equal-area net. As shown in Fig. 30 we have

(a) Fault plane (chosen in this case with the aid of local geology): strike N 90° E, dip 44° N.
(b) Auxiliary plane: strike N 54° W, dip 52° SW.
(c) Slip vector $C$: strike N 36° E, plunge 38°.
(d) $P$ axis: strike N 161° W, plunge 4°.
(e) $T$ axis: strike N 96° E, plunge 70°.
(f) The diagram represents reverse faulting with a minor left-lateral component.

### *6.2.2. Pitfalls in Using P-Wave First Motion Data*

Unlike arrival times, which have a range of values for their errors, a P-wave first motion reading is either correct or wrong. One of the most difficult tasks in operating a microearthquake network is to ensure that the direction of motion recorded on the seismograms corresponds to the true direction of ground motion. Care must be taken to check the station polarities. Large nuclear explosions or large teleseismic events often are used to ensure accuracy of station polarities and to correct the polarities if necessary (Houck *et al.*, 1976).

Because the P-wave first motion plot depends on the earthquake location and the take-off angles of seismic rays, one must have a reasonably

accurate location for the focus and a sufficiently realistic velocity model of the region before one attempts any fault-plane solution. Engdahl and Lee (1976) showed that proper ray tracing is essential in fault-plane solutions, especially in areas of large lateral velocity variations. We must also emphasize that fault-plane solutions may be ambiguous or not even possible if the station distribution is poor or some station polarities are uncertain. For example, Lee *et al.* (1979b) showed how drastically different fault-plane solutions were obtained if two key stations were ignored because their P-wave first motions might be wrong.

If the number of P-wave first motion readings is small, it is a common practice to determine nodal planes from a composite P-wave first motion plot of a group of earthquakes that occurred closely in space and time. Such a practice should be used with caution because it assumes that the focal mechanisms for these earthquakes are identical, which may not be true.

### *6.2.3. Computer versus Manual Solution*

Many attempts have been made to determine the fault-plane solution by computer rather than by the manual method described in the preceding section. For examples of computer solution, readers are referred to the works of Kasahara (1963), Wickens and Hodgson (1967), Udias and Baumann (1969), Dillinger *et al.* (1971), Chandra (1971), Keilis-Borok *et al.* (1972), Shapira and Bath (1978), and Brillinger *et al.* (1980).

Basically, most computer programs for fault-plane solutions try to match the observed P-wave first motions on the focal sphere with those that are expected theoretically from a pair of orthogonal planes at the focus. To find the best match, we let a pair of orthogonal planes assume a sequence of positions, sweeping systematically through the complete solid angle at the focus. In any position, we may compute a score to see how well the data are matched and choose the pair of orthogonal planes with the best score as the nodal planes. Recently, Brillinger *et al.* (1980) developed a probability model for determining the nodal planes directly.

Since the manual method for determining the nodal planes is fast if the P-wave first motion plot is printed along with the earthquake location, as for example, in the HYPO71 program, we believe that the manual method is desirable in order to keep in close touch with the data. The problem of fault-plane solution in practice involves decision making because the observed data are never perfect. Since human beings generally make better decisions than computer programs do, one must master the manual method in order to check out the computer solutions. However, if large amounts of earthquake data are to be processed, computer solutions

should ease the burden of routine manipulations and allow the human analysts to concentrate on verifications.

## 6.3. Simultaneous Inversion for Hypocenter Parameters and Velocity Structure

The principal data measured from seismograms collected by a microearthquake network are first P-arrival times and directions of first P-motion from local earthquakes. These data contain information on the tectonics and structure of the earth underneath the network. In this section, we show how to extract information about the velocity structure from the arrival times. In addition to the hypocenter parameters (origin time, epicenter coordinates, and focal depth), each earthquake contributes independent observations to the potential data set for determining the earth's velocity structure, provided that the total number of observations exceeds four.

Crosson (1976a,b) developed a nonlinear least squares modeling procedure to estimate simultaneously the hypocenter parameters, station corrections, and parameters for a layered velocity model by using arrival times from local earthquakes. This approach has been applied to several seismic networks. Readers may refer to works, for example, by Steppe and Crosson (1978), Crosson and Koyanagi (1979), Hileman (1979), Horie and Shibuya (1979), and Sato (1979).

Independently, Aki and Lee (1976) developed a similar method for a general three-dimensional velocity model. Because lateral velocity variations are known to exist in the earth's crust (e.g., across the San Andreas fault as discussed by Engdahl and Lee, 1976), the method developed by Aki and Lee and extended by Lee *et al.* (1982a) is more general than Crosson's and will be treated here.

### *6.3.1. Formulation of the Simultaneous Inversion Problem*

The problem of simultaneous inversion for hypocenter parameters and velocity structure may be formulated by generalizing Geiger's method of determining hypocenter parameters. As with the earthquake location problem, arrival times of any seismic phases can be used in the simultaneous inversion. However, the following discussion will be restricted to first P-arrival times, although generalization to include other seismic arrivals is straightforward.

We are given a set of first P-arrival times observed at $m$ stations from a set of $n$ earthquakes, and we wish to determine the hypocenter parameters

and the P-velocity structure underneath the stations. Let us denote the first P-arrival time observed at the $k$th station for the $j$th earthquake as $\tau_{jk}$ along the ray path $\Gamma_{jk}$.

Since there are $n$ earthquakes, the total number of hypocenter parameters to be determined is $4n$. Let us denote the hypocenter parameters for the $j$th earthquake by $(t_j^0, x_j^0, y_j^0, z_j^0)$, where $t_j^0$ is the origin time and $x_j^0, y_j^0$, and $z_j^0$ are the hypocenter coordinates. Thus, all the hypocenter parameters for $n$ earthquakes may be considered as components of a vector in a Euclidean space of $4n$ dimensions, i.e., $(t_1^0, x_1^0, y_1^0, z_1^0, t_2^0, x_2^0, y_2^0, z_2^0, \ldots, t_n^0, x_n^0, y_n^0, z_n^0)^{\mathrm{T}}$, where the superscript T denotes the transpose.

The earth underneath the stations may be divided into a total of $L$ rectangular blocks with sides parallel to the $x$, $y$, and $z$ axes in a Cartesian coordinate system. Let each block be characterized by a P-velocity denoted as $v$. If $l$ is the index for the blocks, then the velocity of the $l$th block is $v_l$, $l = 1, 2, \ldots, L$. We further assume that the set of $n$ earthquakes and the set of $m$ stations are contained within the block model. Thus, the velocity structure underneath the stations is represented by the $L$ parameters of block velocity. These $L$ velocity parameters may be considered as components of a vector in a Euclidean space of $L$ dimensions, i.e., $(v_1, v_2, \ldots, v_L)^{\mathrm{T}}$.

Assuming that every block of the velocity model is penetrated by at least one ray path, the total number of parameters to be determined in the simultaneous inversion problem is $(4n + L)$. These hypocenter and velocity parameters may also be considered as components of a vector $\boldsymbol{\xi}$ in a Euclidean space of $(4n + L)$ dimensions, i.e.,

$$\boldsymbol{\xi} = (t_1^0, x_1^0, y_1^0, z_1^0, t_2^0, x_2^0, y_2^0, z_2^0, \ldots, t_n^0, x_n^0, y_n^0, z_n^0, v_1, v_2, \ldots, v_L)^{\mathrm{T}} \tag{6.24}$$

In order to formulate the simultaneous inversion problem as a nonlinear optimization problem, we assume a trial parameter vector $\boldsymbol{\xi}^*$ given by

$$\boldsymbol{\xi}^* = (t_1^*, x_1^*, y_1^*, z_1^*, t_2^*, x_2^*, y_2^*, z_2^*, \ldots, t_n^*, x_n^*, y_n^*, z_n^*, v_1^*, v_2^*, \ldots, v_L^*)^{\mathrm{T}} \tag{6.25}$$

The arrival time residual at the $k$th station for the $j$th earthquake may be defined in a manner similar to Eq. (6.7) as

$$\begin{gathered} r_{jk}(\boldsymbol{\xi}^*) = \tau_{jk} - T_{jk}(\boldsymbol{\xi}^*) - t_j^* \\ k = 1, 2, \ldots, m, \qquad j = 1, 2, \ldots, n \end{gathered} \tag{6.26}$$

where $\tau_{jk}$ is the first P-arrival time observed at the $k$th station for the $j$th earthquake, $T_{jk}(\boldsymbol{\xi}^*)$ is the corresponding theoretical travel time from the

trial hypocenter $(x_j^*, y_j^*, z_j^*)$ of the $j$th earthquake, and $t_j^*$ is the trial origin time of the $j$th earthquake. Our objective is to adjust the trial hypocenter and velocity parameters $(\boldsymbol{\xi}^*)$ simultaneously such that the sum of the squares of the arrival time residuals is minimized. We now generalize Geiger's method as given in Section 6.1.2 for our present problem.

The objective function for the least-squares minimization [Eq. (6.8)] as applied to the simultaneous inversion is

$$F(\boldsymbol{\xi}^*) = \sum_{j=1}^{n} \sum_{k=1}^{m} [r_{jk}(\boldsymbol{\xi}^*)]^2 \tag{6.27}$$

where $r_{jk}(\boldsymbol{\xi}^*)$ is given by Eq. (6.26). We may consider the set of arrival time residuals $r_{jk}(\boldsymbol{\xi}^*)$, for $k = 1, 2, \ldots, m$, and $j = 1, 2, \ldots, n$, as components of a vector $\mathbf{r}$ in a Euclidean space of $mn$ dimensions, i.e.,

$$\mathbf{r} = (r_{11}, r_{12}, \ldots, r_{1m}, r_{21}, r_{22}, \ldots, r_{2m}, \ldots, r_{n1}, r_{n2}, \ldots, r_{nm})^{\mathrm{T}} \tag{6.28}$$

The adjustment vector [Eq. (6.10)] now becomes

$$\boldsymbol{\delta\xi} = (\delta t_1, \delta x_1, \delta y_1, \delta z_1, \delta t_2, \delta x_2, \delta y_2, \delta z_2, \ldots, \delta t_n, \delta x_n, \delta y_n, \delta z_n, \delta v_1, \delta v_2, \ldots, \delta v_L)^{\mathrm{T}} \tag{6.29}$$

and it is to be determined from a set of linear equations similar to Eq. (6.19). We then replace the trial parameter vector $\boldsymbol{\xi}^*$ by $(\boldsymbol{\xi}^* + \boldsymbol{\delta\xi})$ and repeat the iteration until some cutoff criteria are met.

To apply the Gauss–Newton method to the simultaneous inversion problem, a set of linear equations is to be solved for the adjustment vector $\boldsymbol{\delta\xi}$ at each iteration step. In this case, we may generalize Eq. (6.11) or equivalently, Eq. (6.18), to read

$$\mathbf{B}\,\boldsymbol{\delta\xi} = -\mathbf{r} \tag{6.30}$$

where $\mathbf{B}$ is the Jacobian matrix generalized to include a set of $n$ earthquakes and a set of $L$ velocity parameters, i.e.,

$$\mathbf{B} = \left(\begin{array}{ccccc|c} \mathbf{A}_1 & \mathbf{0} & \mathbf{0} & \ldots & \mathbf{0} & \\ \mathbf{0} & \mathbf{A}_2 & \mathbf{0} & \ldots & \mathbf{0} & \\ & & & \vdots & & \mathbf{C} \\ \mathbf{0} & \mathbf{0} & \mathbf{0} & \ldots & \mathbf{A}_n & \end{array}\right) \tag{6.31}$$

where the $\mathbf{0}$'s are $m \times 4$ matrices with zero elements, the $\mathbf{A}$'s are $m \times 4$ Jacobian matrices given in a manner similar to Eq. (6.13) as

$$\mathbf{A}_j = -\begin{pmatrix} 1 & \partial T_{j1}/\partial x & \partial T_{j1}/\partial y & \partial T_{j1}/\partial z \\ 1 & \partial T_{j2}/\partial x & \partial T_{j2}/\partial y & \partial T_{j2}/\partial z \\ \vdots & \vdots & \vdots & \vdots \\ 1 & \partial T_{jm}/\partial x & \partial T_{jm}/\partial y & \partial T_{jm}/\partial z \end{pmatrix}\Bigg|_{\xi^*} \tag{6.32}$$

and $\mathbf{C}$ is a $mn \times L$ matrix. Each row of the velocity coefficient matrix $\mathbf{C}$ has $L$ elements and describes the sampling of the velocity blocks of a particular ray path. If $\Gamma_{jk}$ is the ray path connecting the $k$th station and the $j$th earthquake, then the elements of the $i$th row [where $i = k + (j - 1)m$] of $\mathbf{C}$ are given by

$$C_{il} = -\Pi_{jkl}(\partial T_{jk}/\partial v_l)|_{\xi^*} \qquad \text{for} \quad l = 1, 2, \ldots, L \tag{6.33}$$

where $\Pi_{jkl}$ is defined by

$$\Pi_{jkl} = \begin{cases} 1 & \text{if the } l\text{th block is penetrated by the ray path } \Gamma_{jk} \\ 0 & \text{otherwise} \end{cases} \tag{6.34}$$

If $u_l$ is the slowness in the $l$th block defined by

$$u_l = 1/v_l \tag{6.35}$$

then we have

$$\delta u_l = -\delta v_l/v_l^2 \tag{6.36}$$

To approximate $\partial T_{jk}/\partial v_l$ in Eq. (6.33) to first-order accuracy, we note that $\partial T_{jk}/\partial u_l \simeq \partial T_{jkl}/\partial u_l$, where $T_{jkl}$ is the travel time spent by the ray $\Gamma_{jk}$ in the $l$th block. In addition, we note that $T_{jkl} = u_l S_{jkl}$, where $S_{jkl}$ is the length of the ray path $\Gamma_{jk}$ in the $l$th block. Assuming that the dependence of $S_{jkl}$ on $u_l$ is of second order, $\partial T_{jkl}/\partial u_l \simeq S_{jkl} = v_l T_{jkl}$. Hence Eq. (6.33) becomes

$$C_{il} = \Pi_{jkl} T_{jkl}(\xi^*)/v_l^* \qquad \text{for} \quad l = 1, 2, \ldots, L \tag{6.37}$$

because $(\partial T_{jk}/\partial v_l)\,\delta v_l = (\partial T_{jk}/\partial u_l)\,\delta u_l$, and using Eq. (6.36).

Since each ray path samples only a small number of blocks, most elements of matrix $\mathbf{C}$ are zero. Therefore, the matrix $\mathbf{B}$ as given by Eq. (6.31) is sparse, with most of its elements being zero.

Equation (6.30) is a set of $mn$ equations written in matrix form, and by Eqs. (6.28), (6.29), (6.31), (6.32), and (6.37), it may be rewritten as

$$\delta t_j + \left.\frac{\partial T_{jk}}{\partial x}\right|_{\xi^*} \delta x_j + \left.\frac{\partial T_{jk}}{\partial y}\right|_{\xi^*} \delta y_j + \left.\frac{\partial T_{jk}}{\partial z}\right|_{\xi^*} \delta z_j - \sum_{l=1}^{L} \frac{\Pi_{jkl} T_{jkl}}{v_l^*} \delta v_l = r_{jk}(\boldsymbol{\xi}^*) \tag{6.38}$$

$$\text{for } k = 1, 2, \ldots, m, \quad j = 1, 2, \ldots, n$$

Equation (6.38) is a generalization of Eq. (6.19) for the simultaneous inversion problem.

### 6.3.2. *Numerical Solution of the Simultaneous Inversion Problem*

In the previous subsection, we have shown that the simultaneous inversion problem may be formulated in a manner similar to Geiger's method of determining origin time and hypocenter. The computations involve the following steps:

(1) Guess a trial parameter vector $\boldsymbol{\xi}^*$ as given by Eq. (6.25).
(2) Compute the theoretical travel time $T_{jk}$ and its spatial partial derivatives $\partial T_{jk}/\partial x$, $\partial T_{jk}/\partial y$, and $\partial T_{jk}/\partial z$ evaluated at $(x_j^*, y_j^*, z_j^*)$ for $k = 1, 2, \ldots, m$ and $j = 1, 2, \ldots, n$.
(3) Compute matrix **B** as given by Eqs. (6.31), (6.32), and (6.37), and compute vector **r** as given by Eqs. (6.28) and (6.26).
(4) Solve the system of $mn$ linear equations as given by Eq. (6.30) for the adjustment vector $\boldsymbol{\delta\xi}$ with $(4n + L)$ elements. This may be accomplished via the normal equations approach, or the generalized inversion approach as discussed in Chapter 5.
(5) Replace the trial parameter vector $\boldsymbol{\xi}^*$ by $(\boldsymbol{\xi}^* + \boldsymbol{\delta\xi})$.
(6) Repeat steps 2–5 until some cutoff criteria are met. At this point, we set $\boldsymbol{\xi} = \boldsymbol{\xi}^*$ as our solution for the hypocenter and velocity parameters.

Although numerical solution for the simultaneous inversion is computationally straightforward, the pitfalls discussed in Section 6.1.3 apply here also. The set of $mn$ linear equations to be solved in step 4 can be very large. Typically a few thousand equations and several hundred unknowns are involved. Because of the positions of the zero elements in matrix **B** [Eq. (6.31)], the arrival time residuals of one earthquake are coupled to those of another earthquake only through the velocity coefficient matrix **C** in Eq. (6.30). Therefore, it is possible to decouple mathematically the hypocenter parameters from the velocity parameters in the inversion procedure as shown by Pavlis and Booker (1980) and Spencer and Gubbins (1980). Consequently, large amounts of arrival time data can be used in

the simultaneous inversion without having to solve a very large set of equations. Furthermore, explosion data also can be included in the inversion.

Since the velocity can be different from block to block in the simultaneous inversion problem, three-dimensional ray tracing must be used in computing travel times and derivatives in step 2. The problem of ray tracing in a heterogeneous medium has been discussed in Chapter 4. For an application of simultaneous inversion using data from a microearthquake network, readers may refer, for example, to Lee *et al.* (1982a).

## 6.4. Estimation of Earthquake Magnitude

Intensity of effects and amplitudes of ground motion recorded by seismographs show that there are large variations in the size of earthquakes. Earthquake intensity is a measure of effects (e.g., broken windows, collapsed houses, etc.) produced by an earthquake at a particular point of observation. Thus, the effects of an earthquake may be collapsed houses at city A, broken windows at city B, and almost nothing damaged at city C. Unfortunately, intensity observations are subject to uncertainties of personal estimates and are limited by circumstances of reported effects. Therefore, it is desirable to have a scale for rating earthquakes in terms of their energy, independent of the effects produced in populated areas.

In response to this practical need, C. F. Richter proposed a magnitude scale in 1935 based solely on amplitudes of ground motion recorded by seismographs. Richter's procedure to estimate earthquake magnitude followed a practice by Wadati (1931) in which the calculated ground amplitudes in microns for various Japanese stations were plotted against their epicentral distances. Wadati employed the resulting amplitude-vs-distance curves to distinguish between deep and shallow earthquakes, to calculate the absorption coefficient for surface waves, and to make a rough comparison between the sizes of several strong earthquakes. Realizing that no great precision is needed, Richter (1935) took several bold steps to make the estimation of earthquake magnitude simple and easy to carry out. Consequently, Richter's magnitude scale has been widely accepted, and quantification of earthquakes has become an active research topic in seismology.

### *6.4.1. Local Magnitude for Southern California Earthquakes*

The Richter magnitude scale was originally devised for local earthquakes in southern California. Richter recognized that these earth-

quakes originated at depths not much different from 15 km, so that the effects caused by focal depth variations could be ignored. He could also skip the tedious procedure of reducing the amplitudes recorded on seismograms to true ground motions. This is because the Southern California Seismic Network at that time was equipped with Wood–Anderson instruments which have nearly constant displacement amplification over the frequency range appropriate for local earthquakes. Therefore, Richter (1935, 1958, pp. 338–345) defined the local magnitude $M_L$, of an earthquake observed at a station to be

$$M_L = \log A - \log A_0(\Delta) \tag{6.39}$$

where $A$ is the maximum amplitude in millimeters recorded on the Wood–Anderson seismogram for an earthquake at epicentral distance of $\Delta$ km, and $A_0(\Delta)$ is the maximum amplitude at $\Delta$ km for a standard earthquake. The local magnitude is thus a number characteristic of the earthquake and independent of the location of the recording stations.

Three arbitrary choices enter into the definition of local magnitude: (1) the use of the standard Wood–Anderson seismograph; (2) the use of common logarithms to the base 10; and (3) the selection of the standard earthquake whose amplitudes as a function of distance $\Delta$ are represented by $A_0(\Delta)$. The zero level of $A_0(\Delta)$ can be fixed by choosing its value at a particular distance. Richter chose it to be 1 $\mu$m (or 0.001 mm) at a distance of 100 km from the earthquake epicenter. This is equivalent to assigning an earthquake to be magnitude 3 if its maximum trace amplitude is 1 mm on a standard Wood–Anderson seismogram recorded at 100 km. In other words, to compute $M_L$ a table of $(-\log A_0)$ as a function of epicentral distance in kilometers is needed. Richter arbitrarily chose $(-\log A_0) = 3$ at $\Delta = 100$ km so that the earthquakes he dealt with did not have negative magnitudes. Other entries of this $(-\log A_0)$ table were constructed from observed amplitudes of a series of well-located earthquakes, and the table of $(-\log A_0)$ is given in Richter (1958, p. 342).

In practice, we need to know the approximate epicentral distances of the recording stations. The maximum trace amplitude on a standard Wood–Anderson seismogram is then measured in millimeters, and its logarithm to base 10 is taken. To this number we add the quantity tabulated as $(-\log A_0)$ for the corresponding station distance from the epicenter. The sum is a value of local magnitude for that seismogram. We repeat the same procedure for every available standard Wood–Anderson seismogram. Since there are two components (EW and NS) of Wood–Anderson instruments at each station, we average the two magnitude values from a given station to obtain the station magnitude. We then

average all the station magnitudes to obtain the local magnitude $M_L$ for the earthquake.

### *6.4.2. Extension to Other Magnitudes*

In the 1940s, B. Gutenberg and C. F. Richter extended the local magnitude scale to include more distant earthquakes. Gutenberg (1945a) defined the surface-wave magnitude $M_S$ as

$$M_S = \log A - \log A_0(\Delta^\circ) \tag{6.40}$$

where $A$ is the maximum combined horizontal ground amplitude in micrometers for surface waves with a period of 20 sec, and $(-\log A_0)$ is tabulated as a function of epicentral distance $\Delta$ in degrees in a similar manner to that for local magnitude (Richter, 1958, pp. 345–347).

A difficulty in using the surface-wave magnitude scale is that it can be applied only to shallow earthquakes that generate observable surface waves. Gutenberg (1945b) thus defined the body-wave magnitude $m_b$ to be

$$m_b = \log(A/T) - f(\Delta, h) \tag{6.41}$$

where $A/T$ is the amplitude-to-period ratio in micrometers per second, and $f(\Delta, h)$ is a calibration function of epicentral distance $\Delta$ and focal depth $h$. In practice, the determination of earthquake magnitude $M$ (either body-wave or surface-wave) may be generalized to the form (Bath, 1973, pp. 110–118):

$$M = \log(A/T) + C_1 \log(\Delta) + C_2 \tag{6.42}$$

where $C_1$ and $C_2$ are constants. A summary on magnitude scales may be found in Duda and Nuttli (1974).

### *6.4.3. Estimating Magnitude for Microearthquakes*

Because Wood–Anderson instruments seldom give useful records for earthquakes with magnitude less than 2, we need a convenient method for estimating magnitude of local earthquakes recorded by microearthquake networks with high-gain instruments. One approach (e.g., Brune and Allen, 1967; Eaton *et al.*, 1970b) is to calculate the ground motion from the recorded maximum amplitude, and from this compute the response expected from a Wood–Anderson seismograph. As Richter (1958, p. 345) pointed out, the maximum amplitude on the Wood–Anderson record may not correspond to the wave with maximum amplitude on a different instrument's record. This problem can, in principle, be solved by converting the entire seismogram to its Wood–Anderson equivalent and determining

magnitude from the latter. Indeed, Bakun *et al.* (1978a) verified that a Wood–Anderson equivalent from a modern high-gain seismograph can be obtained that matches closely the Wood–Anderson seismogram observed at the same site. It takes some effort, however, to calibrate and maintain a microearthquake network so that the ground motion can be calculated (see Section 2.2.5). In the USGS Central California Microearthquake Network, the maximum amplitude and corresponding period of seismic signals can be measured from low-gain stations at small epicentral distances, and from high-gain stations at larger epicentral distances. In this way it is possible to extend Richter's method of calculating magnitude for local earthquakes recorded in microearthquake networks. However, it may be difficult to relate this type of local magnitude scale to the original Richter scale as discussed by Thatcher (1973).

Another approach is to use signal duration instead of maximum amplitude. This idea appears to originate from Bisztricsany (1958) who determined the relationship between earthquakes with magnitudes 5 to 8 and durations of their surface waves at epicentral distances between 4 and 160°. Solov'ev (1965) applied this technique in the study of the seismicity of Sakhalin Island, but used the total signal duration instead. Tsumura (1967) studied the determination of magnitude from total signal duration for local earthquakes recorded by the Wakayama Microearthquake Network in Japan. He derived an empirical relationship between total signal duration and the magnitude determined by the Japan Meteorological Agency using amplitudes.

Lee *et al.* (1972) established an empirical formula for estimating magnitudes of local earthquakes recorded by the USGS Central California Microearthquake Network using signal durations. For a set of 351 earthquakes, they computed the local magnitudes (as defined by Richter, 1935) from Wood–Anderson seismograms or their equivalents. Correlating these local magnitudes with the signal durations measured from seismograms recorded by the USGS network, they obtained the following empirical formula:

$$\hat{M} = -0.87 + 2.00 \log \tau + 0.0035\, \Delta \tag{6.43}$$

where $\hat{M}$ is an estimate of Richter magnitude, $\tau$ is signal duration in seconds, and $\Delta$ is epicentral distance in kilometers. In an independent work, Crosson (1972) obtained a similar formula using 23 events recorded by his microearthquake network in the Puget Sound region of Washington state.

Since 1972, the use of signal duration to determine magnitude and also seismic moment of local earthquakes has been investigated by several

authors, e.g., Hori (1973), Real and Teng (1973), Herrmann (1975), Bakun and Lindh (1977), Griscom and Arabasz (1979), Johnson (1979), and Suteau and Whitcomb (1979). Duration magnitude $M_D$ for a given station is usually given in the form

$$M_D = a_1 + a_2 \log \tau + a_3 \Delta + a_4 h \tag{6.44}$$

where $\tau$ is signal duration in seconds, $\Delta$ is epicentral distance in kilometers, $h$ is focal depth in kilometers, and $a_1$, $a_2$, $a_3$ and $a_4$ are empirical constants. These constants usually are determined by correlating signal duration with Richter magnitude for a set of selected earthquakes and taking epicentral distance and focal depth into account.

It is important to note that different authors may define signal duration differently. In practice, total duration of the seismic signal of an earthquake is difficult to measure. Lee *et al.* (1972) defined signal duration to be the time interval in seconds between the onset of the first P-wave and the point where the seismic signal (peak-to-peak amplitude) no longer exceeds 1 cm as it appears on a Geotech Develocorder viewer with 20× magnification. This definition is arbitrary, but it is easy to apply, and duration measurements are reproducible by different readers. Since the background seismic noise is about 0.5 cm (peak-to-peak), this definition is equivalent to a cutoff point where the signal amplitude is approximately twice that of the noise. Because magnitude is a rough estimate of the size of an earthquake, the definition of signal duration is not very critical. However, it should be consistent and reproducible for a given microearthquake network. For a given earthquake, signal duration should be measured for as many stations as possible. In practice, a sample of 6 to 10 stations is adequate if the chosen stations surround the earthquake epicenter and if stations known to record anomalously long or short durations are ignored. Duration magnitude is then computed for each station, and the average of the station magnitudes is taken to be the earthquake magnitude.

Using signal duration to estimate earthquake magnitude has become a common practice in microearthquake networks, as evidenced by recent surveys of magnitude practice (Adams, 1977; Lee and Wetmiller, 1978). In addition, studies to improve determination of magnitudes of local earthquakes have been carried out. For example, Johnson (1979, Chapter 2) presented a robust method of magnitude estimation based on the decay of coda amplitudes using digital seismic traces; Suteau and Whitcomb (1979) studied relationships between local magnitude, seismic moment, coda amplitudes, and signal duration.

## 6.5. Quantification of Earthquakes

As pointed out by Kanamori (1978b), it is not a simple matter to find a single measure of the size of an earthquake, because earthquakes result from complex physical processes. In the previous section, we described the Richter magnitude scale and its extensions. Since Richter magnitude is defined empirically, it is desirable to relate it to the physical processes of earthquakes. In the past 30 years, considerable advances have been made in relating parameters describing an earthquake source with observed ground motion. Readers are referred to an excellent treatise on quantitative methods in seismology by Aki and Richards (1980).

### *6.5.1. Quantitative Models of Earthquakes*

Reid's elastic rebound theory (Reid, 1910) suggests that earthquakes originate from spontaneous slippage on active faults after a long period of elastic strain accumulation. Faults may be considered as the slip surfaces across which discontinuous displacement occurs in the earth, and the faulting process may be modeled mathematically as a shear dislocation in an elastic medium (see Savage, 1978, for a review). A shear dislocation (i.e., slip) is equivalent to a double-couple body force (Maruyama, 1963; Burridge and Knopoff, 1964). The scaling parameter of each component couple of a double-couple body force is its moment. Using the equivalence between slip and body forces, Aki (1966) introduced the seismic moment $M_0$ as

$$M_0 = \mu \int_A D(A)\, dA = \mu \bar{D} A \tag{6.45}$$

where $\mu$ is the shear modulus of the medium, $A$ is the area of the slipped surface or source area, and $\bar{D}$ is the slip $D(A)$ averaged over the area $A$. Hence the seismic moment of an earthquake is a direct measure of the strength of an earthquake caused by fault slip. If an earthquake occurs with surface faulting, we may estimate its rupture length $L$ and its average slip $\bar{D}$. The source area $A$ may be approximated by $Lh$, where $h$ is the focal depth. A reasonable estimate for $\mu$ is $3 \times 10^{11}$ dynes/cm$^2$. With these quantities, we can estimate the seismic moment using Eq. (6.45). For more discussion on seismic moment, readers may refer to Brune (1976), and Aki and Richards (1980).

From dislocation theory, the seismic moment can be related to the far-field seismic displacement recorded by seismographs. For example, Hanks and Wyss (1972) showed how to determine seismic source param-

eters using body-wave spectra. The seismic moment $M_0$ may be determined by

$$M_0 = (\Omega_0/\psi_{\theta\phi})4\pi\rho R v^3 \tag{6.46}$$

where $\Omega_0$ is the long-period limit of the displacement spectrum of either P or S waves, $\psi_{\theta\phi}$ is a function accounting for the body-wave radiation pattern, $\rho$ is the density of the medium, $R$ is a function accounting for spreading of body waves, and $v$ is the body-wave velocity. Similarly, seismic moment can also be determined from surface waves or coda waves (e.g., Aki, 1966, 1969). Thus, if seismic moment is determined from seismograms and if we assume the source area to be the aftershock area, then we can estimate the average slip $\bar{D}$ from Eq. (6.45).

Actually, seismic moment is only one of the three parameters that can be determined from a study of seismic wave spectra. For example, Hanks and Thatcher (1972) showed how various seismic source parameters are related if one accepts Brune's (1970) source model. The far-field displacement spectrum is assumed to be described by three spectral parameters. These parameters are (1) the long-period spectral level $\Omega_0$, (2) the spectral corner frequency $f_0$, and (3) the parameter $\epsilon$ which controls the high-frequency ($f > f_0$) decay of spectral amplitudes. They can be extracted from a log–log plot of the seismic wave spectrum (spectral level $\Omega$ vs frequency $f$). If we further assume that the physical interpretation of these spectral parameters as given by Brune (1970) is correct, then the source dimension $r$ for a circular fault is given by

$$r = 2.34v/2\pi f_0 \tag{6.47}$$

where $v$ and $f_0$ are seismic velocity and corner frequency, respectively. The stress drop $\Delta\sigma$ is given by

$$\Delta\sigma = 7M_0/16r^3 \tag{6.48}$$

Similar formulas for strike-slip and dip-slip faults have been summarized by Kanamori and Anderson (1975, pp. 1074–1075).

The stress drop $\Delta\sigma$ is an important parameter and is defined as the difference between the initial stress $\sigma_0$ before an earthquake and the final stress $\sigma_1$ after the earthquake

$$\Delta\sigma = \sigma_0 - \sigma_1 \tag{6.49}$$

The mean stress $\bar{\sigma}$ is defined as

$$\bar{\sigma} = \tfrac{1}{2}(\sigma_0 + \sigma_1) \tag{6.50}$$

and is related to the change in the strain energy $\Delta W$ before and after an earthquake by (Kanamori and Anderson, 1975, p. 1075)

(6.51) $$\Delta W = A\bar{D}\bar{\sigma}$$

The radiated seismic energy $E_s$ is

(6.52) $$E_s = \eta\, \Delta W$$

where $\eta$ is the seismic efficiency. $\eta$ is less than 1 because only part of the strain energy change is released as radiated seismic energy.

Kanamori and Anderson (1975) discussed the theoretical basis of some empirical relations in seismology. They showed that for large earthquakes the surface-wave magnitude $M_S$ is related to rupture length $L$ by

(6.53) $$M_S \sim \log L^2$$

and the seismic moment $M_0$ by

(6.54) $$M_0 \sim L^3$$

Thus we have

(6.55) $$\log M_0 \sim \tfrac{3}{2} M_S$$

which is empirically observed. Gutenberg and Richter (1956) related the surface-wave magnitude $M_S$ to the seismic energy $E_s$ empirically by

(6.56) $$\log E_s = 1.5 M_S + 11.8$$

Kanamori and Anderson (1975, p. 1086) showed that

(6.57) $$E_s \sim L^3$$

and by using Eq. (6.53), we have

(6.58) $$\log E_s \sim \tfrac{3}{2} M_S$$

which agrees with the Gutenberg–Richter relation given in Eq. (6.56).

### *6.5.2. Applications to Microearthquake Networks*

The preceding subsection shows that seismic moment is a fundamental quantity. The $M_L$ and $M_S$ magnitude scales as originally defined by Richter and Gutenberg can be related to seismic moment approximately. Indeed, Hanks and Kanamori (1979) proposed a moment–magnitude scale by defining

(6.59) $$M = \tfrac{2}{3} \log M_0 - 10.7$$

This moment–magnitude scale is consistent with $M_L$ in the range 3–6, with $M_S$ in the range 5–8, and with $M_W$ introduced by Kanamori (1977) for great earthquakes ($M \geq 8$). Because the duration magnitude scale $M_D$ is usually

tied to Richter's local magnitude $M_L$, one would expect that this moment–magnitude scale is also consistent with $M_D$ in the range of 0–3. However, this consistency is yet to be confirmed.

Many present-day microearthquake networks are not yet sufficiently equipped and calibrated for spectral analysis of recorded ground motion. In the past, special broadband instruments with high dynamic range recording have been constructed by various research groups for spectral analysis of local earthquakes (e.g., Tsujiura, 1966, 1978; Tucker and Brune, 1973; Johnson and McEvilly, 1974; Bakun *et al.*, 1976; Helmberger and Johnson, 1977; Rautian *et al.*, 1978). Alternatively, one uses accelerograms from strong motion instruments (e.g., Anderson and Fletcher, 1976; Boatwright, 1978). Several authors have used recordings from microearthquake networks for spectral studies (e.g., Douglas *et al.*, 1970; Douglas and Ryall, 1972; Bakun and Lindh, 1977; Bakun *et al.*, 1978b). In addition, O'Neill and Healy (1973) proposed a simple method of estimating source dimensions and stress drops of small earthquakes using P-wave rise time recorded by microearthquake networks.

In order to determine earthquake source parameters from seismograms, it is necessary in general to have broadband, on-scale records in digital form. If such records were available, D. J. Andrews (written communication, 1979) suggested that it would be desirable to determine the following two integrals:

$$A = \int u(t)\, dt, \qquad B = \int [\dot{u}(t)]^2\, dt \tag{6.60}$$

where $u$ is ground displacement, $\dot{u}$ is ground velocity, $t$ is time, and the integrals are over the time duration of each seismic phase or over the entire record. At distances much greater than the source dimension, both displacement and velocity of ground motion return to zero after the passage of the seismic waves. Thus the two integrals given by Eq. (6.60) are the two simplest nonvanishing integrals of the ground motion. The integral $A$ is the long-period spectral level $\Omega_0$ and is related to seismic moment by Eq. (6.46). The integral $B$ is proportional to the energy that is propagated to the station. If the spectrum of ground motion follows the simple Brune (1970) model with $\varepsilon = 1$, the corner frequency $f_0$ is related to the integrals $A$ and $B$ by

$$f_0 = (4^{1/3}/2\pi)B^{1/3}/A^{2/3} \tag{6.61}$$

Whereas the numerical coefficient may be different in other models, the quantity $B^{1/3}/A^{2/3}$, having dimension of time$^{-1}$, can be expected to be a robust measure of a characteristic frequency. Andrews believes that this procedure is better than the traditional method of finding corner frequency

from a log–log plot of the seismic wave spectrum. Boatwright (1980) has used the integral $B$ to calculate the total radiated energy.

As pointed out by Aki (1980b), the basis of any magnitude scale depends on the separation of amplitude of ground motion into source and propagation effects. For example, Richter's local magnitude scale depends on the observation that the maximum trace amplitude $A_m$ recorded by the standard Wood–Anderson seismographs can be written as

$$A_m(\Delta) = S \cdot F(\Delta) \tag{6.62}$$

where $S$ depends only on the earthquake source, and $F(\Delta)$ describes the response of the rock medium to the earthquake source and depends only on epicentral distance $\Delta$. Thus, if we equate

$$\log S = M_L \tag{6.63}$$

where $M_L$ is Richter's local magnitude, and take the logarithm of both sides of Eq. (6.62), we have

$$M_L = \log A_m(\Delta) - \log F(\Delta) \tag{6.64}$$

which is equivalent to Eq. (6.39) defining Richter's local magnitude.

The seismogram of an earthquake generally shows some ground vibrations long after the body waves and surface waves have passed. This portion of the seismogram is referred to as the coda. Coda waves are believed to be backscattering waves due to lateral inhomogeneities in the earth's crust and upper mantle (Aki and Chouet, 1975). They showed that the coda amplitude, $A(\omega,t)$ could be expressed by

$$A(\omega,t) = S \cdot t^{-a} \exp(-\omega t/2Q) \tag{6.65}$$

where $S$ represents the coda source factor at frequency $\omega$, $t$ is the time measured from the origin time, $a$ is a constant that depends on the geometrical spreading, and $Q$ is the quality factor. The separation of coda amplitude into source and propagation effects as expressed by Eq. (6.65) has been confirmed by observations (e.g., Rautian and Khalturin, 1978; Tsujiura, 1978).

We may now give a theoretical basis for estimating magnitude ($M_D$) using signal duration. Taking the logarithm of both sides of Eq. (6.65) and ignoring the effects of $Q$ and frequency, we have

$$\log A(t) = \log S - a \log t \tag{6.66}$$

For estimating magnitudes, signal durations are usually measured starting from the first P-onsets to some constant cutoff value $C$ of coda amplitude. Because the signal duration is usually greater than the travel time of the

first P-arrival, we may substitute signal duration $\tau$ for $t$ and $C$ for $A(t = \tau)$ in Eq. (6.66) and obtain

$$\log C = \log S - a \log \tau \tag{6.67}$$

Thus, if we equate

$$\log S = M_D \tag{6.68}$$

then we obtain

$$M_D = \log C + a \log \tau \tag{6.69}$$

Since $\log C$ is a constant, Eq. (6.69) is identical to the usual definition of duration magnitude [Eq. (6.44)] to first-order terms. Herrmann (1975), Johnson (1979), and Suteau and Whitcomb (1979) also presented a similar theoretical basis for estimating magnitude from properties of the coda waves. Herrmann (1980) also used coda waves to estimate $Q$.

By taking advantage of the properties of coda waves, we may determine source parameters and the quality factor of the medium as discussed, for example, by Aki (1980a,b). We expect that such studies will soon be applied to data from microearthquake networks on a routine basis.

In this section, we have not treated seismic moment tensor inversion. This method has been discussed in Aki and Richards (1980, pp. 50–60), and readers may refer to works, for example, by Stump and Johnson (1977), Patton and Aki (1979), and Ward (1980) for applications to synthetic and teleseismic data. Although we are not aware of any published literature that applies this method to microearthquake data, we expect to see such publications soon. Furthermore, we have not treated any statistical techniques as applied to the study of earthquake sequences. Readers may refer, for example, to Vere-Jones (1970) for a review. In recent years, point process analysis (e.g., Cox and Lewis, 1966) has been introduced into statistics to analyze a sequence of times of events in manners similar to those of ordinary time series analysis. Applications of point process analysis to microearthquake data may be found, for example, in Udias and Rice (1975), Vere-Jones (1978), and Kagan and Knopoff (1980).

# 7. General Applications

Data from microearthquake networks have been applied to many seismological problems, especially in detailed studies of seismicity and focal mechanism. These in turn provide valuable information for (1) identifying active faults and earthquake precursors, (2) estimating earthquake risk, and (3) studying the earthquake generating process. In this chapter, we summarize some general applications of microearthquake networks. Because of the vast amounts of existing literature, it is inevitable that many references (especially those not written in English) have not been cited here.

From an operational point of view, microearthquake networks may be classified as either permanent or temporary types. Permanent microearthquake networks usually consist of stations in which signals are telemetered to a central recording center in order to reduce the labor in collecting and processing seismic data. Telemetering places severe limitations on where stations can be set up (line of sight for radio-telemetering or availability of telephone lines) and usually requires a long lead time before a station is operating. Temporary microearthquake networks are usually designed to be extremely portable and can be deployed for operation quickly. Thus, they are most valuable for responding to large earthquakes or for studies in remote areas. However, temporary networks require large amounts of manual labor to collect and process the data. For practical reasons, most seismological research centers maintain both permanent and temporary networks. In fact, a combination of both permanent and temporary stations proves most fruitful for many applications.

## 7.1. Permanent Networks for Basic Research

In a given region large earthquakes usually occur at intervals of tens or hundreds of years. Therefore, long-term studies must be conducted to

collect the necessary data. To study microearthquakes, we must have high-sensitivity seismographs located at least within 100 km of earthquake sources. If microearthquakes have shallow focal depths (<10 km), then we must have a station spacing of less than 20 km to determine focal depths reliably. Consequently, microearthquake networks consist of densely deployed stations and necessitate moderate to large operations in data collecting, processing, and analysis.

At present, about 100 permanent microearthquake networks are in operation throughout the world. These networks consist of a few stations to a few hundred stations. In Table II (see p. 171), we have compiled a list of existing permanent microearthquake networks by geographic regions.[1] This list is not complete because information about some microearthquake networks is not available to us. Also, we have omitted seismic networks that are not primarily concerned with microearthquakes. Examples of the omitted networks include those operated by the Seismographic Stations of the University of California and by the Japan Meteorological Agency, arrays for detecting nuclear explosions as described in Section 1.1.1, the large aperture seismic network in France (Massinon and Plantet, 1976), and the Graefenberg array in Germany (Harjes and Seidl, 1978). Included in Table II are operating institution(s), start date, geographic location, areal coverage, number of stations, average station spacing, and annual number of located earthquakes. The values given in various table columns are very approximate as most networks change their operating characteristics frequently. The average station spacing is computed by dividing the areal coverage by the number of stations and taking the square root. It is a rough measure of how well hypocentral coordinates can be determined. The annual number of located earthquakes depends on factors such as seismicity, areal coverage of the network, etc. General results from permanent microearthquake networks are too numerous to be summarized here. Readers are referred to network publications which may be obtained by writing to the operating institution. An excellent summary of microearthquake networks in Japan with bibliography is given in Suzuki *et al.* (1979).

## 7.2. Temporary Networks for Reconnaissance Surveys

Temporary microearthquake networks consisting of portable seismographs are usually deployed for reconnaissance surveys. The simplest type of portable seismograph consists of a geophone and a recorder with built-

[1] Tables for Chapter 7 begin on p. 171.

in amplifier and power supply. The smoked paper recorder is very popular because it is reliable and gives a visual seismogram. A few commercial companies in the United States manufacture these portable units at a cost of about $5000 per unit. Analog or digital magnetic tape recorders are used if more detailed seismic data are desired. They are more expensive (about $10,000 per unit) and require a playback facility (about $30,000). Operation of temporary networks on land is rather simple, but operation at sea requires entirely different instrumentation (see Section 2.4).

Examples of reconnaissance surveys on land and at sea are listed in Table III (p. 178) and Table IV (p. 186), respectively. In both tables, we group the surveys by geographic location, and within the same location, in chronological order. These tables are by no means complete, but they should give the reader a general overview of what has been done.

## 7.3. Aftershock Studies

As discussed in Chapter 1, aftershock studies have greatly stimulated the development of microearthquake networks. Because numerous aftershocks generally follow a moderate or large earthquake, vast quantities of data can be collected in a short period of time. The occurrence of a damaging earthquake also justifies detailed studies. Temporary stations are usually deployed quickly after damaging earthquakes and are commonly operated until the aftershocks subside to a low level. If the earthquake occurs within an existing seismic network, temporary stations may be deployed for augmentation, and additional permanent stations may also be added.

Examples of aftershock studies in the microearthquake range of magnitude are listed in Table V on p. 188. Included in this table are data on the main shock, brief description of the field observation, number of microearthquakes observed and located, and reference. Because of the large amount of existing literature, this table is selective and references usually are given to the final report if possible. Values given in Table V are often approximate and are not given if they are not obvious in the published papers.

## 7.4. Induced Seismicity Studies

Earthquakes may sometimes be induced by human activities, such as testing nuclear weapons, mining, filling reservoirs, and injecting fluid underground. Microearthquake networks have been applied to study some of these problems, and we summarize them here.

### *7.4.1. Nuclear Explosions*

In the 1960s, it was noted that increased earthquake activity often accompanied large underground nuclear explosions. A dense microearthquake network (consisting of telemetered and portable stations) was set up at the Nevada Test Site by the U.S. Geological Survey, and several temporary networks by other institutions were deployed to study this problem. Results are summarized in Table VI on p. 193.

### *7.4.2. Mining Activities*

Rockbursts have often occurred in mining operations. Geophysicists in South Africa showed that rockbursts were earthquakes induced by stress concentrations due to mining. Microearthquake networks with stations extremely close to the source have been used in studying the mine tremors; some of the results are summarized in Table VII on p. 194. The review by Cook (1976) gave an excellent summary of seismicity associated with mining. Readers may also refer to Hardy and Leighton (1977, 1980).

### *7.4.3. Filling Reservoirs*

Seismicity of an area may be modified by filling reservoirs. There are several cases where reservoirs may have triggered moderate-size earthquakes. There are also cases where the seismicity has increased, showed no change, or even decreased. Many reviews have been written on the subject (e.g., Gupta and Rastogi, 1976; Simpson, 1976). Some examples of microearthquake observations made near reservoirs are summarized in Table VIII (p. 195). Because of various difficulties, long-term and good-quality seismic data for studying induced seismicity are rare. However, this problem has been recognized, and microearthquake networks are now routinely deployed to monitor seismicity before, during, and after reservoir filling. We expect much improved data soon.

### *7.4.4. Fluid Injection*

When fluid is injected underground at high pressure, earthquakes may be induced. The most famous case is the Denver, Colorado, earthquakes studied in detail by Healy *et al.* (1968). Similar cases were studied in Los Angeles, California, by Teng *et al.* (1973), at Matsushiro, Japan, by Ohtake (1974), and at Dale, New York, by Fletcher and Sykes (1977). Fluid injection was also used in an earthquake control experiment at

Rangely, Colorado, by Raleigh *et al.* (1976). In all these cases microearthquake networks were effective in mapping the seismicity to show that it was related to the fluid injection, and in determining the focal mechanism to show that tectonic stress was released.

## 7.5. Geothermal Exploration

Microearthquake networks can be an effective tool in geothermal exploration (e.g., Ward, 1972; Combs and Hadley, 1977; Gilpin and Lee, 1978; Majer and McEvilly, 1979). Through reconnaissance surveys, microearthquakes have been observed in many geothermal areas around the world, and microseismicity has been shown to correlate with geothermal activity. By detailed mapping of microearthquakes in geothermal areas, active faults may be located along which steam and hot waters are brought to the earth's surface. Numerous microearthquake surveys have been conducted in geothermal areas. Some examples of these studies have been summarized in Table III along with reconnaissance surveys for other purposes. Recently, a special issue of the *Journal of Geophysical Research* was devoted to studies of the Coso geothermal area in California; papers by Reasenberg *et al.* (1980), Walter and Weaver (1980), and Young and Ward (1980) used data from a microearthquake network supplemented by a temporary array.

Two applications of microearthquake networks in geothermal studies have been pioneered by H. M. Iyer and his colleagues (Iyer, 1975, 1979; Iyer and Hitchcock, 1976a,b; Steeples and Iyer, 1976a,b; Iyer and Stewart, 1977; Iyer *et al.*, 1979). In one approach, array processing techniques were used to study seismic noise anomalies in order to identify potential geothermal sources. In another approach, teleseismic P-delays across a microearthquake network were used to search for anomalous regions in the crust and upper mantle that might contain magma.

## 7.6. Crustal and Mantle Structure

Arrival times and hypocenter data from temporary or permanent microearthquake networks have been used in several ways to determine the seismic velocity structure of the crust and mantle. Sources of data include local, regional, and teleseismic earthquakes, and explosions recorded at local and regional distances. First P-arrival times are most often used, but later P- and S-phases can also be added to the analysis.

Many studies have utilized well-located microearthquakes or quarry explosions as energy sources to construct standard time–distance plots. These plots are then interpreted by the usual refraction methods. For example, mine tremors from the Witwatersrand gold mining region of South Africa were recorded as far away as 500 km on portable instruments laid out in linear arrays (Willmore *et al.*, 1952; Gane *et al.*, 1956). The mine tremors were precisely located by a permanent network in the mining region. Local events and microearthquake networks were also used in this way in Hawaii (Eaton, 1962) and in Japan (Mikumo *et al.*, 1956; Watanabe and Nakamura, 1968). Data from deep crustal reflections as well as from direct and refracted waves were used by Mizoue (1971) to study crustal structure in the Kii Peninsula. Hadley and Kanamori (1977) supplemented local microearthquake data with that from artificial sources and teleseisms to study the seismic velocity structure of the Transverse Ranges in southern California. Data from the USGS Central California Microearthquake Network have been used in a variety of special studies. Seismic properties of the San Andreas fault zone and the adjacent regions have been determined (Kind, 1972; Mayer-Rosa, 1973; Healy and Peake, 1975; Peake and Healy, 1977). Matumoto *et al.* (1977) developed and applied the "minimum apparent velocity" method to interpret data from local explosions and earthquakes in Central America in terms of crustal properties.

The time-term technique has been applied to arrival time data from microearthquake networks. Explosive sources generally were used (e.g., Hamilton, 1970; Wesson *et al.*, 1973b; McCollom and Crosson, 1975). Direct measurements of apparent velocities of P-waves from regional events have been made with microearthquake networks. From these measurements, crustal and mantle velocity structure beneath the networks have been determined (e.g., Kanamori, 1967; Burdick and Powell, 1980).

In more recent years the widespread use of computers has encouraged development of more advanced modeling techniques. For example, arrival time data from local earthquakes and artificial sources may be combined and then inverted simultaneously for hypocenter parameters, station corrections, and velocity structure (see Section 6.3). In one modeling technique, the velocity structure was allowed to vary only with depth (e.g., Crosson, 1976a,b; Steppe and Crosson, 1978; Crosson and Koyanagi, 1979; Hileman, 1979; Horie and Shibuya, 1979; Sato, 1979). In another approach, the velocity structure was modeled in three dimensions (e.g., Aki and Lee, 1976; Lee *et al.*, 1982a). A nonlinear least squares technique described by Mitchell and Hashim (1977) used local P- and S-readings from a microearthquake network to compute apparent velocities and points of intersection of the travel time lines for refracted phases.

The inversion of arrival times from teleseismic events to yield a three-dimensional velocity structure beneath a seismic network was pioneered by K. Aki and his colleagues. This method was applied to data from the LASA array in Montana (Aki *et al.*, 1976) and to data from the NORSAR array in Norway (Aki *et al.*, 1977). This approach has since been further developed and applied particularly to data from microearthquake networks, for example, to the Tarbela array in Pakistan (Menke, 1977), to the St. Louis University network in the New Madrid, Missouri, seismic region (Mitchell *et al.*, 1977), to networks in Japan (Hirahara, 1977; Hirahara and Mikumo, 1980), to USGS microearthquake networks in central California (Zandt, 1978; Cockerham and Ellsworth, 1979), in Yellowstone National Park, Wyoming (Zandt, 1978; Iyer *et al.*, 1981), and in Hawaii (Ellsworth and Koyanagi, 1977), and to the Southern California Seismic Network (Raikes, 1980).

## 7.7. Other Applications

In addition to those discussed above, there are several other applications of microearthquake networks. For example, microearthquake networks have been used to monitor seismicity around volcanoes, nuclear waste disposal sites, and nuclear power plants. In fact, several of the earliest microearthquake networks were set up to study volcanoes (e.g., Eaton, 1962). Many of the permanent microearthquake networks listed in Table II are located in volcanic regions (e.g., Hawaii, Iceland, and Oregon), and their primary function is to monitor seismicity as an aid for forecasting volcanic eruptions. Crosson *et al.* (1980) described such an application for Mt. St. Helens, which erupted cataclysmically on May 18, 1980. Microearthquake networks often are used to map active faults in the vicinity of nuclear waste disposal sites and nuclear power plants. Results from such studies usually are too specific in nature and commonly are not published in scientific journals.

**TABLE II. Examples of Permanent Microearthquake Networks**

| Country | Microearthquake network | Operating or coordinating institution | Start date | Geographic location | Areal coverage ($km^2$) | Number of stations | Station spacing (km) | Annual number of located earthquakes |
|---|---|---|---|---|---|---|---|---|
| | | | | *Asia* | | | | |
| China | Beijing region | State Seism. Bureau, Beijing, China | 1966 | Northern Hopei | 120,000 | 21 | 76 | ~500 |
| | Taiwan | Acad. Sinica, Taipei, Taiwan | 1972 | Taiwan | 30,000 | 22 | 37 | 1500 |
| Japan | Abuyama | Abuyama Seism. Obs., Kyoto Univ., Takastsuki-shi Osaka-fu, Japan | 1967 | Osaka-fu, Honshu | 10,000 | 13 | 28 | |
| | Akita | Akita Geophys. Obs., Tohoku Univ., Sendai, Japan | 1966 | Akita, Honshu | 10,000 | 6 | 41 | |
| | Dodaira | Dodaira Microearthq. Obs., Earthq. Res. Inst., Tokyo Univ., Tokyo, Japan | 1966 | Kanto district, Honshu | 10,000 | 5 | 45 | |
| | Hirosaki | Hirosaki Earthq. Obs., Hirosaki Univ., Hirosaki, Japan | 1972 | Aomori-ken, Honshu | 1000 | 7 | 12 | |
| | Hokkaido | Res. Cent. Earthq. Pred., Hokkaido Univ., Sapporo, Japan | 1976 | Southern Hokkaido | 25,000 | 9 | 53 | |
| | Hokuriku | Hokuriku Microearthq. Obs., DPRI, Kyoto Univ., Kyoto, Japan | 1968 | Fukui-ken, Honshu | 5000 | 7 | 27 | |
| | Hokushin | Hokushin Obs., Earthq. Res. Inst., Tokyo Univ., Tokyo, Japan | 1967 | Nagoya-ken, Honshu | 10,000 | 7 | 38 | |

(*continued*)

**TABLE II** (*Continued*)

| Country | Microearthquake network | Operating or coordinating institution | Start date | Geographic location | Areal coverage ($km^2$) | Number of stations | Station spacing (km) | Annual number of located earthquakes |
|---|---|---|---|---|---|---|---|---|
| Japan | Kamitakara | Kamitakara Geophys. Obs., DPRI, Kyoto Univ., Kyoto, Japan | 1966 | Gifu-ken, Honshu | 1000 | 3 | 18 | |
| | Kanto-Tokai | Nat. Res. Cent. Disast. Prevent., Sakura-mura, Niihari-gun, Ibaraki-ken, Japan | 1973 | Ibaraki-ken, Honshu | 40,000 | 10 | 63 | |
| | Kitakami | Kitakami Seism. Obs., Tohoku Univ., Sendai, Japan | 1971 | Iwate-ken, Honshu | 10,000 | 14 | 27 | |
| | Kochi | Kochi Earthq. Obs., Kochi Univ., Kochi, Japan | 1967 | Kochi-ken, Shikoku | 3000 | 5 | 24 | |
| | Nagoya | Res. Cent. Earthq. Pred., Nagoya Univ., Nagoya, Japan | 1976 | Central Honshu | 20,000 | 13 | 39 | |
| | Shiraki | Shiraki Microearthq. Obs., Earthq. Res. Inst., Tokyo Univ., Tokyo, Japan | 1968 | Hiroshima-ken, Honshu | 2000 | 3 | 26 | |
| | Takayama | Takayama Seism. Obs., Nagoya Univ., Nagoya, Japan | 1970 | Gifu-ken, Honshu | 2000 | 4 | 22 | |
| | Tohoku | Obs. Cent. Earthq. Pred., Tohoku Univ., Sendai, Japan | 1975 | Tohoku district, Honshu | 40,000 | 16 | 50 | |
| | Tokushima | Tokushima Seism. Obs., Kyoto Univ., Kyoto, Japan | 1972 | Tokushima-ken, Shikoku | 2000 | 4 | 22 | |
| | Tottori | Tottori Microearthq. Obs., DPRI, Kyoto Univ., Kyoto, Japan | 1964 | Tottori-ken, Honshu | 8000 | 8 | 32 | |

| | | | | | | | | |
|---|---|---|---|---|---|---|---|---|
| | Wakayama | Wakayama Microearthq. Obs., Earthq. Res. Inst., Tokyo Univ., Tokyo, Japan | 1965 | Wakayama-ken, Honshu | 20,000 | 12 | 41 | |
| Pakistan | Tarbela/Chashma | Govt. of Pakistan, and Lamont–Doherty Geol. Obs., Palisades, New York | 1973 | Northern Pakistan | 50,000 | 32 | 40 | 2000 |
| USSR | Dushanbe | Tadzhik Inst. of Seism. Const. and Seismology, Dushanbe, USSR | 1955 | Tadzhik SSR | 15,000 | 18 | 29 | ~2000 |
| | Garm | Inst. Phys. of the Earth, Moscow, USSR | 1950 | Tadzhik SSR | 10,000 | 16 | 25 | 3500 |
| | | | | *Australia and New Zealand* | | | | |
| Australia | Adelaide | Dept of Physics, Univ. of Adelaide, Adelaide, Australia | 1962 | South Australia | 150,000 | 9 | 130 | 60 |
| | New South Wales | School of Earth Sci., Australian Natl. Univ., Canberra, Australia | | New South Wales | | 9 | | |
| | Tasmania | Geology Dept., Univ. of Tasmania, Hobart, Australia | 1972 | Tasmania | 20,000 | 8 | 50 | 100 |
| New Zealand | Pukaki | Seism. Obs., DSIR, Wellington, New Zealand | 1975 | Central South Island | 3000 | 10 | 17 | ~300 |
| | Wellington | Seism. Obs., DSIR, Wellington, New Zealand | 1975 | Wellington region | 5000 | 11 | 21 | 1000 |
| | | | | *Europe* | | | | |
| France | Rhinegraben | Inst. Phys. Globe, Univ. of Strasbourg, Strasbourg, France | | Rhinegraben | 3000 | 5 | 24 | 150 |

*(continued)*

TABLE II (*Continued*)

| Country | Microearthquake network | Operating or coordinating institution | Start date | Geographic location | Areal coverage ($km^2$) | Number of stations | Station spacing (km) | Annual number of located earthquakes |
|---|---|---|---|---|---|---|---|---|
| Germany | Rhinegraben | Geophys. Inst., Univ. of Karlsruhe, Karlsruhe, Germany | 1966 | Rhinegraben | 10,000 | 8 | 35 | 150 |
| Iceland | Hengill–Hellisheidi | Sci. Inst., Univ. of Iceland, Reykjavik, Iceland | 1974 | SW Iceland | 5000 | 8 | 25 | |
| Italy | Ancona | Inst. Geof., Litosfera, Milano, Italy | 1973 | Central Italy, East coast | 400 | 5 | 9 | |
| Romania | Vrancea | Inst. Hydroelec. Bucharest, Romania | 1977 | Carpathians | 40,000 | 7 | 76 | 100 |
| Sweden | Southern Sweden | Hagfors Obs., FOA Fack, S-10450 Stockholm, Sweden | 1980 | Southern Sweden | 200,000 | 20 | 100 | |
| Switzerland | Switzerland | Swiss Seism. Serv. Zurich, Switzerland | 1974 | Swiss Alps and Alpine Forelands | 15,000 | 14 | 33 | 300 |
| U.K. | Lownet | Inst. Geol. Sci. Edinburgh, Scotland, UK | 1969 | Lowland Valley, Scotland | 10,000 | 7 | 38 | |
| | | | | *North and Central America* | | | | |
| Canada | Eastern Canada | Earth Physics Br., Dept. Energy, Mines and Resources, Ottawa, Canada | 1974 | Southern Quebec | 20,000 | 4 | 70 | |
| | Western Canada | Earth Physics Br., Dept. Energy, Mines and Resources, Ottawa, Canada | 1975 | Southwestern British Columbia | 10,000 | 4 | 50 | |
| Costa Rica | Costa Rica | Univ. Costa Rica, San Jose, Costa Rica | 1976 | Costa Rica | 10,000 | 10 | 32 | |
| Guatemala | Guatemala | Inst. Nacional de Sismologia, Guatemala City, Guatemala | 1975 | Guatemala | 40,000 | 30 | 37 | ~2000 |

| | | | | | | | | |
|---|---|---|---|---|---|---|---|---|
| Mexico | Cerro Prieto | Centro Investig. Cientif. Educ. Super. Ensenada, Ensenada, B.C., Mexico | 1977 | Cerro Prieto, Northern Baja | 400 | 6 | 8 | ~200 |
| Nicaragua | Nicaragua | Inst. de Investigaciones Sismicas, Managua, Nicaragua | 1975 | Nicaragua | 40,000 | 16 | 50 | ~2000 |
| U.S. | Adak | CIRES, Univ. Colorado, Boulder, Colorado | 1974 | Adak, Alaska | 7500 | 14 | 23 | 900 |
| | Alaska | Geophys. Inst., Univ. Alaska, Fairbanks, Alaska | 1977 | Fairbanks, Alaska Peninsula, Kodiak Island, Seward Peninsula | 800,000 | 50 | 100 | 4000 |
| | Alaska Peninsula (2 subnets) | Lamont-Doherty Geol. Obs., Columbia Univ., Palisades, New York | 1973 | Shumagin Islands and Unalaska Island | 66,000 | 20 | 57 | 1000 |
| | Albuquerque Basin | Off. Earthq. Studies, U.S. Geol. Survey, Albuquerque, New Mexico | 1976 | Central New Mexico | 20,000 | 13 | 39 | 200 |
| | Central California | Off. Earthq. Studies, U.S. Geol. Survey, Menlo Park, California | 1967 | Central California | 50,000 | 250 | 14 | 4000 |
| | Eastern Washington | Geophys. Program, Univ. Washington Seattle, Wash. | 1969 | Eastern Washington | 10,000 | 32 | 18 | |
| | Hawaii | Hawaii Volcan. Obs., U.S. Geol. Survey, Hawaii Is., Hawaii | 1961 | Hawaii Island | 10,000 | 40 | 16 | 4000 |
| | INEL | Idaho Natl. Eng. Lab., Idaho Falls, Idaho | 1973 | Southeast Idaho | 6000 | 6 | 32 | |
| | Kansas | Kansas Geol. Survey, Lawrence, Kansas | 1977 | Eastern Kansas | 50,000 | 12 | 65 | 12 |
| | Los Angeles Basin | Dept. of Geol. Sci., Univ. Southern Calif., Los Angeles, California | 1971 | Los Angeles Basin, Southern Calif. | 4000 | 25 | 13 | 200 |
| | Nevada | Seismol. Lab., Univ. of Nevada, Reno, Nevada | 1970 | Western Nevada and Eastern California | 100,000 | 50 | 45 | 1000 |

*(continued)*

TABLE II (*Continued*)

| Country | Microearthquake network | Operating or coordinating institution | Start date | Geographic location | Areal coverage ($km^2$) | Number of stations | Station spacing (km) | Annual number of located earthquakes |
|---|---|---|---|---|---|---|---|---|
| U.S. | New Madrid | Dept. of Earth and Atm. Sci., St. Louis Univ., St. Louis, Missouri | 1974 | Southeast Missouri | 20,000 | 17 | 34 | 200 |
| | Northeastern United States (7 member networks) | Weston Obs., Boston College, Boston, Mass. | 1975 | Northeastern United States | 200,000 | 110 | 43 | 100 |
| | Northern Caribbean | Lamont–Doherty Geol. Obs., Columbia Univ., Palisades, New York | 1975 | Netherland Antilles, Puerto Rico, Virgin Is., West Indies | 30,000 | 15 | 45 | |
| | Oklahoma | Oklahoma Geophys. Obs., Univ. of Oklahoma, Norman, Oklahoma | 1977 | Oklahoma | 150,000 | 10 | 122 | 60 |
| | Oregon | Off. Earthq. Studies, U.S. Geol. Survey, Menlo Park, California | 1980 | Cascade Range, Oregon | 37,500 | 32 | 34 | 100 |
| | Puerto Rico | Off. Earthq. Studies, U.S. Geol. Survey, Denver, Colorado | 1975 | Puerto Rico | 10,000 | 15 | 26 | 300 |
| | Southeastern United States (12 member networks) | Virginia Polytechnic Inst., Blacksburg, Virginia | 1977 | Southeastern United States | 250,000 | 83 | 55 | 100 |
| | Southern Alaska | Off. Earthq. Studies, U.S. Geol. Survey, Menlo Park, California | 1972 | Southern Alaska | 230,000 | 50 | 60 | 5000 |
| | Southern California | Seismol. Lab., Cal. Inst. Tech. Pasadena, California | 1973 | Southern California | 100,000 | 150 | 26 | 6000 |
| | Southern Great Basin | Off. Earthq. Studies, U.S. Geol. Survey, Denver, Colorado | 1978 | Southern Nevada, NW Arizona, SE California | 100,000 | 50 | 45 | 500 |

| | | | | | | | | |
|---|---|---|---|---|---|---|---|---|
| | Wasatch Front | Dept. Geol. and Geophys., Univ. of Utah, Salt Lake City, Utah | 1974 | Northern Utah | 30,000 | 43 | 26 | 1000 |
| | Western Washington | Geophys. Program, Univ. Washington, Seattle, Wash. | 1969 | Puget Sound Region, Western Washington | 30,000 | 17 | 42 | 400 |
| | Yellowstone | Off. Earthq. Studies, U.S. Geol. Survey, Menlo Park, California | 1972 | Yellowstone Natl. Park and vicinity, Idaho–Wyoming–Montana | 8000 | 20 | 20 | 200 |
| West Indies | Eastern Caribbean | Seismic Res. Unit, Univ. West Indies, Trinidad | 1978 | Various Leeward and Windward Islands | 70,000 | 11 | 80 | |

**TABLE III. Examples of Reconnaissance Microearthquake Surveys on Land**

| Country | Province/ State | Locality | Seismographs | Number of Instr. | Number of Sites | Time Year | Time Duration | Number of microearthquakes Observed | Number of microearthquakes Located | Reference |
|---|---|---|---|---|---|---|---|---|---|---|
| | | | | *Africa* | | | | | | |
| Botswana | | Okavango Delta | Smoked paper portable | 5 | — | 1974 | ~3 months | ~0.5/day | ~50 | Scholz *et al.* (1976) |
| Tanzania/ Kenya | | E. African Rift | Modified ocean-bottom type | 5 | 14 | 1968–1969 | 5–10 days/site | Up to 30/day | 100 | Rykounov *et al.* (1972) |
| Ethiopia | | NW Ethiopian Rift | Smoked paper portable | — | 27 | 1969 | 6 weeks | 5 | | Molnar *et al.* (1970) |
| Kenya | | Gregory Rift | Smoked paper portable | 3 | 28 | 1967 | ~700 hr | ~500 | | Tobin *et al.* (1969) |
| | | Kenya Rift | Smoked paper portable | — | 70 | 1969–1970 | ~2500 hr | 0–390/day | 19 | Molnar and Aggarwal (1971) |
| Uganda | | Ruwenzori and other districts | Smoked paper portable | 4 | 28 | 1973 | ~3 months | 5–20/day | ~200 | Maasha (1975) |
| | | Sempaya, Kitagata, and Lake Kitagata | Smoked paper portable | 1 | — | 1973 | 4 days | 0 | | Maasha (1976) |
| | | | | — | — | 1973 | 24 hr | 12 | 6 | |
| | | | | — | — | 1973 | — | — | | |
| | | | | *Antarctica* | | | | | | |
| | | Syowa station | Standard station | — | — | 1967–1970 | — | ~100 | | Kaminuma (1971) |
| | | McMurdo Sound | Temporary stations | 3 | 3 | 1974–1976 | ~1 month | ~25 | | Kaminuma (1976) |
| | | | | *Asia* | | | | | | |
| Afghanistan | | Hindu Kush | Smoked paper portable and 1 permanent | 12 | 12 | 1977 | ~5 weeks | — | ~1200 | Chatelain *et al.* (1980) |
| Iran | | Teheran region | Smoked paper and magnetic tape | 3 | 11 | 1974 | ~1 month | ~300 | 37 | Hedayati *et al.* (1976, 1978) |
| Iraq | | Iraq | 3-component portable | 1 set | 42 | 1974–1975 | 180 hr | 23 | | Alsinawi and Banno (1976) |
| Israel | | Dead Sea–Jordan Valley Rift | Smoked paper portable | 3 | 20 | 1972–1973 | 7–40 days/site | — | | Wu *et al.* (1973) |

| | | | | | | | | | | |
|---|---|---|---|---|---|---|---|---|---|---|
| Israel/Jordan | | Dead Sea region | Ink-pen portable | 3 | 3 | 1976 | 5 months | — | ~30 | Ben-Menahem *et al.* (1977) |
| Japan | Honshu | Gobo, Wakayama Pref. | Electronic type | 2 | 3 | 1952 | 46 hr | 82 | | Miyamura (1959a) |
| | Honshu | Wakayama Pref. | Accelerograph and electronic type | 8 | 25 | 1952–1956 | ~6 months | ~2000 | ~100 | Miyamura (1959b, 1960) |
| | Honshu | Mt. Tsukuba, Kanto Pref. | Ultrasensitive | 3 | 1 | 1955 | 48 hr | ~200/day | | Asada (1957) |
| | Honshu | Matsushiro | Ultrasensitive | 4 | 1 | 1956 | 13 days | 121 | | Asada *et al.* (1958) |
| | Honshu | Neo Valley | Smoked paper portable | 4 | 6 | 1956–1962 | — | 139 | 97 | Muramatu *et al.* (1963) |
| | Honshu | Kii Peninsula | Accelerograph and electronic type | 10 | 10 | 1957–1962 | — | — | ~300 | Miyamura *et al.* (1966) |
| | Honshu | Mt. Tsukuba | Radio telerecording | 6 | 6 | 1958 | — | — | 55 | Miyamura and Tsujiura (1959) |
| | Honshu | Kanto and Chubu region | Magnetic tape recording | 2 | 2 | 1961–1962 | 212 days | 519 | Hundreds | Miyamura *et al.* (1962) |
| | | | | | | 1962 | 42 days | 215 | | |
| | | | | | | 1962 | 42 days | 291 | | |
| | Honshu | Hachiman, Gifu Pref. | Magnetic tape recording | 4 | 4 | 1963 | 720 hr | 195 | 71 | Miyamura *et al.* (1964) |
| | Honshu | Neo Valley fault | Temporary and permanent type | 13 | 13 | 1963 | ~1 month | 1489 | Hundreds | Miki *et al.* (1965) |
| | Honshu | Neo Valley fault | Data from cooperative observations | — | — | 1963–1964 | — | — | ~100 | Watanabe and Nakamura (1967) |
| | Honshu | Wakayama | 7 array type and 3 individual | 33 | 33 | 1965 | 15 days | 2600 | | Hori and Matumoto (1967) |
| | Honshu | W. Kii Peninsula | 10 temporary and 7 permanent | 17 | 17 | 1965 | 15 days | 470 | ~360 | Watanabe and Kuroiso (1967) |
| | Kyushu | N. Shimabara Peninsula | 1 tripartite array | 3 | 3 | 1966 | 2 weeks | — | 19 | Kubotera and Kikuchi (1967) |
| | Honshu | Mt. Minakami, Matsushiro | 1 tripartite array | 3 | 3 | 1966 | 14 hr | >1500 | 255 | Watanabe *et al.* (1967) |
| | Honshu | NE Honshu | 1 tripartite array and 7 portable | 10 | 20 | 1967 | 20 days | ~1000 | ~50 | Hamaguchi *et al.* (1973) |
| | Honshu | Tsukechi and Sakashita | Paper recording | 1 | 1 | 1968 | ~14 days | 48 | | Watanabe and Iida (1970) |
| | | | | 1 | 1 | 1968 | 76 days | 348 | | |
| | Honshu | S. Neo Valley fault | Smoked paper and magnetic tape recording | 11 | 11 | 1968 | — | ~400 | ~50 | Ooida *et al.* (1971) |

*(continued)*

TABLE III (*Continued*)

| Country | Province/ State | Locality | Seismographs | Number of | | Time | | Number of microearthquakes | | Reference |
|---|---|---|---|---|---|---|---|---|---|---|
| | | | | Instr. | Sites | Year | Duration | Observed | Located | |
| Japan | Honshu | Mikawa district | Smoked paper and magnetic tape recording | 8 | 8 | 1969 | 75 days | ~600 | ~120 | Ooida and Yamada (1972) |
| | Honshu | Hiroshima–Shimane border area | 2 tripartite, 1 single, and 4 permanent | 11 | 13 | 1969 | 3 weeks | ~500 | ~160 | Kayano *et al.* (1970) |
| | Honshu | Miura-Boso region | Magnetic tape recording | 2 | 2 | 1970 | 10 days | ~120 | 58 | Ishibashi and Tsumura (1971) |
| | Honshu | W. Sizuoka Pref. | 4 temporary type | 4 | 4 | 1970 | 2 months | — | ~100 | Yamada and Ooida (1972) |
| | Honshu | N. Gifu Pref. | 7 temporary type and 2 permanent | 9 | 9 | 1971 | 1 month | — | ~100 | Yamada *et al.* (1972) |
| | Honshu | Atera fault | Magnetic tape recording | 3 | 1 | 1971 | 2.5 months | — | ~100 | Ikami *et al.* (1972) |
| | Honshu | Ashio, Tochigi Pref. | Tripartite array | 3 | 3 | 1972–1973 | — | ~5–10/day | ~150 | Ogino (1974) |
| | Hokkaido | Noboribetsu hot spring, Iburi Province | Tripartite array | 3 | 3 | 1974 | 13 days | 22 | 2 | Hirota (1977) |
| Pakistan | | Quetta | Magnetic tape recording | 1 | 1 | 1962 | — | Numerous | | DeNoyer (1964) |
| Taiwan | | Hsintien–Ilan area | Up to 19 smoked paper portables and 7 permanent | 26 | 26 | 1974 | 3 months | — | ~260 | Tsai *et al.* (1975) |
| | | Kaohsiung–Pingtung | 11 Smoked paper portables and 6 permanent | 17 | 17 | 1977 | ~3 months | 2800 | >525 | Lin *et al.* (1979) |
| Turkey | | Marmara Sea region | Radio telemetered type | 7 | 7 | 1971 | 2 months | — | 65 | Crampin and Ucer (1975) |
| | | | *Australia and New Zealand* | | | | | | | |
| New Zealand | South Island | Marlborough region | Smoked paper portable | 7 | 56 | 1972 | 3 months | ~2000 | >230 | Arabasz and Robinson (1976) |

| | | | | | | | | | | |
|---|---|---|---|---|---|---|---|---|---|---|
| | North Island | Central North Island | Smoked paper portable | 4 | 8 | 1971–1972 | — | 44 | 29 | Evison *et al.* (1976) |
| | South Island | Alpine fault zone and Fiordland region | Smoked paper portable | 10 | 72 | 1972 | 10 weeks | — | ~200 | Scholz *et al.* (1973a) |
| | South Island | NW Nelson region | Smoked paper portable | 7 | 9 | 1973 | — | 2–12/day | 33 | Robinson and Arabasz (1975) |
| | South Island | Alpine fault zone near Haast | Smoked paper portable | 8 | 8 | 1973 | 32 days | 122 | 60 | Caldwell and Frohlich (1975) |
| | South Island | Clarence Fault | Smoked paper portable | 6 | 6 | 1975 | 13 days | ~2/day | ~70 | Kieckhefer (1977) |
| | | | | *Europe* | | | | | | |
| Finland | | Kuusamo region | Telemetered | 3 | 3 | 1972 | 3 weeks | 12 regional events | | Koschyk and Steinwachs (1977) |
| France/Italy | | Western Alps | Smoked paper portable | 11<br>16 | —<br>— | 1977<br>1978 | 1 month<br>1 month | 1800 | 250 | Frechet and Pavoni (1979) |
| Iceland | | Mid-Atlantic Ridge | Smoked paper portable | 3 | 78 | 1967 | ~2000 hr | >1000 | | Ward *et al.* (1969) |
| | | Mid-Atlantic Ridge | 2 tripartite arrays and smoked paper portable | 5 and 2 arrays | 154 | 1968 | 38 hr/site | — | >600 | Ward and Bjornsson (1971) |
| | | Geothermal areas | Smoked paper portable | 3 | 24 | 1970 | 1204 hr | ~600 | | Conant (1972) |
| | | Mid-Atlantic Ridge, Reykjanes Peninsula | Smoked paper, broadband and radio telemetered | 13<br>23 | 13<br>23 | 1971<br>1972 | ~2 weeks<br>~7 weeks | 20/day<br>12–24/day | >150<br>>150 | Klein *et al.* (1973) |
| | | Mid-Atlantic Ridge, Reykjanes Peninsula | Smoked paper, broadband and radio telemetered | 23 | 23 | 1972 | ~6 weeks | 17,000 | 2514 | Klein *et al.* (1977) |
| | | Mid-Atlantic Ridge, Tjednes Peninsula | Magnetic tape recording | 7 | 7 | 1972–1973 | 2.5 months | ~900 | 208 | Zverev *et al.* (1978) |
| Italy | | Stromboli | Magnetic tape recording | 6 | 15 | 1973 | ~1 week | 1329 | | Del Pezzo *et al.* (1975) |
| | | Etna | Magnetic tape recording | 5 | 14 | 1973 | 76 hr | Many | | Lo Bascio *et al.* (1976) |
| USSR | | Anapa region, Caucasus | SKM-3, SKD, SMTR instruments | — | 1 | 1968–1970 | 2 years | 500 | 81 | Aronovich *et al.* (1972) |
| Switzerland | | Swiss Alps | Smoked paper portable | 5 | — | 1975–1976 | 7 weeks | 83 | | Pavoni (1977) |

*(continued)*

TABLE III (*Continued*)

| Country | Province/ State | Locality | Seismographs | Number of Instr. | Number of Sites | Time Year | Time Duration | Number of microearthquakes Observed | Number of microearthquakes Located | Reference |
|---|---|---|---|---|---|---|---|---|---|---|
| | | | *North and Central America* | | | | | | | |
| Canada | Quebec | St. Lawrence Valley | Hot stylus portable | 7 | 16 | 1970 | 6–7 weeks | — | 28 | Leblanc *et al.* (1973) |
| | Quebec | St. Lawrence Valley | Telemetered and portable | 20 | 19 | 1974 | ~2 months | — | 35 | Leblanc and Buchbinder (1977) |
| El Salvador | | Ahuachapan geothermal area | Magnetic tape recording | 5 | 3 | 1969–1970 | 6 months | ~500 | 17 | Ward and Jacob (1971) |
| El Salvador, Guatemala, Nicaragua | | Central American volcanoes | Smoked paper portable | 1 | 7 | 1972 | ~300 hr | ~1000 | | Wood (1974) |
| Mexico | Baja Calif. | San Miguel fault zone | Smoked paper portable | 3 | 22 | 1970–1973 | ~800 hr | ~1000 | ~20 | Reyes *et al.* (1975) |
| | N. Baja Calif. | Agua Blanca and San Miguel faults | Smoked paper portable | 5 | 15 | 1974 | 2 months | — | ~200 | Johnson *et al.* (1976) |
| U.S. | Alaska | Katmai Natl. Monument | Tripartite array and 2 single | 5 | — | 1965 | 39 days | >1800 | ~560 | Matumoto and Ward (1967) |
| | Alaska | Denali fault zone, Mt. McKinley Natl. Park | High-gain portable | 3 | 7 | 1965 | 236 hr | 520 | | Boucher *et al.* (1968) |
| | Alaska | Denali fault between Mt. McKinley Natl. Park and Haines | Smoked paper portable | 4 | 22 | 1967 | 1–3 days/site | A few events/day | | Boucher and Fitch (1969) |
| | Alaska | Crillon Lake, Fair-weather Fault zone | Smoked paper portable | 1 | 1 | 1968 | 53 hr | 87 | | Page (1969) |
| U.S./Canada | Alaska and British Columbia | SE Alaska and NW British Columbia | Hot stylus portable | 4 | 7 | 1969 | 81 days | 140 | 77 | Rogers (1976) |
| U.S. | California | San Jacinto fault SE of Anza | Caltech trailer | 6 | 12 | 1966–1967 | ~5 weeks | — | ~100 | Arabasz *et al.* (1970) |

| | | | | | | | | | |
|---|---|---|---|---|---|---|---|---|---|
| California | San Andreas fault system | Caltech trailer | 8 | ~60 | 1964–1966 | >35,000 hr total | 0–75/day | | Brune and Allen (1967) |
| California | Coast of N. California | Smoked paper portable | 5 | 25 | 1968 | — | — | 160 | Seeber *et al.* (1970) |
| California | The Geysers, Sonoma County | Magnetic tape recording | 6 | 6 | 1968 | 120 hr | 29 | 19 | Lange and Westphal (1969) |
| California | Lassen Peak Volcano | USGS 10-day portable | 8 | 8 | 1969 | 13 days | — | 29 | Unger and Coakley (1971) |
| California | Mono Lake, N. Owens Valley | USGS 10-day portable and others | 29 | 31 | 1970 | 20 days | 140 | 74 | Pitt and Steeples (1975) |
| California | Geysers geothermal area | USGS telemetered type | 8 | 8 | 1971 | 3 weeks | — | 53 | Hamilton and Muffler (1972) |
| California | Whittier fault | USGS telemetered type | 11 | 25 | 1971–1972 | ~9 months | — | 31 | Lamar (1973) |
| California | Elsinore fault zone | Smoked paper portable | 6 | 20 | 1972 | >5000 hr | 0.5–3.7/day | 53 | Langenkamp and Combs (1974) |
| California | Cape Mendocino | 8 Radio telemetered type and 2 permanent | 10 | 10 | 1972 | 3 months | >400 | 150 | Simila *et al.* (1975) |
| California | Fontana–San Bernardino area | Smoked paper portable | 6 | 16 | 1972–1973 | 6000 hr | — | ~70 | Hadley and Combs (1974) |
| California | Long Valley geothermal area | USGS 10-day portable | 16 | 20 | 1973 | 5 weeks | — | 76 | Steeples and Pitt (1976) |
| California | Mesa geothermal area, Imperial Valley | Smoked paper portable | 6 | 6 | 1973 | ~5 weeks | Hundreds | 36 | Combs and Hadley (1977) |
| California | San Jacinto Valley, Riverside County | Smoked paper portable | 6 | 10 | 1973 | 6 weeks | 0–17/day | ~100 | Cheatum and Combs (1973) |
| California | Coso geothermal area, China Lake | 6 smoked paper and 9 magnetic tape | 15 | 15 | 1974 | 33 days | >2000 | 78 | Combs and Rotstein (1976) |
| California | Salton Sea geothermal area | 5 smoked paper and 2 permanent | 7 | 7 | 1975 | 8 weeks | 2–3/day | ~100 | Gilpin and Lee (1978) |
| California | San Andreas Fault from Carrizo Plains to Lake Hughes | Caltech trailer | 7 | 20 | 1976 | 38–69 days | — | ~165 | Carlson *et al.* (1979) |
| California | Auburn | Smoked paper portable | 8 | 8 | 1976 | 11 weeks | 15 | 15 | McNally *et al.* (1978b) |
| California | Auburn | Smoked paper portable | 5 | 5 | 1976 | 3 months | 22 | 22 | Cramer *et al.* (1978) |
| California | The Geysers, Sonoma County | Radio telemetered, triggered digital, and smoked paper | 16 | — | 1976<br>1977 | 5 days<br>11 days | 70<br>340 | 40 | Majer (1978) |

(*continued*)

TABLE III (*Continued*)

| Country | Province/ State | Locality | Seismographs | Number of Instr. | Number of Sites | Time Year | Time Duration | Number of microearthquakes Observed | Number of microearthquakes Located | Reference |
|---|---|---|---|---|---|---|---|---|---|---|
| U.S. | Colorado | San Luis Valley | Smoked paper portable | 3 | 8 | 1974 | 3 weeks | 6 | 1 | Keller and Adams (1976) |
| | Hawaii | Hawaiian Ridge | Ocean-bottom type and land-based | — | — | 1976–1977 | 8 months | 359 | 65 | Estill and Odegard (1978) |
| | Idaho | Snake River, Stanley/ Sunbeam | Smoked paper portable | 9 | ~29 | 1972 | 3 weeks<br>8 days | 0<br>40 | 0<br>18 | Pennington *et al.* (1974) |
| | Montana and Utah | Intermountain seismic belt | Smoked paper portable | 6 | 82 | 1969 | ~50 days | — | 120 | Sbar *et al.* (1972b) |
| | Montana and Wyoming | Hebgen Lake–Yellowstone Park region | Smoked paper portable | 6 | 6 | 1972 | — | 16/day | 182 | Trimble and Smith (1975) |
| | Montana | Helena–Marysville area | Smoked paper portable | 6 | 3 | 1973 | ~2 months | — | 97 | Freidline *et al.* (1976) |
| | Nevada | Fallon area | Film and magnetic tape recording | 5 | 7 | 1963 | 70 days | 216 | 187 | Mickey (1966) |
| | Nevada | Fairview Peak area | Magnetic tape recording | 24 | 24 | 1965 | 129 days | 1386 | 224 | Westphal and Lange (1967) |
| | Nevada | Fairview Peak and Reno areas | High-gain portable | 2 | 10 | 1965 | 115 hr<br>65 hr | ~200/day | | Oliver *et al.* (1966) |
| | Nevada | Fairview Peak area | Magnetic tape recording | 4 | 4 | 1966 | 6 weeks | 31/day | 315 | Stauder and Ryall (1967) |
| | Nevada and California | Nevada seismic zone | Smoked paper portable | 6 | 29 | 1969 | ~3000 hr | ~1000 | 281 | Gumper and Scholz (1971) |
| | Nevada | Buffalo Valley, Grass Valley, Buena Vista Valley | Smoked paper and radio telemetered | — | — | 1976 | 8 weeks | ~120 | ~70 | Majer (1978) |
| | New Jersey | Sterling Mine, Ogdensburg | 1 high-gain and 8 permanent | 9 | 8 | 1962–1963 | 730 hr | 8 | 5 | Isacks and Oliver (1964) |
| | New Jersey | Lake Hopatcong | Smoked paper portable | 4 | 6 | 1969 | 24 days | 26 | 13 | Sbar *et al.* (1975) |
| | New Mexico | Socorro | High-gain | 2 | 3 | 1960–1962 | 20 months | Several hundred | 20 | Sanford and Holmes (1962) |

| | | | | | | | | | | |
|---|---|---|---|---|---|---|---|---|---|---|
| | New Mexico | Socorro | High-gain | 5 | 6 | 1960–1965 | — | — | 34 | Sanford and Long (1965) |
| | Tennessee and Missouri | SE Missouri and W. Tennessee | Smoked paper portable | 4 | 12 | 1968 | 11 days | 45 | 6 | Lammlein *et al.* (1971) |
| | Tennessee | Maryville–Alcoa area | Smoked paper portable | 5 | 5 | 1976 | 50 days | 11 | 4 | Sodbinow and Bollinger (1978) |
| | Virgin Is. and Puerto Rico | E. Puerto Rico and the Virgin Is. | 4 high-gain portables and 2 permanent | 6 | 8 | 1965 | 2 weeks | 77 | 19 | Murphy *et al.* (1970) |
| | Virginia | Hot Springs area | Smoked paper portable | 3 | 7 | 1973 | 440 hr | 43 | | Bollinger and Gilbert (1974) |
| | Virginia | Central Virginia seismic zone | Smoked paper portable | 3 | 26 | 1974 | 91.5 days | ~11 | | Bollinger (1975) |
| | Washington | Mt. Rainier Volcano | USGS 10-day portable | 5 | 5 | 1968 | 30 days | ~345 | 65 | Unger and Decker (1970) |
| | Washington | Mt. Rainier Volcano | USGS 10-day portable | 9 | 9 | 1969 | ~1 month | 10/day | 67 | Unger and Mills (1972) |
| | Wyoming | Yellowstone Natl. Park | — | 12 | ~29 | 1972–1976 | ~26 weeks | — | ~1000 | Smith *et al.* (1977) |
| West Indies | St. Lucia | Sulphur Springs geothermal region | Slow-speed tape recording | 5 | 5 | 1974–1975 | 39 days | — | 7 | Aspinall *et al.* (1976) |
| | | | | *South America* | | | | | | |
| Colombia | | Bucaramanga | 3-component portable and 2 permanent | 8 | 8 | 1976 | 3.5 days | 27 | 23 | Pennington *et al.* (1979) |

**TABLE IV. Examples of Reconnaissance Microearthquake Surveys at Sea**

| Location | Seismographs | Number of | | Time | | Number of microearthquakes | | Reference |
|---|---|---|---|---|---|---|---|---|
| | | Instr. | Sites | Year | Duration | Observed | Located | |
| | | | *Atlantic Ocean* | | | | | |
| Mid-Atlantic Ridge near 45°35′ N | Magnetic tape recording and ocean-bottom type | 1 | 2 | 1972 | 8 days | 6–30/day | | Francis and Porter (1972) |
| Mid-Atlantic Ridge near 37° N | Magnetic tape recording and ocean-bottom type | 2 | 2 | 1973 | ~18 days | 699 | 50–60 | Francis *et al.* (1977) |
| Mid-Atlantic Ridge near 37° N | Telemetered radio sonobuoys | >3 | — | 1973 | 11 days | 104 | 59 | Reid and MacDonald (1973) |
| Mid-Atlantic Ridge near 36°30′ N, median valley | Expendable radio telemetered sonobuoys | 3 | — | 1973 | 72 hr | 112 | 29 | Spindel *et al.* (1974) |
| Mid-Atlantic Ridge, E. St. Paul's fracture zone | Ocean-bottom type | 4 | 4 | 1974 | ~6 days | >300 | >6 | Francis *et al.* (1978) |
| Mid-Atlantic Ridge near 45° N, median valley | Ocean-bottom type | 3 | 3 | 1975 | ~8 days | >450 | 91 | Lilwall *et al.* (1977, 1978) |
| Reykjanes Ridge near 59° N | Ocean-bottom type | 2 | 2 | 1977 | 7.5 days | 100 | 34 | Lilwall *et al.* (1980) |

| | | | | | | | | |
|---|---|---|---|---|---|---|---|---|
| | | | *Indian Ocean* | | | | | |
| 50 km NW of RRR triple junction | Ocean-bottom type | 1 | 1 | 1976 | ~2 weeks | 38 | | Solomon *et al.* (1977) |
| | | | *Pacific Ocean* | | | | | |
| Mendocino escarpment, NW coast of California | Ocean-bottom type | 2 | 2 | 1966–1971 | ~5 years | ~650 | ~200 | Nowroozi (1973) |
| Japan Trench, off Sanriku | Ocean-bottom type | 4 | 4 | 1970 | ~9 days | 1–12 locals/day | 25 | Nagumo *et al.* (1976) |
| Gulf of California, Mexico | Telemetered sonobuoys | — | — | 1972 | ~6 weeks | ~1100 | | Reid *et al.* (1973) |
| Galapagos spreading center | Sonobuoys | — | — | 1972 | 86 min | 58 | | Northrop (1974) |
| Galapagos spreading center, near Galapagos Island | Sonobuoys | — | — | 1972 | ~55 hr | 15–80/hr | | MacDonald and Mudie (1974) |
| Gulf of California, Mexico | Telemetered sonobuoys and 2 land stations | 8 | 3 | 1972–1973 | 2/week | ~2000 | ~75 | Reichle and Reid (1977) |
| Central Basin fault, Philippine Sea | Ocean-bottom type | 1 | 1 | 1973 | 63 hr | 120 | | Shimamura *et al.* (1975) |
| Central part of Fiji Plateau | Ocean-bottom type | 1 | 1 | 1973 | 10 days | 117 | | Nagumo *et al.* (1975) |
| Gorda Ridge | Quadripartite sonobuoy array, radio telemetered and tape recorded | 1 array | 2 | 1973 | ~20 hr | 69 | 10 | Jones and Johnson (1978) |
| Blanco fracture zone | 2 tripartite sonobuoy arrays | 2 arrays | 4 | 1973 | 26 hr | 38 | 32 | Johnson and Jones (1978) |
| E. Pacific Rise and Rivera fracture zone | Ocean-bottom capsules in 3 separate tripartite arrays | 1 array | 3 | 1974 | ~29 days | ~1000 | ~100 | Prothero *et al.* (1976); Reid and Prothero (1981) |

**TABLE V. Examples of Micro-Aftershock Studies**

| Main shock | | | | | Number of microearthquakes | | |
|---|---|---|---|---|---|---|---|
| Date | Name | Magnitude | Field observation | Time period | Observed | Located | Reference |
| Jun. 28, 1948 | Fukui (Hukui), Japan | 7.3 | Tripartite array of 3 high-gain, short-period, vertical-comp. stations | Jul. 14–Aug. 10, 1948 | 262 | 0 | Asada and Suzuki (1949) |
| Oct. 5, 1948 | Ashkhabad, USSR | 7.6 | 4 temporary stations (magnification of 3000) | Jul.–Oct. 1949 | 1500 | 150 | Rustanovich (1957) |
| | | | 7 temporary stations (magnification of 10,000 to 35,000) | Jun.–Sep. 1953 | 1500 | 100 | Rustanovich (1957) |
| Dec. 26, 1949 | Imaichi, Japan | 6.7 | Tripartite array of 3 high-gain, short-period, horizontal-comp. stations | Dec. 29, 1949–Jan. 10, 1950 | 623 | 0 | Asada and Suzuki (1950) |
| Aug. 19, 1961 | Kitamino, Japan | 7.0 | Tripartite array with one 3-comp. and 2 vertical-comp. stations | Aug. 27–Sep. 20, 1961 | 694 | 149 | Miyamura *et al.* (1961) |
| Mar. 28, 1964 | Alaska | 8.3 | Quadripartite array with one 3-comp. and 3 vertical-comp. stations | May 19–Jun. 7, 1964 | 9061 | 797 | Aki *et al.* (1966) |
| | | | 2 tripartite arrays with 5 high-gain short-period stations | Jul. 2–5, 1964 | — | 249 | Matumoto and Page (1966) |
| Jun. 16, 1964 | Niigata, Japan | 7.5 | 15 temporary stations to augment existing stations by various groups | Jun. 23–Jul. 6, 1964 | — | 400 | Kayano (1968) |
| Nov. 16, 1964 | Corralitos, California | 5.0 | 3 temporary stations to augment existing stations | Nov. 16–23, 1964 | >100 | 35 | McEvilly (1966) |
| Aug. 1965 | Matsushiro swarms, Japan | (Swarm) | 16 temporary stations to augment existing stations | Oct. 1965–Oct. 1967 | — | 8061 | Hagiwara and Iwata (1968) |
| | | | Tripartite array at 4 sites | Oct. 1965–May 1967 | — | >30,000 | Hamada (1968) |
| Sep. 10, 1965 | Antioch, California | 4.9 | 1 temporary station to augment existing stations | Sep. 11–20, 1965 | 106 | 29 | McEvilly and Casaday (1967) |
| Jun. 28, 1966 | Parkfield, California | 5.5 | Data from Univ. of California Seismographic Stations plus temporary stations by various groups | Jun. 28, 1966–Jan. 12, 1967 | — | 201 | McEvilly *et al.* (1967) |

| | | | | | | | |
|---|---|---|---|---|---|---|---|
| | | | 13 USGS and 5 ESSA temporary stations plus 3 permanent stations operated by Univ. of Calif., Berkeley | Jul. 1–Sep. 15, 1966 | — | 630 | Eaton *et al.* (1970b) |
| Sep. 12, 1966 | Truckee, California | 6.0 | 1 tripartite array to augment existing stations | Sep. 16–29, 1966 | ~14,000 | 108 | Ryall *et al.* (1968) |
| Apr. 9, 1968 | Borrego Mountain, California | 6.4 | 20 temporary stations to augment existing stations | Apr. 12–Jun. 12, 1968 | >10,000 | 533 | Hamilton (1972) |
| May 16, 1968 | Tokachi-Oki, offshore Japan | 7.9 | 1 temporary station | May 18–Aug. 1968 | 52,000 | 0 | Hamaguchi *et al.* (1970) |
| | | | Data from Urakawa Seismological Observatory | May 1964–Dec. 1972 | ~20,000 | | Motoya (1974) |
| | | | 4 ocean-bottom seismographic stations (1 lost) | May–Jun. 1969 | ~600 | ~100 | Nagumo *et al.* (1970) |
| Jun. 1968 | Santa Barbara Channel, California | 5.2 (swarm) | 4 temporary stations to augment existing stations | Jun. 26–Aug. 3, 1968 | — | 63 | Sylvester *et al.* (1970) |
| Aug. 18, 1968 | Wachi, Japan | 5.6 | Data from Abuyama Seismological Observatory | Feb. 1968–Apr. 1969 | 9000 | ~200 | Watanabe and Kuroiso (1969) |
| Apr. 28, 1969 | Coyote Mountain, California | 5.8 | Up to 26 temporary stations and 2 permanent stations | May 2–13, 1969 | — | 127 | Thatcher and Hamilton (1973) |
| Aug. 13, 1969 | Kanuma, Japan | 4.0 | 1 tripartite array to augment existing stations | Aug. 29–Sep. 6, 1969 | 188 | 103 | Kaminuma *et al.* (1970) |
| Aug. 31, 1969 | Kamikochi, Japan | 5.0 | Data from Hokushin Seismological Observatory and its satellite stations | Aug. 31–Sep. 29, 1969 | — | 54 | Ohtake (1970a) |
| Sep. 9, 1969 | Central Gifu, Japan | 6.6 | 3 temporary stations to augment existing stations | Sep. 16–Nov. 10, 1969 | ~2000 | 59 | Sasaki *et al.* (1970) |
| | | | 1 tripartite array | Sep. 15–Oct. 5, 1969 | | ~500 | Anonymous (1970) |
| | | | Temporary network with 5 high-frequency stations | Sep. 1969–Feb. 1970 | >3000 | ~1800 | Watanabe and Kuroiso (1970) |
| Sep. 29, 1969 | Ceres, South Africa | 6.3 | Up to 7 temporary stations | Oct.–Nov. 1969 | 2000 | 125 | Green and Bloch (1971) |
| Apr. 9, 1970 | Matsushiro, Japan | 5.0 | Data from Hokushin Seismological Observatory and its satellite stations | Apr.–May 1970 | ~5000 | ~100 | Ohtake (1970b) |
| May 1970 | Danville, California | 4.3 (swarm) | 7 temporary stations to augment existing stations | May 1–Jul. 31, 1970 | ~5000 | 426 | Lee *et al.* (1971) |
| Jan. 5, 1971 | Offshore of Atsumi Peninsula, Japan | 6.1 | Data from Inuyama and Wakayama seismic networks | Jan.–Mar. 1971 | ~200 | 40 | Ooida and Ito (1972) |

(*continued*)

TABLE V (*Continued*)

| Main shock | | | | | Number of microearthquakes | | |
|---|---|---|---|---|---|---|---|
| Date | Name | Magnitude | Field observation | Time period | Observed | Located | Reference |
| Feb. 9, 1971 | San Fernando, California | 6.4 | Data from 7 temporary stations plus permanent stations | Feb. 10–11, 1971 | — | 47 | Hanks *et al.* (1971) |
| | | | 19 temporary stations | Feb. 12–13, 1971 | — | 164 | Wesson *et al.* (1971) |
| | | | 1 broadband digital seismic system for studying source parameters | Feb. 10–18, Dec. 23–24, 1971 | — | 167 | Tucker and Brune (1973) |
| May 23, 1971 | Adirondacks, New York | 3.6 (swarm) | 6 temporary stations using high-gain, short-period seismographs | May 25–Sep. 7, 1971 | ~10,000 | 54 | Sbar *et al.* (1972a) |
| Feb. 24, 1972 | Bear Valley, California | 5.0 | Data from USGS Central California Microearthquake Network | 1971–1972 | — | 3087 | Ellsworth (1975) |
| Feb. 29, 1972 | Offshore of Hachijojima, Japan | 7.0 | 2 temporary stations to augment the existing Dodaira Microearthquake Observatory | Feb.–Apr. 1972 | — | ~50 | Kasahara *et al.* (1973a) |
| Dec. 4, 1972 | Offshore of Hachijojima, Japan | 7.2 | 2 temporary stations to augment existing stations | Dec. 1972 | — | ~100 | Kasahara *et al.* (1973b) |
| Dec. 23, 1972 | Managua, Nicaragua | 6.2 | 9 portable smoked paper recording seismographs | Jan. 3–Feb. 7, 1973 | — | 171 | Ward *et al.* (1974) |
| 1972–1974 | Columbia Basin, Washington | (Swarm) | Up to 7 temporary stations at selected periods | 1972–1974 | ~400 | 121 | Malone *et al.* (1975) |
| Feb. 21, 1973 | Point Mugu, California | 6.0 | 19 temporary stations to augment existing stations | Feb. 21–Apr. 12, 1973 | — | 142 | Stierman and Ellsworth (1976) |
| | | | A five-station sonobuoy array | 4 hr total (beginning 7 hr after the main shock) | 28 | 9 | Bradner and Brune (1974) |
| Feb. 28, 1973 | Delaware–New Jersey | 3.8 | 4 temporary stations | Mar. 2–4, 1973 | — | 5 | Sbar *et al.* (1975) |
| Mar. 25, 1973 | Gulf of California, Mexico | 5.5 | 4 long-life sonobuoys | Mar. 26, 1973 (6 hrs) | 40 | 12 | Reichle *et al.* (1976) |
| | | | 3 sonobuoy arrays | Apr. 26–27, 1973 | 60 | 10 | |
| Sep. 13, 1973 | Agua Caliente Springs, California | 4.8 | 4 temporary stations to augment existing stations | Sep. 13–23, 1973 | — | 46 | Allison *et al.* (1978) |

| | | | | | | | |
|---|---|---|---|---|---|---|---|
| Nov. 30, 1973 | Eastern Tennessee | 4.6 | 8 temporary stations | Dec. 2–12, 1973 | — | 18 | Bollinger *et al.* (1976) |
| May 9, 1974 | Izu-Hanto-Oki, Japan | 6.9 | 2 temporary stations and 1 permanent station | May 13–31, 1974 | — | 399 | Karakama *et al.* (1974) |
| May 31, 1974 | Guaymas Basin, Gulf of California | 6.3 | Several sonobuoy arrays | June 1–2, 1974 | — | 23 | Reichle *et al.* (1976) |
| Jun. 12, 1974 | Borgarfjordur, Iceland | 6.3 | Temporary array of 9 short-period stations | Jun. 28–Jul. 15, 1977 | — | 563 | Einarsson *et al.* (1977) |
| Jan. 23, 1975 | Brawley, California | 4.7 (swarm) | Data from USGS Imperial Valley array and strong-motion records at AIR | Jan. 23–31, 1975 | — | 264 | Johnson and Hadley (1976) |
| Jun. 30, 1975 | Yellowstone Park, Wyoming | 6.1 | Up to 15 temporary stations to augment 21 existing stations | Jul. 2–19, 1975 | — | 97 | Pitt *et al.* (1979) |
| Jul. 8, 1975 | Canal de las Ballenas, Gulf of California, Mexico | 6.5 | An array of 4 portable seismographs plus 6 short-life sonobuoys | Jul. 11–16, 1975 | >200 | 51 | Munguia *et al.* (1977) |
| Jul. 12, 1975 | Maniwaki, Quebec, Canada | 4.2 | 3 portable seismographs, 2 permanent stations, and 1 high-gain array | Jul. 13–16, 1975 | 14 | 1 | Horner *et al.* (1978) |
| Aug. 1, 1975 | Oroville, California | 5.9 | Up to 16 telemetered stations | Aug. 5–31, 1975 | — | 336 | Lahr *et al.* (1976) |
| | | | 4 temporary stations plus Oroville station | Aug. 1–31, 1975 | — | 243 | Savage *et al.* (1975) |
| 1975–1977 | Izu Peninsula, Japan | 5.4 (swarm) | Up to 5 temporary stations to augment existing stations | Jul. 1975–May 1977 | 8532 | ~4000 | Tsumura *et al.* (1977) |
| Feb. 4, 1976 | Guatemala | 7.5 | A temporary seismic network | Feb. 9–27, 1976 | — | 258 | Langer and Bollinger (1979) |
| May 6, 1976 | Friuli, Italy | 6.3 | 4 digital seismographs, to augment existing stations | May 8–Jun. 14, 1976 | 100 | 30 | Gebrande *et al.* (1977) |
| | | | 9 mobile stations to augment existing stations | May 6, 1966–Apr. 13, 1977 | — | — | Cagnetti and Pasquale (1979) |
| 1976–1977 | Palmdale, California | 3.0 (swarm) | 7 movable seismographic trailers to augment existing stations | Nov. 1976–Nov. 1977 | ~700 | | McNally *et al.* (1978a) |
| Jan. 8, 1977 | Briones Hills, California | 4.3 (swarm) | Stations from Univ. of Calif. and USGS | Jan. 8–9, 1977 | 68 | 8 | Bolt *et al.* (1977) |
| Mar. 4, 1977 | Romania | 7.2 | Up to 10 mobile stations to augment existing stations | Mar.–May, 1977 | — | >140 | Fuchs *et al.* (1979) |
| Apr. 6, 1977 | Eguzon, France | 3.4 | Data from L.D.G. Seismic Network in France | Apr. 5–30, 1977 | 45 | 33 | Delhaye and Santoire (1977a) |
| Apr. 27, 1977 | Cosne d'Allier, France | 3.8 | Data from L.D.G. Seismic Network in France | Apr. 22–May 10, 1977 | 126 | 94 | Delhaye and Santoire (1977b) |

*(continued)*

TABLE V (*Continued*)

| Main shock | | | | | Number of microearthquakes | | |
|---|---|---|---|---|---|---|---|
| Date | Name | Magnitude | Field observation | Time period | Observed | Located | Reference |
| Jan. 14, 1978 | Izu-Oshima-Kinkai, Japan | 7.0 | Data from Izu Peninsula Network and other stations | Jun. 1977–Jun. 1978 | — | >1000 | Tsumura *et al.* (1978) |
| Feb. 18, 1978 | St. Donat, Quebec, Canada | 4.1 | 3 portable seismographs | Feb. 19–21, 1978 | 2 | 1 | Horner *et al.* (1979) |
| Jun. 20, 1978 | Thessaloniki, Greece | 6.4 | 10 portable seismographs | Jul. 3–23, 1978 | — | 42 | Carver and Henrisey (1978) |
| Aug. 13, 1978 | Santa Barbara, California | 5.1 | Data from S. Calif. Seismic Network and USC Network | Aug. 13–18, 1978 | — | 71 | Lee *et al.* (1978) |
| Sep. 3, 1978 | Swabian Jura, Germany | 5.7 | 8 event recording stations to augment existing stations | Sep. 3–mid-Oct., 1978 | ~325 | ~150 | Haessler *et al.* (1980) |
| Sep. 16, 1978 | Tabas-E-Golshan, Iran | 7.7 | 9 portable seismographs | Oct. 1978 | 6000 | 62 | Berberian *et al.* (1979) |
| Nov. 29, 1978 | Oaxaca, Mexico | 7.8 | 12 portable seismographs | Dec. 1–12, 1978 | — | 88 | Singh *et al.* (1980) |
| Feb. 28, 1979 | St. Elias, Alaska | 7.1 | Data from USGS Alaska Seismic Network, 4 portable seismographs, and 4 Canadian stations | Feb. 28–Mar. 31, 1979 | — | 308 | Stephens *et al.* (1980) |
| Mar. 14, 1979 | Petatlan, Guerrero, Mexico | 7.6 | 15 digital recorders, 4 smoked paper seismographs | Mar. 14–16, 1979 | Thousands | 29 | Meyer *et al.* (1980) |
| Aug. 6, 1979 | Coyote Lake, California | 5.7 | Data from USGS Central California Microearthquake Network | Aug. 6–21, 1979 | >1000 | 150 | Lee *et al.* (1979a) |
| | | 5.9 | Stations from Univ. of California and 2 others | Aug. 6–16, 1979 | — | 31 | Uhrhammer (1980a) |
| Oct. 15, 1979 | Imperial Valley, Mexico–California border | 6.6 | Data from Southern California Seismic Network | First 20 days after the main shock | — | >2000 | Johnson and Hutton (1981) |
| Jan. 24, 1980 | Livermore, California | 5.9 | Data from USGS Central California Microearthquake Network and 4 portable seismographs | Jan. 24–Feb. 26, 1980 | — | ~600 | Cockerham *et al.* (1980) |

TABLE VI. Examples of Microearthquake Studies of Nuclear Explosions

| Nuclear explosion | | | | | Number of microearthquakes | | |
|---|---|---|---|---|---|---|---|
| Date | Name | Size (megaton) | Field observation | Time period | Observed | Located | Reference |
| Jan. 19, 1968 | Faultless | < 1 | A small tripartite array 10 km SW of ground zero | Mar. 9–15, 1968 | 28 | 27 | Boucher *et al.* (1969) |
| Apr. 26, 1968 | Boxcar | ~ 1 | A small tripartite array 14 km SSE of ground zero | Apr. 22–Jun. 3, 1968 | ~2000 | ~ 100 | Ryall and Savage (1969) |
| Dec. 19, 1968 | Benham | 1.1 | 20 portable and 7 telemetered stations within 32 km of ground zero installed 12 days prior to shot | 70 days | 3836 | ~600 | Hamilton and Healy (1969); Hamilton *et al.* (1971); Stauder (1971) |
| Sep. 16, 1969 | Jorum | ~ 1 | 10 portable and 14 telemetered stations within 32 km of ground zero | 20 days | 278 | ~250 | Hamilton *et al.* (1971) |
| Mar. 26, 1970 | Handley | > 1 | 11 portable and 14 telemetered stations within 32 km of ground zero | 60 days | 719 | ~500 | Hamilton *et al.* (1971) |

**TABLE VII. Examples of Microearthquake Studies of Mine Tremors**

| Geographic location | Field observation | Time period | Number of microearthquakes | | Reference |
|---|---|---|---|---|---|
| | | | Observed | Located | |
| East Rand Proprietary Mines, Johannesburg, S. Africa | 6 telemetered stations within 3 km of the foci | Jul. 7–Aug. 1, 1950 | 146 | 100 | Gane *et al.* (1952) |
| | 8 cabled stations within 1 km of the foci | Jan. 13–Jun. 30, 1961 | ~1000 | 187 | Cook (1963) |
| | 10 cabled stations within 1.5 km of the foci | Jun. 20–Sep. 30, 1972 | 450 | 441 | McGarr and Wiebols (1977) |
| | 10 cabled stations within 1.5 km of the foci | Oct. 16–Dec. 4, 1972; Feb. 13–Mar. 31, 1973 | ~500 | ~200 | McGarr *et al.* (1975) |
| | 6 close-in stations within 150 m of the foci | Mar. 1973 | ~300 | | McGarr and Green (1978) |
| Columbia and Geneva Coal Mines, Utah | 3 high-gain portables and 1 tripartite array | Jul. 23–Aug. 26, 1970 | | 272 | Smith *et al.* (1974) |
| Wappingers Falls Quarry, New York | 5 high-gain portables within 3 km of the quarry | Jun. 8–13, 1974 | >100 | 42 | Pomeroy *et al.* (1976) |
| Grangesberg Iron Ore Mine, Sweden | Swedish Seismograph Network and a 3-dimensional geophone array around the mine | Aug. 1974–Jun. 1978 | 505 | — | Bath (1979) |
| Star Mine, Burke, Idaho | 21 geophones on 5 levels of the mine | 1975 | — | — | Brady and Leighton (1977) |
| Ruhr coal mining district, Germany | 3 arrays, each with 5 cabled stations within 3 km of the foci | Dec. 1, 1978–Jun. 6, 1979 | ~200 | 73 | Casten and Cete (1980) |

TABLE VIII. Examples of Microearthquake Studies of Reservoirs

| Impounding year | Reservoir | Location | Field observation | Time period | Seismicity | Reference |
|---|---|---|---|---|---|---|
| 1935 | Lake Mead | Arizona | Up to 4 stations, about 80 km apart | 1938–1944 | ~4000 events observed and ~400 located | Carder (1945) |
| | | | Up to 4 stations, about 80 km apart | 1938–1949, 1950–1952, 1966 | ~300 events per year observed | Carder (1970) |
| | | | 9 telemetered stations, ~20 km apart | Jul. 10, 1972–Dec. 5, 1973 | 678 events located | Rogers and Lee (1976) |
| 1938 | Flathead Lake | Montana | Temporary and regional stations | Apr. 1969–Apr. 1971 | 54 events located | Dunphy (1972) |
| | | | 9 telemetered stations, about 20 km apart | Oct. 13–Nov. 27, 1971 | 259 events located | Stevenson (1976) |
| 1950 | Anderson | California | Data from USGS Central Calif. Microearthquake Network | Jan. 1969–Sep. 1973 | ~500 events located | Bufe (1976) |
| 1952 | Clark Hill | South Carolina | Up to 5 smoked paper portable seismographs | 1974–1975 | >1000 events observed | Talwani (1976) |
| 1958 | Kariba | Zambia | 3 stations, about 150 km apart, plus regional stations | 1959–1971 | ~2000 events observed and ~500 located | Archer and Allen (1969, 1972); Gough and Gough (1970) |
| 1959 | Hsinfengkiang | Kwangtung, China | 4 stations about 10 km apart | Jul. 1971–Dec. 1972 | 258,247 events observed and 25,513 located | Shen *et al.* (1974) |
| | | | 9 smoked paper portable seismographs added, Jan.–Mar. 1972 | | Fault-plane studies | Anonymous (1974) |
| | | | | | Fault-plane and $V_p/V_s$ studies | Wang *et al.* (1976) |
| 1960 | Kurobe | Honshu, Japan | 1 high-gain station at dam site | May 1963–Apr. 1970 | 1182 events with S–P ≤ 1 sec | Hagiwara and Ohtake (1972) |

*(continued)*

TABLE VIII (*Continued*)

| Impounding year | Reservoir | Location | Field observation | Time period | Seismicity | Reference |
|---|---|---|---|---|---|---|
| 1962 | Koyna (Shivajisagar) | India | 4 stations about 50 km apart plus later additions and POO station about 100 km away | Oct. 1963–Dec. 1973 | ~25,000 events observed and ~3000 located | Guha *et al.* (1971, 1974) |
| 1965 | Kremasta | Greece | Regional network of 4 stations, nearest 115 km | Sep. 1965–Nov. 1966 | ~2300 events observed and 161 located | Comninakis *et al.* (1968) |
| | | | 1 mobile station added | Nov. 1–6, 1966 | 54 events located | Steinwachs (1971) |
| 1967 | Mangla | Pakistan | 3 stations about 15 km apart | Jan. 1966–Nov. 1968 | ~60 events observed | Adams and Ahmed (1969) |
| | | | | Jan. 1966–Mar. 1973 | ~150 events observed | Brown (1974) |
| 1967 | Nurek | Tadzhik SSR, USSR | 13 stations about 30 km apart | Since 1955 | Increased seismicity after major filling in 1972, then returned to normal | Soboleva and Mamadaliev (1976) |
| 1968 | Lake Benmore | South Island, New Zealand | New Zealand Seismic Network plus preliminary micro-earthquake survey | 1956–1972 | Minor increase of seismicity | Adams (1974) |
| 1968 | Lake Keowee | South Carolina | Up to 16 stations about 5 km apart | Jan.–Mar. 1978 | ~100 events located | Talwani *et al.* (1979) |
| 1969 | Nagawado | Honshu, Japan | 1 high-gain 3-comp. station | Mar. 1970–Mar. 1973 | 534 events with S–P < 4 sec | Anonymous (1975) |

| | | | | | | |
|---|---|---|---|---|---|---|
| 1971 | Talbingo | Australia | 3 temporary stations plus up to 5 telemetered stations | 1969–1972 | Minor increase of seismicity | Timmel and Simpson (1973) |
| 1971 | Schlegeis | Austria | Up to 2 stations near dam site | May 1971–May 1973 | 176 events observed | Blum and Fuchs (1974) |
| | | | 6 temporary stations deployed Mar. 25–Apr. 30, 1974 | 1971–1977 | 550 events observed and 30 events located | Blum *et al.* (1977) |
| 1972 | Gordon–Pedder | Tasmania | 2 telemetered stations | 1972–1978 | Seismicity increased with water load | Shirley (1980) |
| 1973 | McNaughton | Canada | 8 telemetered stations about 40 km apart | 1972–1974 | Swarms observed before and after filling; no seismicity change during loading | Ellis *et al.* (1976) |
| 1973 | Emosson | Switzerland | 4 telemetered ink portable stations | 1974–1977 | No seismicity change during loading | Bock (1978) |
| 1974 | Ramganga | India | Seismic Observatory near dam site plus 1 temporary station | Jul. 16–Sep. 19, 1975 | No seismicity change during loading | Singh *et al.* (1976) |
| 1974 | Lake Jocassee | South Carolina | Up to 7 smoked paper portable seismographs | Nov. 8, 1975–May 31, 1976 | >1000 events observed and >300 located | Talwani (1977) |
| 1975 | Manic 3 | Quebec, Canada | 1 telemetered station, 3 portable seismographs, and 1 telemetered array of 6 elements | Dec. 1974–Aug. 1977 | >1000 events observed and >72 located | Leblanc and Anglin (1978) |
| 1975 | Toktogul | Kirgizia, USSR | Portable seismographs and 7 telemetered stations to augment existing stations | 1965–1979 | Initial filling produced two bursts of seismicity | Simpson *et al.* (1981) |

# 8. Applications for Earthquake Prediction

Theories of earthquake processes developed within the framework of plate tectonics serve to explain seismicity on a global scale. But at present they do not allow estimates of location, time, and magnitude precise enough to be applied to short-term earthquake prediction. If damaging earthquakes are the result of episodic stress accumulation and subsequent strain release, a means to monitor the changing stress field on a more precise scale must be found. Microearthquake networks can play an important role in earthquake prediction research because they can provide some information on changes in the local stress field. However, data from microearthquake networks probably are not sufficient to predict earthquakes, and other types of data (e.g., geodetic, tilt, strain, geochemical) may be needed as well. In this chapter we summarize a few examples from the very extensive literature on seismic precursors to earthquakes. Readers may refer to Rikitake (1976, 1979) for a more complete review on the classification and use of earthquake precursors.

First we will discuss some methods and results in searching for temporal and spatial seismicity patterns. These methods involve examination of an earthquake catalog that covers a specific area for a given period of time. Although the results from these studies can suggest the future time, place, or magnitude of a large earthquake, they are generally useful only for long-term prediction. An exception to this is the possibility of identifying probable foreshocks as they are occurring, and of tracking the seismicity pattern as the forthcoming large earthquake approaches.

More detailed studies of the behavior of earthquakes in a relatively small region have suggested that temporal changes of certain parameters relating to the earthquake mechanism or to the surrounding rock medium might have occurred. Velocity anomalies were among the earliest predictors specifically examined and reported. Many enthusiastic claims were

made for their potential usefulness, but their success in predicting earthquakes has been rather limited. Because of the extensive literature on this subject and the impetus these early studies gave to the search for other predictors, we have devoted a section to it. Temporal variations of many other seismic parameters, such as $b$-slopes and focal mechanisms, have also been investigated and will be summarized in a later section.

In this chapter, we discuss earthquake prediction based largely on data from microearthquake networks, although many seismic precursors were identified by using data from regional or global networks. In either case, most precursors were not discovered until after the earthquakes had occurred. One exception is the case for the recent Oaxaca, Mexico, earthquake. An announcement of a forthcoming major earthquake near Oaxaca was published in the scientific literature before its occurrence. By studying seismicity patterns of shallow earthquakes located from teleseismic data, Ohtake *et al.* (1977) identified a seismic gap along the west coast of southern Mexico. This allowed them to estimate the magnitude and the location of an earthquake that would occur in the gap. Because they had no reliable basis for predicting the time of occurrence, they urged that a program including monitoring microearthquake activity be carried out in the Oaxaca region. On the other hand, Garza and Lomnitz (1978) argued on the basis of statistical methods applied to the seismicity data, that the evidence for a seismic gap near Oaxaca was inconclusive. However, Garza and Lomnitz had no doubt that a large earthquake would occur near Oaxaca sooner or later.

Following the suggestion by Ohtake *et al.* (1977), a portable microearthquake array was deployed in the Oaxaca region in early November, 1978 by K. C. McNally and colleagues. A major earthquake ($M_s = 7.8$) occurred within the array on November 29, 1978, as anticipated (Singh *et al.*, 1980). According to McNally, the microearthquake array provided unique data for studying the foreshock–main-shock–aftershock sequence. Readers may refer to articles in *Geofisica Internacional* **17**, *numbers 2 and 3, 1978*, for details.

## 8.1. Seismicity Patterns

At least three problems are involved in the study of seismicity patterns for earthquake prediction. First, can past occurrences of earthquakes be used to predict a large earthquake? Second, can the search for spatial and temporal patterns of seismicity be more systematic and more objective? Can pattern recognition techniques developed in other scientific disciplines be adapted to earthquake prediction research? Are the space–time

patterns that are observed in one region applicable to others? Third, do unusual seismicity patterns occur before large earthquakes, and can they be detected by a microearthquake network? These three problems will be discussed in this section using some examples from the published literature available to us in mid-1980.

### *8.1.1. Concept of Seismic Gaps*

Earthquake occurrence in space and time has been studied for many years. For example, Imamura (1929) found a recurrence interval of 123 years in studying the 600-year earthquake history of the southern part of central Japan. He noted that the last severe earthquake activity had ended 75 years before; he suggested a disastrous event could be expected soon and urged taking advantage of this knowledge "in order to render the occurrence comparatively harmless." Fedotov (1965,1968) and Fedotov *et al.* (1969, 1972) developed the concept of "seismic cycle" from studying the seismicity of the great shallow earthquakes in the Kamchatka–Kuriles–northeast Japan region. They found recurrence intervals of a few hundred years and issued long-term earthquake forecasts as much as 15 years in advance. Independently, a series of papers by Mogi (1968a,b,c, 1969a,b) have documented the regularity of occurrence of the great shallow earthquakes in the northwest portion of the circum-Pacific seismic belt, from Japan to Alaska. The rupture zones of the great shallow earthquakes were delineated by the spatial extent of their aftershock distributions.

Three fundamental observations were made by Fedotov and Mogi. First, great earthquakes occurred quite regularly in space and time. Second, the rupture zones of adjacent great earthquakes did not overlap each other to any extent. Third, the spatial distribution of seismicity for a given time interval was characterized by gaps. These seismic gaps coincided with the rupture zones of great earthquakes that occurred before this time interval. Mogi (1979) defined these as seismic gaps of the first kind. The regularity of occurrence of great earthquakes suggested that seismic gaps would be the likely locations for future great earthquakes. The concept of seismic gaps and the subsequent filling in by great earthquakes and their aftershocks has been studied extensively. In addition to the pioneering work of Fedotov and Mogi, readers may refer to Sykes (1971), Kelleher (1970, 1972), Kelleher *et al.* (1973), Chang *et al.* (1974), Kelleher and Savino (1975), Ohtake *et al.* (1977), McCann *et al.* (1979), and Sykes *et al.* (1980).

Seismic gaps may not always be filled in by the occurrence of a large earthquake and its aftershocks. For example, Lahr *et al.* (1980) suggested that the St. Elias, Alaska, earthquake of February 28, 1979 ($M_S = 7.1$)

only partially filled in a seismic gap that had previously been recognized by Kelleher (1970), and that the unfilled portion of the gap might be a primary site for the occurrence of another large earthquake. The aftershock data used by Lahr and his colleagues were believed to be complete to $M_L = 3.5$.

In some detailed studies of smaller magnitude earthquakes, seismicity in the focal region of a future large earthquake was observed to decrease before the occurrence of the large event. Such a change in seismicity has been considered as a premonitory phenomenon useful for earthquake prediction. Mogi (1979) defined premonitory gaps as seismic gaps of the second kind in order to distinguish them from the seismic gaps of the first kind, which we discussed earlier in this subsection. For example, Mogi (1969a) observed that in many cases seismicity took on a doughnut-shaped pattern. For a period of 20 years or more before the main earthquake, the doughnut hole region became relatively aseismic, while the surrounding region became relatively more seismic. Immediately before the occurrence of the main earthquake, foreshocks would tend to occur in the doughnut hole region where the main shock would eventually take place. Aftershocks would fill in the doughnut hole region, and the entire region would gradually return to a state of broadly distributed seismicity. After many decades, this type of seismicity pattern might repeat itself. Seismic gaps of the second kind have been identified in many different tectonic situations and over a wide range of earthquake magnitudes. Readers may refer, for example, to Mogi (1979) and Wyss and Habermann (1979).

### *8.1.2. Some Examples of Seismicity Patterns*

The concept of seismic gaps has been applied to earthquakes of all magnitudes. We now briefly summarize a few examples of seismicity patterns observed in California, New Zealand, and Japan.

In central California, small-scale regularity in the pattern of strain accumulation and release was demonstrated by Bufe *et al.* (1977) for a 9-km zone on the Calaveras fault from 1963 to 1976. Recurrence intervals between earthquakes of magnitude 3 to 4 in the zone were shown to be dependent on the strain released in the previous large earthquake and in the smaller earthquakes in the interim.

Ishida and Kanamori (1978) studied the seismicity in the region surrounding the San Fernando, California, earthquake of February 9, 1971 ($M_L = 6.4$). The following seismicity patterns were observed around the epicenter of the main shock before its occurrence: (1) earthquakes showed a northeast–southwest alignment 7–10 years before; (2) a seismic gap started to form 3–6 years before, with no earthquakes located within 15

km of the pending main shock epicenter; and (3) seismicity showed a noticeable increase 2 years before.

Ishida and Kanamori (1980) reported similar variations in seismicity before the Kern County, California, earthquake of July 21, 1952 ($M_S = 7.7$). These variations took the general form of quiescence followed by clustering of earthquakes in the immediate vicinity of the forthcoming main shock. They also observed that similar variations occurred in earlier years, but were not followed by large earthquakes. Kanamori (1978a) suggested that additional observations of other features (such as changes in the shape of the seismic waveform or anomalous crustal deformation) might be required to identify those regions that were most likely to produce a large earthquake.

Bakun *et al.* (1980) and Bakun (1980) have studied in detail the relation of recent seismicity to the mapped fault traces along portions of the San Andreas fault system in central California. The locations and directivity of microearthquake sources (Bakun *et al.*, 1978b) associated with a magnitude 4.1 earthquake were found to correlate well with bends and discontinuous offsets in the mapped active strands of the San Andreas fault. These observations were used to extend and refine the model of "stuck" and "creeping" patches of an active fault surface (e.g., Wesson *et al.*, 1973a) and could be explained by Segall and Pollard's (1980) theory of stability for mechanically interacting fault segments in an elastic material. Furthermore, the seismicity patterns associated with this earthquake were similar in many respects to those observed for large earthquakes (e.g., Kelleher and Savino, 1975). Bakun *et al.* (1980) demonstrated that fault geometry played a dominant role in the seismicity patterns associated with relatively small earthquakes and suggested that studies of large earthquakes should include an examination of the details of the fault trace geometry.

Evison (1977) identified a precursory swarm pattern for 11 large earthquakes (3 in California and 8 in New Zealand) ranging in magnitude from 4.9 to 7.1. He divided the precursory pattern into four episodes and extracted from each of the 11 earthquake data sets three parameters that might be diagnostic for long-term earthquake prediction. These episodes were characterized by: (1) a period of normal seismicity; (2) a precursory swarm, with magnitude of the largest event noted as $M_p$; (3) a precursory gap time (the time from the onset of the precursory swarm to the main shock) of length $T_p$; and (4) the main shock with magnitude $M_m$. Evison showed that regression relations between $M_m$ and $M_p$, and $\log_{10} T_p$ and $M_p$ could be used to estimate the magnitude and the precursor time of the forthcoming main shock.

Sekiya (1977) identified similar precursory swarm patterns preceding 11 earthquakes in Japan, ranging in magnitude from 4.1 to 7.9. The relation

between earthquake magnitude $M$ and precursor time $T$ generally agreed with those found by other investigators using other precursory phenomena.

Yamashina and Inoue (1979) studied the seismicity patterns preceding a shallow earthquake of magnitude 6.1 that occurred on June 3, 1978, in southwest Japan. They traced the development of a circular gap, about 5 km in diameter, starting 6 months before the main shock. However, they did not observe an increase in seismicity within the gap before the occurrence of the earthquake.

These results show that for some tectonic environments great shallow earthquakes are repetitive in time, and that the seismicity preceding them has some identifiable patterns. More importantly, it appears that similar seismicity patterns can be identified for earthquakes of all magnitudes. This raises the possibility that the long-term seismicity of a region could be estimated from the short-term seismicity which is easier to obtain. In other words, how is the short-term seismicity related to the long-term?

Although many short-term microearthquake surveys have been made throughout the world (see Section 7.2 for a summary), this question does not seem to have a simple answer. For instance, a microearthquake survey by Brune and Allen (1967) suggested that there might be an inverse correlation between short-term microseismicity and long-term seismicity in some places along the San Andreas fault in southern California. They found that the microseismicity at the time of the survey was at a low level along the portion of the San Andreas fault that broke in the 1857 earthquake. Results from the USGS Central California Microearthquake Network were similar: microseismicity along the portion of the San Andreas fault that broke in 1906 was also low. On the other hand, Ben-Menahem *et al.* (1977) studied the seismicity of the Dead Sea region by combining data from a 2000-year historical record, from a few decades of macroseismic data and instrumental recordings, and from a 5-month microearthquake survey. They reported that all these sources of data were consistent with a $b$-slope value of 0.86.

Although the microseismicity recorded over a few years may be similar to the seismicity recorded over a longer period of time (e.g., Asada, 1957; Rikitake, 1976), one would not rely too heavily on short-term microseismicity data for earthquake prediction purposes. One would always like to work with the longest possible earthquake history in order to avoid seismicity fluctuations that may not be significant.

### *8.1.3. Pattern Recognition Techniques*

In recent years pattern recognition techniques have been developed and applied to data from earthquake catalogs. The goal has been to identify

diagnostic features in the seismicity of an area that will be reliable predictors of future earthquakes, either in time or in space. Computer algorithms are formally defined and used to make an objective search of the data set for the occurrence of specific patterns. When pattern recognition techniques were first adapted to the seismicity problem in the 1960s and early 1970s, the only catalog data available were those for the larger, regional earthquake networks. This restricted the studies to events of magnitude 4 and greater. More recently, catalogs from microearthquake networks have become available, and pattern recognition techniques have been applied to these data as well. Pattern recognition techniques can be divided into two classes, and are summarized briefly.

In the first technique, temporal variations of seismicity over a region are characterized by a few, simple time-series functions. Precursory features of these functions are identified, and then the functions are tested on other data sets. The definition and development of such functions is discussed, for example, by Keilis-Borok and Malinovskaya (1964) and Keilis-Borok *et al.* (1980a). Three time-series functions have been formally defined and studied. Briefly, these are referred to as pattern B (bursts of aftershocks), pattern S (swarms of activity), and pattern $\Sigma$ (cumulative energy).

Pattern B is said to occur when an earthquake has an abnormally large number of aftershocks concentrated at the beginning of its aftershock sequence. The occurrence of pattern B was found to precede strong earthquakes in southern California, New Zealand, and Italy (Keilis-Borok *et al.*, 1980a).

Pattern S is said to occur when a group of earthquakes, concentrated in space and time, happens at a time when the seismicity of the region is above normal. This pattern may be considered as a variation of pattern B, although it is computed over a much longer time window. Keilis-Borok *et al.* (1980a) reported that in southern California all earthquakes predicted by pattern B were also predicted by pattern S: there were seven successful predictions, one failure to predict, and one false prediction.

Pattern $\Sigma$ is said to occur when the sum of the earthquake energies, raised to a power less than 1 and computed using a sliding time window, exceeds a threshold value for that region. The summation is carried out for earthquakes with magnitude less than the magnitude of the earthquake to be predicted. The success of pattern $\Sigma$ as a predictor depends critically on the choice of the threshold level and on the consistency with which earthquake magnitudes are calculated. Pattern $\Sigma$ has had some success as a predictor in California, New Zealand, and the region of Tibet and the Himalayas (Keilis-Borok *et al.*, 1980a,b).

These patterns (B, S, and $\Sigma$) are computed from seismicity over a broad region and are not capable of defining the focal region of a predicted event.

Keilis-Borok *et al.* (1980b) suggested that these patterns should be used primarily to "stimulate the search for medium- and short-term precursors in the region, and to search for similar long-term precursors elsewhere."

Application of the S pattern recognition technique to microearthquake data from the Lake Jocassee area, South Carolina, was reported by Sauber and Talwani (1980). They used events ranging in magnitude from −0.6 to 2.0 to predict events of magnitude between 2.0 and 2.6. A modified form of the Keilis-Borok algorithm was used. Of eight alarms given by the algorithm, five were successful predictions, and three were false predictions; two events were not predicted.

This first pattern recognition technique suggests that precursory seismic activity may precede some earthquakes. But the development of algorithms to detect these precursors and the compilation of a complete (to some cutoff magnitude) and accurate earthquake catalog are difficult to accomplish in practice.

The second technique of pattern recognition attempts to correlate the seismicity of a region with its geomorphological characteristics. These characteristics can include detailed knowledge of structural lineaments and their intersections, topographic elevation and relief, fault length, type, and density, relative area of sedimentary cover, and so on. The methods of preparing the seismicity and geomorphological data for input to the computer, and the computer algorithms themselves, are highly formalized (see, e.g., Gelfand *et al.*, 1976).

The object of this technique is to characterize the geomorphological settings where large earthquakes have occurred in the past and can be expected to occur again. It should also identify geomorphological settings where large earthquakes have not occurred in the past and should not be expected in the future. The time of occurrence of a predicted event cannot be determined. In a sense, this technique complements the first one described previously, in which the area of the predicted occurrence is not well determined, but the predicted time of occurrence can be approximated roughly.

Gelfand *et al.* (1976) applied spatial pattern recognition procedures to earthquakes in California. Depending on which geomorphological features were being examined, the results met with varying degrees of success. Generally, areas of potentially dangerous earthquakes ("D" areas) were characterized by proximity to the ends of intersections of major faults and by relatively low elevation or subsidence against a background of weaker uplift. By contrast, nondangerous areas ("N" areas) were characterized by higher elevations or stronger uplift, but less contrast in topographic relief. Their general result suggests that dangerous earthquakes occur at identifiable places along faults, and not at arbitrary locations. This implies

that faults have special properties that act to initiate or retard rupture. As discussed in Section 8.1.1, Bakun (1980) has found good correspondence in central California between mapped bends and breaks in fault traces and the spatial occurrence of small earthquakes and microearthquakes.

Examples of other areas studied on the basis of geomorphological characteristics include central Asia (Gelfand *et al.*, 1972), China (Xiao and Li, 1979), and Italy (Caputo *et al.*, 1980).

### *8.1.4. Foreshock Activity*

How to identify foreshocks within the general seismicity pattern of a region is a challenging problem. Nearly all previous identifications of foreshocks were not made until after the occurrence of the main shocks. If foreshock activity is to be used as a premonitory indicator, it must be identified before the main shock occurs.

The works of Fedotov, Mogi, Kelleher, Sykes, and others cited previously have laid a foundation for interpreting foreshock activity within the framework of seismic gaps. They studied large earthquakes that occurred infrequently and were recorded throughout the world, and whose major foreshocks could be recorded by standard regional stations. Better understanding of the characteristics of foreshock activity, especially in predicting earthquakes of smaller magnitudes, will require finer resolution of seismicity which could only be provided by microearthquake networks.

In reporting on foreshocks of a minor earthquake, Hagiwara *et al.* (1963) noted that they accidentally recorded several "micro-foreshocks" because they happened to be in the epicentral region carrying out microearthquake observations for other purposes. They suggested that many foreshocks might be undetected by standard regional stations but could be recorded by the higher sensitivity stations of a microearthquake network.

Wesson and Ellsworth (1973) studied seismicity patterns in the years preceding moderate to large earthquakes in California, such as Kern County (1952), Watsonville (1963), Corralitos (1964), Parkfield (1966), Borrego Mountain (1968), Santa Rosa (1969), San Fernando (1971), and Bear Valley (1972). They found that seismicity was higher than usual in the focal regions of these earthquakes before their occurrence. In particular, hypocenters of microearthquakes were observed to concentrate near the focal region of the Bear Valley earthquake starting a few months before its occurrence. Such detailed observations were possible because of a dense station coverage by a microearthquake network operating there. Similarly, Wu *et al.* (1976) reported 527 foreshocks recorded at a close-in station 20 km from the epicenter of the Haicheng earthquake of February 4, 1975 ($M_S = 7.3$). These foreshocks occurred within four days

of the main shock, and their epicenters were concentrated spatially.

Wyss *et al.* (1978) examined the seismicity before four large earthquakes (Kamchatka, USSR; Friuli, Italy; Assam, India; and Kalapana, Hawaii). On the basis of this, as well as results reported by other investigators, they concluded that systematic patterns observed in foreshock seismicity were similar for earthquakes throughout the world. They also suggested that some "precursory cluster events" appeared to have radiation properties different from the background earthquakes (see Section 8.3.3).

Utsu (1978) attempted to discriminate foreshock sequences from swarms on the basis of magnitude statistics as follows. Let $M_1$, $M_2$, and $M_3$ be the magnitudes of the largest, second largest, and third largest events in a foreshock sequence or a swarm. He selected 245 shallow swarms or foreshock sequences in Japan using the following criteria: (1) $M_1 - M_2 \leq 0.6$, and $M_1 \geq 5.0$ for the period 1926–1964; and (2) $M_1 - M_2 \leq 0.6$, and $M_1 \geq 4.5$ for the period 1965–1977. From this data set, Utsu was able to identify 77% of the foreshock sequences (10 out of 13) if he stipulated the following conditions: (1) $0.4 \leq M_1 - M_2 \leq 0.6$; (2) $M_1 - M_3 \geq 0.7$; and (3) $M_2$ precedes $M_3$ in time. He would have mistaken 7% of the swarms (17 out of 232) as foreshock sequences.

Jones and Molnar (1979) summarized the characteristics of foreshocks associated with major earthquakes throughout the world. Their primary data sources were issues of the International Seismological Summary and bulletins of the International Seismological Center. They observed that foreshock seismicity was often characterized by a pattern of increases and decreases, accompanied by changes in its geographic location relative to the forthcoming main shock epicenter and aftershock zone. The number of foreshocks per day appeared to increase as the time to the main shock approached. This relationship seemed to be independent of the main shock magnitude. The magnitude of the largest foreshock did not appear to be related to the magnitude of the main shock. Extension of the work by Jones and Molnar to lower magnitude earthquakes should be possible as more earthquake catalogs are produced from microearthquake networks.

Kodama and Bufe (1979) studied foreshock occurrence for 29 earthquakes of magnitude 3.5 or greater located along the San Andreas fault in central California. Only 10 of the 29 earthquakes appeared to have foreshocks. The foreshock pattern often was one of an increase of activity, a period of quiescence, and then more foreshocks within 24 hr of the main shock. The time interval between the start of the seismicity increase and the occurrence of the main shock was found to be weakly dependent on the main shock magnitude.

## 8.2. Temporal Variations of Seismic Velocity

Compressional wave velocity ($V_p$) and shear wave velocity ($V_s$) may be determined from the P-wave arrival time ($t_p$) and the S-wave arrival time ($t_s$) either as a ratio ($V_p/V_s$) or individually. The velocity ratio is determined traditionally by the Wadati method (Wadati, 1933). In this method, the observed P-arrival time ($t_p$) is plotted as the abscissa and the observed S–P interval time ($t_s - t_p$) is plotted as the ordinate for a set of arrival time data from an earthquake. Such a graph is known as a Wadati diagram. If Poisson's ratio is constant along the travel path, then the P-wave and the S-wave travel paths will be identical. Under this assumption, the graph of ($t_s - t_p$) versus $t_p$ is a straight line and its slope is $(V_p/V_s) - 1$ (Kisslinger and Engdahl, 1973). For a set of earthquakes, a Wadati diagram may be constructed and a least squares line may be fitted to the data for each earthquake. From the slopes of these fitted lines, we obtain $V_p/V_s$ as a function of time. Thus, temporal variation of seismic velocity ratios may be examined.

In addition to the Wadati method, changes in P-wave velocity or S-wave velocity may be examined by the following two methods. In practice, there are many refinements. In the first method, the epicentral coordinates of the earthquake must be known. Dividing the difference in epicentral distance by the difference in arrival time between two stations gives an apparent velocity (either $V_p$ or $V_s$) between the two stations. Depending on the variation of velocity along the travel path, the apparent velocity may not always represent the actual velocity within the earth. But it is a change in this apparent velocity that is of interest here. The second method generally uses regional or teleseismic P-arrival times to compute a P-wave residual. The P-residual is simply the difference between the observed P-arrival time and the arrival time computed on the basis of a given earth model or a given travel time table. A refinement of this method is to determine relative P-residuals by computing the differences in residuals relative to a fixed station within or near the area of interest. Temporal variation in P-residuals (or S-residuals) may reflect temporal variation in $V_p$ (or $V_s$) near the stations. Following Rikitake (1976), the first method will be referred to as the $V_p$ (or $V_s$) anomaly method, and the second method as the P-residual method.

According to Rikitake (1976), investigating temporal changes in seismic velocity as a premonitory phenomenon in earthquake prediction was first attempted by Hayakawa (1950), and his results were negative. In the 1950s, a seismic network was established at Garm, USSR, for earthquake prediction research (Riznichenko, 1975). In the early 1960s, specific results concerning velocity changes as a diagnostic precursor to earthquake

occurrence in the Garm region were published. The paper by Kondratenko and Nersesov (1962) often is cited as being the first to report a positive correlation between temporal changes in the velocity ratio $V_p/V_s$ and the later occurrence of a significant earthquake. From the early 1960s until the late 1970s, reports on changes in velocity or velocity ratio increased dramatically. In addition to those in the USSR, premonitory velocity anomalies for some earthquakes in China, Japan, the United States, and other places were also reported. Readers may refer to Rikitake (1976) for a general review.

In this section, we summarize both the positive and negative results in the search for precursory velocity anomalies, and discuss a few of the problems that should be considered before relating a temporal velocity anomaly to the future occurrence of an earthquake.

### *8.2.1. Investigations of Velocity Anomalies*

Table IX summarizes some examples of investigations in which $V_p/V_s$ or P-residual anomalies have been reported. It is apparent that the inferred velocity changes are quite small, regardless of the magnitude of the targeted earthquakes. In this table, many of the figures given for precursor times and sizes of velocity changes are estimated from illustrations in the original papers, as some authors do not specifically list these data. Others may obtain slightly different results.

Table X summarizes some examples of investigations reporting negative results in the search for precursory velocity anomalies. Most negative results reported are from California along the San Andreas fault system. The reason may be the predominantly strike-slip focal mechanisms and relatively shallow focal depths.

Temporal variations of velocity have also been investigated by techniques other than the Wadati method or P-residual method. For example, McNally and McEvilly (1977) studied the first P-motions for a set of 400 earthquakes along the San Andreas fault in central California. They found that the inconsistencies in first P-motions could be explained by lateral refraction of the P-waves along the higher velocity material southwest of the fault zone from earthquakes located to the northeast. Velocity contrast across the fault could be determined by geometrical interpretation of the laterally refracted wave path. McNally and McEvilly suggested that a closely spaced array of seismometers normal to the fault should be capable of monitoring stress-related velocity changes within the earthquake source region.

As another example, Fitch and Rynn (1976) described an inversion method in which localized volumes of anomalously low seismic velocity

**TABLE IX. Examples of Investigations Searching for Velocity Anomalies with Positive Results**

| Earthquake | | | Anomaly | | Data | | |
|---|---|---|---|---|---|---|---|
| Region | Date | Magnitude | Precursor time | Max. size | Source | Analysis method | Reference |
| California (central) | | | | | | | |
| Bear Valley | 2/24/72 | 5.0 | 2 months | 0.3 sec | Local events | P-residual | Robinson *et al.* (1974) |
| Stone Canyon | 9/4/72 | 4.6 | 2 months | 25% increase | Local events | Variation of mean focal depth | Bufe *et al.* (1974) |
| California (north) | | | | | | | |
| Oroville | 8/1/75 | 5.7 | ~3 years | 0.1-sec delay | Novaya Zemlya explosions | Relative P-residual | Cramer *et al.* (1977) |
| California (south) | | | | | | | |
| Newhall | 4/76 | 4.7 | | | Quarry blasts | Smoothed $V_p/V_s$, and $V_p$ | Whitcomb (1977) |
| San Fernando | 2/9/71 | 6.4 | 3.5 years | −10% | Local events | $V_p/V_s$ | Whitcomb *et al.* (1973) |
| | | | | −19% | Local events | P-residual | |
| Pt. Mugu | 2/21/73 | 6.0 | 180 days | 0.5–1.0 sec | Teleseisms | P-delay, and $V_p$ from 2 station time differences | G. S. Stewart (1973) |
| | | | 380 days | −20% | Local events | | |
| New York | | | | | | | |
| Blue Mtn. Lake | 6/20/71 | 3.1 | 6 days | −9% | Local events | $V_p/V_s$ | Scholz *et al.* (1973b) |
| | 7/10/71 | 3.3 | 6 days | −14% | Local events | $V_p/V_s$ | Aggarwal *et al.* (1973) |
| | 7/27/71 | 2.5 | 3.5 days | −11% | Local events | $V_p/V_s$ | |
| | 8/3/73 | 2.6 | 4 days | −15% | Local events | $T_s/T_p$ | Aggarwal *et al.* (1975) |
| South Carolina | | | | | | | |
| Lake Jocassee | 1/13/76 | 2.5 | 17 days | −16% | Local events | $T_s/T_p$ | Stevenson (1977) |
| | 2/23/77 | 2.3 | 14 days | −16% | Local events | $T_s/T_p$ | Talwani *et al.* (1977) |
| | 11/25/77 | 2.2 | 13 days | −17% | Local events | $T_s/T_p$ | Talwani *et al.* (1978) |
| Monticello Reservoir | 8/27/78 | 2.5 | 15 days | −6% | Local events | $T_s/T_p$ | Rastogi and Talwani (1980) |
| | 9/15/78 | 2.3 | 15 days | −12% | Local events | $T_s/T_p$ | Rastogi and Talwani (1980) |
| Alaska | | | | | | | |
| Adak Is. | 2/22/76 | 5.0 | 4–5 weeks | 0.2 sec | Local events | P-delay (and other factors) | Engdahl and Kisslinger (1977) |
| Windy Is. | 9/28/71 | 3.8 | 50 days | −5% | Local events | $V_p/V_s$ | Kisslinger and Engdahl (1974) |
| Hawaii | | | | | | | |
| Kalapana | 11/20/75 | 7.2 | 3.5 years | 0.2 sec | Teleseisms | P-delay | Johnston (1978) |
| China | | | | | | | |
| Hsinfengkiang, | 3/19/62 | 6.1 | 11 months | −11% | Local events | $V_p/V_s$ | Feng (1977) |

| | | | | | | | |
|---|---|---|---|---|---|---|---|
| Kwantung Prov. | | | | | | | |
| Yongshan-Daguan | 5/11/74 | 7.1 | 8 years and 5 months | −11% | Local events | $V_p/V_s$ | Feng (1975) |
| Haicheng | 2/4/75 | 7.3 | 4 years | −10% | 147 local events | $V_p/V_s$ | Feng *et al.* (1976) |
| Songpan-Pingwu | 8/16/76 | 7.2 | | | Local events | $V_p/V_s$ | Feng *et al.* (1980) |
| Iran | | | | | | | |
| Teheran | 11/21/74 | 2.1 | 1 day | −16% | Local events | Wadati $V_p/V_s$ | Hedayati *et al.* (1978) |
| | to | 2.4 | 2 days | | | | |
| | 12/13/74 | 2.8 | 3 days | | | | |
| Japan | | | | | | | |
| North Miyagi | 4/30/62 | 6.5 | 1 year | −70% | Local and regional events | $T_s/T_p$ | Ohtake (1973) |
| North Nagano | 9/21/68 | 5.3 | 3–4 months | −33% | Local and regional events | $T_s/T_p$ | Ohtake (1973) |
| Chugoku-Kinki | 1967 | 5.0 | 50 days | −9% | Local events | $V_p/V_s$ | Brown (1973); Rikitake (1976) |
| | 1968 | 5.0 | 52 days | −7% | Local events | $V_p/V_s$ | |
| Matsushiro | 1965–1967 | Swarms | 2.5–3.5 years | −0.4 sec | Teleseisms | P-residuals | Wyss and Holcomb (1973) |
| SE Akita | 10/16/70 | 6.2 | 2 years | −16% | Local events | $T_s/T_p$ | Hasegawa *et al.* (1975) |
| Central Gifu | 9/9/69 | 6.6 | 3 years | ~1 sec | 400 shallow, local events | P-residual | Utsu (1975) |
| Izu-Hanto-oki | 5/9/74 | 6.9 | 9 years | ~1 sec | | | |
| Izu-Hanto-oki | 5/9/74 | 6.9 | 10 years | −1.5 sec | Local events | P-residual, single station | Ohtake (1976) |
| Off Izu peninsula | 5/9/74 | 6.9 | 11 years | −5% | Local events | $V_p/V_s$ | Sekiya (1977) |
| New Zealand | | | | | | | |
| Gisborne | 3/4/66 | 6.2 | 480 days | 0.5 sec | Teleseisms 1964–1968 | P-residual | Sutton (1974) |
| Gisborne | 3/4/66 | 6.2 | 550 days | 0.4 sec | Teleseisms | P-residual | Wyss and Johnston (1974) |
| Seddon | 4/23/66 | 6.1 | 360 days | 0.4 sec | Teleseisms | P-residual | |
| Gisborne | 3/4/66 | 6.2 | 1.6 years | −19% | Local events | $V_p/V_s$ to single station | Evison (1975) |
| Seddon | 4/23/66 | 6.0 | 1.4 years | −7% | Local events | | |
| Inangahua | 5/23/68 | 7.1 | 3 years | −17% | Local events | | |
| Arthur's Pass | 3/3/72 | 3.5 | 10 days | 7% | Local events | $T_s/T_p$ | Rynn and Scholz (1978) |
| USSR | | | | | | | |
| Garm | 1956 | 5.5 | 3 months | −6% | Local events | $T_s/T_p$ | Semenov (1969) |
| | 1956 | 4.8 | 2 months | −6% | | | |
| | 1957 | 4.1 | 1 month | −6% | | | |
| | 1959 | 5.5 | 2¼ months | −5% | | | |
| | 1960 | 4.1 | 1¼ months | −5% | | | |
| | 1961 | 4.8 | 1 month | −7% | | | |
| | 1962 | 4.5 | 1½ months | −4% | | | |
| | 1962 | 4.5 | 1¼ months | −6% | | | |
| | 1963 | 4.1 | 1 month | −10% | | | |
| | 1963 | 4.8 | 1¼ months | −5% | | | |
| | 1964 | 4.1 | ¾ month | −7% | | | |
| | 1966 | 5.5 | 2¾ months | −7% | | | |
| | 1967 | 4.8 | 1 month | −5% | | | |
| Garm | 3/22/69 | 5.7 | 1.2 years | 0.4 sec | Teleseisms | P-residual | Wyss (1975) |

**TABLE X. Examples of Investigations Searching for Velocity Anomalies with Negative Results**

| Region | Date | Magnitude | Seismic receivers | Seismic source | Analysis method | Reference |
|---|---|---|---|---|---|---|
| California (central) | | | | | | |
| San Andreas fault | 10/69–11/74 | | USGS Network | 8 Novaya Zemlya explosions | P-residual | Robinson and Iyer (1976) |
| Bear Valley | 2/24/72 | 5.0 | USGS Network | Local earthquakes | P-residual | Steppe *et al.* (1977) |
| | 9/4/72 | 4.6 | | | | |
| | 1/15/73 | 4.1 | | | | |
| Bear Valley | 8/74–5/75 | 2.9–3.3 | 51 field instruments | 17 explosive charges (250 kg) | Cross-correlation | Peake *et al.* (1977) |
| San Andreas fault | 7/61–6/73 | 4.5–5.4 | UCB Network | 70 Quarry blasts | $T_s$, $T_P$, $T_s/T_p$ | McEvilly and Johnson (1973, 1974) |
| San Andreas fault | 1/71–12/72 | | UCB Network | Tonga Islands teleseisms | 2-station relative P-residual | Cramer and Kovach (1974) |
| | 2/24/72 | 5.1 | | | | |
| | 10/3/72 | 4.9 | | | | |
| Hollister | 5/74–12/74 | | 30 stns. of USGS Network | Circum-Pacific teleseisms | 2-station relative P-residual | Cramer (1976) |
| | 11/28/74 | 5.1 | | | | |
| Bear Valley | 12/71–2/73 | | Stone Canyon Observatory | 175 Local earthquakes | $T_s$, $T_p$, $V_p/V_s$ | Bakun *et al.* (1973) |
| | 2/24/72 | 5.0 | | | | |
| | 9/4/72 | 4.6 | | | | |
| | 1/15/73 | 4.2 | | | | |
| Parkfield | 11/65–8/67 | | UCB Network and GHC (USGS) station | Quarries, regionals, teleseisms | $T_p$ difference at station pairs | Boore *et al.* (1975) |
| | 6/28/66 | 5.5 | | | | |
| California (north) | | | | | | |
| Oroville | 12/70–3/76 | | ORV and JAS stations | 46 NTS explosions | $T_p$ difference between ORV–JAS | Bolt (1977b) |
| | 8/1/75 | 5.7 | | | | |
| Oroville | 8/68–3/76 | | ORV, MGL, and KPK stations | NTS explosions | 2-station relative P-residual | Cramer *et al.* (1977) |
| | 8/1/75 | 5.7 | | | | |

| | | | | | | |
|---|---|---|---|---|---|---|
| California (south) | | | | | | |
| Entire area | 1965–1971 | | S. Calif. Seismic Network | Aleutian explosions, Marianas teleseisms | P-residual | Kanamori and Chung (1974) |
| | 1962–1973 | | S. Calif. Seismic Network | Corona, Eagle Mtn. explosions | P-residual | Allen and Helmberger (1973) |
| Borrego Mtn. | 1968 | 6.4 | | | | |
| San Fernando | 1971 | 6.4 | | | | |
| Galway Lake | 6/1/75 | 5.2 | S. Calif. Seismic Network | Quarry blasts | P-residual | Kanamori and Fuis (1976) |
| Goat Mtn. | 11/15/75 | 4.7 | | | | |
| Goat Mtn. | 12/14/75 | 4.7 | | | | |
| Entire area | 1972–1976 | | S. Calif. Seismic Network | Teleseisms | P-residual | Raikes (1978); Whitcomb (1977) |
| Palmdale | 6/74–6/76 | | 4 Hz geophone array | Air gun | P-residual | Leary *et al.* (1979) |
| Utah | | | | | | |
| Wasatch Front | 10/74–3/77 | | Wasatch Front Seismic Network | Mine blasts | P-residual | Gaiser (1977) |
| Washington | | | | | | |
| Centralia | 4/72–5/75 | | W. Washington Seismic Network | Mine explosions | Relative P-residual | Chou and Crosson (1978) |
| Aleutian Is. | | | | | | |
| Adak Canyon | 5/2/71 | 6.8 | 1 Aleutian, and 2 Alaskan stations | Fiji-Tonga deep focus earthquakes | Relative P-residual | Engdahl (1975) |
| Seymour Canyon | 7/71–4/73 | | Amchitka Network | Local events | $V_p/V_s$ (Wadati) | Kisslinger and Engdahl (1974) |
| South Africa | | | | | | |
| Johannesburg | 3/27/73 | $3\frac{3}{4}$ | Underground geophone array | Mine tremors | $V_p$, $V_s$, $V_p/V_s$ | McGarr (1974) |
| Japan | | | | | | |
| Matsushiro, Tsukuba, and Kamikineusu | 2/62–6/73 | | Standard stations | NTS explosions | P-residual | Utsu (1973) |
| Oshima Is. | 1968–1976 | | 10 stns. in S. Kanto district | 500 kg explosions yearly at Oshima Is. | P-residual | Kakimi and Hasegawa (1977) |
| Boso Peninsula | 1971–1973 | | 10 stns. in S. Kanto district | 800 kg explosions yearly, near Tateyama | P-residual | Asano *et al.* (1979) |

could be identified using arrival time data from local earthquakes. They suggested that the inversion method could, in principle, resolve near-source effects, whereas the Wadati method would require the velocity changes to be regional in scale in order to be detected. In general, simultaneous inversion of source and path parameters (as discussed in Section 6.3) could be applied to study temporal velocity changes. However, as pointed out by Aki and Lee (1976), data from more closely spaced stations within a microearthquake network than were presently available would be required.

Finally, sources other than earthquakes or explosives may be used to study temporal velocity changes. For example, vibroseismic and air gun techniques may be applied (e.g., Brandsaeter *et al.*, 1979; Leary *et al.*, 1979; Clymer, 1980).

### *8.2.2. Alternative Interpretations of Velocity Anomalies*

Some reported velocity anomalies might be caused by factors other than stress changes in the vicinity of an impending earthquake. Thus, temporal changes in seismic velocity might not always be indicative of imminent rock failure according to the dilatancy model of earthquake processes, which was proposed by Nur (1972). We now give a few examples of alternative interpretations of velocity anomalies.

Kanamori and Hadley (1975) found small but systematic temporal velocity changes in a study of about 20 quarry blasts in southern California. They suggested that these changes might be due to "minor local effects such as the change in ground water level, changes in the water content in the rocks near the source or the station, etc."

Aftershocks of two moderate earthquakes along the San Andreas fault south of Hollister in central California were studied by Healy and Peake (1975). They used 24 stations that were part of the USGS Central California Microearthquake Network, and 57 temporary stations that were deployed for aftershock studies. Wadati diagrams showed considerable scatter until data points for stations east and west of the fault were plotted separately. The slope obtained from the Wadati diagrams for the westside stations yielded a $V_p/V_s$ ratio of 1.71, and that for the eastside stations of 1.79. On the basis of this and detailed analysis of other arrival time data, they concluded that "large spatial variations in $V_s/V_p$ are probably masking any temporal changes in $V_s/V_p$ that occur in the data."

Lindh *et al.* (1978b) showed that two precursory P-residual anomalies reported for central California earthquakes could also be explained by sampling problems in the original arrival time data. Reanalysis of the seismograms showed that, in some cases, earthquakes used during the anomalous period were of too low a magnitude, hence too emergent to be

read reliably. During the anomalous period, some of the earthquakes used also had shallow focal depths relative to the majority of the earthquakes in the source region.

Along more theoretical lines, a number of authors have studied the problems associated with investigating velocity changes. Three examples are given below.

The effect on the Wadati diagram of a layered medium in which the ratio $V_p/V_s$ differs by a small but reasonable amount from one layer to another was studied by Kisslinger and Engdahl (1973). They found that at distances large compared to the focal depth, the slope obtained from a Wadati diagram was most representative of the $V_p/V_s$ ratio in the deepest layer encountered by the seismic wave. In this case the origin time was no longer given by the intercept on the P-arrival time axis.

Picking S-wave onsets is usually difficult, especially if only vertical-component seismograms are available. Kanasewich *et al.* (1973) computed synthetic seismograms to illustrate the effect that a S- to P-wave conversion near the receiver had in producing an earlier apparent S-arrival. They demonstrated that large errors in picking S-arrivals might occur if only vertical-component seismograms were used. For stations underlaid by sedimentary layers only a few kilometers thick, errors of a few seconds might occur even if horizontal-component seismograms were read. They suggested that misidentification of S-arrivals might be fairly common in practice. In regions with lateral velocity changes, such as across a fault zone, it might be difficult to identify the same arrival phase from station to station because of phase conversions along the travel path.

Crampin (1978) studied the propagation of seismic waves through a medium characterized by systems of parallel cracks. He demonstrated that crack orientation and geometry could play a primary role in producing velocity anomalies and in distinguishing between the various dilatancy models. He suggested that the orientation of the principal stress axes could produce an anisotropic crack system, making some velocity anomalies very difficult to observe. This might explain why velocity anomalies were most often reported in regions with thrust-type focal mechanisms and rarely in regions with strike-slip mechanisms. On the other hand, polarization anomalies for the shear phases should always be observable, and thus might be a reliable means to recognize dilatant episodes (see, also, Crampin and McGonigle, 1981).

## 8.3. Temporal Variations of Other Seismic Parameters

Many other kinds of earthquake precursors have been reported. These include temporal changes in $b$-slope, amplitude or amplitude ratio of cer-

tain seismic waves, seismic wave spectrum, focal depth, and orientation of the principal stress axes. The goal is to find some precursors that can discriminate between background earthquakes and foreshock activity. Although some earlier studies used data from regional networks, they have produced encouraging results and have suggested directions for more detailed investigations. Thus, a major reason to establish a microearthquake network is to provide the necessary data for studying earthquake precursors.

### *8.3.1. Changes in b-Slope*

As discussed in Section 1.1.2, the frequency of earthquakes as a function of magnitude may be represented by the Gutenberg–Richter relation

$$\log N = a - bM \tag{8.1}$$

where $N$ is the number of earthquakes of magnitude $M$ or greater, and $a$ and $b$ are numerical constants. The parameter $b$ is often referred to as $b$-slope, and it describes the rate of increase of earthquakes as magnitude decreases. Studies in many areas of the world have shown that the $b$-slope values usually are within the range of 0.6–1.2. This range corresponds to an increase in the number of earthquakes of 4 to 16 times for each decrease of magnitude by one unit.

For a given sample of earthquake magnitude data, if we plot $N$ versus $M$, then the $b$-slope may be estimated from the slope of the least squares line fitted through the data points. Alternatively, the $b$-slope may be computed by Utsu's formula (Utsu, 1965) in a form given by Aki (1965)

$$b = \log(e)/(\bar{M} - M_{\min}) \tag{8.2}$$

where $\log(e) \simeq 0.4343$, $\bar{M}$ is the average magnitude, and $M_{\min}$ is the minimum magnitude in a given sample of data. Aki (1965) showed that Eq. (8.2) was the maximum likelihood estimate of the $b$-slope and derived confidence limits for this estimate. As pointed out by Hamilton (1967), Eq. (8.2) may be written as

$$\bar{M} = M_{\min} + \log(e)/b \tag{8.3}$$

Therefore, the nature of the frequency–magnitude relation is measured equivalently by $b$ or $\bar{M}$ (Wyss and Lee, 1973). Readers interested in a more detailed discussion of $b$-slope and its significance in earthquake statistics are referred to Utsu (1971). We now summarize a few examples of $b$-slope studies as they relate directly to earthquake prediction.

Suyehiro *et al.* (1964) calculated $b$-slopes from foreshock and aftershock activity associated with a magnitude 3.3 earthquake on January 22,

1964, near the Matsushiro Seismological Observatory. The data set consisted of 25 foreshocks and 173 aftershocks, with magnitudes as small as −2. Foreshock activity started about 4 hr before the main shock, and aftershock activity lasted about 14 hr. Computed $b$-slopes were 0.35 for the foreshocks and 0.76 for the aftershocks. Background seismicity of the Matsushiro region had a $b$-slope of 0.8.

Temporal changes in $b$-slope associated with an earthquake swarm in mid-1970 near Danville, California, were studied by Bufe (1970). The swarm activity could not be easily partitioned into a foreshock–aftershock series. However, Bufe found that the $b$-slope decreased from a regional value of about 1.04 to 0.6–0.8 before episodes of relatively large magnitude earthquakes, and returned to normal soon after these episodes. About 2400 events were used in this study.

Pfluke and Steppe (1973) investigated spatial variations of $b$-slope along the San Andreas fault system in central California. The region between Mount Diablo and Parkfield was divided into 10 geographic zones, based upon tectonic and seismic considerations. The data set consisted of 1452 earthquakes with magnitude $\geq 1.8$ from 1969 to 1972 as listed in the catalogs of the USGS Central California Microearthquake Network. Using the method developed by Utsu (1965, 1966), they found significant differences in the $b$-slopes computed for the relatively small geographic zones. For example, in two areas characterized by fault creep, the higher $b$-slope occurred in the area with low seismicity, and the lower $b$-slope occurred in the area with high seismicity.

Using data from the same earthquake catalogs, Wyss and Lee (1973) studied $b$-slope variation as a function of time prior to the larger events listed. Four events ranging in magnitude from 3.9 to 5.0 were selected for study. A constant event window was used to compute temporal variation of $\bar{M}$, or equivalently, the $b$-slope. The number of earthquakes kept within the event window was either 25, 36, or 50. At times of low seismicity, the event window might cover a time period as long as 1 year, thereby reducing the chances of detecting significant temporal changes in $b$-slope. Each of the four events studied showed precursory decreases in $b$-slope prior to their occurrence. However, not all temporal decreases in $b$-slope were followed by a significant earthquake. A precursory decrease in $b$-slope was also observed by Stephens *et al.* (1980) to have occurred before the 1979 St. Elias, Alaska, earthquake.

Udias (1977) computed $b$-slopes for two aftershock sequences and a swarm near Bear Valley in central California. He used data from the short-period, high-gain seismic system operated at the San Andreas Observatory by the University of California at Berkeley. For the two aftershock sequences, the $b$-slope values were 1.12 and 0.96; whereas for the

swarm, the $b$-slope value was 0.46. Udias suggested that the differences in $b$-slopes might reflect spatial variations in the rock properties of the source region, although he could not rule out the possibility of a temporal change.

The studies just presented suggest that changes in $b$-slope might be temporal or spatial, and it would be difficult to tell them apart in some cases. Furthermore, it is difficult to prepare a complete and uniform earthquake catalog (to some cutoff magnitude) over a long period of time. The reasons include changes in instrumentation and in data processing procedures which take place frequently for some seismic networks.

### *8.3.2. Temporal Variations in Focal Depth*

Reliable calculation of earthquake focal depth requires at least one station located at an epicentral distance comparable to the focal depth. Unless the average station spacing in a microearthquake network is comparable to the focal depth of the earthquakes in the region, it may be difficult to study temporal variations in focal depth. Because microearthquakes usually are shallow, it may be difficult and costly to achieve an average station spacing that meets this requirement. Therefore, this type of temporal change has not often been reported.

An example of investigating temporal variations in focal depth is given by Bufe *et al.* (1974). They studied the earthquakes along the Bear Valley section of the San Andreas fault for a 23 month period which included the magnitude 4.6 Stone Canyon earthquake of September 4, 1972. Mean focal depth was calculated by averaging the depths for all events within a 30-day time window and then stepping the window forward in increments of 10 days. Starting about 60 days before the Stone Canyon earthquake, mean focal depth began to increase from 5.5 km to about 7 km. Mean focal depth returned nearly to normal about 10–20 days before the main shock.

Temporal variations in focal depth may be only apparent and may be caused by a dilatancy-induced velocity decrease. To test this hypothesis, Wu and Crosson (1975) computed travel times in a model consisting of a triaxial ellipsoid with velocity lower than that of the surrounding medium. A hypothetical distribution of seismic stations and hypocenters, along with reasonable velocity values, was chosen to be compatible with the study by Bufe *et al.* (1974). Wu and Crosson relocated the earthquake hypocenters using the calculated travel times and a constant velocity model. They concluded that any tendency toward an increase in focal depth was an order of magnitude less than that reported by Bufe *et al.*, and suggested that the increase in focal depth could be real and might not be caused by the effect of a dilatancy-induced velocity decrease.

### *8.3.3. Changes in Source Characteristics*

It is important in earthquake prediction to distinguish a foreshock sequence from the background seismicity of a region, or from a swarm that will not culminate in a much larger earthquake. An obvious hypothesis to be tested is whether genuine foreshocks have different source characteristics than background seismicity or swarms. Changes in source characteristics may be inferred, for example, from studies of waveforms, amplitudes, and spectra of seismic waves, and from fault-plane solutions. In this subsection, we summarize a few examples of different approaches to investigate changes in source characteristics.

There is some evidence that variations in the ratio of P to S amplitudes may be useful. The amplitude ratio (P/S) for an earthquake at a given station is usually determined from the maximum P amplitude and the maximum S amplitude recorded on a given component of the station's seismogram. It depends mainly on the following factors: (1) the orientation of the fault plane at the source; (2) the direction of rupture during the earthquake; (3) the propagation path of the seismic waves; and (4) the position of the recording station with respect to the earthquake hypocenter. If the earthquakes being studied occur relatively close to one another, then the amplitude ratio should depend mostly on the first two factors. If these earthquakes have the same source characteristics, then the amplitude ratio at a given station should be constant.

Chin *et al.* (1978) studied amplitude ratios from vertical-component recordings of P and SV phases from foreshocks and aftershocks of the magnitude 7.3 Haicheng, China, earthquake of February 4, 1975. The amplitude ratios (P/SV) for the foreshocks were found to be quite stable with time, although their values differed from station to station. However, the amplitude ratios (P/SV) for the aftershocks were found to be highly variable at all stations. In order to distinguish foreshocks from swarms, Chin *et al.* also studied amplitude ratios (P/SV) for five earthquake swarms occurring elsewhere in China. They found that these ratios for the swarms were unstable with time.

The amplitude ratios (P/SV) for three main shocks in California ranging in magnitude from 4.3 to 5.7 were examined by Lindh *et al.* (1978a). Because of low background seismicity in the focal regions prior to the foreshock sequences, they were restricted to comparing amplitude ratios between foreshocks and aftershocks. The amplitude ratios (P/SV) were measured from short-period, vertical-component seismograms at one station near each of the three focal regions. They found that the amplitude ratios showed significant decreases from foreshocks to aftershocks in all cases. These amplitude ratio changes were attributed to a slight rotation

of the fault plane, of the order of 5–20°, at the time of the main shock. As an alternative explanation, they suggested changes in the attenuation properties of the material surrounding the focal regions.

Jones and Molnar (1979) measured amplitude ratios (P/S) for foreshocks from three earthquake sequences—one in the Philippines and two in eastern Europe. They used seismograms recorded at WWSSN stations that were sufficiently close to these earthquakes so that the foreshocks were well recorded. The amplitude ratios were found to be stable with time for each of the foreshock sequences, suggesting that the focal mechanisms for the foreshocks did not change.

Theoretical expressions for the amplitude ratio P/SV derived by Kisslinger (1980) show that this ratio cannot distinguish between conjugate mechanisms or determine the sense of slip on the fault plane. He suggested that routine observations of the P/SV ratio at a well-placed station could detect changes in focal mechanisms without the need for more detailed fault-plane solutions. Such solutions usually are based on the directions of the first P-motions from vertical-component seismograms (see Section 6.2) and may be supplemented by the polarization directions for the S-arrivals from three-component seismograms. The orientation of the principal stress axes may be inferred from fault-plane solutions. Changes in the orientation of the compressional stress axes have been investigated as a possible earthquake precursor, and we now summarize a few examples.

The orientation of the compressional stress axes using small earthquakes has been studied in the Garm region, USSR. Nersesov *et al.* (1973) identified three stages of temporal behavior: (1) a quiet period, lasting several years, was characterized by random distribution of the azimuths of the compressional stress axes; (2) a shorter period, of the order of 1 year, was distinguished by an alignment of the compressional stress axes along one of the two preferred directions, in this case 110–170°; and (3) a period beginning 3 to 4 months before the main shock was characterized by a process of realignment, in which the axes of compressional stress rotated to the second preferred direction, in this case 15–70°. After the main shock, the stress system returned to its initial state as described by (1).

Bolt *et al.* (1977) studied the Briones Hills earthquake swarm of January 1977 in central California, in which the largest event ($M_L$ = 4.3) was considered to be the main shock. The fault-plane solution for the main shock was found to be consistent with the regional right-lateral, strike-slip motion along a northwest trending fault. The largest foreshock ($M_L$ = 4.0) had a fault-plane solution that was rotated approximately 90° clockwise from that of the main shock. The waveforms recorded at a station about 6

km from the swarm were quite similar, but the amplitude ratios (P/S) were larger for the foreshocks than for the rest of the events.

Earthquake precursors for a magnitude 5 earthquake near the Adak Microearthquake Network in the central Aleutian Islands were investigated by Engdahl and Kisslinger (1977). During the 5 week period before the main shock, six foreshocks occurred. Of these, the first and the last had thrust-type focal mechanisms similar to the background earthquakes. The remaining foreshocks were found to have the thrust-type focal mechanisms also, but the principal stress axes were rotated nearly 90°.

As discussed in Section 6.5, if digital waveform data are available, the earthquake source may be characterized in some detail. Thus, studying waveforms may be the most direct approach in identifying earthquake precursors. However, obtaining meaningful results from waveform data usually requires tedious labor, if it could be done at all. There is now a tendency toward digital recording to overcome the traditional difficulties in dynamic range and bandwidth. We expect that more detailed studies of earthquake source characteristics will be forthcoming (e.g., Brune *et al.*, 1980).

Changes of seismic wave spectra have been reported for foreshocks, aftershocks, and swarms. A few examples related to earthquake prediction are summarized next. An early report of a temporal variation of seismic spectra was given by Suyehiro (1968). A tremendous swarm of earthquakes occurred at Matsushiro, Japan, from August 1965 through 1967. Fortunately, tripartite recordings of local seismicity were made before the swarm started, during the swarm, and in 1967. Suyehiro found that the waveforms of preswarm earthquakes had significantly higher frequency content than those of the swarm and postswarm events; waves with frequency content greater than 200 Hz showed considerable attenuation with time. He attributed this temporal change to extensive fracturing of rocks in the focal region caused by the swarm itself.

Tsujiura (1979) studied waveform variations in earthquake swarms at seven areas in Japan and in the foreshocks preceding the magnitude 7 Izu-Oshima-Kinkai earthquake of January 14, 1978. Earthquakes from a given swarm were found to have a similar waveform. However, the waveforms for the foreshocks varied significantly, even for those events that occurred relatively close in time.

An earthquake of magnitude 5.5 occurred along the San Andreas fault near Parkfield, California, in 1934, and also in 1966. Both had a foreshock of magnitude 5.1 which occurred 17 min and 25 sec, and 17 min and 17 sec, respectively, before the main shock. Bakun and McEvilly (1979) showed that the first several seconds of the waveforms for the foreshocks were nearly identical, as were the waveforms of the main shocks. This

suggested that the locations and the focal mechanisms for the foreshock pair and for the main shock pair were identical. However, the P-wave spectra were consistent with a northwest direction of rupture for the foreshocks, and a southeast direction of rupture for the main shocks.

Ishida and Kanamori (1980) examined the spectra of some pre-1949 background earthquakes and of foreshocks preceding the magnitude 7.7 Kern County, California, earthquake of July 21, 1952. The frequency of the spectral peak was found to be systematically higher for the foreshocks than for the events occurring before 1949. They suggested that this result was consistent with a model of stress concentration around the eventual hypocenter of the main shock.

**Note Added in Proof**

In May, 1980, a symposium on earthquake prediction was held in New York, hosted by the Lamont–Doherty Geological Observatory of Columbia University. A collection of 51 research papers from this symposium has just been published:

Simpson, D. W., and Richards, P. G., eds. (1981). "Earthquake Prediction, an International Review," American Geophysical Union, Washington, D.C.

Major topics in this volume include: seismicity patterns, geological and seismological evidence for recurrence times along major fault zones, seismic and nonseismic long-term and intermediate-term precursors to earthquakes, short-term and immediate precursors to earthquakes, theoretical and laboratory investigations, and reviews of national programs in Japan, China, and the United States.

# 9. Discussion

Microearthquake studies have grown tremendously in the last two decades. The use of microearthquakes as a tool in understanding tectonic processes was recognized in the 1950s. Permanent networks and portable arrays were developed specifically for studying microearthquakes. Telemetry transmission was tested and proved feasible. In the 1960s, instrumentation development for telemetered microearthquake networks was started. Many data acquisition and processing procedures were automated, including hypocenter locations by computers.

With funds available for research in earthquake hazards reduction (especially for earthquake prediction), many microearthquake networks were established in the 1970s. Telemetry transmission and centralized recording systems were improved. Much effort went into streamlining data acquisition and processing procedures, but progress has been slow. More intensive use of computers to analyze microearthquake data increased our knowledge about the distribution of microearthquakes and their relation to the faulting process. However, we also learned that microearthquake networks can generate far greater amounts of data than can be coped with effectively. To help solve this problem, a combined effort by the USGS and several universities to develop interactive computing facilities for microearthquake networks has been undertaken by P. L. Ward and colleagues (1980). There is also an increasing use of digital electronics and microprocessors to collect, process, and analyze microearthquake data (see, e.g., Allen and Ellis, 1980; Prothero, 1980).

The capital cost for either a permanent station or a temporary station is about $5000. The total operating cost for a permanent station is also about $5000 per year, and that for a temporary station may be a few times more. Given a limited amount of financial support, it may not be effective to operate a dense microearthquake network of permanent stations over a large area. An alternative is to have a relatively sparse network of permanent stations and to use a mobile array of temporary stations that provides

denser station coverage for a portion of the network area at a time. This allows the permanent stations to monitor the general seismicity of the entire area, and the temporary stations to fill in the details.

The average station spacing $\xi$ in a microearthquake network is related to the network area $A$ and the number of stations $N$ by $\xi = (A/N)^{1/2}$. Since reducing $\xi$ by a factor of 2 requires increasing $N$ by a factor of 4, it is not practical to have small station spacing over a large area. Let us consider the problem of monitoring an area of 100 km $\times$ 100 km with a network of 100 stations. If the stations are permanent and distributed evenly over the area, then the average station spacing is 10 km, which is not adequate for some detailed microearthquake studies. An alternative plan is to equip the network with 75 permanent stations and a mobile array of 25 temporary stations. The average spacing for the permanent stations is increased to 11.6 km, but the network location capability is not degraded significantly. If we use the mobile array to supplement the permanent stations and to occupy one-tenth of the network area at a time, we will achieve an effective station spacing of 5.6 km. Thus, we can carry out detailed microearthquake studies without increasing the total number of stations. In practice, such a combination of permanent and mobile stations has not yet been fully exploited.

There are two major difficulties in operating a microearthquake network on a continuing basis: (1) obtaining adequate financial support and management year after year, and (2) maintaining high standards of quality in network operations, especially with respect to data processing and analysis. A microearthquake network can become unmanageable if the tasks to achieve the desired goals are not clearly defined and performed. For example, if the scientific goal is to map the geometry of active faults in a given area, then it is not necessary to operate the network continuously in time. Furthermore, because the fault geometry can be defined by well-located earthquakes, it is not necessary to save all the waveform data. The main tasks then are to operate a microearthquake network that surrounds the target area, and to collect first P-arrival times and first P-motion data for precise earthquake locations and fault-plane solutions. It is not easy to strike the proper balance between the desire to collect, process, and analyze as much data as possible, and the ability to perform these tasks with high standards of quality.

It is tempting to rely on partial or total automation in the routine operation of a microearthquake network in order to reduce the staff and the cost. However, development and implementation of automatic procedures requires substantial amounts of resources and some lead time. It is easy to overlook this fact and thereby end up with disappointing results.

Automation usually does not reduce costs, but often opens up new possibilities in data analysis.

Finally, because a microearthquake network is a complex tool, it is not possible for one person to understand every facet of the network operations and its many practical applications. Successful operation of a microearthquake network requires (1) well-defined tasks to achieve the desired goals; (2) a team of scientists, engineers, and technicians; and (3) effective management and adequate financial support. To get the best results from microearthquake networks also requires sharing experience and collaborating in research on national and international levels.

# Appendix: Glossary of Abbreviations and Unusual Terms

This glossary defines abbreviations and some unusual terms used in this volume. By "unusual terms" we mean those terms whose definitions may be difficult to find elsewhere, or whose meaning has enough variation that we felt it necessary to define them specifically as used in this book. This glossary is by no means complete. We have chosen not to define many words, particularly if their meaning is rather well known, or if they are adequately defined in the following standard references:

Aki, K., and Richards, P. (1980). "Methods of Quantitative Seismology." Freeman, San Francisco, California.

Bates, R. L., and Jackson, J. A., editors (1980). "Glossary of Geology," 2nd ed. American Geological Institute, Falls Church, Virginia.

James, R. C., and James, G. (1976). "Mathematics Dictionary," 4th ed. Van Nostrand Reinhold, New York.

Lapedes, D. N., editor (1978). "Dictionary of Scientific and Technical Terms." 2nd ed. McGraw-Hill, New York.

Richter, C. F. (1958). "Elementary Seismology." Freeman, San Francisco, California.

*Glossary*

**AGC:** Automatic gain control. System that automatically changes the gain of an amplifier or other piece of equipment so that the desired output signal remains essentially constant despite variations in input strength. See Section 2.2.3.

**BPI:** Bits per inch. Commonly used to measure the density of information recorded on a digital magnetic tape. For example, a nine-track 800 BPI tape contains information at a density of 800 bits/inch/track. Because a byte is usually coded as 9 bits across a magnetic tape, the effective information density in this example is 800 bytes/inch.

**Cholesky method:** An efficient method of solving a set of linear equations $\mathbf{Ax} = \mathbf{b}$ if the matrix $\mathbf{A}$ is symmetric and positive definite. Matrix $\mathbf{A}$ is said to be positive definite if $\mathbf{x}^T\mathbf{Ax} > 0$ for all $\mathbf{x} \neq \mathbf{0}$. The method is based on the Cholesky decomposition of $\mathbf{A}$ into $\mathbf{LL}^T$, where $\mathbf{L}$ is a lower triangular matrix. It is commonly used to solve a set of normal equations.

**Coda magnitude:** Type of earthquake magnitude. It is based on either the duration of coda waves or some of their characteristics. Some authors have used this term interchangeably with duration magnitude; this practice is technically incorrect. *See* Duration magnitude. For a definition of coda waves, see Aki and Richards (1980, p. 526).

**Compensation signals:** Signals that are recorded on an analog magnetic tape along with the

data and in the same tape track as the data. They are used during the playback of data in order to correct for the effects of tape-speed variations.

**CPU:** Central processing unit of a computer. It is the unit that performs the interpretation and execution of computer instructions.

**CPU time for a computer job:** Actual time taken by the central processing unit of a computer to complete a given job. For a computationally intensive job, the CPU time is the dominant factor in determining the computing cost charged to a user.

**dB:** Decibel. Unit for describing the ratio of two powers or intensities. If $P_1$ and $P_2$ are two measurements of power, the first is said to be $n$ decibels greater, where $n = 10 \cdot \log_{10}(P_1/P_2)$. Since the power of a sinusoidal wave is proportional to the square of the amplitude, and if $A_1$ and $A_2$ are the corresponding amplitudes for $P_1$ and $P_2$, we have $n = 20 \cdot \log_{10}(A_1/A_2)$.

**dB/octave:** Decibels per octave. Used as a unit to express the change of amplitude over a frequency interval. *See* dB; Octave.

**Develocorder:** Multichannel (up to 20) galvanometric instrument that records analog signals continuously on 16-mm microfilm. Processing of the film is performed continuously within the instrument so that the analog film record can be viewed at 10× magnification approximately 10 min. later. It is manufactured by Teledyne Geotech, and is commonly used to record seismic and timing signals from a microearthquake network.

**Direct-mode tape recording:** Technique to record analog signals by amplitude modulation on magnetic tapes.

**Discriminator:** Electronic component that converts variations in signal frequency (relative to a reference or carrier frequency) to variations in signal amplitude. Its function is exactly opposite to that of a voltage-controlled oscillator.

**Duration magnitude:** Type of earthquake magnitude. It is based on the duration of seismic waves (i.e., signal duration). In practice, signal duration is often measured as the interval from the first P-arrival time to the time where the signal amplitude no longer exceeds some prescribed value. *See* Coda magnitude.

**Earthquake swarm:** Type of earthquake sequence characterized by a long series of large and small shocks with no one outstanding, principal event.

**Euclidean length of a vector:** If $\mathbf{x}$ is an $n$-vector with components $x_i$, $i = 1, 2, \ldots, n$, then its Euclidean length is $\|\mathbf{x}\| = (\Sigma_{i=1}^{n} x_i^2)^{1/2}$. It is the 2-norm of a vector and is the most commonly used vector norm. *See* Norm of a vector.

**EW:** East–west direction.

**FDM:** Frequency division multiplexing. Technique for combining and transmitting two or more signals over a common path by using a different frequency band for each signal.

**FFT:** Fast Fourier transform. It is an algorithm that efficiently computes the discrete Fourier transform.

**First motion of P-waves:** Refers to the direction of the initial motion of P-waves recorded on a seismogram at a given station from a given earthquake. For a vertical component seismogram, the common convention is that the up and down directions on the seismogram correspond to the up and down directions of ground motion, respectively. *See* Section 6.2; *see also* Polarity of a station.

**FM:** Frequency modulation. Technique of converting signals for the purpose of transmission or recording. In frequency modulation, variations in signal amplitude are converted to variations in frequency relative to a reference frequency or carrier frequency.

**Geophone:** Term that is commonly used for an electromagnetic seismometer that is light weight and responds to high-frequency ground motion (e.g., greater than 1 Hz).

**Helicorder:** A multichannel (up to three) galvanometric instrument that records analog signals continuously on a sheet of thermally sensitive paper by means of a hot stylus. The sheet of paper is wrapped around a cylindrical drum so that a standard-size seismogram is

produced every 24 hr. It is manufactured by Teledyne Geotech, and is commonly used to produce a low-speed, instantaneously visible seismogram for monitoring purposes.

**HYP071:** A computer program written by Lee and Lahr (1975) for determining hypocenter, magnitude, and first motion pattern of local earthquakes.

**IBM:** International Business Machines Corporation, a manufacturer of computers and related products.

**Ill conditioned:** A set of equations is said to be ill conditioned if the solution of the equations is very sensitive to small changes in the coefficients of the equations.

**IRIG:** Inter-Range Instrumentation Group. This group was responsible for standardization of time-code formats and timing techniques at the White Sands Missle Range, New Mexico, in the 1960s.

**IRIG-C:** Time-code format devised by the Inter-Range Instrumentation Group (IRIG). In this format, time is coded at a rate of 2 pulses per second. *See* Time-code generator.

**IRIG-E:** Time code format devised by the Inter-Range Instrumentation Group (IRIG). In this format, time is coded at a rate of 10 pulses per second. *See* Time-code generator.

**Julian day:** Number of days since January 1 in a given calendar year. For example, the Julian day for March 10, 1981 is 69. It is a compact way to identify and count the days in a given year.

**$M$:** Often used to denote the magnitude of an earthquake. Some authors are careful to specify how they define $M$, while others are not.

**$m_b$:** Body-wave magnitude of an earthquake. See Section 6.4.2.

**$M_D$:** Duration magnitude of an earthquake. See Section 6.4.2.

**$M_L$:** Local magnitude of an earthquake. See Section 6.4.1.

**$M_0$:** Seismic moment of an earthquake. See Section 6.5.1.

**$M_S$:** Surface-wave magnitude of an earthquake. See Section 6.4.2.

**NCER:** National Center for Earthquake Research. This organization is now the Office of Earthquake Studies within the U.S. Geological Survey.

**NOAA:** National Oceanic and Atmospheric Administration.

**Nonsingular matrix:** A square matrix is said to be nonsingular if its determinant is nonzero.

**Norm of a vector:** Number that measures the general size of the elements of a vector. If $\mathbf{x}$ is an $n$-vector, then the 1, 2, and $\infty$ norms of $\mathbf{x}$ are defined by

$$\|\mathbf{x}\|_1 = \sum_{i=1}^{n} |x_i|, \qquad \|\mathbf{x}\|_2 = \left[ \sum_{i=1}^{n} x_i^2 \right]^{1/2}$$

$$\|\mathbf{x}\|_\infty = \max\{|x_i|; i = 1, 2, \ldots, n\}$$

respectively. *See* Euclidean length of a vector.

**NS:** North–south direction.

**NTS:** Nevada Test Site. Many of the United States nuclear explosions are set off at this site.

**OBS:** Ocean-bottom seismograph. See Section 2.4.

**Octave:** Interval between any two frequencies that have a ratio of 2 to 1. For example, the interval between 10 and 20 Hz is 1 octave, and the interval between 2 and 32 Hz is 4 octaves.

**Oscillomink:** Multichannel (up to 16) galvanometric instrument that records analog signals continuously on paper by means of an ink jet. It is manufactured by Siemens Corp., and is commonly used to record seismic and timing signals, which are played back from analog magnetic tapes.

**Polarity of a station:** Term used to indicate the correspondence between the direction of the first motion of P-waves as it appears on the seismogram and the actual direction of the first motion of P-waves arriving at the station site. A vertical-component seismograph station is

said to have the correct polarity if the up (or down) direction of the first P-motion on the seismogram corresponds to the up (or down) direction of the ground motion. Otherwise, it is said to have reversed polarity.

**P-phase:** The part of the seismic signal recorded on a seismogram, which is interpreted to represent the ground motion associated with P-waves.

**P/SV amplitude ratio:** Ratio of the maximum amplitude of the P-phase to the maximum amplitude of the S-phase of an earthquake as measured from the vertical component seismogram recorded at a given station. It is assumed that the travel path from the earthquake source to the receiving station is the same for the P-phase and the S-phase in question. In general, the SV-wave motion (see Aki and Richards, 1980, p. 531) is not entirely in the vertical direction. Thus, in practice, it is usually the ratio of the maximum amplitude of the vertical component of the P-phase to the maximum amplitude of the vertical component of the SV-phase that is measured.

**P-waves:** Compressional elastic waves are called P-waves in seismology, where P stands for primary.

***Q*:** Quality factor of an imperfect elastic medium. It is a dimensionless measure of the internal friction in a volume of material. [See Aki and Richards (1980, p. 168–169)].

**Seismometer:** Instrument that detects ground motion and converts it to a signal that can be amplified and recorded. This definition is consistent with the current usage, and differs from an earlier definition which defines seismometer as a calibrated seismograph.

**Singular matrix:** A square matrix is said to be singular if its determinant is zero.

**S–P time interval:** Time interval between the S-wave arrival time and the P-wave arrival time.

**S-phase:** The part of the seismic signal recorded on a seismogram, which is interpreted to represent the ground motion associated with S-waves.

**SVD:** Singular-value decomposition. See Section 5.1.4.

**Swarm:** *See* Earthquake swarm.

**S-waves:** Elastic shear waves are called S-waves in seismology, where S stands for secondary.

**Time-code generator:** A crystal-controlled pulse generator that produces a train of pulses with various predetermined widths and spacings. It is designed such that the time of day (and sometimes the Julian day of the year) can be decoded from the pulse train. It is used to provide a continuous time base for physical measurements.

$t_p$: P-wave arrival time or travel time, depending on the context. It is most commonly used for the first P-wave that arrives at a given station.

**Tripartite array:** Array of seismographs deployed at the corners of a triangle. The sides of the triangle are usually 1 km or so in length, and the triangle is usually equilateral in shape. A fourth station often occupies the center of the triangle, and serves as a central recording site. Although this type of array was popular at one time, it is no longer commonly deployed. The reason is that the benefits from such a geometry often are not balanced by the logistical difficulties.

$t_s$: S-wave arrival time or travel time, depending on the context.

$t_s/t_p$: Ratio of S-wave travel time to P-wave travel time. In determining this ratio, it is commonly assumed that the S-wave and the P-wave travel the same path from an earthquake source to a given station.

**uhf:** Ultrahigh frequency. The band of frequencies from 300 to 3000 MHz in the radio spectrum is referred to as the uhf band.

**USGS:** United States Geological Survey.

**UTC:** Universal Time Coordinated: A time scale defined by the International Time Bureau and agreed upon by international convention.

**VCO:** Voltage-controlled oscillator: An electronic component which converts variations in signal amplitude to variations in frequency relative to a reference frequency. The converted signal may then be combined with other converted signals by the frequency division multiplexing technique.

**Vector norm:** *See* Norm of a vector.

**vhf:** Very high frequency. The band of frequencies from 30 to 300 MHz in the radio spectrum is referred to as the vhf band.

**Voice-grade circuit:** Circuit for transmitting voice-frequency signals in the frequency band from 300 to 3000 Hz.

$V_p$: P-wave velocity, most often given in km/sec.

$V_{pp}$: Volts (peak-to-peak), which is the voltage of a sinusoidal electrical signal as measured from one peak to an adjacent trough.

$V_p/V_s$: Ratio of P-wave velocity to S-wave velocity.

$V_s$: S-wave velocity, most often given in km/sec.

**WWSSN:** World-Wide Standardized Seismograph Network (see Oliver and Murphy, 1971)

**WWV:** Call letters for a radio station maintained by the National Bureau of Standards. It transmits a standard time broadcast, which is coded such that Universal Time Coordinated can be determined by an appropriate receiver. Broadcast frequencies for WWV are 2.5, 5, 10, 20, and 25 mHz.

**WWVB:** Call letters for a radio station maintained by the National Bureau of Standards. It transmits a standard time broadcast at 60 kHz, which is coded such that Universal Time Coordinated can be determined by an appropriate receiver.

# References


Acton, F. S. (1970). "Numerical Methods That Work." Harper & Row, New York.

Adams, R. D. (1974). Statistical studies of earthquakes associated with Lake Benmore, New Zealand. *Eng. Geol. (Amsterdam)* **8**, 155–169.

Adams, R. D., ed. (1977). Survey of practice in determining magnitudes of near earthquakes. Part 2. Europe, Asia, Africa, Australia, and Pacific. *World Data Cent. A Solid Earth Geophys.* **SE-8**, 1–67.

Adams, R. D., and Ahmed, A. (1969). Seismic effects at Mangla Dam, Pakistan. *Nature (London)* **222**, 1153–1155.

Adby, P. R., and Dempster, M. A. H. (1974). "Introduction to Optimization Methods." Chapman & Hall, London.

Aggarwal, Y. P., Sykes, L. R., Armbruster, J., and Sbar, M. L. (1973). Premonitory changes in seismic velocities and prediction of earthquakes. *Nature (London)* **241**, 101–104.

Aggarwal, Y. P., Sykes, L. R., Simpson, D. W., and Richards, P. G. (1975). Spatial and temporal variations in $t_s/t_p$ and in P wave residuals at Blue Mountain Lake, New York: Application to earthquake prediction. *J. Geophys. Res.* **80**, 718–732.

Aki, K. (1965). Maximum likelihood estimate of b in the formula log $N = a - bM$ and its confidence limits. *Bull. Earthquake Res. Inst., Univ. Tokyo* **43**, 237–239.

Aki, K. (1966). Generation and propagation of G waves from the Niigata earthquake of June 16, 1964. Part 2. Estimation of earthquake moment, released energy, and stress-strain drop from the G wave spectrum. *Bull. Earthquake Res. Inst., Univ. Tokyo* **44**, 73–88.

Aki, K. (1969). Analysis of the seismic coda of local earthquakes as scattered waves. *J. Geophys. Res.* **74**, 615–631.

Aki, K. (1980a). Attenuation of shear-waves in the lithosphere for frequencies from 0.05 to 25 Hz. *Phys. Earth Planet. Inter.* **21**, 50–60.

Aki, K. (1980b). "Local Earthquake Seismology." Lectures given at U.S. Geological Survey, July 1980.

Aki, K., and Chouet, B. (1975). Origin of coda waves: Source, attenuation, and scattering effects. *J. Geophys. Res.* **80**, 3322–3342.

Aki, K., and Lee, W. H. K. (1976). Determination of three-dimensional velocity anomalies under a seismic array using first P arrival times from local earthquakes. Part I. A homogeneous initial model. *J. Geophys. Res.* **81**, 4381–4399.

Aki, K., and Richards, P. (1980). "Methods of Quantitative Seismology." Freeman, San Francisco, California.

Aki, K., Hori, M., and Matumoto, H. (1966). Microaftershocks observed at a temporary array station on the Kenai Peninsula. *In* "The Prince William Sound Alaska Earthquake of 1964 and Aftershocks" (L. E. Leipold, ed.), Vol. II, Parts B & C, pp. 131–156. US Govt. Printing Office, Washington, D.C.

Aki, K., Christoffersson, A., and Husebye, E. S. (1976). Three-dimensional seismic structure of the lithosphere under Montana LASA. *Bull. Seismol. Soc. Am.* **66,** 501–524.

Aki, K., Christoffersson, A., and Husebye, E. S. (1977). Determination of the three-dimensional seismic structure of the lithosphere. *J. Geophys. Res.* **82,** 277–296.

Allen, C. R., and Helmberger, D. V. (1973). Search for temporal changes in seismic velocities using large explosions in southern California. *Stanford Univ. Publ., Geol. Sci.* **13,** 436–445.

Allen, R. V. (1978). Automatic earthquake recognition and timing from single traces. *Bull. Seismol. Soc. Am.* **68,** 1521–1532.

Allen, R. V., and Ellis, J. O. (1980). An automatic on-line monitor for microearthquake networks. *Trans. Am. Geophys. Union* **61,** S41.

Allison, M. L., Whitcomb, J. H., Cheatum, C. E., and McEuen, R. B. (1978). Elsinore fault seismicity: The September 13, 1973, Agua Caliente Springs, California, earthquake series. *Bull. Seismol. Soc. Am.* **68,** 429–440.

Alsinawi, S. A., and Banno, I. S. (1976). The first microearthquake recording in Iraq. *Tectonophysics* **36,** T1–T6.

Ambuter, B. P., and Solomon, S. C. (1974). An event recording system for monitoring small earthquakes. *Bull. Seismol. Soc. Am.* **64,** 1181–1188.

Anderson, J. A., and Wood, H. O. (1925). Description and theory of the torsion seismometer. *Bull. Seismol. Soc. Am.* **15,** 1–72.

Anderson, J. G., and Fletcher, J. B. (1976). Source properties of a Blue Mt. Lake earthquake. *Bull. Seismol. Soc. Am.* **66,** 677–683.

Anderson, K. R. (1978). Automatic processing of local earthquake data. Ph.D. Thesis, Massachusetts Institute of Technology, Cambridge.

Anonymous (1970). Aftershock observations of the earthquake of the central part of Gifu Prefecture, September 9, 1969. *Bull. Earthquake Res. Inst., Univ. Tokyo* **48,** 1155–1163 (in Japanese with English abstract).

Anonymous (1974). A preliminary analysis of the mechanism of microearthquakes in the region of Hsinfengkiang Reservoir. *Sci. Geol. Sin.* pp. 234–245 (in Chinese with English abstract).

Anonymous (1975). An observation of microearthquakes at Nagawado Dam in Nagano Prefecture. *Bull. Earthquake Res. Inst., Univ. Tokyo* **50,** 47–51 (in Japanese with English abstract).

Anonymous (1978). NBS time via satellites. *Nat. Bureau Standards Publ. (U.S.)* **TFS-602.**

Anonymous (1979). "Geophysical Data Interchange Assessment 1978." Nat. Acad. Sci., Washington, D.C.

Arabasz, W. J., and Robinson, R. (1976). Microseismicity and geologic structure in the northern South Island, New Zealand. *N. Z. J. Geol. Geophys.* **19,** 569–601.

Arabasz, W. J., Brune, J. N., and Engen, G. R. (1970). Locations of small earthquakes near the trifurcation of the San Jacinto fault southeast of Anza, California. Bull. Seismol. Soc. Am. **60,** 617–627.

Archer, C. B., and Allen, N. J. (1969). A catalogue of earthquakes in the Lake Kariba area: 1959 to 1968. *Rep. Meteorol. Serv. Salisbury* pp. 1–35.

Archer, C. B., and Allen, N. J. (1972). A supplementary catalogue of earthquakes in the Lake Kariba area: 1969 to 1971. *Rep. Meteorol. Serv., Salisbury* pp. 1–5.

Armstrong, B. H. (1969). Acoustic emission prior to rockbursts and earthquakes. *Bull. Seismol. Soc. Am.* **59,** 1259–1279.

Aronovich, Z. I., Zarayskiy, M. P., and Yakusheva, V. N. (1972). The seismicity of the Anapa region according to instrument data. *Izv., Acad. Sci., USSR, Phys. Solid Earth (Engl. Transl.)* No. 1, pp. 79–85.

Asada, T. (1957). Observations of near-by microearthquakes with ultra sensitive seismometers. *J. Phys. Earth* **5**, 83–113.

Asada, T., and Suzuki, Z. (1949). On microearthquakes having accompanied aftershocks of the Fukui earthquake of June 28, 1948. *Geophys. Notes, Tokyo Univ.* **2**, No. 16, 1–14.

Asada, T., and Suzuki, Z. (1950). On microearthquakes observed after the Imaichi earthquake, Dec. 26, 1949. *Bull. Earthquake Res. Inst., Univ. Tokyo* **28**, 415–420.

Asada, T., Suyehiro, S., and Akamatu, K. (1958). Observation of near-by microearthquakes with ultra sensitive seismometers at Matsushiro, Japan. *J. Phys. Earth* **6**, 23–33.

Asano, S., Ichinose, Y., Koresawa, S., Hasegawa, I., Iizuka, S., and Suzuki, H. (1979). A study of change in the velocity of seismic waves in the southern Kanto area by Tateyama explosions. *Bull. Earthquake Res. Inst., Univ. Tokyo* **54**, 119–134 (in Japanese with English abstract).

Aspinall, W. P., Michael, M. O., and Tomblin, J. F. (1976). Evidence for fluid bodies beneath the Sulphur Springs geothermal region, St. Lucia, West Indies. *Geophys. Res. Lett.* **3**, 87–90.

Backus, G., and Gilbert, J. F. (1967). Numerical applications of a formalism for geophysical inverse problems. *Geophys. J. R. Astron. Soc.* **13**, 247–276.

Backus, G., and Gilbert F. (1968). The resolving power of gross earth data. *Geophys. J. R. Astron. Soc.* **16**, 169–205.

Backus, G., and Gilbert, F. (1970). Uniqueness in the inversion of inaccurate gross earth data. *Philos. Trans. R. Soc. London, Ser. A* **266**, 123–192.

Bacon, C. F. (1975). Acoustic emission along the San Andreas fault in southern central California. *Calif. Geol.* **28**, 147–154.

Bakun, W. H. (1980). Seismic activity on the southern Calaveras fault in central California. *Bull. Seismol. Soc. Am.* **70**, 1181–1197.

Bakun, W. H., and Dratler, J. (1976). Empirical transfer functions for stations in the central California seismological network. *Geol. Surv. Open-File Rep. (U.S.)* **76-259**, 76 pp.

Bakun, W. H., and Lindh, A. G. (1977). Local magnitudes, seismic moments, and coda durations for earthquakes near Oroville, California. *Bull. Seismol. Soc. Am.* **67**, 615–629.

Bakun, W. H., and McEvilly, T. V. (1979). Earthquakes near Parkfield, California: comparing the 1934 and 1966 sequences, *Science*, 205, 1375-1377.

Bakun, W. H., Stewart, R. M., and Tocher, D. (1973). Variations in $V_p/V_s$ in Bear Valley in 1972. *Stanford Univ. Publ., Geol. Sci.* **13**, 453–462.

Bakun, W. H., Bufe, C. G., and Stewart, R. M. (1976). Body wave spectra of central California earthquakes. *Bull. Seismol. Soc. Am.* **66**, 363–384.

Bakun, W. H., Houck, S. T., and Lee, W. H. K. (1978a). A direct comparison of "synthetic" and actual Wood-Anderson seismograms. *Bull. Seismol. Soc. Am.* **68**, 1199–1202.

Bakun, W. H., Stewart, R. M., and Bufe, C. G. (1978b). Directivity in the high frequency radiation of small earthquakes. *Bull. Seismol. Soc. Am.* **68**, 1253–1263.

Bakun, W. H., Stewart, R. M., Bufe, C. G., and Marks, S. M. (1980). Implication of seismicity for failure of a section of the San Andreas fault. *Bull. Seismol. Soc. Am.* **70**, 185–201.

Bard, Y. (1974). "Nonlinear Parameter Estimation." Academic Press, New York.

Bath, M. (1973). "Introduction to Seismology." Wiley, New York.

Bath, M. (1979). A rockburst sequence at the Grangesberg iron ore mines in central Sweden. *Riv. Ital. Geofis. Sci. Affini* **5**, 5–10.

Ben-Israel, A., and Greville, T. N. E. (1974). "Generalized Inverses." Wiley (Interscience), New York.

Ben-Menahem, A., Aboodi, E., Vered, M., and Kovach, R. L. (1977). Rate of seismicity of the Dead Sea region over the past 4000 years. *Phys. Earth Planet. Inter.* **14**, 17–27.

Berberian, M., Asudeh, I., Bilham, R. G., Scholz, C. H., and Soufleris, C. (1979). Mechanism of the main shock and the aftershock study of the Tabas E-Golshan (Iran) earthquake of September 16, 1978: A preliminary report. *Bull. Seismol. Soc. Am.* **69**, 1851–1859.

Berry, A. (1898). "A Short History of Astronomy from Earliest Times through the Nineteenth Century." Dover, New York.

Billings, M. P. (1954). "Structural Geology," 2nd ed. Prentice-Hall, Englewood Cliffs, New Jersey.

Bisztricsany, E. (1958). A new method for the determination of the magnitude of earthquakes. *Geofiz. Kozl.* **7**, 69–96 (in Hungarian with English abstract).

Blair, B. E. (1974). Time and frequency dissemination: An overview of principles and techniques. NBS Monogr. (*U.S.*) **140**, 233–313.

Blum, R., and Fuchs, K. (1974). Observation of low magnitude seismicity at a reservoir in the eastern Alps. *Eng. Geol. (Amsterdam)* **8**, 99–106.

Blum, R., Bock, G., Fuchs, K., Merkler, G., and Widmann, R. (1977). Correlation between micro-activity and variation of water level at the Schlegeis Reservoir. *J. Geophys.* **43**, 561–567.

Boatwright, J. (1978). Detailed spectral analysis of two small New York state earthquakes. *Bull. Seismol. Soc. Am.* **68**, 1117–1131.

Boatwright, J. (1980). A spectral theory for circular seismic sources: Simple estimates of source dimension, dynamic stress drop and radiated seismic energy. *Bull. Seismol. Soc. Am.* **70**, 1–27.

Bock, G. (1978). Induced seismicity: Model and observations at Schlegeis-.and Emosson-Reservoir. Ph.D. Thesis, University of Karlsruhe, Karlsruhe (in German).

Bollinger, G. A. (1975). A microearthquake survey of the central Virginia seismic zone. *Earthquake Notes* **46**, 3–13.

Bollinger, G. A., and Gilbert, M. C. (1974). A reconnaissance microearthquake survey of the Hot Springs, Virginia area. *Bull. Seismol. Soc. Am.* **64**, 1715–1720.

Bollinger, G. A., Langer, C. J., and Harding, S. T. (1976). The eastern Tennessee earthquake sequence of October through December, 1973. *Bull. Seismol. Soc. Am.* **66**, 525–547.

Bolt, B. A. (1960). The revision of earthquake epicentres, focal depths and origin times using a high-speed computer. *Geophys. J. R. Astron. Soc.* **3**, 433–440.

Bolt, B. A. (1970). Earthquake location for small networks using the generalized inverse matrix. *Bull. Seismol. Soc. Am.* **60**, 1823–1828.

Bolt, B. A. (1977a). The seismographic stations of the University of California, Berkeley. *Earthquake Inf. Bull.* **9**, 4–12.

Bolt, B. A. (1977b). Constancy of P travel times from Nevada explosions to Oroville Dam station 1970 to 1976. *Bull. Seismol. Soc. Am.* **67**, 27–32.

Bolt, B. A., and Turcotte, T. (1964). Computer location of local earthquakes within the Berkeley seismographic network. *In* "Computers in the Mineral Industries" (G. A. Parks, ed.), pp. 561–576. Stanford University, Stanford, California.

Bolt, B. A., Stifler, J., and Uhrhammer, R. (1977). The Briones Hills earthquake swarm of January 8, 1977, Contra Costa County, California. *Bull. Seismol. Soc. Am.* **67**, 1555–1564.

Bolt, B. A., Okubo, P., and Uhrhammer, R. A. (1978). Optimum station distribution and determination of hypocenters for small seismographic networks. *U.S. Army Eng. Waterways Exp., St., Misc. Paper* **S-78-9**, 1–43.

Boore, D. M., Lindh, A. G., McEvilly, T. V., and Tolmachoff, W. W. (1975). A search for

travel-time changes associated with the Parkfield, California, earthquake of 1966. *Bull. Seismol. Soc. Am.* **65**, 1407–1418.

Boucher, G., and Fitch, T. J. (1969). Microearthquake seismicity of the Denali fault. *J. Geophys. Res.* **74**, 6638–6648.

Boucher, G., Matumoto, T., and Oliver, J. (1968). Localized microearthquakes in the Denali fault zone. *J. Geophys. Res.* **73**, 4789–4793.

Boucher, G., Ryall, A., and Jones, A. E. (1969). Earthquakes associated with underground nuclear explosions. *J. Geophys. Res.* **74**, 3808–3820.

Bradner, H., and Brune, J. N. (1974). The use of sonobuoys in determining hypocenters of aftershocks of the February 21, 1973 Pt. Mugu earthquake. *Bull. Seismol. Soc. Am.* **64**, 99–101.

Brady, B. T., and Leighton, F. W. (1977). Seismicity anomaly prior to a moderate rock burst: A case study. *Int. J. Rock Mech. Miner. Sci. Geomech. Abstr.* **14**, 127–132.

Brandsaeter, H., Farestveit, A., and Ursin, B. (1979). A new high-resolution or deep penetration airgun array. *Geophysics* **44**, 865–879.

Brillinger, D. R., Udias, A., and Bolt, B. A. (1980). A probability model for regional focal mechanism solutions. *Bull. Seismol. Soc. Am.* **70**, 149–170.

Brown, R. (1973). Precursory changes in $V_p/V_s$ before strike-slip events. *Stanford Univ. Publ., Geol. Sci.* **13**, 463–472.

Brown, R. L. (1974). Seismic activity following impounding of Mangla Reservoir. *Eng. Geol. (Amsterdam)* **8**, 79–93.

Brune, J. N. (1970). Tectonic stress and the spectra of seismic shear waves from earthquakes. *J. Geophys. Res.* **75**, 4997–5009.

Brune, J. N. (1976). The physics of earthquake strong motion. *In* "Seismic Risk and Engineering Decisions" (C. Lomnitz and E. Rosenblueth, eds.), pp. 141–177. Elsevier, Amsterdam.

Brune, J. N., and Allen, C. R. (1967). A microearthquake survey of the San Andreas fault system in southern California. *Bull. Seismol. Soc. Am.* **57**, 277–296.

Brune, J. N., Simons, R. A., Vernon, F., Canales, L., and Reyes, A. (1980). Digital seismic event recorders: Description and examples from the San Jacinto fault, the Imperial fault, the Cerro Prieto fault, and the Oaxaca, Mexico, subduction fault. *Bull. Seismol. Soc. Am.* **70**, 1395–1410.

Bufe, C. G. (1970). Frequency—magnitude variations during the 1970 Danville earthquake swarm. *Earthquake Notes* **41**, 3–7.

Bufe, C. G. (1976). The Anderson Reservoir seismic gap—induced aseismicity? *Eng. Geol., (Amsterdam)* **10**, 255–262.

Bufe, C. G., Pfluke, J. H., and Wesson, R. L. (1974). Premonitory vertical migration of microearthquakes in central California: Evidence of dilatancy biasing? *Geophys. Res. Lett.* **1**, 221–224.

Bufe, C. G., Harsh, P. W., and Burford, R. O. (1977). Steady-state seismic slip. A precise recurrence model. *Geophys. Res. Lett.* **4**, 91–94.

Buland, R. (1976). The mechanics of locating earthquakes. *Bull. Seismol. Soc. Am.* **66**, 173–187.

Bungum, H., and Husebye, E. S. (1974). Analysis of the operational capabilities for detection and location of seismic events at Norsar. *Bull. Seismol. Soc. Am.* **64**, 637–656.

Burdick, L. J., and Powell, C. (1980). Apparent velocity measurements for the lower mantle from a wide aperture array. *J. Geophys. Res.* **85**, 3845–3856.

Burridge, R., and Knopoff, L. (1964). Body force equivalents for seismic dislocations. *Bull. Seismol. Soc. Am.* **54**, 1875–1888.

Byerly, P. (1942). "Seismology." Prentice-Hall, Englewood Cliffs, New Jersey.

Cagnetti, V., and Pasquale, V. (1979). The earthquake sequence in Friuli, Italy, 1976. *Bull. Seismol. Soc. Am.* **69**, 1797–1818.

Caldwell, J. G., and Frohlich, C. (1975). Microearthquake study of the Alpine fault zone near Haast, South Island, New Zealand. *Bull. Seismol. Soc. Am.* **65**, 1097–1104.

Capon, J. (1973). Signal processing and frequency wavenumber spectrum analysis for a large aperture seismic array. *Methods Comput. Phys.* **13**, 1–59.

Caputo, M., Keilis-Borok, V., Oficerova, E., Ranzman, E., Rotwain, I., and Solovjeff, A. (1980). Pattern recognition of earthquake-prone areas in Italy. *Phys. Earth Planet. Inter.* **21**, 305–320.

Carder, D. S. (1945). Seismic investigations in the Boulder Dam area, 1940 to 1944, and the influence of reservoir loading on local earthquake activity. *Bull. Seismol. Soc. Am.* **35**, 175–192.

Carder, D. S. (1970). Reservoir loading and local earthquakes. *Geol. Soc. Am., Eng. Geol. Case Hist.* **8**, 51–61.

Carlson, R., Kanamori, H., and McNally, K. (1979). A survey of microearthquake activity along the San Andreas fault from Carrizo Plains to Lake Hughes. *Bull. Seismol. Soc. Am.* **69**, 177–186.

Carmichael, D., Carpenter, G., Hubbard, A., McCamy, K., and McDonald, W. (1973). A recording ocean bottom seismograph. *J. Geophys. Res.* **78**, 8748–8750.

Carver, D., and Henrisey, R. (1978). Preliminary report on the aftershocks of the June 20, 1978, Thessaloniki, Greece, earthquake. *Geol. Surv. Open-File Rep. (U.S.)* **78-1099**, 1–11.

Casten, U., and Cete, A. (1980). Induced seismicity in the mining industry ot the Ruhr coal field. *Glueckauf-Forschungsh.* **41**, 12–16 (in German).

Cerveny, V., and Hron, F. (1980). The ray series method and dynamic ray tracing system for three dimensional inhomogeneous media. *Bull. Seismol. Soc. Am.* **70**, 47–77.

Cerveny, V., Molotkov, I. A., and Psencik, I. (1977). "Ray Method in Seismology." Univ. Karlova Press, Prague.

Chambers, J. M. (1977). "Computational Methods for Data Analysis." Wiley, New York.

Chander, R. (1975). On tracing seismic rays with specified end points. *J. Geophys.* **41**, 173–177.

Chandra, U. (1971). Combination of P and S data for the determination of earthquake focal mechanism. *Bull. Seismol. Soc. Am.* **61**, 1655–1673.

Chang, C. C., Wei, K. Y., and Sung, L. Y. (1974). Probability of the times of earthquake occurrence (II). *Acta Geophys. Sin.* **17**, 200–208 (in Chinese with English abstract).

Chatelain, J. L., Roecker, S. W., Hatzfeld, D., and Molnar, P. (1980). Microearthquake seismicity and fault plane solutions in the Hindu Kush region and their tectonic implications. *J. Geophys. Res.* **85**, 1365–1387.

Cheatum, C., and Combs, J. (1973). Microearthquake study of the San Jacinto Valley, Riverside County, California. *Stanford Univ. Publ., Geol. Sci.* **13**, 1–10.

Chin, Y., Chao, Y., Chen, Y., Yen, C. C., and Cho, Y. J. (1978). A characteristic feature of the dislocation model of the foreshocks of the Haicheng earthquake, Liaoning Province. *Chinese Geophys.* **1**, 55–65.

Chou, C. W., and Booker, J. R. (1979). A Backus-Gilbert approach to inversion of travel time data for three dimensional velocity structure. *Geophys. J. R. Astron. Soc.* **59**, 325–344.

Chou, C. W., and Crosson, R. S. (1978). Seismic P velocity monitoring from mining explosions near Centralia, Washington. *Geophys. Res. Lett.* **5**, 97–100.

Claerbout, J. F. (1976). "Fundamentals of Geophysical Data Processing." McGraw-Hill, New York.

Cleary, J. R., Wright, C., and Muirhead, K. J. (1968). The effects of local structure upon measurements of the travel time gradient at the Warramunga seismic array. *Geophys. J. R. Astron. Soc.* **16**, 21–29.

Clymer, R. W. (1980). High-precision travel-time monitoring with seismic reflection techniques. Ph.D. Thesis, University of California, Berkeley.

Cockerham, R. S., and Ellsworth, W. L. (1979). Three-dimensional large-scale mantle structure in central California. *Trans. Am. Geophys. Union* **60**, 875.

Cockerham, R. S., Lester, F. W., and Ellsworth, W. L. (1980). A preliminary report on the Livermore Valley earthquake sequence January 24-February 26, 1980. *Geol. Surv. Open-File Rep. (U.S.)* **80-714**, 1–45.

Combs, J., and Hadley, D. (1977). Microearthquake investigation of the Mesa geothermal anomaly, Imperial Valley, California. *Geophysics* **42**, 17–33.

Combs, J., and Rotstein, Y. (1976). Microearthquake studies at the Coso geothermal area, China Lake, California. *Proc. U.N. Symp. Dev. Use Geotherm. Resour., 2nd, 1975* Vol. 2, pp. 909–912.

Comninakis, P., Drakopoulos, J., Moumoulidis, G., and Papazachos, B. (1968). Foreshock and aftershock sequences of the Cremasta earthquake and their relation to waterloading of the Cremasta artificial lake. *Ann. Geofis.* **21**, 39–71.

Conant, D. A. (1972). A microearthquake survey of geothermal areas in Iceland, 1970. *Earthquake Notes* **43**, 19–32.

Cook, N. G. W. (1963). The seismic location of rockbursts. *In* "Proceedings of the Fifth Rock Mechanics Symposium," pp. 493–516. Pergamon, Oxford.

Cook, N. G. W. (1976). Seismicity associated with mining. *Eng. Geol. (Amsterdam)* **10**, 99–122.

Corbishley, D. J. (1970). Structure under seismic arrays. *Geophys. J. R. Astron. Soc.* **21**, 415–425.

Courant, R., and John, F. (1965). "Introduction to Calculus and Analysis," Vol. 1. Wiley (Interscience), New York.

Courant, R., and John, F. (1974). "Introduction to Calculus and Analysis," Vol. 2. Wiley (Interscience), New York.

Cox, D. R., and Lewis, P. A. W. (1966). "The Statistical Analysis of Series of Events." Methuen, London.

Cramer, C. H. (1976). Teleseismic residuals prior to the November 28, 1974, Thanksgiving Day earthquake near Hollister, California. *Bull. Seismol. Soc. Am.* **66**, 1233–1248.

Cramer, C. H., and Kovach, R. L. (1974). A search for teleseismic travel-time anomalies along the San Andreas fault zone. *Geophys. Res. Lett.* **1**, 90–92.

Cramer, C. H., Bufe, C. G., and Morrison, P. W. (1977). P wave travel-time variations before the August 1, 1975 Oroville, California earthquake. *Bull. Seismol. Soc. Am.* **67**, 9–26.

Cramer, C. H., Toppozada, T. R., and Parke, D. L. (1978). Seismicity of the Foothills fault system of the Sierra Nevada between Folsom and Oroville, California. *Bull. Seismol. Soc. Am.* **68**, 245–249.

Crampin, S. (1970). A method for the location of near seismic events using travel-times along ray paths. *Geophys. J. R. Astron. Soc.* **21**, 535–539.

Crampin, S. (1978). Seismic-wave propagation through a cracked solid: Polarization as a possible dilatancy diagnostic. *Geophys. J. R. Astron. Soc.* **53**, 467–496.

Crampin, S., and Fyfe, C. J. (1974). Automatic analysis of tape recordings from seismic networks. *Geophys. J. R. Astron. Soc.* **39**, 155–168.

Crampin, S., and McGonigle, R. (1981). The variation of delays in stress-induced anisotropic polarization anomalies. *Geophys. J. R. Astron. Soc.* **64**, 115–131.

Crampin, S., and Ucer, S. B. (1975). The seismicity of the Marmara Sea region of Turkey. *Geophys. J. R. Astron. Soc.* **40**, 269–288.

Crosson, R. S. (1972). Small earthquakes, structure, and tectonics of the Puget Sound region. *Bull. Seismol. Soc. Am.* **62**, 1133–1171.

Crosson, R. S. (1976a). Crustal structure modeling of earthquake data. Part 1. Simultaneous least squares estimation of hypocenter and velocity parameters. *J. Geophys. Res.* **81**, 3036–3046.

Crosson, R. S. (1976b). Crustal structure modeling of earthquake data. Part 2. Velocity structures of the Puget Sound region, Washington. *J. Geophys. Res.* **81**, 3047–3053.

Crosson, R. S., and Koyanagi, R. Y. (1979). Seismic velocity structure below the island of Hawaii from earthquake data. *J. Geophys. Res.* **84**, 2331–2342.

Crosson, R. S., Endo, E. T., Malone, S. D., Noson, L. J., and Weaver, C. S. (1980). Eruption of Mt. St. Helens: Seismology. *Nature (London)* **285**, 529–531.

Dahlquist, G., and Bjorck, A. (1974). "Numerical Methods." Prentice-Hall, Englewood Cliffs, New Jersey.

Delhaye, A., and Santoire, J. P. (1977a). Seismic activity in the Eguzon region (Indre) recorded by the L.D.G. network in April 1977. *Rapp. CEA/LDG/TDG* No. 8/77, pp. 1–8.

Delhaye, A., and Santoire, J. P. (1977b). Seismic activity in the Cosne d'Allier region (Allier) recorded by the L.D.G. network in May 1977. *Rapp. CEA/LDG/TDG* No. 9/77, pp. 1–19.

Del Pezzo, E., Guerra, I., Lo Bascio, A., Luongo, G., Nappi, G., and Scarpa, R. (1975). Microtremors and volcanic explosions at Stromboli. Part 2. *Bull. Volcanol.* **38**, 1023–1036.

Dennis, J. E., Gay, D. M., and Welsch, R. E. (1979). An adaptive nonlinear least-squares algorithm. *Cornell Univ.* **TR77-321.**

DeNoyer, J. (1964). High frequency microearthquakes recorded at Quetta, Pakistan. *Bull. Seismol. Soc. Am.* **54**, 2133–2139.

Dewey, J. W. (1971). Seismicity studies with the method of joint hypocenter determination. Ph.D. Thesis, University of California, Berkeley.

Dey-Sarkar, S. K., and Chapman, C. H. (1978). A simple method for the computation of body-wave seismograms. *Bull. Seismol. Soc. Am.* **68**, 1577–1593.

Dillinger, W. H., Pope, A. J., and Harding, S. T. (1971). The determination of focal mechanisms using P and S wave data. *NOAA Tech. Rep.* **NOS 44**, 1–56.

Douglas, A. (1967). Joint epicentre determination. *Nature (London)* **215**, 47–48.

Douglas, B. M., and Ryall, A. (1972). Spectral characteristics and stress drop for microearthquakes near Fairview Peak, Nevada. *J. Geophys. Res.* **77**, 351–359.

Douglas, B. M., Ryall, A., and Williams, R. (1970). Spectral characteristics of central Nevada microearthquakes. *Bull. Seismol. Soc. Am.* **60**, 1547–1559.

Draper, N. R., and Smith, H. (1966). "Applied Regression Analysis." Wiley, New York.

Duda, S. J., and Nuttli, O. W. (1974). Earthquake magnitude scales. *Geophys. Surv.* **1**, 429–458.

Dunphy, G. J. (1972). Seismic activity of the Kerr Dam—S. W. Flathead Lake area, Montana. *NOAA Tech. Rep.* **ERL236-ESI21**, 59–61.

Eaton, J. P. (1962). Crustal structure and volcanism in Hawaii. *Geophys. Monogr., Am. Geophys. Union*, **6**, 13–29.

Eaton, J. P. (1969). HYPOLAYR, a computer program for determining hypocenters of local earthquakes in an earth consisting of uniform flat layers over a half space. *Geol. Surv. Open-File Rep. (U.S.)* 155.

Eaton, J. P. (1976). Tests of the standard (30 hz) NCER FM multiplex telemetry system, augmented by two timing channels and a compensation reference signal, used to record multiplexed seismic network data on magnetic tape. *Geol. Surv. Open-File Rep. (U.S.)* **76-374**, 1–61.

Eaton, J. P. (1977). Frequency response of the USGS short period telemetered seismic system and its suitability for network studies of local earthquakes. *Geol. Surv. Open-File Rep. (U.S.)* **77-844**, 1–45.

Eaton, J. P., and Van Schaack, J. R. (1977). Factors limiting the sensitivity and dynamic range of a seismic system employing analog magnetic tape recording and a seismic amplifier with adjustable gain settings and several output levels. *Geol. Surv. Open-File Rep. (U.S.)* **77-224**, 1–14.

Eaton, J. P., Lee, W. H. K., and Pakiser, L. C. (1970a). Use of microearthquakes in the study of the mechanics of earthquake generation along the San Andreas fault in central California. *Tectonophysics* **9**, 259–282.

Eaton, J. P., O'Neill, M. E., and Murdock, J. N. (1970b). Aftershocks of the 1966 Parkfield—Cholame, California, earthquake: A detailed study. *Bull. Seismol. Soc. Am.* **60**, 1151–1197.

Eckart, C., and Young, G. (1939). A principal axis transformation for non-Hermitian matrices. *Am. Math. Soc. Bull.* **45**, 118–121.

Einarsson, P., Klein, F. W., and Bjornsson, S. (1977). The Borgarfjordur earthquakes of 1974 in west Iceland. *Bull. Seismol. Soc. Am.* **67**, 187–208.

Eliseevnin, V. A. (1965). Analysis of rays propagating in an inhomogeneous medium. *Sov. Phys. Acoust. (Engl. Transl.)* **10**, 242–245.

Ellis, R. M., Dragert, H., and Ozard, J. M. (1976). Seismic activity in the McNaughton Lake area, Canada. *Eng. Geol. (Amsterdam)* **10**, 227–238.

Ellsworth, W. L. (1975). Bear Valley, California, earthquake sequence of February to March 1972. *Bull. Seismol. Soc. Am.* **65**, 483–506.

Ellsworth, W. L., and Koyanagi, R. Y. (1977). Three-dimensional crust and mantle structure of Kilauea Volcano, Hawaii. *J. Geophys. Res.* **82**, 5379–5394.

Engdahl, E. R. (1973). Relocation of intermediate depth earthquakes in the central Aleutians by seismic ray tracing. *Nature (London)* **245**, 23–25.

Engdahl, E. R. (1975). Effects of plate structure and dilatancy on relative teleseismic P wave residuals. *Geophys. Res. Lett.* **2**, 420–422.

Engdahl, E. R., and Gunst, R. H. (1966). Use of a high speed computer for the preliminary determination of earthquake hypocenters. *Bull. Seismol. Soc. Am.* **56**, 325–336.

Engdahl, E. R., and Kisslinger, C. (1977). Seismological precursors to a magnitude 5 earthquake in the central Aleutian Islands. *J. Phys. Earth* **25S**, 243–250.

Engdahl, E. R., and Lee, W. H. K. (1976). Relocation of local earthquakes by seismic ray tracing. *J. Geophys. Res.* **81**, 4400–4406.

Espinosa, A. F., Sutton, G. H., and Miller, H. J. (1962). A transient technique for seismograph calibration. *Bull. Seismol. Soc. Am.* **52**, 767–779.

Estill, R. E., and Odegard, M. E. (1978). Hawaiian Ridge seismicity from the Makapuu ocean-bottom seismograph. *Geophys. Res. Lett.* **5**, 485–486.

Eterno, J. S., Burns, D. S., Frier, L. J., and Buck, S. W. (1974). "Special Event Detection for an Unattended Seismic Observatory," Rep. No. R-765. Charles Stark Draper Lab., Massachusetts Institute of Technology, Cambridge.

Evison, F. F. (1975). Determination of precursory velocity anomalies in New Zealand from observatory data on local earthquakes. *Geophys. J. R. Astron. Soc.* **43**, 957–972.

Evison, F. F. (1977). The precursory earthquake swarm. *Phys. Earth Planet. Inter.* **15**, 19–23.

Evison, F. F., Robinson, R., and Arabasz, W. J. (1976). Microearthquakes, geothermal activity, and structure, central North Island. *N. Z. J. Geol. Geophys.* **19**, 625–637.

Fedotov, S. A. (1965). On regularities in distribution of strong earthquakes of Kamchatka, Kurile Islands and northeastern Japan. *Tr. Inst. Fiz. Zemli, Akad. Nauk SSSR* **36**, 66–93.

Fedotov, S. A. (1968). The seismic cycle, quantitative seismic zoning and long term seismic forecasting. *In* "Seismic Zoning of the USSR" (S. V. Medvedev, ed.), pp. 121–150. Science Press, Moscow (Engl. transl., 1976, pp. 133–166).

Fedotov, S. A., Bagdasarova, A. M., Kuzin, I. P., and Tarakanov, R. Z. (1969). Seismicity in the south of the Kurile Island Arc. The disastrous Etorofu earthquake of 6 November 1958 and the seismic regime of the southern Kurile zone before and after it. *In* "Earthquakes and the Deep Structure of the South Kurile Island Arc" (S. A. Fedotov, ed.), Science Press, Moscow (Engl. transl., 1971, pp. 58–121).

Fedotov, S. A., Gusev, A. A., and Boldyrev, S. A. (1972). Progress of earthquake prediction in Kamchatka. *Tectonophysics* **14**, 279–286.

Feng, D. Y. (1975). Anomalous variations of seismic velocity ratio before the Yongshan—Daguan earthquake on May 11, 1974. *Acta Geophys. Sin.* **18**, 235–239 (in Chinese with English abstract).

Feng, D. Y., Wang, Z. Y., Gu, J. P., Sheng, G. Y., and Li, K. L. (1980). Anomalous variations of seismic velocity ratio before the Song-pan—Pingwu Earthquake (M = 7.2) of 1976. *Acta Seismol. Sin.* **2**, 54–64 (in Chinese with English abstract).

Feng, R. (1977). On the variations of the velocity ratio before and after the Xinfengjiang Reservoir impounding earthquake of M = 6.1. *Acta Geophys. Sin.* **20**, 211–221 (in Chinese with English abstract).

Feng, R., Pang, Q. Y., Fu, Z. X., Zheng, J. Z., Sun, C. C., and Li, B. X. (1976). Variations of $V_p/V_s$ before and after the Haicheng earthquake of 1975. *Acta Geophys. Sin.* **19**, 295–305 (in Chinese with English abstract).

Fitch, T. J., and Rynn, J. M. W. (1976). Inversion for $V_p/V_s$ in shallow source regions. *Geophys. J. R. Astron. Soc.* **44**, 253–267.

Fletcher, J. B. (1980). Spectra from high dynamic range digital recordings of Oroville, California aftershocks and their source parameters. *Bull. Seismol. Soc. Am.* **70**, 735–755.

Fletcher, J. B., and Sykes, L. R. (1977). Earthquakes related to hydraulic mining and natural seismic activity in western New York state. *J. Geophys. Res.* **82**, 3767–3780.

Fletcher, R. (1980). "Practical Methods of Optimization," Vol. 1. Wiley, New York.

Flinn, E. A. (1960). Local earthquake location with an electronic computer. *Bull. Seismol. Soc. Am.* **50**, 467–470.

Forsythe, G. E., and Moler, C. B. (1967). "Computer Solution of Linear Algebraic Systems." Prentice-Hall, Englewood Cliffs, New Jersey.

Forsythe, G. E., Malcolm, M. A., and Moler, C. B. (1977). "Computer Methods for Mathematical Computations." Prentice-Hall, Englewood Cliffs, New Jersey.

Francis, T. J. G. (1977). Ocean bottom seismographs. *Earthquake Inf. Bull.* **9**, 9–15.

Francis, T. J. G., and Porter, I. T. (1972). Microearthquake survey of the Mid-Atlantic Ridge. *Nature (London)* **240**, 547–549.

Francis, T. J. G., Porter, I. T., Lane, R. D., Osborne, P. J., Pooley, J. E., and Tomkins, P. K. (1975). Ocean bottom seismograph. *Mar. Geophys. Res.* **2**, 195–213.

Francis, T. J. G., Porter, I. T., and McGrath, J. R. (1977). Ocean-bottom seismograph observations on the Mid-Atlantic Ridge near lat. 37 degrees N. *Geol. Soc. Am. Bull.* **88**, 664–677.

Francis, T. J. G., Porter, I. T., and Lilwall, R. C. (1978). Microearthquakes near the eastern end of St. Paul's fracture zone. *Geophys. J. R. Astron. Soc.* **53**, 201–217.

Frechet, J., and Pavoni, N. (1979). Seismicity study of the Brianconnais zone between Pelvoux and Argentera, western Alps, using a net of portable seismic stations. *Eclogae Geol. Helv.* **72/3**, 763–779 (in French with English abstract).

Freidline, R. A., Smith, R. B., and Blackwell, D. D. (1976). Seismicity and contemporary tectonics of the Helena, Montana area. *Bull. Seismol. Soc. Am.* **66**, 81–95.

Fuchs, K., Bonjer, K. P., Bock, G., Cornea, I., Radu, C., Enescu, D., Jianu, D., Nourescue, A., Merkler, G., Moldoveanu, T., and Tudorache, G. (1979). The Romanian earthquake of March 4, 1977 Part II. Aftershocks and migration of seismic activity. *Tectonophysics* **53**, 225–247.

Fung, Y. C. (1969). "A First Course in Continuum Mechanics." Prentice-Hall, Englewood Cliffs, New Jersey.

Gaiser, J. E. (1977). Origin corrected travel-time variations measured across the Wasatch Front. M.S. Thesis, University of Utah, Salt Lake City.

Gamburtsev, G. A., and Gal'perin, Y. I. (1960a). Results of investigations of weak local earthquakes in southwestern Turkmenia with the aid of the correlation method. *In* "G. A. Gamburtsev, Selected Papers," pp. 390–393. Press Acad. Sci. USSR, Moscow (in Russian).

Gamburtsev, G. A., and Gal'perin, Y. I. (1960b). Experience gathered in research on weak earthquakes of the Khaitsk epicentral zone of the Tadzhik Socialist Soviet Republic. *In* "G. A. Gamburtsev, Selected Papers," pp. 400–426. Press Acad. Sci. USSR, Moscow (in Russian).

Gane, P. G., Hales, A. L., and Oliver, H. A. (1946). A seismic investigation of the Witwatersrand earth tremors. *Bull. Seismol. Soc. Am.* **36**, 49–80.

Gane, P. G., Logie, H. J., and Stephen, J. H. (1949). Triggered telerecording seismic equipment. *Bull. Seismol. Soc. Am.* **39**, 117–143.

Gane, P. G., Seligman, P., and Stephen, J. H. (1952). Focal depths of Witwatersrand tremors. *Bull. Seismol. Soc. Am.* **42**, 239–250.

Gane, P. G., Atkins, A. R., Sellschop, P. F., and Seligman, P. (1956). Crustal structure in the Transvaal. *Bull. Seismol. Soc. Am.* **46**, 293–316.

Garmany, J., Orcutt, J. A., and Parker, R. L. (1979). Travel time inversion: A geometrical approach. *J. Geophys. Res.* **84**, 3615–3622.

Garza, T., and Lomnitz, C. (1978). The Oaxaca gap: A case history. *Geol. Surv. Open-File Rep. (U.S.)* **78-943**, 173–188.

Gear, W. C. (1971). "Numerical Initial Value Problems in Ordinary Differential Equations." Prentice-Hall, Englewood Cliffs, New Jersey.

Gebrande, H., Miller, H., and Schmedes, E. (1977). Digital registrations of aftershocks of the Friuli earthquake 1976. *Publ. Inst. Geophys. Pol. Acad. Sc.* **A-6(117)**, 75–84.

Geiger, L. (1912). Probability method for the determination of earthquake epicenters from the arrival time only. *Bull. St. Louis Univ.* **8**, 60–71.

Gelfand, I. M., and Fomin, S. V. (1963). "Calculus of Variations." Prentice-Hall, Englewood Cliffs, New Jersey.

Gelfand, I. M., Guberman, S. I., Izvekova, M. L., Keilis-Borok, V. I., and Ranzman, E. J. (1972). Criteria of high seismicity, determined by pattern recognition. *Tectonophysics* **13**, 415–422.

Gelfand, I. M., Guberman, S. A., Keilis-Borok, V. I., Knopoff, L., Press, F., Ranzman, E. Y., Rotwain, I. M., and Sadovsky, A. M. (1976). Pattern recognition applied to earthquake epicenters in California. *Phys. Earth Planet. Inter.* **11**, 227–283.

Gerver, M., and Markushevich, V. (1966). Determination of a seismic wave velocity from the travel-time curve. *Geophys. J. R. Astron. Soc.* **11**, 165–173.

Gerver, M., and Markushevich, V. (1967). On the characteristic properties of travel-time curves. *Geophys. J. R. Astron. Soc.* **13**, 241–246.

Gill, P. E., and Murray, W. (1978). Algorithms for the solution of the nonlinear least-squares problem. *SIAM J. Numer. Anal.* **15**, 977–992.

Gill, P. E., Murray, W., and Wright, M. H. (1981). "Practical Optimization." Academic Press, London.

Gilpin, B., and Lee, T. C. (1978). A microearthquake study in the Salton Sea geothermal area, California. *Bull. Seismol. Soc. Am.* **68**, 441–450.

Golub, G. H., and Reinsch, C. (1970). Singular value decomposition and least squares solutions. *Numer. Math.* **14**, 403–420.

Gough, D. I., and Gough, W. I. (1970). Load-induced earthquakes at Lake Kariba. 2. *Geophys. J. R. Astron. Soc.* **21**, 79–101.

Green, R. (1973). A portable multi-channel seismic recorder and a data processing system. *Bull. Seismol. Soc. Am.* **63**, 423–431.

Green, R. W. E., and Bloch, S. (1971). The Ceres, South Africa, earthquake of September 29, 1969. Part I. Report on some aftershocks. *Bull. Seismol. Soc. Am.* **61**, 851–859.

Griscom, M., and Arabasz, W. J. (1979). Local magnitude ($M_L$) in the Wasatch Front and Utah region: Wood-Anderson calibration, coda duration estimates of $M_L$, and $M_L$ versus $m_b$. *In* "Earthquake Studies in Utah 1850 to 1978" (W. J. Arabasz, R. B. Smith, and W. D. Richins, eds.), pp. 433–443, University of Utah.

Guha, S. K., Gosavi, P. D., Padale, J. G., and Marwadi, S. C. (1971). An earthquake cluster at Koyna. *Bull. Seismol. Soc. Am.* **61**, 297–315.

Guha, S. K., Gosavi, P. D., Agarwal, B. N. P., Padale, J. G., and Marwadi, S. C. (1974). Case histories of some artificial crustal disturbances. *Eng. Geol. (Amsterdam)* **8**, 59–77.

Gumper, F. J., and Scholz, C. H. (1971). Microseismicity and tectonics of the Nevada seismic zone. *Bull. Seismol. Soc. Am.* **61**, 1413–1432.

Gupta, H. K., and Rastogi, B. K. (1976). "Dams and Earthquakes." Elsevier, Amsterdam.

Gutenberg, B. (1945a). Amplitudes of surface waves and magnitudes of shallow earthquakes. *Bull. Seismol. Soc. Am.* **35**, 3–12.

Gutenberg, B. (1945b). Amplitudes of P, PP, and S and magnitude of shallow earthquakes. *Bull. Seismol. Soc. Am.* **35**, 57–69.

Gutenberg, B. (1945c). Magnitude determination for deep focus earthquakes. *Bull. Seismol. Soc. Am.* **35**, 117–130.

Gutenberg, B., and Richter, C. F. (1941). Seismicity of the Earth. *Geol. Soc. Am., Spec. Pap.* **34**, 1–133.

Gutenberg, B., and Richter, C. F. (1956). Earthquake magnitude, intensity, energy, and acceleration (second paper). *Bull. Seismol. Soc. Am.* **46**, 105–145.

Hadley, D., and Combs, J. (1974). Microearthquake distribution and mechanisms of faulting in the Fontana—San Bernardino area of southern California. *Bull. Seismol. Soc. Am.* **64**, 1477–1499.

Hadley, D., and Kanamori, H. (1977). Seismic structure of the Transverse Ranges, California. *Geol. Soc. Am. Bull.* **88**, 1469–1478.

Haessler, H., Hoang-Trong, P., Schick, R., Schneider, G., and Strobach, K. (1980). The September 3, 1978, Swabian Jura earthquake. *Tectonophysics* **68**, 1–14.

Hagiwara, T. (1964). Brief description of the project proposed by the earthquake prediction research group of Japan. *Proc. U.S.-Japan Conf. Res. Relat. Earthquake Prediction Probl., 1964* pp. 10–12.

Hagiwara, T., and Iwata, T. (1968). Summary of the seismographic observation of Matsushiro swarm earthquakes. *Bull. Earthquake Res. Inst., Univ. Tokyo* **46**, 485–515.

Hagiwara, T., and Ohtake, M. (1972). Seismic activity associated with the filling of the reservoir behind the Kurobe Dam, Japan, 1963–1970. *Tectonophysics* **15**, 241–254.

Hagiwara, T., Karakama, I., Kayano, I., and Kaminuma, K. (1963). Foreshocks, aftershocks and an earthquake swarm detected by the microearthquake observation. *Bull. Earthquake Res. Inst., Univ. Tokyo* **41**, 659–680.

Hamada, K. (1968). Ultra microearthquakes in the area around Matsushiro. *Bull. Earthquake Res. Inst., Univ. Tokyo* **46**, 271–318.

Hamaguchi, H., Hasegawa, A., and Kasahara, M. (1970). Microearthquake activity excited by the Tokachi-Oki earthquake of 1968. *J. Seismol. Soc. Japan* **23**, 72–81 (in Japanese with English abstract).

Hamaguchi, H., Watanabe, H., Takano, K., Gumper, F. J., and Boucher, G. (1973). Microearthquake survey in northeastern Honshu, Japan. *J. Phys. Earth* **21**, 1–18.

Hamilton, R. M. (1967). Mean magnitude of an earthquake sequence. *Bull. Seismol. Soc. Am.* **57**, 1115–1116.

Hamilton, R. M. (1970). Time-term analysis of explosion data from the vicinity of the Borrego Mountain, California, earthquake of 9 April 1968. *Bull. Seismol. Soc. Am.* **60**, 367–381.

Hamilton, R. M. (1972). Aftershocks of the Borrego Mountain earthquake from April 12 to June 12, 1968. *Geol. Surv. Prof. Pap. (U.S.)* **787**, 31–54.

Hamilton, R. M., and Healy, J. H. (1969). Aftershocks of the Benham nuclear explosion. *Bull. Seismol. Soc. Am.* **59**, 2271–2281.

Hamilton, R. M., and Muffler, L. J. P. (1972). Microearthquakes at The Geysers geothermal area, California. *J. Geophys. Res.* **77**, 2081–2086.

Hamilton, R. M., Smith, B. E., Fischer, F. G., and Papanek, P. J. (1971). Seismicity of the Pahute Mesa area, Nevada test site: 8 December 1968 through 31 December 1970. *Geol. Surv. Spec. Stud. (U.S.)* **89**, 1–170.

Hamming, R. W. (1962). "Numerical Methods for Scientists and Engineers." McGraw-Hill, New York.

Hanks, T. C., and Kanamori, H. (1979). A moment-magnitude scale. *J. Geophys. Res.* **84**, 2348–2350.

Hanks, T. C., and Thatcher, W. (1972). A graphical representation of seismic source parameters. *J. Geophys. Res.* **77**, 4393–4405.

Hanks, T. C., and Wyss, M. (1972). The use of body wave spectra in the determination of seismic source parameters. *Bull. Seismol. Soc. Am.* **62**, 561–589.

Hanks, T. C., Jordan, T. H., and Minster, J. B. (1971). Precise locations of aftershocks of the San Fernando earthquake—2300 (GMT) February 10-1700 February 11, 1971. *Geol. Surv. Prof. Pap. (U.S.)* **733**, 21–23.

Hardy, H. R., and Leighton, F. W., ed. (1977). "Proceedings, First Conference on Acoustic Emission/Microseismic Activity in Geologic Structures and Material." Trans Tech, Clausthal, Germany.

Hardy, H. R., and Leighton, F. W., ed. (1980). "Proceedings, Second Conference on Acoustic Emission/Microseismic Activity in Geologic Structures and Materials." Trans Tech, Clausthal, Germany.

Harjes, H. P., and Seidl, D. (1978). Digital recording and analysis of broad band seismic data at the Graefenberg (GRF) array. *J. Geophys.* **44**, 511–523.

Hasegawa, A., Hasegawa, T., and Hori, S. (1975). Premonitory variation in seismic velocity related to the southeastern Akita earthquake of 1970. *J. Phys. Earth* **23**, 189–203.

Hayakawa, M. (1950). Time variation of the seismic wave velocity (preliminary report). *Japan Geol. Surv. Rep., Spec. No.* pp. 7–24.

Hayman, R. B., and Shannon, W. E. (1979). Seismological service of Canada: Instrumentation and data processing. *Phys. Earth Planet. Inter.* **18**, 95–104.

Healy, J. H., and O'Neill, M. E. (1977). Calibration of seismographic systems: USGS stations in the central California network. *Geol. Surv. Open-File Rep. (U.S.)* **77-736**, 1–176.

Healy, J. H., and Peake, L. G. (1975). Seismic velocity structure along a section of the San Andreas fault near Bear Valley, California. *Bull. Seismol. Soc. Am.* **65**, 1177–1197.

Healy, J. H., Rubey, W. W., Griggs, D. T., and Raleigh, C. B. (1968). The Denver earthquakes. *Science* **161**, 1301–1310.

Hedayati, A., Brander, J. L., and Berberian, M. (1976). Microearthquake survey of Tehran region, Iran. *Bull. Seismol. Soc. Am.* **66**, 1713–1725.

Hedayati, A., Brander, J. L., and Mason, R. G. (1978). Instances of premonitory crustal velocity ratio changes in Iran. *Tectonophysics* **44**, T1–T6.

Helmberger, D. V., and Johnson, L. R. (1977). Source parameters of moderate size earthquakes and the importance of receiver crustal structure in interpreting observations of local earthquakes. *Bull. Seismol. Soc. Am.* **67**, 301–313.

Henyey, T. L., Teng, T. L., McRaney, J. K., and Manov, D. V. (1979). A sea-floor seismic monitoring network around an off shore oilfield platform and recording of the August 13, 1978 Santa Barbara earthquake. *Proc.—Annu. Offshore Technol. Conf.* **11**, 2219–2223.

Herrmann, R. B. (1975). The use of duration as a measure of seismic moment and magnitude. *Bull. Seismol. Soc. Am.* **65**, 899–913.

Herrmann, R. B. (1979). FASTHYPO—a hypocenter location program. *Earthquake Notes* **50**, 25–37.

Herrmann, R. B. (1980). Q estimates using the coda of local earthquakes. *Bull. Seismol. Soc. Am.* **70**, 447–468.

Hileman, J. A. (1979). Inversion of phase times for hypocenters and shallow crustal velocities, Mojave Desert, California. *Bull. Seismol. Soc. Am.* **69**, 387–396.

Hirahara, K. (1977). A large scale three-dimensional seismic structure under the Japan Islands and the Sea of Japan. *J. Phys. Earth* **25**, 393–417.

Hirahara, K., and Mikumo, T. (1980). Three-dimensional seismic structure of subducting lithospheric plates under the Japan Islands. *Phys. Earth Planet. Inter.* **21**, 109–119.

Hirota, T. (1977). Observation of microearthquakes in the region of Noboribetsu Hot Spring, Iburi Province. *Hokkaido Geol. Surv. Rep.* **49**, 101–106 (in Japanese).

Honda, H. (1962). Earthquake mechanism and seismic waves. *J. Phys. Earth* **10**, 1–97.

Honda, H., and Emura, K. (1958). Some charts for studying the mechanism of earthquake. *Sci. Rep. Tohoku Univ., 5th Ser. Geophys.* **9**, 113–115.

Hori, M. (1973). Determination of earthquake magnitude of the local and near earthquake by the Dodaira Microearthquake Observatory. *Bull. Earthquake Res. Inst., Univ. Tokyo* **10**, 1–4 (in Japanese with English abstract).

Hori, M., and Matumoto, H. (1967). Observation of ultra microearthquakes by seismometer array method in the vicinity of Wakayama, central Japan. *J. Seismol. Soc. Japan* **20**, 41–49 (in Japanese with English abstract).

Horie, A., and Shibuya, K. (1979). P-wave velocity structure down to 150 km in Kanto district—simultaneous determination of velocity structure, hypocenter parameters and station corrections by using inversion technique. *J. Seismol. Soc. Japan* **32**, 125–140 (in Japanese with English abstract).

Horner, R. B., Stevens, A. E., Hasegawa, H. S., and LeBlanc, G. (1978). Focal parameters of the July 12, 1975, Maniwaki, Quebec, earthquake—an example of interplate seismicity in eastern Canada. *Bull. Seismol. Soc. Am.* **68**, 619–640.

Horner, R. B., Wetmiller, R. J., and Hasegawa, H. S. (1979). The St. Donat, Quebec, earthquake sequence of February 18–23, 1978. *Can. J. Earth Sci.* **16**, 1892–1898.

Houck, S. T., Guerrero, J. D., Miller, A. E., and Lee, W. H. K. (1976). Handbook for USGS central California microearthquake network, 1969 to 1975. *Geol. Surv. Open-File Rep. (U.S.)* **76-282**, 1–241.

Howe, S., ed. (1976). NBS Time and Frequency Dissemination Services." Nat. Bur. Stand., Boulder, Colorado.

Ichikawa, M. (1980). Automatic processing system of seismograms in Japan Meteorological Agency. *Q. J. Seismol., Japan Meteorol. Agency* **44**, 15–34 (in Japanese with English abstract).

Ichikawa, M., Fujisawa, I., and Yoshida, H. (1980). System for earthquake parameter rapid determination and some results obtained. *Q. J. Seismol., Japan Meteorol. Agency* **44**, 35–85 (in Japanese with English abstract).

Iida, K. (1939). Observations sur les seismes enregistres par le microsismographe construit dernierement (2). *Bull. Earthquake Res. Inst., Univ. Tokyo* **17**, 741–782 (in Japanese with French abstract).

Iida, K. (1940). Observations sur les seismes enregistres par le microsismographe (3). *Bull. Earthquake Res. Inst., Univ. Tokyo* **18**, 575–674 (in Japanese with French abstract).

Ikami, A., Ankyu, T., and Aoki, H. (1972). Low seismic activity associated with the Atera fault, central Japan. *J. Seismol. Soc. Japan.* **25**, 232–242 (in Japanese with English abstract).

Imamura, A. (1929). On the chronic and acute earth tiltings in the Kii Peninsula. *Japan J. Astron. Geophys.* **7**, 31–45.

Imamura, A., Kodaira, T., and Imamura, H. (1932). The earthquake swarms of Nagusa and vicinity. *Bull. Earthquake Res. Inst., Univ. Tokyo* **10**, 636–648.

Isacks, B., and Oliver, J. (1964). Seismic waves with frequencies from 1 to 100 cycles per second recorded in a deep mine in northern New Jersey. *Bull. Seismol. Soc. Am.* **54**, 1941–1979.

Ishibashi, K., and Tsumura, K. (1971). Temporary observation of microearthquakes in the southern part of the Kanto district. *Bull. Earthquake Res. Inst., Univ. Tokyo* **49**, 97–113 (in Japanese with English abstract).

Ishida, M., and Kanamori, H. (1978). The foreshock activity of the 1971 San Fernando earthquake, California. *Bull. Seismol. Soc. Am.* **68**, 1265–1279.

Ishida, M., and Kanamori, H. (1980). Temporal variation of seismicity and spectrum of small earthquakes preceding the 1952 Kern County, California, earthquake. *Bull. Seismol. Soc. Am.* **70**, 509–527.

Ishimoto, M., and Iida, K. (1939). Observations sur les seismes enregistres par le microsismographe construit dernierement (1). *Bull. Earthquake Res. Inst., Univ. Tokyo* **17**, 443–478 (in Japanese with French abstract).

Iyer, H. M. (1975). Anomalous delays of teleseismic P waves in Yellowstone National Park. *Nature (London)* **253**, 425–427.

Iyer, H. M. (1979). Deep structure under Yellowstone Park, USA: A continental hot spot. *Tectonophysics* **56**, 165–197.

Iyer, H. M., and Hitchcock, T. (1976a). Seismic noise as a geothermal exploration tool: Techniques and results. *Proc. U.N. Symp. Dev. Use Geotherm. Resour., 2nd, 1975* Vol. 2, pp. 1075–1083.

Iyer, H. M., and Hitchcock, T. (1976b). Seismic noise survey in Long Valley, California. *J. Geophys. Res.* **81**, 821–840.

Iyer, H. M., and Stewart, R. M. (1977). Teleseismic technique to locate magma in the crust and upper mantle. *Bull.-Oreg., Dep. Geol. Miner. Ind.* **96**, 281–299.

Iyer, H. M., Oppenheimer, D. H., and Hitchcock, T. (1979). Abnormal P-wave delays in the Geyser—Clear Lake geothermal area. *Science* **204**, 495–497.

Iyer, H. M., Evans, J. R., Zandt, G., Stewart, R. M., Coakley, J. M., and Roloff, J. N. (1981). A deep magma body under the Yellowstone Caldera, Wyoming: Delineation using teleseismic P-wave residuals and tectonic interpretation. *Geol. Soc. Am. Bull.* **92**, 792-798, and 1471-1646.

Jackson, D. D. (1972). Interpretation of inaccurate, insufficient and inconsistent data. *Geophys. J. R. Astron. Soc.* **28**, 97–109.

Jackson, P. L. (1970). Digital simulation of seismic rays. Ph.D. Thesis, University of Michigan, Ann Arbor.

Jacob, K. H. (1970). Three-dimensional seismic ray tracing in a laterally heterogenous spherical earth. *J. Geophys. Res.* **75**, 6675–6689.

Jensen, E. G. (1976a). OES compensation and timing multiplexer. *Geol. Surv. Open-File Rep. (U.S.)* **76-385**, 1–10.

Jensen, E. G. (1976b). Automatic gain control system for telemetry. *Geol. Surv. Open-File Rep. (U.S.)* **76-820**, 1–9.

Jensen, E. G. (1977). Crystal VCO center frequency stabilizer. *Geol. Surv. Open-File Rep. (U.S.)* **77-184**, 1–9.

Johnson, C. E. (1979). I. CEDAR: An approach to the computer automation of short-period local seismic networks. II. Seismotectonics of the Imperial Valley of southern California. Ph.D. Thesis, California Institute of Technology, Pasadena.

Johnson, C. E., and Hadley, D. M. (1976). Tectonic implications of the Brawley earthquake swarm, Imperial Valley, California, January 1975. *Bull. Seismol. Soc. Am.* **66**, 1133–1144.

Johnson, C. E., and Hutton, L. K. (1981). The 15 October, 1979 Imperial Valley earthquake: A study of aftershocks and prior seismicity. *Geol. Surv. Prof. Pap. (U.S.)* (in press).

Johnson, L. R., and McEvilly, T. V. (1974). Near-field observations and source parameters of central California earthquakes. *Bull. Seismol. Soc. Am.* **64**, 1855–1886.

Johnson, S. H., and Jones, P. R. (1978). Microearthquakes located on the Blanco fracture zone with sonobuoy arrays. *J. Geophys. Res.* **83**, 255–261.

Johnson, T. L., Madrid, J., and Koczynski, T. (1976). A study of microseismicity in northern Baja California, Mexico. *Bull. Seismol. Soc. Am.* **66**, 1921–1929.

Johnston, A. C. (1978). Localized compressional velocity decrease precursory to the Kalapana, Hawaii, earthquake. *Science* **199**, 882–885.

Jones, L. M., and Molnar, P. (1979). Some characteristics of foreshocks and their possible relationship to earthquake prediction and premonitory slip on faults. *J. Geophys. Res.* **84**, 3596–3608.

Jones, P. R., and Johnson, S. H. (1978). Sonobuoy array measurements of active faulting on the Gorda Ridge. *J. Geophys. Res.* **83**, 3435–3440.

Julian, B. R. (1970). "Ray Tracing in Arbitrarily Heterogeneous Media," Tech. Note 1970-45. Lincoln Lab., Massachusetts Institute of Technology, Cambridge.

Julian, B. R., and Gubbins, D. (1977). Three-dimensional seismic ray tracing. *J. Geophys.* **43**, 95–113.

Jupp, D. L. B., and Vozoff, K. (1975). Stable iterative methods for the inversion of geophysical data. *Geophys. J. R. Astron. Soc.* **42**, 957–976.

Kagan, Y. Y., and Knopoff, L. (1980). Spatial distribution of earthquakes: the two-point correlation function. *Geophys. J. R. Astron. Soc.* 62, 303–320.

Kakimi, T., and Hasegawa, I. (1977). Observations of changes in seismic wave velocity in south Kanto district, south of Tokyo, by the explosion seismic method. *J. Phys. Earth* **25S**, 105–113.

Kaminuma, K. (1971). Microearthquakes observed at Syowa Station, Antarctica. *Japanese Antarctic Expedition Rep.* **40**, 65–73 (in Japanese with English abstract).

Kaminuma, K. (1976). Seismicity in Antarctica. *J. Phys. Earth* **24**, 381–395.

Kaminuma, K., Tsumura, K., Matumoto, H., and Karakama, I. (1970). Microseismic observation at Kobugahara, Tochigi prefecture—aftershock observations of the earthquake, August 13, 1969. *Bull. Earthquake Res. Inst., Univ. Tokyo* **48**, 53–63 (in Japanese with English abstract).

Kanamori, H. (1967). Upper mantle structure from apparent velocities of P waves recorded at Wakayama Microearthquake Observatory. *Bull. Earthquake Res. Inst., Univ. Tokyo* **45**, 657–678.

Kanamori, H. (1977). The energy release in great earthquakes. *J. Geophys. Res.* **82**, 2981–2987.

Kanamori, H. (1978a). Nature of seismic gaps and foreshocks. *Geol. Surv. Open-File Rep. (U.S.)* **78-943**, 319–334.

Kanamori, H. (1978b). Quantification of earthquakes. *Nature (London)* **271**, 411–414.

Kanamori, H., and Anderson, D. L. (1975). Theoretical basis of some empirical relations in seismology. *Bull. Seismol. Soc. Am.* **65**, 1073–1095.

Kanamori, H., and Chung, W. Y. (1974). Temporal changes in P wave velocity in southern California. *Tectonophysics* **23**, 67–78.

Kanamori, H., and Fuis, G. (1976). Variation of P wave velocity before and after the Galway Lake earthquake ($M_L = 5.2$) and the Goat Mountain earthquakes ($M_L = 4.7, 4.7$) in the Mojave Desert, California. *Bull. Seismol. Soc. Am.* **66**, 2017–2037.

Kanamori, H., and Hadley, D. (1975). Crustal structure and temporal velocity change in southern California. *Pure Appl. Geophys.* **113**, 257–280.

Kanasewich, E. R., Alpaslan, T., and Hron, F. (1973). The importance of S-wave precursors in shear-wave studies. *Bull. Seismol. Soc. Am.* **63**, 2167–2176.

Karakama, I., Tsumura, K., Takahashi, M., Ogino, I., and Sakai, K. (1974). Observation of the aftershocks of the Izu-Hanto-oki earthquake of 1974: Preliminary report of observations at Shinokamo, Matsuzaki & Okuno in the Izu Peninsula. *Bull. Earthquake Res. Inst., Univ. Tokyo* **14**, 55–67 (in Japanese with English abstract).

Karal, F. C., and Keller, J. B. (1959). Elastic wave propagation in homogeneous and inhomogeneous media. *J. Acoust. Soc. Am.* **31**, 694–705.

Kasahara, J., Koresawa, S., Tsumura, K., Nagumo, S., and Nakamura, I. (1973a). Aftershock observation of the earthquake of February 29, 1972 in the east off Hachijo-jima. *J. Seismol. Soc. Japan.* **26**, 305–315 (in Japanese with English abstract).

Kasahara, J., Koresawa, S., Nakamura, I., Tsumura, K., and Nagumo, S. (1973b). Foreshocks and aftershocks of an earthquake east of Hachijo-jima, December 4, 1972. *J. Seismol. Soc. Japan.* **26**, 326–335 (in Japanese with English abstract).

Kasahara, K. (1963). Computer program for a fault-plane solution. *Bull. Seismol. Soc. Am.* **53**, 1–13.

Kasper, J., and Hutchinson, C. (1979). Omega: Global navigation by VLF fix. *IEEE Spectrum* **16** (5), 59–63.

Kayano, I. (1968). Determination of origin times, epicenters and focal depths of aftershocks of the Niigata earthquake of June 16, 1964: A preliminary report of the cooperative

study of aftershocks of the Niigata earthquake. *Bull. Earthquake Res. Inst., Univ. Tokyo* **46**, 223–269.

Kayano, I., Kubota, S., and Takahashi, M. (1970). Microearthquake activity in the border region between Hiroshima and Shimane prefectures, western Japan. *Bull. Earthquake Res. Inst., Univ. Tokyo* **48**, 1069–1087.

Keilis-Borok, V. I., and Malinovskaya, L. N. (1964). One regularity in the occurrence of strong earthquakes. *J. Geophys. Res.* **69**, 3019–3024.

Keilis-Borok, V. I., Pisarenko, V. F., Pyatetskii-Shapiro, I. I., and Zhelankina, T. S. (1972). Computer determination of earthquake mechanism. *In* "Computational Seismology" (V. I. Keilis-Borok, ed.), pp. 32–45. Consultants Bureau, New York.

Keilis-Borok, V. I., Knopoff, L., Rotvain, I. M., and Sidorenko, T. M. (1980a). Bursts of seismicity as long term precursors of strong earthquakes. *J. Geophys. Res.* **85**, 803–811.

Keilis-Borok, V. I., Knopoff, L., and Allen, C. R. (1980b). Long-term premonitory seismicity in Tibet and the Himalayas. *J. Geophys. Res.* **85**, 813–820.

Kelleher, J. A. (1970). Space—time seismicity of the Alaska—Aleutian seismic zone. *J. Geophys. Res.* **75**, 5745–5756.

Kelleher, J. A. (1972). Rupture zones of large South American earthquakes and some predictions. *J. Geophys. Res.* **77**, 2087–2103.

Kelleher, J. A., and Savino, J. (1975). Distribution of seismicity before large strike-slip and thrust-type earthquakes. *J. Geophys. Res.* **80**, 260–271.

Kelleher, J. A., Sykes, L. R., and Oliver, J. (1973). Possible criteria for predicting earthquake locations and their application to major plate boundaries of the Pacific and the Caribbean. *J. Geophys. Res.* **78**, 2547–2585.

Keller, G. R., and Adams, H. E. (1976). A reconnaissance microearthquake survey of the San Luis Valley, southern Colorado. *Bull. Seismol. Soc. Am.* **66**, 345–347.

Keller, H. B. (1968). "Numerical Methods for Two Point Boundary Value Problems." Ginn (Blaisdell), Boston, Massachusetts.

Keller, H. B. (1976). "Numerical Solution of Two Point Boundary Value Problems." Soc. Ind. Appl. Math., Philadelphia, Pennsylvania.

Kieckhefer, R. M. (1977). Microseismicity in the vicinity of the Clarence fault, New Zealand. *N. Z. J. Geol. Geophys.* **20**, 165–177.

Kijko, A. (1978). Methods of the optimal planning of regional seismic networks. *Publ. Inst. Geophys. Pol. Acad. Sci.* **A-7 (119)**, 3–63.

Kind, R. (1972). Residuals and velocities of $P_n$ waves recorded by the San Andreas seismograph network. *Bull. Seismol. Soc. Am.* **62**, 85–100.

Kisslinger, C. (1980). Evaluation of S to P amplitude ratios for determining focal mechanisms from regional network observations. *Bull. Seismol. Soc. Am.* **70**, 999–1014.

Kisslinger, C., and Engdahl, E. R. (1973). The interpretation of the Wadati diagram with relaxed assumptions. *Bull. Seismol. Soc. Am.* **63**, 1723–1736.

Kisslinger, C., and Engdahl, E. R. (1974). A test of the Semyenov prediction technique in the central Aleutian Islands. *Tectonophysics* **23**, 237–246.

Klein, F. W. (1978). Hypocenter location program—HYPOINVERSE: Users guide to versions 1, 2, 3, and 4. *Geol. Surv. Open-File Rep. (U.S.)* **78-694**, 1–113.

Klein, F. W., Einarsson, P., and Wyss, M. (1973). Microearthquakes on the Mid-Atlantic plate boundary on the Reykjanes Peninsula in Iceland. *J. Geophys. Res.* **78**, 5084–5099.

Klein, F. W., Einarsson, P., and Wyss, M. (1977). The Reykjanes Peninsula, Iceland, earthquake swarm of September 1972 and its tectonic significance. *J. Geophys. Res.* **82**, 865–888.

Kodama, K. P., and Bufe, C. G. (1979). Foreshock occurrence in central California. *Earthquake Notes* **50**, 9–20.

Kondratenko, A. M., and Nersesov, I. L. (1962). Some results of the study of change in the velocity of longitudinal waves and relation between the velocity of longitudinal and transverse waves in a focal zone. *Tr. Inst. Fiz. Zemli, Akad. Nauk SSSR* **25** (102), 130–150.

Koschyk, K., and Steinwachs, M. (1977). The Blue Road geotraverse: Investigations of local earthquakes in the land uplift area of Fennoscandia by mobile seismograph stations. *Geol. Foeren. Stockholm Foerh.* **99**, 36–38.

Kubotera, A., and Kikuchi, S. (1967). Seismic observation in Shimabara Peninsula—on the activity of Volcano Unzen. *Spec. Contrib. Geophys. Inst., Kyoto Univ.* **7**, 161–168.

Kuroiso, A., and Watanabe, H. (1977). On the telemetered array system for microearthquake observation at Abuyama Seismological Observatory. *J. Seismol. Soc. Japan* **30**, 91–106 (in Japanese with English abstract).

Lahr, J. C. (1979). HYPOELLIPSE: A computer program for determining local earthquake hypocentral parameters, magnitude, and first motion pattern. *Geol. Surv. Open-File Rep. (U.S.)* **79-431**, 1–239.

Lahr, J. C., Stephens, C. D., Hasegawa, H. S., and Boatwright, J. (1980). Alaskan seismic gap only partially filled by 28 February 1979 earthquake. *Science* **207**, 1351–1354.

Lahr, K. M., Lahr, J. C., Lindh, A. G., Bufe, C. G., and Lester, F. W. (1976). The August 1975 Oroville earthquakes. *Bull. Seismol. Soc. Am.* **66**, 1085–1099.

Lamar, D. L. (1973). Microseismicity of the Whittier fault, California. *In* "Guidebook of the Tertiary Geology of Eastern Orange and Los Angeles Counties, California" (M. S. Woyski *et al.*, eds.), pp. 61–65. South Coast Geol. Soc., Tustin, California.

Lammlein, D. R., Sbar, M. L., and Dorman, J. (1971). A microearthquake reconnaissance of southeastern Missouri and western Tennessee. *Bull. Seismol. Soc. Am.* **61**, 1705–1716.

Lanczos, C. (1956). "Applied Analysis." Prentice-Hall, Englewood Cliffs, New Jersey.

Lanczos, C. (1961). "Linear Differential Operators." Van Nostrand-Reinhold, Princeton, New Jersey.

Lange, A. L., and Westphal, W. H. (1969). Microearthquakes near The Geysers, Sonoma County, California. *J. Geophys. Res.* **74**, 4377–4378.

Langenkamp, D., and Combs, J. (1974). Microearthquake study of the Elsinore fault zone, southern California. *Bull. Seismol. Soc. Am.* **64**, 187–203.

Langer, C. J., and Bollinger, G. A. (1979). Secondary faulting at the terminus of a seismogenic strike-slip fault: Aftershocks of the 1976 Guatemala earthquake. *Bull. Seismol. Soc. Am.* **69**, 427–444.

Latham, G. V., and Nowroozi, A. A. (1968). Waves, weather, and ocean bottom microseisms. *J. Geophys. Res.* **73**, 3945–3956.

Lawson, C. L., and Hanson, R. J. (1974). "Solving Least Squares Problems." Prentice-Hall, Englewood Cliffs, New Jersey.

Leary, P. C., Malin, P. E., Phinney, R. A., Brocher, T., and von Collin, R. (1979). Systematic monitoring of millisecond travel time variations near Palmdale, California. *J. Geophys. Res.* **84**, 659–666.

Leblanc, G., and Anglin, F. (1978). Induced seismicity at the Manic 3 Reservoir, Quebec. *Bull. Seismol. Soc. Am.* **68**, 1469–1485.

Leblanc, G., and Buchbinder, G. (1977). Second microearthquake survey of the St. Lawrence Valley near La Malbaie, Quebec. *Can. J. Earth Sci.* **14**, 2778–2789.

Leblanc, G., Stevens, A. E., Wetmiller, R. J., and DuBerger, R. (1973). A microearthquake survey of the St. Lawrence Valley near La Malbaie, Quebec. *Can. J. Earth Sci.* **10**, 42–53.

Lee, W. H. K., and Lahr, J. C. (1975). HYP071 (revised): A computer program for determining hypocenter, magnitude, and first motion pattern of local earthquakes. *Geol. Surv. Open-File Rep. (U.S.)* **75-311**, 1–116.

Lee, W. H. K., and Wetmiller, R. J. (eds.) (1978). Survey of practice in determining magnitudes of near earthquakes. Part 1: North, Central, and South America. *World Data Cent. A Solid Earth Geophys., Rep.* **SE-9**, 1–102.

Lee, W. H. K., Eaton, M. S., and Brabb, E. E. (1971). The earthquake sequence near Danville, California, 1970. *Bull. Seismol. Soc. Am.* **61**, 1771–1794.

Lee, W. H. K., Bennett, R. E., and Meagher, K. L. (1972). A method of estimating magnitude of local earthquakes from signal duration. *Geol. Surv. Open-File Rep. (U.S.)* 28.

Lee, W. H. K., Johnson, C. E., Henyey, T. L., and Yerkes, R. F. (1978). A preliminary study of the Santa Barbara, California, earthquake of August 13, 1978 and its major aftershocks. *Geol. Surv. Circ. (U.S.)* **797**, 1–11.

Lee, W. H. K., Herd, D. G., Cagnetti, V., Bakun, W. H., and Rapport, A. L. (1979a). A preliminary study of the Coyote Lake earthquake of August 6, 1979 and its major aftershocks. *Geol. Surv. Open-File Rep. (U.S.)* **79-1621**, 1–43.

Lee, W. H. K., Yerkes, R. F., and Simirenko, M. (1979b). Recent earthquake activity and focal mechanisms in the western Transverse Ranges, California. *Geol. Surv. Circ. (U.S.)* **799-A**, 1–26.

Lee, W. H. K., Nelson, G., Ward, P. L., and Zhao, Z. H. (1981). Users' manual for HYPO81A: A program to determine hypocenter and magnitude of local earthquakes using minicomputers. In preparation.

Lee, W. H. K., Aki, K., and Thurber, C. (1982a). Determination of three-dimensional velocity anomalies under a seismic array using first P arrival times from local earthquakes. Part II. A heterogeneous initial model. In preparation.

Lee, W. H. K., Pereyra, V., and Keller, H. B. (1982b). Solving two-point ray-tracing problems in a heterogeneous medium. Part 2. Numerical solutions of two- and three-dimensional velocity models. In preparation.

Lehner, F. E., and Press, F. (1966). A mobile seismograph array. *Bull. Seismol. Soc. Am.* **56**, 889–897.

Lentini, M., and Pereyra, V. (1977). An adaptive finite difference solver for nonlinear two-point boundary problems with mild boundary layers. *SIAM J. Numer. Anal.* **14**, 91–111.

Lester, F. W., Bufe, C. G., Lahr, K. M., and Stewart, S. W. (1975). Aftershocks of the Oroville earthquake of August 1, 1975. *Spec. Rep.—Calif., Div. Mines Geol.* **124**, 131–138.

Levenberg, K. (1944). A method for the solution of certain non-linear problems in least squares. *Q. Appl. Math.* **2**, 164–168.

Lilwall, R. C., and Francis, T. J. G. (1978). Hypocentral resolution of small ocean bottom seismic networks. *Geophys. J. R. Astron. Soc.* **54**, 721–728.

Lilwall, R. C., Francis, T. J. G., and Porter, I. T. (1977). Ocean-bottom seismograph observations on the Mid-Atlantic Ridge near 45 degrees N. *Geophys. J. R. Astron. Soc.* **51**, 357–370.

Lilwall, R. C., Francis, T. J. G., and Porter, I. T. (1978). Ocean-bottom seismograph observation on the Mid-Atlantic Ridge near 45 degrees N: Further results. *Geophys. J. R. Astron. Soc.* **55**, 255–262.

Lilwall, R. C., Francis, T. J. G., and Porter, I. T. (1980). Some ocean-bottom seismograph observations on the Reykjanes Ridge at 59 degrees N. *Geophys. J. R. Astron. Soc.* **62**, 321–327.

Lin, M. T., Tsai, Y. B., and Feng, C. C. (1979). Microearthquake studies in southern Taiwan. *Proc. Natl. Sci. Counc., Repub. China* **3**, 347–355.

Lindh, A. G., Fuis, G., and Mantis, C. (1978a). Seismic amplitude measurements suggest foreshocks have different focal mechanisms than aftershocks. *Science* **201**, 56–59.

Lindh, A. G., Lockner, D. A., and Lee, W. H. K. (1978b). Velocity anomalies: An alternative explanation. *Bull. Seismol. Soc. Am.* **68**, 721–734.

Lo Bascio, A., Nappi, G., and Scarpa, R. (1976). Seismicity of Etna during November 1973. *Boll. Geofis. Teor. Appl.* **19**, 92–97.

Long, R. E. (1974). A compact portable seismic recorder. *Geophys. J. R. Astron. Soc.* **37**, 91–98.

Luenberger, D. G. (1973). "Introduction to Linear and Nonlinear Programming." Addison-Wesley, Reading, Massachusetts.

Luk, F., Comer, R., and Lee, W. H. K. (1982). Solving seismic ray-tracing problems in a heterogeneous medium by a general shooting method. In preparation.

Maasha, N. (1975). The seismicity of the Ruwenzori region in Uganda. *J. Geophys. Res.* **80**, 1485–1496.

Maasha, N. (1976). Electrical resistivity and microearthquake surveys of the Sempaya, Lake Kitagata, and Kitagata geothermal anomalies, western Uganda. *Proc. U.N. Symp. Dev. Use Geotherm. Resour., 2nd, 1975* Vol. 2, pp. 1103–1112.

MacDonald, K. C., and Mudie, J. D. (1974). Microearthquakes on the Galapagos spreading centre and the seismicity of fast spreading ridges. *Geophys. J. R. Astron. Soc.* **36**, 245–257.

Majer, E. L. (1978). Seismological investigations in geothermal regions. Ph.D. Thesis, University of California, Berkeley.

Majer, E. L., and McEvilly, T. V. (1979). Seismological investigations at The Geysers geothermal field. *Geophysics* **44**, 246–269.

Maling, D. H. (1973). "Coordinate Systems and Map Projections." George Philip & Son, London.

Malone, S. D., Rothe, G. H., and Smith, S. W. (1975). Details of microearthquake swarms in the Columbia Basin, Washington. *Bull. Seismol. Soc. Am.* **65**, 855–864.

Marquardt, D. W. (1963). An algorithm for least-squares estimation of nonlinear parameters. *J. Soc. Ind. Appl. Math.* **11**, 431–441.

Maruyama, T. (1963). On the force equivalents of dynamical elastic dislocations with reference to the earthquake mechanism. *Bull. Earthquake Res. Inst., Univ. Tokyo* **41**, 467–486.

Massinon, B., and Plantet, J. L. (1976). A large aperture seismic network in France: Description and some results concerning epicenter location and upper mantle anomalies. *Phys. Earth Planet. Inter.* **12**, 118–127.

Mattaboni, P. J., and Solomon, S. C. (1977). MITOBS: A seismometer system for ocean-bottom earthquake studies. *Mar. Geophys. Res.* **3**, 87–102.

Matumoto, T., and Page, R. A. (1966). Microaftershocks following the earthquake: Determination of hypocenters and crustal velocities. *In* "The Prince William Sound Alaska Earthquake of 1964 and Aftershocks" (L. E. Leipold, ed.), Vol. II, Parts B & C, pp. 157–173. US Govt. Printing Office, Washington, D.C.

Matumoto, T., and Ward, P. L. (1967). Microearthquake study of Mount Katmai and vicinity, Alaska. *J. Geophys. Res.* **72**, 2557–2568.

Matumoto, T., Ohtake, M., Latham, G., and Umana, J. (1977). Crustal structure in southern central America. *Bull. Seismol. Soc. Am.* **67**, 121–134.

Mayer-Rosa, D. (1973). Travel-time anomalies and distribution of earthquakes along the Calaveras fault zone, California. *Bull. Seismol. Soc. Am.* **63**, 713–729.

McCann, W. R., Nishenko, S. P., Sykes, L. R., and Krause, J. (1979). Seismic gaps and plate tectonics: Seismic potential for major boundaries. *Pure Appl. Geophys.* **117**, 1082–1147.

McCollom, R. L., and Crosson, R. S. (1975). An array study of upper mantle velocity in Washington state. *Bull. Seismol. Soc. Am.* **65**, 467–482.

McEvilly, T. V. (1966). The earthquake sequence of November 1964 near Corralitos, California. *Bull. Seismol. Soc. Am.* **56**, 755–773.

McEvilly, T. V., and Casaday, K. B. (1967). The earthquake sequence of September, 1965 near Antioch, California. *Bull. Seismol. Soc. Am.* **57**, 113–124.

McEvilly, T. V., and Johnson, L. R. (1973). Earthquakes of strike-slip type in central California: Evidence on the question of dilatancy. *Science* **182**, 581–584.

McEvilly, T. V., and Johnson, L. R. (1974). Stability of P and S velocities from central California quarry blasts. *Bull. Seismol. Soc. Am.* **64**, 343–353.

McEvilly, T. V., Bakun, W. H., and Casaday, K. B. (1967). The Parkfield, California, earthquakes of 1966. *Bull. Seismol. Soc. Am.* **57**, 1221–1244.

McGarr, A. (1974). Earthquake prediction—absence of a precursive change in seismic velocities before a tremor of magnitude $3\frac{3}{4}$. *Science* **185**, 1047–1049.

McGarr, A., and Green, R. W. E. (1978). Microtremor sequences and tilting in a deep mine. *Bull. Seismol. Soc. Am.* **68**, 1679–1697.

McGarr, A., and Wiebols, G. A. (1977). Influence of mine geometry and closure volume on seismicity in a deep-level mine. *Int. J. Rock Mech. Miner. Sci. Geomech. Abstr.* **14**, 139–145.

McGarr, A., Spottiswoode, S. M., and Gay, N. C. (1975). Relationship of mine tremors to induced stresses and to rock properties in the focal region. *Bull. Seismol. Soc. Am.* **65**, 981–993.

McKenzie, D. P. (1969). The relation between fault plane solutions for earthquakes and the directions of the principal stresses. *Bull. Seismol. Soc. Am.* **59**, 591–601.

McMechan, G. A. (1976). Generalized p-delta curves. *Geophys. J. R. Astron. Soc.* **47**, 9–18.

McMechan, G. A., and Mooney, W. D. (1980). Asymptotic ray theory and synthetic seismograms for laterally varying structures: theory and application to the Imperial Valley, California. *Bull. Seismol. Soc. Am.* **70**, 2021–2035.

McNally, K. C., and McEvilly, T. V. (1977). Velocity contrast across the San Andreas fault in central California: Small-scale variations from P wave nodal plane distortion. *Bull. Seismol. Soc. Am.* **67**, 1565–1576.

McNally, K. C., Kanamori, H., and Pechmann, J. C. (1978a). Earthquake swarm along the San Andreas fault near Palmdale, southern California, 1976 to 1977. *Science* **201**, 814–817.

McNally, K. C., Simila, G. W., and Von Dollen, F. J. (1978b). Microearthquake activity adjacent to the Rocklin Pluton near Auburn, California. *Bull. Seismol. Soc. Am.* **68**, 239–243.

Menke, W. H. (1977). Lateral inhomogeneities in P velocity under the Tarbela array of the Lesser Himalayas of Pakistan. *Bull. Seismol. Soc. Am.* **67**, 725–734.

Meyer, R. P., Pennington, W. D., Powell, L. A., Unger, W. L., Guzman, M., Havskov, J., Singh, S. K., Valdes, C., and Yamamoto, J. (1980). A first report on the Petatlan, Guerrero, Mexico earthquake of 14 March 1979. *Geophys. Res. Lett.* **7**, 97–100.

Mickey, W. V. (1966). Seismic clusters. *In* "ESSA Symposium on Earthquake Prediction," pp. 63–68. US Govt. Printing Office, Washington, D.C.

Miki, H., Watanabe, H., and Shimada, M. (1965). Observations of ultra microearthquakes in the vicinity of Neo Valley fault in central Honshu, Japan. *J. Seismol. Soc. Japan* **18**, 103–112 (in Japanese with English abstract).

Mikumo, T., Otsuka, M., and Kamitsuki, A. (1956). On the nature of local earthquakes observed in Wakayama district. *J. Seismol. Soc. Japan* **9**, 218–228 (in Japanese with English abstract).

Mitchell, B. J., and Hashim, B. M. (1977). Seismic velocity determinations in the New Madrid seismic zone: A new method using local earthquakes. *Bull. Seismol. Soc. Am.* **67**, 413–424.

Mitchell, B. J., and Landisman, M. (1969). Electromagnetic seismograph constants by least-squares inversion. *Bull. Seismol. Soc. Am.* **59**, 1335–1348.

Mitchell, B. J., Stauder, W., and Cheng, C. C. (1977). The New Madrid seismic zone as a laboratory for earthquake prediction research. *J. Phys. Earth* **25S**, 43–49.

Miyamura, S. (1959a). Local earthquakes in Kii Peninsula, central Japan. Part I. Reconnaissance observation of minor shocks at Gobo, Wakayama Prefecture. *Bull. Earthquake Res. Inst., Univ. Tokyo* **37**, 347–358 (in Japanese with English abstract).

Miyamura, S. (1959b). Local earthquakes in Kii Peninsula, central Japan. Part III. Temporary seismological network in the neighbourhood of Wakayama. *Bull. Earthquake Res. Inst., Univ. Tokyo* **37**, 609–635 (in Japanese with English abstract).

Miyamura, S. (1960). Local earthquakes in Kii Peninsula, central Japan. Part 4. Location of earthquakes by the temporary network of stations near Wakayama. *Bull. Earthquake Res. Inst., Univ. Tokyo* **38**, 71–112 (in Japanese with English abstract).

Miyamura, S., and Tsujiura, M. (1959). Direction of approach and apparent velocity of near earthquake initial motion. *Bull. Earthquake Res. Inst., Univ. Tokyo* **37**, 359–374 (in Japanese with English abstract).

Miyamura, S., Hori, M., Aki, K., Matumoto, H., and Ando, S. (1961). Observation of aftershocks of the Kita Mino earthquake, Aug. 19, 1961. *Bull. Earthquake Res. Inst., Univ. Tokyo* **39**, 895–908 (in Japanese with English abstract).

Miyamura, S., Hori, M., Aki, K., Tsujiura, M., and Matumoto, H. (1962). Simultaneous operation of two seismometer array stations in a study of microearthquakes in the Kanto and Chubu region. *Bull. Earthquake Res. Inst., Univ. Tokyo* **40**, 885–897 (in Japanese with English abstract).

Miyamura, S., Hori, M., Matumoto, H., and Tsujiura, M. (1964). Observation of microearthquakes by a seismometer array at Hachiman, Gifu prefecture, central Japan. *Bull. Earthquake Res. Inst., Univ. Tokyo* **42**, 257–272 (in Japanese with English abstract).

Miyamura, S., Hori, M., and Matumoto, H. (1966). Local earthquakes in Kii Peninsula, central Japan. Part 5. Development of microearthquake observation network in Kii Peninsula during 1957–1962 and observed seismicity. *Bull. Earthquake Res. Inst., Univ. Tokyo* **44**, 709–729 (in Japanese with English abstract).

Mizoue, M. (1971). Crustal structure from travel times of reflected and refracted seismic waves recorded at Wakayama Microearthquake Observatory and its substations. *Bull. Earthquake Res. Inst., Univ. Tokyo* **49**, 33–62.

Mogi, K. (1968a). Sequential occurrences of recent great earthquakes. *J. Phys. Earth* **16**, 30–36.

Mogi, K. (1968b). Development of aftershock areas of great earthquakes. *Bull. Earthquake Res. Inst., Univ. Tokyo* **46**, 175–203.

Mogi, K. (1968c). Some features of recent seismic activity in and near Japan (1). *Bull. Earthquake Res. Inst., Univ. Tokyo* **46**, 1225–1236.

Mogi, K. (1969a). Some features of recent seismic activity in and near Japan (2). Activity before and after great earthquakes. *Bull. Earthquake Res. Inst., Univ. Tokyo* **47**, 395–417.

Mogi, K. (1969b). Relationship between the occurrence of great earthquakes and tectonic structures. *Bull. Earthquake Res. Inst., Univ. Tokyo* **47**, 429–451.

Mogi, K. (1979). Two kinds of seismic gaps. *Pure Appl. Geophys.* **117**, 1172–1186.

Molnar, P., and Aggarwal, Y. P. (1971). A microearthquake survey in Kenya. *Bull. Seismol. Soc. Am.* **61**, 195–201.

Molnar, P., Fitch, T. J., and Asfaw, L. M. (1970). A microearthquake survey in the Ethiopian rift. *Earthquake Notes* **41**, 37–44.

Mooney, W. D., and Prodehl, C. (1978). Crustal structure of the Rhenish Massif and adjacent areas: A reinterpretation of existing seismic refraction data. *J. Geophys.* **44**, 573–601.

Motoya, Y. (1974). Aftershock sequences recorded during a microearthquake observation at Kamikineusu, Hokkaido (1964–1972). *J. Phys. Earth* **22**, 245–262.

Muirhead, K. J., and Simpson, D. W. (1972). A three-quarter watt seismic station. *Bull. Seismol. Soc. Am.* **62**, 985–990.

Munguia, L., Reichle, M., Reyes, A., Simons, R., and Brune, J. (1977). Aftershocks of the 8 July, 1975 Canal de las Ballenas, Gulf of California, earthquake. *Geophys. Res. Lett.* **4**, 507–509.

Muramatu, I., Endo, Y., Simono, H., Kooketu, H., and Suzuki, S. (1963). Observation of microearthquakes in Mino district in Gifu prefecture, central Japan. *J. Phys. Earth* **11**, 35–48.

Murphy, A. J., Sykes, L. R., and Donnelly, T. W. (1970). Preliminary survey of the microseismicity of the northeastern Caribbean. *Geol. Soc. Am. Bull.* **81**, 2459–2463.

Murray, W., ed. (1972). "Numerical Methods for Unconstrained Optimization." Academic Press, New York.

Nagumo, S., and Kasahara, J. (1976). Ocean-bottom seismograph study of the western margin of the Pacific. *Geophys. Monogr., Am. Geophys. Union* **19**, 155–169.

Nagumo, S., Hasegawa, S., Koresawa, S., and Kobayashi, H. (1970). Ocean-bottom seismographic observation off Sanriku: Aftershock activity of the 1968 Tokachi—Oki earthquake and its relation to the ocean-continent boundary fault. *Bull. Earthquake Res. Inst., Univ. Tokyo* **48**, 793–809.

Nagumo, S., Kasahara, J., and Ouchi, T. (1975). Active seismicity in the Fiji Plateau observed by ocean-bottom seismograph. *J. Phys. Earth* **23**, 279–287.

Nagumo, S., Kasahara, J., and Koresawa, S. (1976). Structure of microearthquake activity around Japan Trench, off Sanriku, obtained by ocean-bottom seismographic network observation. *J. Phys. Earth* **24**, 215–225.

Nasu, N. (1929a). Further study of the aftershocks of the Tango earthquake. *Bull. Earthquake Res. Inst., Univ. Tokyo* **6**, 133–152 (in Japanese with English abstract).

Nasu, N. (1929b). On the aftershocks of the Tango earthquake. *Bull. Earthquake Res. Inst., Univ. Tokyo* **7**, 245–331 (in Japanese with English abstract).

Nasu, N. (1935a). Supplementary study on the stereometrical distribution of the aftershocks of the Great Tango earthquake of 1927. *Bull. Earthquake Res. Inst., Univ. Tokyo* **13**, 335–399.

Nasu, N. (1935b). Recent seismic activities in the Izu Peninsula. (Part 2). *Bull. Earthquake Res. Inst., Univ. Tokyo* **13**, 400–416.

Nasu, N. (1936). The aftershocks of the Formosa earthquake of 1935. *Bull. Earthquake Res. Inst., Univ. Tokyo* **14**, 75–86 (in Japanese with English abstract).

Nersesov, I. L., Lukk, A. A., Ponomarev, V. S., Rautian, T. G., Rulev, B. G., Semenov, A. N., and Simbireva, I. G. (1973). Possibilities of earthquake prediction, exemplified by the Garm area of the Tadzhik SSR. *In* "Earthquake Precursors" (M. A. Sadovskiy, I. L. Nersesov, and L. A. Latynina, eds.), pp. 72–99. Inst. Phys., Moscow.

Noble, B. (1969). "Applied Linear Algebra." Prentice-Hall, Englewood Cliffs, New Jersey.

Nordquist, J. M. (1962). A special purpose program for earthquake location with an electronic computer. *Bull. Seismol. Soc. Am.* **52**, 431–437.

Northrop, J. (1974). Seaquakes on the Nazca—Cocos plate boundary. *Bull. Seismol. Soc. Am.* **64**, 595–606.

Nowroozi, A. A. (1973). Seismicity of the Mendocino escarpment and the aftershock sequence of June 26, 1968: Ocean bottom seismic measurements. *Bull. Seismol. Soc. Am.* **63**, 441–456.

Nur, A. (1972). Dilatancy, pore fluids, and premonitory variations of $t_s/t_p$ travel times. *Bull. Seismol. Soc. Am.* **62**, 1217–1222.

Officer, C. B. (1958). "Introduction to the Theory of Sound Transmission." McGraw-Hill, New York.

Ogino, I. (1974). Seismic activity in Ashio area, Tochigi prefecture. *Bull. Earthquake Res. Inst., Univ. Tokyo* **12**, 159–169 (in Japanese with English abstract).

Ohtake, M. (1970a). On an earthquake activity that occurred near Kamikochi. *Bull Earthquake Res. Inst., Univ. Tokyo* **48**, 65–71 (in Japanese with English abstract).

Ohtake, M. (1970b). Micro-structure of the seismic sequence related to a moderate earthquake. *Bull. Earthquake Res. Inst., Univ. Tokyo* **48**, 1053–1067.

Ohtake, M. (1973). Change in the $V_p/V_s$ ratio related with occurrence of some shallow earthquakes in Japan. *J. Phys. Earth* **21**, 173–184.

Ohtake, M. (1974). Seismic activity induced by water injection at Matsushiro, Japan. *J. Phys. Earth* **22**, 163–176.

Ohtake, M. (1976). Search for precursors of the 1974 Izu-Hanto-oki earthquake, Japan. *Pure Appl. Geophys.* **114**, 1083–1093.

Ohtake, M., Matumoto, T., and Latham, G. V. (1977). Seismicity gap near Oaxaca, southern Mexico as a probable precursor to a large earthquake. *Pure Appl. Geophys.* **115**, 375–385.

Oliver, J., and Murphy, L. (1971). WWNSS: Seismology's global network of observing stations. *Science* **174**, 254–261.

Oliver, J., Ryall, A., Brune, J. N., and Slemmons, D. B. (1966). Microearthquake activity recorded by portable seismographs of high sensitivity. *Bull. Seismol. Soc. Am.* **56**, 899–924.

Omote, S. (1944). Preliminary report on the investigation of the aftershocks of the Tottori earthquake. *Bull. Earthquake Res. Inst., Univ. Tokyo* **22**, 33–41 (in Japanese).

Omote, S. (1950a). On the aftershocks of the Fukui earthquake. Part 2. *Bull. Earthquake Res. Inst., Univ. Tokyo* **28**, 311–318.

Omote, S. (1950b). Aftershocks of Imaichi earthquake observed at Nishi-oashi Station. *Bull. Earthquake Res. Inst., Univ. Tokyo* **28**, 401–413.

Omote, S. (1955). Aftershocks that accompanied the Tottori earthquake of Sept. 10, 1943. (the 2nd paper). *Bull. Earthquake Res. Inst., Univ. Tokyo* **33**, 641–661.

O'Neill, M. E., and Healy, J. H. (1973). Determination of source parameters of small earthquakes from P wave rise time. *Bull. Seismol. Soc. Am.* **63**, 599–614.

Ooida, T., and Ito, K. (1972). Foreshock—aftershock sequence of the earthquake off the Atsumi Peninsula on January 5, 1971. *J. Seismol. Soc. Japan.* **25**, 178–186 (in Japanese with English abstract).

Ooida, T., and Yamada, I. (1972). Microearthquake activity in central Honshu, Japan. Part 2. Seismicity of microearthquake in Mikawa district. *J. Seismol. Soc. Japan.* **25**, 67–74 (in Japanese with English abstract).

Ooida, T., Yamada, I., Tada, T., Ito, K., Sugiyama, K., and Sasaki, Y. (1971). Microearthquake activity in central Honshu, Japan. Part I. Seismicity of microearthquakes

in the vicinity of the Neo Valley fault. *J. Seismol. Soc. Japan.* **24**, 240–247 (in Japanese with English abstract).

Page, R. A. (1969). The Fairweather fault ten years after the southeast Alaska earthquake of 1958. *Bull. Seismol. Soc. Am.* **59**, 1927–1936.

Parker, R. L. (1977). Understanding inverse theory. *Annu. Rev. Earth Planet. Sci.* **5**, 35–64.

Patton, H., and Aki, K. (1979). Bias in the estimate of seismic moment tensor by the linear inversion method. *Geophys. J. R. Astron. Soc.* **59**, 479–495.

Pavlis, G. L., and Booker, J. R. (1980). The mixed discrete continuous inverse problem: Application to the simultaneous determination of earthquake hypocenters and velocity structure. *J. Geophys. Res.* **85**, 4801–4810.

Pavoni, N. (1977). An investigation of microearthquake activity in the central Valais (Swiss Alps). *Publ. Inst. Geophys. (Pol. Acad. Sci.), Ser. A* **5** (116), 317–320.

Peake, L. G., and Healy, J. H. (1977). A method for determination of the lower crustal structure along the San Andreas fault system in central California. *Bull. Seismol. Soc. Am.* **67**, 793–807.

Peake, L. G., Healy, J. H., and Roller, J. C. (1977). Time variance of seismic velocity from multiple explosive sources southeast of Hollister, California. *Bull. Seismol. Soc. Am.* **67**, 1339–1354.

Pennington, W. D., Smith, R. B., and Trimble, A. B. (1974). A microearthquake survey of parts of the Snake River Plain and central Idaho. *Bull. Seismol. Soc. Am.* **64**, 307–312.

Pennington, W. D., Mooney, W. D., Van Hissenhoven, R., Meyer, H., Ramirez, J. E., and Meyer, R. P. (1979). Results of a reconnaissance microearthquake survey of Bucaramanga, Columbia. *Geophys. Res. Lett.* **6**, 65–68.

Pereyra, V., Lee, W. H. K., and Keller, H. B. (1980). Solving two-point seismic ray-tracing problems in a heterogeneous medium. Part 1. A general adaptive finite difference method. *Bull. Seismol. Soc. Am.* **70**, 79–99.

Peters, D. C., and Crosson, R. S. (1972). Application of prediction analysis to hypocenter determination using a local array. *Bull. Seismol. Soc. Am.* **62**, 775–788.

Peterson, J., and Orsini, N. A. (1976). Seismic research observatories: Upgrading the worldwide seismic data network. *Trans. Am. Geophys. Union* **57**, 548–556.

Pfluke, J. H., and Steppe, J. A. (1973). Magnitude—frequency statistics of small earthquakes from San Francisco Bay to Parkfield. *Stanford Univ. Publ., Geol. Sci.* **13**, 13–23.

Phillips, J. D., and McCowan, D. W. (1978). "Ocean Bottom Seismometers for Research: A Reassessment," Tech. Note 1978-40. Lincoln Lab., Massachusetts Institute of Technology, Cambridge.

Pirhonen, S. E., Nurminen, S., Luosto, U., and Korhonen, H. (1979). The Finnish seismic array. *Phys. Earth Planet. Inter.* **18**, 121–126.

Pitt, A. M., and Steeples, D. W. (1975). Microearthquakes in the Mono Lake—northern Owens Valley, California, region from September 28 to October 18, 1970. *Bull. Seismol. Soc. Am.* **65**, 835–844.

Pitt, A. M., Weaver, C. S., and Spence, W. (1979). The Yellowstone Park earthquake of June 30, 1975. *Bull. Seismol. Soc. Am.* **69**, 187–205.

Pomeroy, P. W., Simpson, D. W., and Sbar, M. L. (1976). Earthquakes triggered by surface quarrying: The Wappingers Falls, New York sequence of June, 1974. *Bull. Seismol. Soc. Am.* **66**, 685–700.

Prothero, W. A. (1976). A portable digital seismic recorder with event recording capability. *Bull. Seismol. Soc. Am.* **66**, 979–985.

Prothero, W. A. (1979). An operationally optimized ocean bottom seismometer capsule. *Phys. Earth Planet. Inter.* **18**, 71–77.

Prothero, W. A. (1980). Earthquake signal processing and logging with a battery-powered microcomputer. *Bull Seismol. Soc. Am.* **70**, 2275–2290.

Prothero, W. A., and Brune, J. N. (1971). A suitcase seismic recording system. *Bull. Seismol. Soc. Am.* **61**, 1849–1852.

Prothero, W. A., Reid, I., Reichle, M. S., and Brune, J. N. (1976). Ocean-bottom seismic measurements on the East Pacific Rise and Rivera fracture zone. *Nature (London)* **262**, 121–124.

Quervain, A. De. (1924). Investigations of aftershocks of the large Visper earthquakes on the basis of setting up the portable Quervain-Piccard seismographs in the epicentral area. *Annual Rep. Earthquake Service, Swiss Meteorol. Agency*, 23–25 (in German).

Ragan, D. M. (1973). "Structural Geology: An Introduction to Geometrical Techniques," 2nd ed. Wiley, New York.

Raikes, S. A. (1978). The temporal variation of teleseismic P residuals for stations in southern California. *Bull. Seismol. Soc. Am.* **68**, 711–720.

Raikes, S. A. (1980). Regional variations in upper mantle structure beneath southern California. *Geophys. J. R. Astron. Soc.* **63**, 187–216.

Raleigh, C. B., Healy, J. H., and Bredehoeft, J. D. (1972). Faulting and crustal stress at Rangely, Colorado. *Geophys. Monogr., Am. Geophys. Union* **16**, 275–284.

Raleigh, C. B., Healy, J. H., and Bredehoeft, J. D. (1976). An experiment in earthquake control at Rangely, Colorado. *Science* **191**, 1230–1237.

Rastogi, B. K., and Talwani, P. (1980). Spatial and temporal variation in $t_s/t_p$ at Monticello Reservoir, South Carolina. *Geophys. Res. Lett.* **7**, 781–784.

Rautian, T. G., and Khalturin, V. I. (1978). The use of the coda for determination of the earthquake source spectrum. *Bull. Seismol. Soc. Am.* **68**, 923–948.

Rautian, T. G., Khalturin, V. I., Martynov, V. G., and Molnar, P. (1978). Preliminary analysis of the spectral content of P and S waves from local earthquakes in the Garm, Tadjikistan region. *Bull. Seismol. Soc. Am.* **68**, 949–971.

Real, C. R., and Teng, T. L. (1973). Local Richter magnitude and total signal duration in southern California. *Bull. Seismol. Soc. Am.* **63**, 1809–1827.

Reasenberg, P., Ellsworth, W., and Walter, A. (1980). Teleseismic evidence for a low-velocity body under the Coso geothermal area. *J. Geophys. Res.* **85**, 2471–2483.

Reichle, M. S., and Reid, I. (1977). Detailed study of earthquake swarms from the Gulf of California. *Bull. Seismol. Soc. Am.* **67**, 159–171.

Reichle, M. S., Sharman, G. F., and Brune, J. N. (1976). Sonobuoy and teleseismic study of Gulf of California transform fault earthquake sequences. *Bull. Seismol. Soc. Am.* **66**, 1623–1641.

Reid, H. F. (1910). "The California Earthquake of April 18, 1906, Vol. 2: The mechanics of the earthquake." Carnegie Inst., Washington, D.C.

Reid, I., and MacDonald, K. C. (1973). Microearthquake study of the Mid-Atlantic Ridge near 37 degrees N, using sonobuoys. *Nature (London)* **246**, 88–90.

Reid, I., and Prothero, W. A. (1981). An earthquake sequence studied with ocean-bottom seismographs. *Geophys. J. R. Astron. Soc.* **64**, 381–391.

Reid, I., Reichle, M., Brune, J., and Bradner, H. (1973). Microearthquake studies using sonobuoys: Preliminary results from the Gulf of California. *Geophys. J. R. Astron. Soc.* **34**, 365–379.

Reyes, A., Brune, J., Barker, T., Canales, L., Madrid, J., Reboller, J., and Munguia, L. (1975). A microearthquake survey of the San Miguel fault zone, Baja California, Mexico. *Geophys. Res. Lett.* **2**, 56–59.

Richter, C. F. (1935). An instrumental earthquake magnitude scale. *Bull. Seismol. Soc. Am.* **25**, 1–32.

Richter, C. F. (1958). "Elementary Seismology." Freeman, San Francisco, California.

Richter, C. F., and Nordquist, J. M. (1948). Minimal recorded earthquakes. *Bull. Seismol. Soc. Am.* **38**, 257–262.

Rikitake, T. (1976). "Earthquake Prediction." Elsevier, Amsterdam.

Rikitake, T. (1979). "Earthquake Precursors." Sc-79, Conf. 801, Col. 6. UNESCO Headquarters, Paris.

Riznichenko, Y. V. (1960). Method of detailed investigations of seismicity. *Tr. Inst. Fiz. Zemli, Akad. Nauk SSSR* **9** (176), 1–327 (in Russian).

Riznichenko, Y. V. (1975). G. A. Gamburtsev and seismology. *Izv., Acad. Sci., USSR, Phys. Solid Earth (Engl. Transl.)* No. 2, pp. 84–86.

Roberts, S. M., and Shipman, J. S. (1972). "Two Point Boundary Value Problems: Shooting Methods." Am. Elsevier, New York.

Robinson, R., and Arabasz, W. J. (1975). Microearthquakes in the northwest Nelson region, New Zealand. *N. Z. J. Geol. Geophys.* **18**, 83–91.

Robinson, R., and Iyer, H. M. (1976). Temporal and spatial variations of travel-time residuals in central California for Novaya Zemlya events. *Bull. Seismol. Soc. Am.* **66**, 1733–1747.

Robinson, R., Wesson, R. L., and Ellsworth, W. L. (1974). Variation of P wave velocity before the Bear Valley, California, earthquake of 24 February 1972. *Science* **184**, 1281–1283.

Rogers, A. M., and Lee, W. H. K. (1976). Seismic study of earthquakes in the Lake Mead, Nevada—Arizona region. *Bull. Seismol. Soc. Am.* **66**, 1657–1681.

Rogers, G. C. (1976). A microearthquake survey in northwest British Columbia and southeast Alaska. *Bull. Seismol. Soc. Am.* **66**, 1643–1655.

Rustanovich, D. N. (1957). Some problems of the investigation of the seismic activity of the Ashkhabad region. *Izv. Akad. Nauk SSSR, Ser. Geofiz.* **1**, 9–21 (English translation).

Ryall, A., and Savage, W. U. (1969). A comparison of seismological effects for the Nevada underground test Boxcar with natural earthquakes in the Nevada region. *J. Geophys. Res.* **74**, 4281–4289.

Ryall, A., Van Wormer, J. D., and Jones, A. E. (1968). Triggering of microearthquakes by earth tides, and other features of the Truckee, California, earthquake sequence of September, 1966. *Bull. Seismol. Soc. Am.* **58**, 215–248.

Rykounov, L. N., Sedov, V. V., Savrina, L. A., and Bourmin, V. J. (1972). Study of microearthquakes in the rift zones of east Africa. *Tectonophysics* **15**, 123–130.

Rykunov, L. N., and Sedov, V. V. (1967). An ocean-bottom seismograph. *Izv., Acad. Sci., USSR, Phys. Solid Earth (Engl. Transl.)* No. 8, pp. 537–541.

Rynn, J. M. W., and Scholz, C. H. (1978). Study of the seismic velocity ratio for several regions of the South Island, New Zealand: Evaluation of regional $t_s/t_p$ and near source $V_p/V_s$ values. *Geophys. J. R. Astron. Soc.* **53**, 87–112.

Sanford, A. R., and Holmes, C. R. (1962). Microearthquakes near Socorro, New Mexico. *J. Geophys. Res.* **67**, 4449–4459.

Sanford, A. R., and Long, L. T. (1965). Microearthquake crustal reflections, Socorro, New Mexico. *Bull. Seismol. Soc. Am.* **55**, 579–586.

Sasaki, Y., Watanabe, K., Hibi, K., and Muramatu, I. (1970). On the aftershocks of the earthquake of the central part of Gifu Prefecture, September 9, 1969. *Bull. Earthquake Res. Inst., Univ. Tokyo* **48**, 1209–1216.

Sato, T. (1979). Velocity structure of the crust beneath the northeastern part of Honshu, Japan, as derived from local earthquake data. *J. Phys. Earth* **27**, 239–253.

Sato, Y., and Skoko, D. (1965). Optimum distribution of seismic observation points. (2). *Bull. Earthquake Res. Inst., Univ. Tokyo* **43**, 451–457.

Sauber, J., and Talwani, P. (1980). Application of Keilis-Borok and McNally prediction algorithms to earthquakes in the Lake Jocassee area, South Carolina. *Phys. Earth Planet. Inter.* **21**, 267–281.

Savage, J. C. (1978). Dislocation in seismology. *In* "Dislocation in Solids" (F. R. N. Nabarro, ed.), pp. 251–339. North-Holland Publ., Amsterdam.

Savage, W. U., Tocher, D., and Birkhahn, P. C. (1975). Microaftershock study of the Oroville, California, earthquake sequence of August 1975. *Spec. Rep.—Calif., Div. Mines Geol.* **124**, 123–129.

Sbar, M. L., Armbruster, J., and Aggarwal, Y. P. (1972a). The Adirondack, New York, earthquake swarm of 1971 and tectonic implications. *Bull. Seismol. Soc. Am.* **62**, 1303–1317.

Sbar, M. L., Barazangi, M., Dorman, J., Scholz, C. H., and Smith, R. B. (1972b). Tectonics of the Intermountain Seismic Belt, western United States: Microearthquake seismicity and composite fault plane solutions. *Geol. Soc. Am. Bull.* **83**, 13–28.

Sbar, M. L., Jordon, R. R., Stephens, C. D., Pickett, T. E., Woodruff, K. D., and Sammis, C. G. (1975). The Delaware—New Jersey earthquake of February 28, 1973. *Bull. Seismol. Soc. Am.* **65**, 85–92.

Scholz, C. H., Rynn, J. M. W., Weed, R. W., and Frohlich, C. (1973a). Detailed seismicity of the Alpine fault zone and Fiordland region, New Zealand. *Geol. Soc. Am. Bull.* **84**, 3297–3316.

Scholz, C. H., Sykes, L. R., and Aggarwal, Y. P. (1973b). Earthquake prediction: A physical basis. *Science* **181**, 803–810.

Scholz, C. H., Koczynski, T. A., and Hutchins, D. G. (1976). Evidence for incipient rifting in southern Africa. *Geophys. J. R. Astron. Soc.* **44**, 135–144.

Seeber, L., Barazangi, M., and Nowroozi, A. (1970). Microearthquake seismicity and tectonics of coastal northern California. *Bull. Seismol. Soc. Am.* **60**, 1669–1699.

Segall, P., and Pollard, D. D. (1980). Mechanics of discontinuous faults. *J. Geophys. Res.* **85**, 4337–4350.

Sekiya, H. (1977). Anomalous seismic activity and earthquake prediction. *J. Phys. Earth* **25S**, 85–93.

Semenov, A. M. (1969). Variations in the travel-time of transverse and longitudinal waves before violent earthquakes. *Izv., Acad. Sci., USSR, Phys. Solid Earth (Engl. Transl.)* No. 4, pp. 245–248.

Shampine, L. F., and Gordon, M. K. (1975). "Computer Solution of Ordinary Differential Equations: The Initial Value Problem." Freeman, San Francisco, California.

Shapira, A., and Bath, M. (1977). Short distance hypocenter location in layered media. *Seismol. Inst. Uppsala (Sweden) Rep.* **2-77.**

Shapira, A., and Bath, M. (1978). Source mechanism determination of short distance microearthquakes. *Seismol. Inst. Uppsala (Sweden) Rep.* **1-78.**

Shen, C. K., Chang, C. H., Chen, H. C., Li, T. C., Huang, L. S., Wang, T. C., Yang, C. J., and Lo, H. H. (1974). Earthquakes induced by reservoir impounding and their effect on the Hsinfengkiang Dam. *Sci. Sin.* **17**, 239–272.

Shimamura, H., Tomoda, Y., and Asada, T. (1975). Seismographic observation at the bottom of the Central Basin fault of the Philippine Sea. *Nature (London)* **253**, 177–179.

Shirai, K., and Tokuhiro, I. (1979). Detection of seismic wave onsets. *J. Seismol. Soc. Japan* **32**, 141–147 (in Japanese with English abstract).

Shirley, J. E. (1980). Tasmanian seismicity—natural and reservoir induced. *Bull. Seismol. Soc. Am.* **70**, 2203–2220.

Simila, G. W., Peppin, W. A., and McEvilly, T. V. (1975). Seismotectonics of the Cape Mendocino, California, area. *Geol. Soc. Am. Bull.* **86**, 1399–1406.

Simpson, D. W. (1976). Seismicity changes associated with reservoir loading. *Eng. Geol. (Amsterdam)* **10**, 123–150.

Simpson, D. W., Hamburger, M. W., Pavlov, V. D., and Nersesov, I. L. (1981). Tectonics and seismicity of the Toktogul reservoir region, Kirgizia, USSR. *J. Geophys. Res.* **86**, 345–358.

Singh, S., Agrawal, P. N., and Arya, A. S. (1976). Filling of Ramganga Reservoir, Kalagarh, U. P., India and its possible influence on seismic activity. *Bull. Seismol. Soc. Am.* **66**, 1727–1731.

Singh, S. K., Havskov, J., McNally, K., Ponce, L., Hearn, T., and Vassiliou, M. (1980). The Oaxaca, Mexico, earthquake of 29 November 1978: A preliminary report on aftershocks. *Science* **207**, 1211–1213.

Smith, R. B., Winkler, P. L., Anderson, J. G., and Scholz, C. H. (1974). Source mechanisms of microearthquakes associated with underground mines in eastern Utah. *Bull. Seismol. Soc. Am.* **64**, 1295–1317.

Smith, R. B., Shuey, R. T., Pelton, J. R., and Bailey, J. P. (1977). Yellowstone Hot Spot: Contemporary tectonics and crustal properties from earthquake and aeromagnetic data. *J. Geophys. Res.* **82**, 3665–3676.

Soboleva, O. V., and Mamadaliev, V. A. (1976). The influence of the Nurek Reservoir on local earthquake activity. *Eng. Geol. (Amsterdam)* **18**, 293–305.

Sodbinow, E. S., and Bollinger, G. A. (1978). Seismic studies in central and eastern Tennessee. *Bull. Seismol. Soc. Am.* **68**, 1081–1094.

Solomon, S. C., Mattaboni, P. J., and Hester, R. L. (1977). Microseismicity near the Indian Ocean triple junction. *Geophys. Res. Lett.* **4**, 597–600.

Solov'ev, S. L. (1965). Seismicity of Sakhalin. *Bull. Earthquake Res. Inst., Univ. Tokyo* **43**, 95–102.

Spencer, C., and Gubbins, D. (1980). Travel-time inversion for simultaneous earthquake location and velocity structure determination in laterally varying media. *Geophys. J. R. Astron. Soc.* **63**, 95–116.

Spindel, R. C., Davis, S. B., MacDonald, K. C., Porter, R. P., and Phillips, J. D. (1974). Microearthquake survey of Median Valley of the Mid-Atlantic Ridge at 36° 30′N. *Nature (London)* **248**, 577–579.

Stauder, W. (1962). The focal mechanism of earthquakes. *Adv. Geophys.* **9**, 1–76.

Stauder, W. (1971). Smaller aftershocks of the Benham nuclear explosion. *Bull. Seismol. Soc. Am.* **61**, 417–428.

Stauder, W., and Ryall, A. (1967). Spatial distribution and source mechanism of microearthquakes in central Nevada. *Bull. Seismol. Soc. Am.* **57**, 1317–1345.

Stauder, W., Kramer, M., Fischer, G., Schaefer, S., and Morrissey, S. T. (1976). Seismic characteristics of southeast Missouri as indicated by a regional telemetered microearthquake array. *Bull. Seismol. Soc. Am.* **66**, 1953–1964.

Steeples, D. W. (1979). Microearthquake network in Kansas. *In* "Terrestrial and Space Techniques in Earthquake Prediction Research" (A. Vogel, ed.), pp. 115–130. Vieweg, Braunschweig.

Steeples, D. W., and Iyer, H. M. (1976a). Low velocity zone under Long Valley as determined from teleseismic events. *J. Geophys. Res.* **81**, 849–860.

Steeples, D. W., and Iyer, H. M. (1976b). Teleseismic P wave delays in geothermal exploration. *Proc. U.N. Symp. Dev. Use Geotherm. Resour., 2nd, 1975* Vol. 2, pp. 1199–1206.

Steeples, D. W., and Pitt, A. M. (1976). Microearthquakes in and near Long Valley, California. *J. Geophys. Res.* **81**, 841–847.

Steinwachs, M. (1971). Interpretation of microearthquake recordings in western Greece. *Z. Geophys.* **37**, 867–881 (in German with English abstract).

Stephens, C. D., Lahr, J. C., Fogleman, K. A., and Horner, R. B. (1980). The St. Elias, Alaska earthquake of 28 February 1979: Regional recording of aftershocks and short-term, pre-earthquake seismicity. *Bull. Seismol. Soc. Am.* **70**, 1607–1633.

Steppe, J. A., and Crosson, R. S. (1978). P velocity models of the southern Diablo Range, California, from inversion of earthquake and explosion arrival times. *Bull. Seismol. Soc. Am.* **68**, 357–367.

Steppe, J. A., Bakun, W. H., and Bufe, C. G. (1977). Temporal stability of P velocity anisotropy before earthquakes in central California. *Bull. Seismol. Soc. Am.* **67**, 1075–1090.

Stevenson, D. A. (1977). $V_p/V_s$ anomalies associated with Lake Jocassee, South Carolina, earthquakes, M.S. Thesis, University of South Carolina, Columbia.

Stevenson, P. R. (1976). Microearthquakes at Flathead Lake, Montana: A study using automatic earthquake processing. *Bull. Seismol. Soc. Am.* **66**, 61–80.

Stevenson, P. R. (1978). Program ISDS: An interactive seismic display system for displaying and measuring seismic wave forms. *Geo. Surv. Open-File Rep. (U.S.)* **79-205**, 1–176.

Stewart, G. S. (1973). Prediction of the Pt. Mugu earthquake by two methods. *Stanford Univ. Publ., Geol. Sci.* **13**, 473–478.

Stewart, G. W. (1973). "Introduction to Matrix Computations." Academic Press, New York.

Stewart, S. W. (1977). Real time detection and location of local seismic events in central California. *Bull. Seismol. Soc. Am.* **67**, 433–452.

Stewart, S. W., and O'Neill, M. E. (1980). Calculation of the frequency response of the USGS telemetered short-period seismic system. *Geol. Surv. Open-File Rep. (U.S.)* **80-143**, 1–83.

Stewart, S. W., Lee, W. H. K., and Eaton, J. P. (1971). Location and real-time detection of microearthquakes along the San Andreas fault system in central California. *Bull.—R. Soc. N. Z.* **9**, 205–209.

Stierman, D. J., and Ellsworth, W. L. (1976). Aftershocks of the February 21, 1973 Point Mugu, California earthquake. *Bull. Seismol. Soc. Am.* **66**, 1931–1952.

Strang, G. (1976). "Linear Algebra and its Applications," 1st ed. Academic Press, New York.

Stump, B. W., and Johnson, L. R. (1977). The determination of source properties by the linear inversion of seismograms. *Bull. Seismol. Soc. Am.* **67**, 1489–1502.

Suteau, A. M., and Whitcomb, J. H. (1979). A local earthquake coda magnitude and its relation to duration, moment $M_0$, and local Richter magnitude $M_L$. *Bull. Seismol. Soc. Am.* **69**, 353–368.

Sutton, D. J. (1974). A fall in P wave velocity before the Gisborne, New Zealand, earthquake of 1966. *Bull. Seismol. Soc. Am.* **64**, 1501–1508.

Suyehiro, S. (1968). Change in earthquake spectrum before and after the Matsushiro swarm. *Pap. Meteorol. Geophys.* **19**, 427–435.

Suyehiro, S., Asada, T., and Ohtake, M. (1964). Foreshocks and aftershocks accompanying a perceptible earthquake in central Japan: On the peculiar nature of foreshocks. *Pap. Meteorol. Geophys.* **15**, 71–88.

Suzuki, Z. (1953). A statistical study on the occurrence of small earthquakes, I. *Sci. Rep. Tohoku Univ., Ser. 5*, **5**, 177–182.

Suzuki, Z., Tsumura, K., Oike, K., and Matsumura, K., eds. (1979). "Microearthquake Observatories in Japan," 2nd ed. (in Japanese).

Sykes, L. R. (1971). Aftershock zones of great earthquakes, seismicity gaps, and earthquake prediction for Alaska and the Aleutians. *J. Geophys. Res.* **76**, 8021–8041.

Sykes, L. R. (1977). Research on earthquake prediction and related areas at Columbia University. *J. Phys. Earth* **25S**, 13–29.

Sykes, L. R., Kisslinger, J. B., House, L., Davies, J. N., and Jacob, K. H. (1980). Rupture zones of great earthquakes, Alaska—Aleutian Arc, 1784–1980. *Science* **210**, 1343–1345.

Sylvester, A. G., Smith, S. W., and Scholz, C. H. (1970). Earthquake swarm in the Santa Barbara Channel, California, 1968. *Bull. Seismol. Soc. Am.* **60**, 1047–1060.

Synge, J. L. (1937). "Geometrical Optics." Cambridge Univ. Press, London and New York.

Takahashi, H., and Hamada, K. (1975). Deep borehole observation of the earth's crust activities around Tokyo—introduction of the Iwatsuki observatory. *Pure Appl. Geophys.* **113**, 311–320.

Talwani, P. (1976). Earthquakes associated with the Clark Hill Reservoir, South Carolina —a case of induced seismicity. *Eng. Geol. (Amsterdam)* **10**, 239–253.

Talwani, P. (1977). Stress distribution near Lake Jocassee, South Carolina. *Pure Appl. Geophys.* **115**, 275–281.

Talwani, P., Stevenson, D., Chiang, J., Sauber, J., and Amick, D. (1977). "The Jocassee Earthquakes (March-May '77)," 5th Tech. Rep. University of South Carolina, Columbia.

Talwani, P., Stevenson, D., Sauber, J., Rastogi, B. K., Drew, A., Chiang, J., and Amick, D. (1978). "Seismicity Studies at Lake Jocassee, Lake Keowee and Monticello Reservoir, South Carolina (October 1977 to March 1978)," 7th Tech. Rep. University of South Carolina, Columbia.

Talwani, P., Stevenson, D., Amick, D., and Chiang, J. (1979). An earthquake swarm at Lake Keowee, South Carolina. *Bull. Seismol. Soc. Am.* **69**, 825–841.

Teng, T. L., Real, C. R., and Henyey, T. L. (1973). Microearthquakes and water flooding in Los Angeles. *Bull. Seismol. Soc. Am.* **63**, 859–875.

Thatcher, W. (1973). A note on discrepancies between local magnitude ($M_L$) and microearthquake magnitude scales. *Bull. Seismol. Soc. Am.* **63**, 315–319.

Thatcher, W., and Hamilton, R. M. (1973). Aftershocks and source characteristics of the 1969 Coyote Mountain earthquake, San Jacinto fault zone, California. *Bull. Seismol. Soc. Am.* **63**, 647–661.

Thatcher, W., and Hanks, T. C. (1973). Source parameters of southern California earthquakes. *J. Geophys. Res.* **78**, 8547–8576.

Thurber, C. H., and Ellsworth, W. L. (1980). Rapid solution of ray tracing problems in heterogeneous media. *Bull. Seismol. Soc. Am.* **70**, 1137–1148.

Timmel, K. E., and Simpson, D. W. (1973). Seismic events during filling of Talbingo Reservoir. *Bull. Aust. Natl. Comm. Large Dams* pp. 27–33.

Tobin, D. G., Ward, P. L., and Drake, C. L. (1969). Microearthquakes in the Rift Valley of Kenya. *Geol. Soc. Am. Bull.* **80**, 2043–2046.

Torrieri, D. J. (1972). The uncertainty of pulse position due to noise. *IEEE Trans. Aerosp. Electron. Syst.* **AES-8**, 661–668.

Trimble, A. B., and Smith, R. B. (1975). Seismicity and contemporary tectonics of the Hebgen Lake—Yellowstone Park region. *J. Geophys. Res.* **80**, 733–741.

Truscott, J. R. (1964). The Eskdalemuir seismological station. *Geophys. J. R. Astron. Soc.* **9**, 59–68.

Tsai, Y. B., Feng, C. C., Chiu, J. M., and Liaw, H. B. (1975). Correlation between microearthquakes and geologic faults in the Hsintien–Ilan area. *Petroleum Geol. Taiwan* **12**, 149–167.

Tsujiura, M. (1966). Frequency analysis of seismic waves (1). *Bull. Earthquake Res. Inst., Univ. Tokyo* **44**, 873–891.

Tsujiura, M. (1978). Spectral analysis of the coda waves from local earthquakes. *Bull. Earthquake Res. Inst., Univ. Tokyo* **53**, 1–48.

Tsujiura, M. (1979). The difference between foreshocks and earthquake swarms, as inferred from the similarity of seismic waveform. *Bull. Earthquake Res. Inst., Univ. Tokyo* **54**, 309–315 (in Japanese with English abstract).

Tsumura, K. (1967). Determination of earthquake magnitude from total duration of oscillation. *Bull. Earthquake Res. Inst., Univ. Tokyo* **45**, 7–18.

Tsumura, K., Karakama, I., Ogino, I., Sakai, K., and Takahashi, M. (1977). Observation of the earthquake swarm in the Izu Peninsula (1975–1977). *Bull. Earthquake Res. Inst., Univ. Tokyo* **52**, 113–140 (in Japanese with English abstract).

Tsumura, K., Karakama, I., Ogino, I., and Takahashi, M. (1978). Seismic activities before and after the Izu-Oshima-Kinkai earthquake of 1978. *Bull. Earthquake Res. Inst., Univ. Tokyo* **53**, 675–706 (in Japanese with English abstract).

Tucker, B. E., and Brune, J. N. (1973). Seismograms, S wave spectra, and source parameters for aftershocks of San Fernando earthquake. *In* "San Fernando, California, Earthquake of February 9, 1971" (L. M. Murphy, ed.), Vol. 3, pp. 69–121. U.S. Govt. Printing Office, Washington, D.C.

Udias, A. (1977). Time and magnitude relations for three microaftershock series near Hollister, California. *Bull. Seismol. Soc. Am.* **67**, 173–185.

Udias, A., and Baumann, D. (1969). A computer program for focal mechanism determination combining P and S wave data. *Bull. Seismol. Soc. Am.* **59**, 503–519.

Udias, A., and Rice, J. (1975). Statistical analysis of microearthquake activity near San Andreas Geophysical Observatory, Hollister, California. *Bull. Seismol. Soc. Am.* 65, 809–827.

Uhrhammer, R. A. (1980a). Observations of the Coyote Lake, California earthquake sequence of August 6, 1979. *Bull. Seismol. Soc. Am.* **70**, 559–570.

Uhrhammer, R. A. (1980b). Analysis of small seismographic station networks. *Bull. Seismol. Soc. Am.* **70**, 1369–1380.

Unger, J. D., and Coakley, J. M. (1971). Microearthquakes near Lassen Peak, California. *Geol. Surv. Prof. Pap. (U.S.)* **750C**, 156–157.

Unger, J. D., and Decker, R. W. (1970). The microearthquake activity of Mt. Rainer, Washington. *Bull. Seismol. Soc. Am.* **60**, 2023–2035.

Unger, J. D., and Mills, K. F. (1972). Microearthquakes at Mt. Rainer—1969. *Bull. Seismol. Soc. Am.* **62**, 1079–1081.

Utsu, T. (1965). A method for determining the value of b in a formula $\log n = a - bM$ showing the magnitude—frequency relation for earthquakes. *Geophys. Bull., Hokkaido Univ.* **13**, 99–103 (in Japanese with English abstract).

Utsu, T. (1966). A statistical significance test of the difference in b value between two earthquake groups. *J. Phys. Earth* **14**, 37–40.

Utsu, T. (1971). Aftershocks and earthquake statistics (III)—analyses of the distribution of earthquakes in magnitude, time, and space with special consideration to clustering characteristics of earthquake occurrence (1). *J. Fac. Sci., Hokkaido Univ., Ser. 7*, **3**, 379–441.

Utsu, T. (1973). Temporal variations in travel time residuals of P waves from Nevada sources. *J. Phys. Earth* **21**, 475–480.

Utsu, T. (1975). Detection of a domain of decreased P velocity prior to an earthquake. *J. Seismol. Soc. Japan* **28**, 435–448 (in Japanese with English abstract).

Utsu, T. (1978). An investigation into the discrimination of foreshock sequences from earthquake swarms. *J. Seismol. Soc. Japan* **31**, 129–135 (in Japanese with English abstract).

Van Loan, C. (1976). "Lectures in Least Squares," Tech. Rep. TR 76-279. Cornell University, Ithaca, New York.

Van Schaack, J. (1975). Self-calibrating seismic amplifier and telemetry system. *Geol. Surv. Open-File Rep. (U.S.)* **75-64**, 1–5.

Varghese, T. G., Roy, F., Rao, B. S. S., Suryavanshi, M. P., and Bharthur, R. N. (1979). Exploitation of the Gauribidanur array for seismic monitoring. *Phys. Earth Planet. Inter.* **18**, 87–94.

Vere-Jones, D. (1970). Stochastic models for earthquake occurrence. *J. R. Stat. Soc. B.* 32, 1–62.

Vere-Jones, D. (1978). Space time correlations for microearthquakes—a pilot study. *Suppl. Adv. Appl. Probability* 10, 73–87.

Wadati, K. (1931). Shallow and deep earthquakes. *Geophys. Mag.* **4**, 231–283.

Wadati, K. (1933). On the travel time of earthquake waves. Part II. *Geophys. Mag.* **7**, 101–111.

Wallace, R. E., and Sadovskiy, M. A. (1976). "Collection of Soviet-American Works on Earthquake Prediction," Vol. I. Donish Publ. House, Dushanbe-Moscow, USSR (in Russian).

Walter, A. W., and Weaver, C. S. (1980). Seismicity of the Coso Range, California. *J. Geophys. Res.* **85**, 2441–2458.

Wang, M. Y., Yang, M. Y., and Hu, Y. L. (1976). Mechanism of the reservoir impounding earthquakes at Xinfengjiang and a preliminary endeavour to discuss their causes. *Acta Geophys. Sin.* **19**, 1–17 (in Chinese with English abstract).

Ward, P. L. (1972). Microearthquakes: Prospecting tool and possible hazard in the development of geothermal resources. *Geothermics* **1**, 3–12.

Ward, P. L., and Bjornsson, S. (1971). Microearthquakes, swarms, and the geothermal areas of Iceland. *J. Geophys. Res.* **76**, 3953–3982.

Ward, P. L., and Jacob, K. H. (1971). Microearthquakes in the Ahuachapan geothermal field, El Salvador, Central America. *Science* **173**, 328–330.

Ward, P. L., Palmason, G., and Drake, C. (1969). Microearthquake survey and the Mid-Atlantic Ridge in Iceland. *J. Geophys. Res.* **74**, 665–684.

Ward, P. L., Gibbs, J., Harlow, D., and Aburto, A. Q. (1974). Aftershocks of the Managua, Nicaragua, earthquake and the tectonic significance of the Tiscapa fault. *Bull. Seismol. Soc. Am.* **64**, 1017–1029.

Ward, P. L., Herriot, J., and Jolitz, W. (1980). Decentralized shared computers in the National Earthquake Hazards Reduction Program. *Proc. Natl. USENIX Conf., June 17, 1980.*

Ward, S. N. (1980). A technique for the recovery of the seismic moment tensor applied to the Oaxaca, Mexico earthquake of November, 1978. *Bull. Seismol. Soc. Am.* **70**, 717–734.

Watanabe, H., and Kuroiso, A. (1967). Some properties of microearthquakes in the west of Kii Peninsula, central Honshu, Japan. *J. Seismol. Soc. Japan* **20**, 180–191 (in Japanese with English abstract).

Watanabe, H., and Kuroiso, A. (1969). Seismic activity in the northern part of the Kinki district and related problems. (1). Earthquake swarm accompanying the Wachi earthquake of August 18, 1968. *Spec. Contrib. Geophys. Inst., Kyoto Univ.* **9**, 123–136.

Watanabe, H., and Kuroiso, A. (1970). Aftershocks of the earthquake of the central part of Gifu prefecture, September 9, 1969. *Bull. Earthquake Res. Inst., Univ. Tokyo* **48**, 1195–1208 (in Japanese with English abstract).

Watanabe, H., and Kuroiso, A. (1977). On the automatic data processing system for mi-

croearthquake observation at Abuyama Seismological Observatory. *J. Seismol. Soc. Japan* **30**, 115–118 (in Japanese).

Watanabe, H., and Nakamura, M. (1967). Some properties of microearthquakes in the vicinity of the Neo Valley fault, central Honshu, Japan. *J. Seismol. Soc. Japan* **20**, 106–115 (in Japanese with English abstract).

Watanabe, H., and Nakamura, M. (1968). On the upper crustal structure in the southwestern part of Kinki district, central Japan. *J. Seismol. Soc. Japan* **21**, 32–53 (in Japanese with English abstract).

Watanabe, H., Nakamura, M., and Kuroiso, A. (1967). Observation of microearthquakes around Mt. Minakami. *Bull. Disaster Prev. Res. Inst., Kyoto Univ.* **17**, 23–26.

Watanabe, S., and Iida, K. (1970). Activity of microearthquakes near Atera fault. *J. Seismol. Soc. Japan* **22**, 348–349 (in Japanese).

Weichert, D. H., and Henger, M. (1976). The Canadian seismic array monitor processing system (CANSAM). *Bull. Seismol. Soc. Am.* **66**, 1381–1403.

Wesson, R. L. (1971). Travel-time inversion for laterally inhomogeneous crustal velocity models. *Bull. Seismol. Soc. Am.* **61**, 729–746.

Wesson, R. L., and Ellsworth, W. L. (1973). Seismicity preceding moderate earthquakes in California. *J. Geophys. Res.* **78**, 8527–8546.

Wesson, R. L., Lee, W. H. K., and Gibbs, J. F. (1971). Aftershocks of the San Fernando earthquake. *Geol. Surv. Prof. Pap. (U.S.)* **733**, 24–32.

Wesson, R. L., Burford, R. O., and Ellsworth, W. L. (1973a). Relationship between seismicity, fault creep and crustal loading along the central San Andreas fault. *Stanford Univ. Publ., Geol. Sci.* **13**, 303–321.

Wesson, R. L., Roller, J. C., and Lee, W. H. K. (1973b). Time-term analysis and geological interpretation of seismic travel-time data from the Coast Ranges of central California. *Bull. Seismol. Soc. Am.* **63**, 1447–1471.

Westphal, W. H., and Lange, A. L. (1967). Local seismic monitoring: Fairview Peak area, Nevada. *Bull. Seismol. Soc. Am.* **57**, 1279–1298.

Whitcomb, J. H. (1977). Earthquake prediction related research at the Seismological Laboratory, California Institute of Technology, 1974–1976. *J. Phys. Earth* **25S**, 1–11.

Whitcomb, J. H., Garmany, J. D., and Anderson, D. L. (1973). Earthquake prediction: Variation of seismic velocities before the San Fernando earthquake. *Science* **180**, 632–635.

Wickens, A. J., and Hodgson, J. H. (1967). Computer re-evaluation of earthquake mechanism solutions. *Publ. Dom. Obs. (Ottawa)* **33**, 1–560.

Wiggins, R. A. (1972). The general linear inverse problem: Implication of surface waves and free oscillations for earth structure. *Rev. Geophys. Space Phys.* **10**, 251–285.

Wilkinson, J. H. (1965). "The Algebraic Eigenvalue Problem." Oxford University Press, Oxford.

Willmore, P. L. (1961). Some properties of heavily damped electromagnetic seismographs. *Geophys. J. R. Astron. Soc.* **4**, 389–404.

Willmore, P. L., ed. (1979). Manual of seismological observatory practice. *World Data Cent. A Solid Earth Geophys.* **SE-20**, 1–141.

Willmore, P. L., Hales, A. L., and Gane, P. G. (1952). A seismic investigation of crustal structure in the western Transvaal. *Bull. Seismol. Soc. Am.* **42**, 53–80.

Wolfe, M. A. (1978). "Numerical Methods for Unconstrained Optimization." Van Nostrand-Reinhold, Princeton, New Jersey.

Wood, R. (1974). Microearthquakes at central American volcanoes. *Bull. Seismol. Soc. Am.* **64**, 275–277.

Woodward, R. S. (1929). "Smithsonian Geographical Tables," 3rd ed. Smithsonian Institution, Washington, D.C.

Wu, C., and Crosson, R. S. (1975). Numerical investigation of dilatancy biasing of hypocenter locations. *Geophys. Res. Lett.* **2**, 205–208.

Wu, F. T., Karcz, L., Arieh, E. J., Kafri, U., and Peled, U. (1973). Microearthquakes along the Dead Sea rift. *Geology* **1**, 159–161.

Wu, K. T., Yue, M. S., Wu, H. Y., Chao, S. L., Chen, H. T., Huang, W. Q., Tien, K. Y., and Lu, S. D. (1976). Certain characteristics of Haicheng earthquake (M = 7.3) sequence. *Acta Geophys. Sin.* **19**, 95–109.

Wyss, M. (1975). Precursors to the Garm earthquake of March 1969. *J. Geophys. Res.* **80**, 2926–2930.

Wyss, M., and Habermann, R. E. (1979). Seismic quiescence precursory to a past and a future Kurile Island earthquake. *Pure Appl. Geophys.* **117**, 1195–1211.

Wyss, M., and Holcomb, D. J. (1973). Earthquake prediction based on station residuals. *Nature (London)* **245**, 139–140.

Wyss, M., and Johnston, A. C. (1974). A search for teleseismic P residual changes before large earthquakes in New Zealand. *J. Geophys. Res.* **79**, 3283–3290.

Wyss, M., and Lee, W. H. K. (1973). Time variations of the average earthquake magnitude in central California. *Stanford Univ. Publ., Geol Sci.* **13**, 24–42.

Wyss, M., Habermann, R. E., and Johnston, A. C. (1978). Long term precursory seismicity fluctuations. *Geol. Surv. Open-File Rep. (U.S.)* **78-943**, 869–894.

Xiao, Y. Y., and Li, P. (1979). Employment of pattern recognition for locating strong earthquake zones in Beijing—Tianjin area and its adjacent regions. *Seismol. Geol.* **1**, 66–78 (in Chinese with English abstract).

Yamada, I., and Ooida, T. (1972). Microearthquake activity in central Honshu, Japan (part 3). *J. Seismol. Soc. Japan* **25**, 115–123 (in Japanese with English abstract).

Yamada, I., Miyajima, R., Fujii, I., and Nakamura, M. (1972). Microearthquake activity in northern part of Gifu Prefecture, central Japan (part 1). *J. Seismol. Soc. Japan* **25**, 124–133 (in Japanese with English abstract).

Yamashina, K., and Inoue, Y. (1979). A doughnut-shaped pattern of seismic activity preceding the Shimane earthquake of 1978. *Nature (London)* **278**, 48–50.

Yang, J. P., and Lee, W. H. K. (1976). Preliminary investigations on computational methods for solving the two-point seismic ray-tracing problems in a heterogeneous and isotropic medium. *Geol. Surv. Open-File Rep. (U.S.)* **76–707**, 1–66.

Young, C., and Ward, R. W. (1980). Three-dimensional 1/Q model of the Coso Hot Springs known geothermal resource area. *J. Geophys. Res.* **85**, 2459–2470.

Zandt, G. (1978). Study of three-dimensional heterogeneity beneath seismic arrays in central California and Yellowstone, Wyoming. Ph.D. Thesis, Massachusetts Institute of Technology, Cambridge.

Zverev, S. M., Boldyrev, S. A., Bourmin, V. Yu., and Mironova, V. I. (1978). Weak earthquakes in the northern part of the rift zone of Iceland. *J. Geophys.* **44**, 283–296.

# Author Index

Numbers in italics refer to pages on which the complete references are listed.

## A


Aboodi, E., *234*
Aburto, A. Q., *264*
Acton, F. S., 83, *231*
Adams, H. E., 184, *248*
Adams, R. D., 157, 196, *231*
Adby, P. R., 122, *231*
Agarwal, B. N. P., *242*
Aggarwal, Y. P., 9, 178, 210, *231, 254, 259*
Agrawal, P. N., *260*
Ahmed, A., 196, *231*
Akamatu, K., *233*
Aki, K., 40, 82, 106, 148, 158, 159, 162, 163, 169, 170, 188, 214, 216, *226*, 229, *231, 232, 250, 253, 256*
Allen, C. R., 9, 155, 183, 203, 213, *232, 235, 248*
Allen, N. J., 195, *232*
Allen, R. V., 65, 67–69, 73, 75, *223, 232*
Allison, M. L., 190, *232*
Alpaslan, T., *247*
Alsinawi, S. A., 178, *232*
Ambuter, B. P., 54, 57, *232*
Amick, D., *262*
Anderson, D. L., 159, 160, *247, 265*
Anderson, J. A., 3, 8, *232*
Anderson, J. G., 161, *232, 260*
Anderson, K. R., 65–67, 75, *232*
Ando, S., *253*
Andrews, D. J., 161
Anglin, F., 197, *249*
Ankyu, T., *245*
Aoki, H., *245*
Arabasz, W. J., 157, 180–182, *232, 240, 242, 258*
Archer, C. B., 195, *232*
Arieh, E. J., *266*
Armbruster, J., *231, 259*
Armstrong, B. H., 19, *232*
Aronovich, Z. I., 181, *232*
Arya, A. S., *260*
Asada, T., 6, 8, 179, 188, 203, *233, 259, 261*
Asano, S., 213, *233*
Asfaw, L. M., *254*
Aspinall, W. P., 185, *233*
Asudeh, I., *234*
Atkins, A. R., *241*


## B


Backus, G., 106, 111, *233*
Bacon, C. F., 19, *233*
Bagdasarova, A. M., *240*
Bailey, J. P., *260*
Bakun, W. H., 32–34, 37, 156, 157, 161, 202, 206, 212, 221, *233, 250, 252, 261*
Banno, I. S., 178, *232*
Barazangi, M., *259*
Bard, Y., 122, *233*
Barker, T., *257*
Bates, R. L., *226*
Bath, M., 40, 130, 134, 147, 155, 194, *233, 259*
Baumann, D., 147, *263*
Ben-Israel, A., 114, 118, 120, *233*
Ben-Menahem, A., 179, 203, *234*
Bennett, R. E., *250*
Berberian, M., 192, *234, 244*
Berry, A., 47, *234*
Bharthur, R. N., *264*
Bilham, R. G., *234*
Billings, M. P., 141, *234*
Birkhahn, P. C., *259*
Bisztricsany, E., 156, *234*
Bjorck, A., 105, 118, *238*

Bjornsson, S., 181, *239, 264*
Blackwell, D. D., *241*
Blair, B. E., 31, *234*
Bloch, S., 189, *242*
Blum, R., 197, *234*
Boatwright, J., 161, 162, *234, 249*
Bock, G., 197, *234, 241*
Boldyrev, S. A., *240, 266*
Bollinger, G. A., 185, 191, *234, 249, 260*
Bolt, B. A., 8, 17, 134, 137, 138, 191, 212, 220, *234, 235*
Bonjer, K. P., *241*
Booker, J. R., 112, 152, *236, 256*
Boore, D. M., 212, *234*
Boucher, G., 182, 193, *235, 243*
Bourmin, V. Yu., *258, 266*
Brabb, E. E., *250*
Bradner, H., 190, *235, 257*
Brady, B. T., 194, *235*
Brahe, T., 47
Brander, J. L., *244*
Brandsaeter, H., 214, *235*
Bredehoeft, J. D., *257*
Brillinger, D. R., 147, *235*
Brocher, T., *249*
Brown, R., 211, *235*
Brown, R. L., 196, *235*
Brune, J. N., 8, 9, 19, 20, 41, 155, 158, 159, 161, 183, 190, 203, 221, *232, 235, 254, 255, 257, 263*
Buchbinder, G., 182, *249*
Buck, S. W., *239*
Bufe, C. G., 195, 201, 207, 210, 217, 218, *233, 235, 237, 249, 250, 261*
Buland, R., 130, 138, *235*
Bungum, H., 2, *235*
Burdick, L. J., 169, *235*
Burford, R. O., *235, 265*
Burns, D. S., *239*
Burridge, R., 158, *235*
Byerly, P., 130, 140, *235*

## C

Cagnetti, V., 191, *236, 250*
Caldwell, J. G., 181, *236*
Canales, L., *235, 257*
Capon, J., 2, 58, *236*
Caputo, M., 206, *236*
Carder, D. S., 195, *236*
Carlson, R., 183, *236*
Carmichael, D., 44, *236*
Carpenter, G., *236*
Carver, D., 192, *236*
Casaday, K. B., 188, *252*
Casten, U., 194, *236*
Cerveny, V., 77, 138, *236*
Cete, A., 194, *236*
Chambers, J. M., 128, *236*
Chander, R., 84, *236*
Chandra, U., 147, *236*
Chang, C. C., 200, *236*
Chang, C. H., *259*
Chao, S. L., *266*
Chao, Y., *236*
Chapman, C. H., 95, *238*
Chatelain, J. L., 178, *236*
Cheatum, C. E., 183, *232, 236*
Chen, H. C., *259*
Chen, H. T., *266*
Chen, Y., *236*
Cheng, C. C., *253*
Chiang, J., *262*
Chin, Y., 219, *236*
Chiu, J. M., *262*
Cho, Y. J., *236*
Chou, C. W., 112, 213, *236*
Chouet, B., 162, *231*
Christoffersson, A., *232*
Chung, W. Y., 213, *247*
Claerbout, J. F., 112, *236*
Cleary, J. R., 2, *237*
Clymer, R. W., 214, *237*
Coakley, J. M., 183, *246, 263*
Cockerham, R. S., 170, 192, *237*
Combs, J., 168, 183, *236, 237, 242, 249*
Comer, R. P., 90, *251*
Comninakis, P., 196, *237*
Conant, D. A., 181, *237*
Cook, N. G. W., 167, 194, *237*
Corbishley, D. J., 2, *237*
Cornea, I., *241*
Courant, R., 81, 124, *237*
Cox, D. R., 163, *237*
Cramer, C. H., 183, 210, 212, *237*
Crampin, S., 63, 64, 67, 69, 70, 74, 134, 180, 215, *237, 238*
Crosson, R. S., 9, 17, 148, 156, 169, 170, 213, 218, *236, 238, 252, 256, 261, 266*

D

Dahlquist, G., 105, 118, *238*
Davies, J. N., *262*
Davis, S. B., *260*
Decker, R. W., 185, *263*
Delhaye, A., 191, *238*
Del Pezzo, E., 181, *238*
Dempster, M. A. H., 122, *231*
Dennis, J. E., 128, *238*
DeNoyer, J., 180, *238*
Dewey, J. W., 138, *238*
Dey-Sarkar, S. K., 95, *238*
Dillinger, W. H., 147, *238*
Donnelly, T. W., *254*
Dorman, J., 249, *259*
Douglas, A., 138, *238*
Douglas, B. M., 161, *238*
Dragert, H., *239*
Drake, C. L., 262, *264*
Drakopoulos, J., *237*
Draper, N. R., 113, 137, *238*
Dratler, J., 32–34, 37; *233*
Drew, A., *262*
DuBerger, R., *249*
Duda, S. J., 155, *238*
Dunphy, G. J., 195, *238*

E

Eaton, J. P., 8, 9, 19–21, 23, 25, 26, 30, 38, 39, 41, 51, 96, 134, 155, 169, 170, 189, *238*, *239*, *261*
Eaton, M. S., *250*
Eckart, C., 114, *239*
Einarsson, P., 191, *239*, *248*
Eliseevnin, V. A., 83, *239*
Ellis, J. O., 223, *232*
Ellis, R. M., 197, *239*
Ellsworth, W. L., 138, 170, 190, 206, *237*, *239*, *257*, *258*, *261*, *262*, *265*
Emura, K., 142, *244*
Endo, E. T., *238*
Endo, Y., *254*
Enescu, D., *241*
Engdahl, E. R., 82, 84, 134, 136, 138, 147, 148, 208, 210, 213, 215, 221, *239*, *248*
Engen, G. R., *232*
Espinosa, A. F., 32, *239*
Estill, R. E., 184, *239*
Eterno, J. S., 57, *239*
Euler, L., 84
Evans, J. R., *246*
Evison, F. F., 181, 202, 211, *239*, *240*

F

Farestveit, A., *235*
Fedotov, S. A., 8, 200, 206, *240*
Feng, C. C., *251*, *262*
Feng, D. Y., 211, *240*
Feng, R., 210, *240*
Fischer, F. G., *243*
Fischer, G., *260*
Fitch, T. J., 182, 209, *235*, *240*, *254*
Fletcher, J. B., 41, 161, 167, *232*, *240*
Fletcher, R., 123, 126, 128, *240*
Flinn, E. A., 134, *240*
Fogleman, K. A., *261*
Fomin, S. V., 81, *241*
Forsythe, G. E., 114, 117, 118, 121, *240*
Francis, T. J. G., 17, 43–45, 186, *240*, *241*, *250*
Frechet, J., 181, *241*
Freidline, R. A., 184, *241*
Freier, L. J., *239*
Frohlich, C., 181, *236*, *259*
Fu, Z. X., *240*
Fuchs, K., 191, 197, *234*, *241*
Fuis, G., 213, *247*, *251*
Fujii, I., *266*
Fujisawa, I., *245*
Fung, Y. C., 76, *241*
Fyfe, C. J., 63, 64, 67, 69, 70, 74, *237*

G

Gaiser, J. E., 213, *241*
Gal'perin, Y. I., 7, *241*
Gamburtsev, G. A., 7, *241*
Gane, P. G., 5, 169, 194, *241*, *265*
Garmany, J. D., 95, *241*, *265*
Garza, T., 199, *241*
Gay, D. M., *238*
Gay, N. C., *252*
Gear, W. C., 83, 86, *241*
Gebrande, H., 191, *241*
Geiger, L., 132, *241*
Gelfand, I. M., 81, 205, 206, *241*
Gerver, M., 95, *242*
Gibbs, J. F., *264*, *265*

Gilbert, J. F., 106, 111, *233*
Gilbert, M. C., 185, *234*
Gill, P. E., 123, 126, 128, *242*
Gilpin, B., 168, 183, *242*
Golub, G. H., 121, *242*
Gordon, M. K., 83, 86, 89, *259*
Gosavi, P. D., *242*
Gough, D. I., 195, *242*
Gough, W. I., 195, *242*
Green, R., 41, *242*
Green, R. W. E., 189, 194, *242, 252*
Greville, T. N. E., 114, 118, 120, *233*
Griggs, D. T., *244*
Griscom, M., 157, *242*
Gu, J. P., *240*
Gubbins, D., 82, 85, 152, *246, 260*
Guberman, S. A., *241*
Guberman, S. I., *241*
Guerra, I., *238*
Guerrero, J. D., *245*
Guha, S. K., 196, *242*
Gumper, F. J., 184, *242, 243*
Gunst, R. H., 134, *239*
Gupta, H. K., 167, *242*
Gusev, A. A., *240*
Gutenberg, B., 2–4, 155, 160, *242*
Guzman, M., *252*

H

Habermann, R. E., 201, *266*
Hadley, D. M., 168, 169, 183, 191, 214, *237, 242, 246, 247*
Haessler, H., 192, *242*
Hagiwara, T., 4, 188, 195, 206, *242, 243*
Hales, A. L., *241, 265*
Hamada, K., 18, 188, *243, 262*
Hamaguchi, H., 179, 189, *243*
Hamburger, M. W., *260*
Hamilton, R. M., 169, 183, 189, 193, 216, *243, 262*
Hamming, R. W., 117, *243*
Hanks, T. C., 20, 22, 158–160, 190, *243, 262*
Hanson, R. J., 120, *249*
Harding, S. T., *234, 238*
Hardy, H. R., 167, *243*
Harjes, H. P., 40, 165, *243*
Harlow, D., *264*
Harsh, P. W., *235*
Hasegawa, A., 211, *243*
Hasegawa, H. S., *245, 249*
Hasegawa, I., 213, *233, 247*
Hasegawa, S., *254*
Hasegawa, T., *243*
Hashim, B. M., 169, *253*
Hatzfeld, D., *236*
Havskov, J., *252, 260*
Hayakawa, M., 208, *244*
Hayman, R. B., 40, *244*
Healy, J. H., 27, 32, 33, 35, 37, 161, 167, 169, 193, 214, *243, 244, 255–257*
Hearn, T., *260*
Hedayati, A., 178, 211, *244*
Helmberger, D. V., 161, 213, *232, 244*
Henger, M., 2, *265*
Henrisey, R., 192, *236*
Henyey, T. L., 41, 42, *244, 250, 262*
Herd, D. G., *250*
Herriot, J., *264*
Herrmann, R. B., 134, 157, 163, *244*
Hester, R. L., *260*
Hibi, K., *258*
Hileman, J. A., 148, 169, *244*
Hirahara, K., 170, *244*
Hirota, T., 180, *244*
Hitchcock, T., 168, *245, 246*
Hoang-Trong, P., *242*
Hodgson, J. H., 140, 147, *265*
Holcomb, D. J., 211, *266*
Holmes, C. R., 8, 184, *258*
Honda, H., 140, 142, *244*
Hori, M., 157, 179, *231, 244, 253*
Hori, S., *243*
Horie, A., 148, 169, *244*
Horner, R. B., 191, 192, *245, 261*
Houck, S. T., 50, 72, 146, *233, 245*
House, L., *262*
Howe, S., 31, *245*
Hron, F., 138, *236, 247*
Hu, Y. L., *264*
Huang, L. S., *259*
Huang, W. Q., *266*
Hubbard, A., *236*
Husebye, E. S., 2, *232, 235*
Hutchins, D. G., *259*
Hutchinson, C., 32, *247*
Hutton, L. K., 192, *246*

I

Ichikawa, M., 73, *245*
Ichinose, Y., *233*

Iida, K., 2, 3, 6, 179, *245, 265*
Iizuka, S., *233*
Ikami, A., 180, *245*
Imamura, A., 6, 200, *245*
Imamura, H., *245*
Inoue, Y., 203, *266*
Isacks, B., 184, *245*
Ishibashi, K., 180, *245*
Ishida, M., 201, 202, 222, *245*
Ishimoto, M., 2, 3, 6, *245*
Ito, K., 189, *255*
Iwata, T., 188, *243*
Iyer, H. M., 168, 170, 212, *245, 246, 258, 260*
Izvekova, M. L., *241*

J

Jackson, D. D., 106, 115, *246*
Jackson, J. A., *226*
Jackson, P. L., 82, *246*
Jacob, K. H., 82, 83, 182, *246, 262, 264*
James, G., *226*
James, R. C., *226*
Jensen, E. G., 29, 30, 52, *246*
Jianu, D., *241*
John, F., 81, 124, *237*
Johnson, C. E., 40, 57, 72, 134, 137, 157, 163, 191, 192, *246, 250*
Johnson, L. R., 161, 163, 212, *244, 246, 252, 261*
Johnson, S. H., 187, *246*
Johnson, T. L., 182, *246*
Johnston, A. C., 210, 211, *246, 266*
Jolitz, W., *264*
Jones, A. E., *235, 258*
Jones, L. M., 207, 220, *246*
Jones, P. R., 187, *246*
Jordan, T. H., *243*
Jordon, R. R., *259*
Julian, B. R., 82–85, *246*
Jupp, D. L. B., 106, *246*

K

Kafri, U., *266*
Kagan, Y. Y., 163, *247*
Kakimi, T., 213, *247*
Kaminuma, K., 178, 189, *243, 247*
Kamitsuki, A., *253*
Kanamori, H., 158–160, 169, 201, 202, 213, 214, 222, *236, 242, 243, 245, 247, 252*
Kanasewich, E. R., 215, *247*
Karakama, I., 191, *243, 247, 263*
Karal, F. C., 76, 77, *247*
Karcz, L., *266*
Kasahara, J., 43, 44, 190, *247, 254*
Kasahara, K., 147, *247*
Kasahara, M., *243*
Kasper, J., 32, *247*
Kayano, I., 180, 188, *243, 247, 248*
Keilis-Borok, V. I., 140, 147, 204, 205, *236, 241, 248*
Kelleher, J. A., 200–202, 206, *248*
Keller, G. R., 184, *248*
Keller, H. B., 86, *248, 250, 256*
Keller, J. B., 76, 77, *247*
Kepler, J., 47
Khalturin, V. I., 162, *257*
Kieckhefer, R. M., 181, *248*
Kijko, A., 17, *248*
Kikuchi, S., 179, *249*
Kind, R., 169, *248*
Kisslinger, C., 208, 210, 213, 215, 220, 221, *239, 248*
Kisslinger, J. B., *262*
Klein, F. W., 134, 137, 181, *239, 248*
Knopoff, L., 158, 163, *235, 241, 247, 248*
Kobayashi, H., *254*
Koczynski, T. A., *246, 259*
Kodaira, T., *245*
Kodama, K. P., 207, *249*
Kondratenko, A. M., 8, 209, *249*
Koning, L. P. G., 140
Kooketu, H., *254*
Koresawa, S., *233, 247, 254*
Korhonen, H., *256*
Koschyk, K., 181, *249*
Kovach, R. L., 212, *234, 237*
Koyanagi, R. Y., 148, 169, 170, *238, 239*
Kramer, M., *260*
Krause, J., *252*
Kubota, S., *248*
Kubotera, A., 179, *249*
Kuroiso, A., 60, 74, 179, 189, *249, 264, 265*
Kuzin, I. P., *240*

L

Lahr, J. C., 69, 71, 134, 137, 142, 200, 201, 228, *249, 250, 261*
Lahr, K. M., 191, *249, 250*
Lamar, D. L., 183, *249*

Lammlein, D. R., 185, *249*
Lanczos, C., 105, 107, 112–114, *249*
Landisman, M., 32, *253*
Lane, R. D., *240*
Lange, A. L., 183, 184, *249, 265*
Langenkamp, D., 183, *249*
Langer, C. J., 191, *234, 249*
Lapedes, D. N., *226*
Latham, G. V., 44, *249, 251, 255*
Lawson, C. L., 120, *249*
Leary, P. C., 213, 214, *249*
Leblanc, G., 182, 197, *245, 249*
Lee, T. C., 168, 183, *242*
Lee, W. H. K., 17, 52, 62, 68, 69, 71, 73, 80, 82, 84, 85, 89, 134, 136–138, 142, 147, 148, 153, 156, 157, 169, 189, 192, 195, 214, 216, 217, 228, *231, 233, 239, 245, 250, 251, 256, 258, 261, 265, 266*
Lehner, F. E., 8, *250*
Leighton, F. W., 167, 194, *235, 243*
Lentini, M., 85, 86, *250*
Lester, F. W., 75, *237, 249, 250*
Levenberg, K., 127, *250*
Lewis, P. A. W., 163, *237*
Li, B. X., *240*
Li, K. L., *240*
Li, P., 206, *266*
Li, T. C., *259*
Liaw, H. B., *262*
Lilwall, R. C., 17, 186, *241, 250*
Lin, M. T., 180, *251*
Lindh, A. G., 157, 161, 214, 219, *233, 234, 249, 251*
Lo, H. H., *259*
Lo Bascio, A., 181, *238, 251*
Lockner, D. A., *251*
Logie, H. J., *241*
Lomnitz, C., 199, *241*
Long, L. T., 185, *258*
Long, R. E., 41, *251*
Lu, S. D., *266*
Luenberger, D. G., 122, *251*
Luk, F., 82, 89, *251*
Lukk, A. A., *254*
Luongo, G., *238*
Luosto, U., *256*

M

Maasha, N., 178, *251*
McCamy, K., *236*
McCann, W. R., 200, *252*
McCollom, R. L., 169, *252*
McCowan, D. W., 41, *256*
MacDonald, K. C., 186, 187, *251, 257, 260*
McDonald, W., *236*
McEuen, R. B., *232*
McEvilly, T. V., 161, 168, 188, 209, 212, 221, *233, 234, 246, 251, 252, 259*
McGarr, A., 194, 213, *252*
McGonigle, R., 215, *237*
McGrath, J. R., *240*
McKenzie, D. P., 146, *252*
McMechan, G. A., 138, *252*
McNally, K. C., 183, 191, 199, 209, *236, 252, 260*
McRaney, J. K., *244*
Madrid, J., *246, 257*
Majer, E. L., 168, 183, 184, *251*
Malcolm, M. A., *240*
Malin, P. E., *249*
Maling, D. H., 141, *251*
Malinovskaya, L. N., 204, *248*
Malone, S. D., 190, *238, 251*
Mamadaliev, V. A., 196, *260*
Manov, D. V., *244*
Mantis, C., *251*
Marks, S. M., *233*
Markushevich, V., 95, *242*
Marquardt, D. W., 128, *251*
Martynov, V. G., *257*
Maruyama, T., 158, *251*
Marwadi, S. C., *242*
Mason, R. G., *244*
Massinon, B., 60, 165, *251*
Matsumura, K., *261*
Mattaboni, P. J., 44, 45, *251, 260*
Matumoto, H., 179, 231, 244, 247, *253*
Matumoto, T., 169, 182, 188, *235, 251, 255*
Mayer-Rosa, D., 169, *251*
Meagher, K. L., *250*
Menke, W. H., 170, *252*
Merkler, G., 234, *241*
Meyer, H., *256*
Meyer, R. P., 192, *252, 256*
Michael, M. O., *233*
Mickey, W. V., 184, *252*
Miki, H., 179, *252*
Mikumo, T., 169, 170, *244, 253*
Miller, A. E., *245*
Miller, H., *241*
Miller, H. J., *239*

Miller, R., 44
Mills, K. F., 185, *263*
Minster, J. B., *243*
Mironova, V. I., *266*
Mitchell, B. J., 32, 169, 170, *253*
Miyajima, R., *266*
Miyamura, S., 6, 179, 188, *253*
Mizoue, M., 169, *253*
Mogi, K., 200, 201, 206, *253, 254*
Moldoveanu, T., *241*
Moler, C. B., 114, *240*
Molnar, P., 178, 207, 220, *236, 246, 254, 257*
Molotkov, I. A., *236*
Mooney, W. D., 138, *252, 254, 256*
Morrison, P. W., *237*
Morrissey, S. T., *260*
Motoya, Y., 189, *254*
Moumoulidis, G., *237*
Mudie, J. D., 187, *251*
Muffler, L. J. P., 183, *243*
Muirhead, K. J., 41, 237, *254*
Munguia, L., 191, *254, 257*
Muramatu, I., 179, *254, 258*
Murdock, J. N., *239*
Murphy, A. J., 185, *254*
Murphy, L., 5, *230, 255*
Murray, W., 122, 128, *242, 254*

N

Nagumo, S., 43, 44, 187, 189, *247, 254*
Nakamura, I., *247*
Nakamura, M., 169, 179, *265, 266*
Nakano, H., 140
Nappi, G., *238, 251*
Nasu, N., 6, *254*
Nelson, G., *250*
Nersesov, I. L., 7, 8, 209, 220, *249, 254, 260*
Nishenko, S. P., *252*
Noble, B., 105, 136, *254*
Nordquist, J. M., 3, 134, *255, 258*
Northrop, J., 187, *255*
Noson, L. J., *238*
Nourescue, A., *241*
Nowroozi, A. A., 44, 187, *249, 255, 259*
Nur, A., 214, *255*
Nurminen, S., *256*
Nuttli, O. W., 155, *238*

O

Odegard, M. E., 184, *239*
Officer, C. B., 77–79, 94, 96, *255*
Oficerova, E., *236*
Ogino, I., 180, *247, 255, 263*
Ohtake, M., 167, 189, 195, 199, 200, 211, *243, 251, 255, 261*
Oike, K., *261*
Okubo, P., *234*
Oliver, H. A., *241*
Oliver, J., 5, 8, 41, 184, 228, 230, *235, 245, 248, 255*
Omote, S., 6, *255*
O'Neill, M. E., 27, 32, 33, 35–38, 161, *239, 244, 255, 261*
Ooida, T., 179, 180, 189, *255, 266*
Oppenheimer, D. H., *246*
Orcutt, J. A., *241*
Orsini, N. A., 19, *256*
Osborne, P. J., *240*
Otsuka, M., *253*
Ouchi, T., *254*
Ozard, J. M., *239*

P

Padale, J. G., *242*
Page, R. A., 182, 188, *251, 256*
Pakiser, L. C., *239*
Palmason, G., *264*
Pang, Q. Y., *240*
Papanek, P. J., *243*
Papazachos, B., *237*
Parke, D. L., *237*
Parker, R. L., 106, *241, 256*
Pasquale, V., 191, *236*
Patton, H., 163, *256*
Pavlis, G. L., 152, *256*
Pavlov, V. D., *260*
Pavoni, N., 181, *241, 256*
Peake, L. G., 169, 212, 214, *244, 256*
Pechmann, J. C., *252*
Peled, U., *266*
Pelton, J. R., *260*
Pennington, W. D., 184, 185, *252, 256*
Peppin, W. A., *259*
Pereyra, V., 82, 85, 86, 88, 89, *250, 256*
Peters, D. C., 17, *256*
Peterson, J., 19, *256*
Pfluke, J. H., 217, *235, 256*

Phillips, J. D., 41, *256, 260*
Phinney, R. A., *249*
Pickett, T. E., *259*
Pirhonen, S. E., 2, *256*
Pisarenko, V. F., *248*
Pitt, A. M., 183, 191, *256, 260*
Plantet, J. L., 60, 165, *251*
Pollard, D. D., 202, *259*
Pomeroy, P. W., 194, *256*
Ponce, L., *260*
Ponomarev, V. S., *254*
Pooley, J. E., *240*
Pope, A. J., *238*
Porter, I. T., 186, *240, 241, 250*
Porter, R. P., *260*
Powell, C., 169, *235*
Powell, L. A., *252*
Press, F., 8, *241, 250*
Prodehl, C., 138, *254*
Prothero, W. A., 41, 44, 45, 57, 187, *223, 256, 257*
Psencik, I., *236*
Pyatetskii-Shapiro, I. I., *248*

Q

Quervain, A. De., 2, *257*

R

Radu, C., *241*
Ragan, D. M., 141, 143, 144, *257*
Raikes, S. A., 170, 213, *257*
Raleigh, C. B., 18, 146, 168, *244, 257*
Ramirez, J. E., *256*
Ranzman, E. Y., *236, 241*
Rao, B. S. S., *264*
Rapport, A. L., *250*
Rastogi, B. K., 167, 210, *242, 257, 262*
Rautian, T. G., 161, 162, *254, 257*
Real, C. R., 157, *257, 262*
Reasenberg, P., 168, *257*
Reboller, J., *257*
Reichle, M. S., 187, 190, 191, *254, 257*
Reid, H. F., 139, 158, *257*
Reid, I., 42, 43, 186, 187, *257*
Reinsch, C., 121, *242*
Reyes, A., 182, *235, 254, 257*
Rice, J., 163, *263*
Richards, P. G., 40, 106, 158, 163, 222, *226,* 229, *231*
Richter, C. F., 1–5, 130, 131, 153–156, 160, *226, 242, 257, 258*
Rikitake, T., 7, 198, 203, 208, 209, 211, *258*
Riznichenko, Y. V., 7, 208, *258*
Roberts, S. M., 86, *258*
Robinson, R., 180, 181, 210, 212, *232, 240, 258*
Roecker, S. W., *236*
Rogers, A. M., 195, *258*
Rogers, G. C., 182, *258*
Roller, J. C., *256, 265*
Roloff, J. N., *246*
Rothe, G. H., *251*
Rotstein, Y., 183, *237*
Rotvain, I. M., *248*
Rotwain, I. M., *236, 241*
Roy, F., *264*
Rubey, W. W., *244*
Rulev, B. G., *254*
Rustanovich, D. N., 7, 188, *258*
Ryall, A., 161, 184, 189, 193, *235, 238, 255, 258, 260*
Rykounov, L. N., 178, *258*
Rykunov, L. N., 43, *258*
Rynn, J. M. W., 209, 211, 240, *258, 259*

S

Sadovskiy, M. A., 8, *264*
Sadovsky, A. M., *241*
Sakai, K., *247, 263*
Sammis, C. G., *259*
Sanford, A. R., 8, 184, 185, *258*
Santoire, J. P., 191, *238*
Sasaki, Y., 189, *255, 258*
Sato, T., 148, 169, *258*
Sato, Y., 17, *258*
Sauber, J., 205, *259, 262*
Savage, J. C., 158, *259*
Savage, W. U., 191, 193, *258, 259*
Savino, J., 200, 202, *248*
Savrina, L. A., *258*
Sbar, M. L., 184, 190, *231, 249, 256, 259*
Scarpa, R., *238, 251*
Schaefer, S., *260*
Schick, R., *242*
Schmedes, E., *241*
Schneider, G., *242*

Scholz, C. H., 178, 181, 184, 210, 211, *234, 242, 258–260, 262*
Sedov, V. V., 43, *258*
Seeber, L., 183, *259*
Segall, P., 202, *259*
Seidl, D., 40, 165, *243*
Sekiya, H., 202, 211, *259*
Seligman, P., *241*
Sellschop, P. F., *241*
Semenov, A. M., 8, 211, *259*
Semenov, A. N., *254*
Shampine, L. F., 83, 86, 89, *259*
Shannon, W. E., 40, *244*
Shapira, A., 134, 147, *259*
Sharman, G. F., *257*
Shen, C. K., 195, *259*
Sheng, G. Y., *240*
Shibuya, K., 148, 169, *244*
Shida, T., 140
Shimada, M., *252*
Shimamura, H., 187, *259*
Shipman, J. S., 86, *258*
Shirai, K., 67, *259*
Shirley, J. E., 197, *259*
Shuey, R. T., *260*
Sidorenko, T. M., *248*
Simbireva, I. G., *254*
Simila, G. W., 183, *252, 259*
Simirenko, M., *250*
Simono, H., *254*
Simons, R. A., *235, 254*
Simpson, D. W., 41, 167, 197, 222, *231, 254, 256, 260, 262*
Singh, S., 197, *260*
Singh, S. K., 192, 199, *252, 260*
Skoko, D., 17, *258*
Slemmons, D. B., *255*
Smith, B. E., *243*
Smith, H., 113, 137, *238*
Smith, R. B., 184, 185, 194, *241, 256, 259, 260, 262*
Smith, S. W., *251, 262*
Soboleva, O. V., 196, *260*
Sodbinow, E. S., 185, *260*
Solomon, S. C., 44, 45, 54, 57, 187, *232, 251, 260*
Solov'ev, S. L., 156, *260*
Solovjeff, A., *236*
Soufleris, C., *234*
Spence, W., *256*
Spencer, C., 152, *260*
Spindel, R. C., 186, *260*
Spottiswoode, S. M., *252*
Stauder, W., 9, 18, 139, 140, 184, 193, *253, 260*
Steeples, D. W., 18, 168, 183, *256, 260*
Steinwachs, M., 181, 196, *249, 260*
Stephen, J. H., *241*
Stephens, C. D., 192, 217, *249, 259, 261*
Steppe, J. A., 148, 169, 212, 217, *256, 261*
Stevens, A. E., *245, 249*
Stevenson, D. A., 210, *261, 262*
Stevenson, P. R., 41, 51, 73, 195, *261*
Stewart, G. S., 210, *261*
Stewart, G. W., 105, 114, *261*
Stewart, R. M., 168, *233, 246*
Stewart, S. W., 32, 35, 36, 38, 54, 58–60, 63–65, 67–70, 74, *250, 261*
Stierman, D. J., 190, *261*
Stifler, J., *234*
Strang, G., 105, *261*
Strobach, K., *242*
Stump, B. W., 163, *261*
Sugiyama, K., *255*
Sun, C. C., *240*
Sung, L. Y., *236*
Suryavanshi, M. P., *264*
Suteau, A. M., 157, 163, *261*
Sutton, D. J., 211, *261*
Sutton, G. H., *239*
Suyehiro, S., 216, 221, *233, 261*
Suzuki, H., *233*
Suzuki, S., *254*
Suzuki, Z., 4, 6, 7, 165, 188, *233, 261*
Sykes, L. R., 9, 167, 200, 206, *231, 240, 248, 252, 254, 259, 261, 262*
Sylvester, A. G., 189, *262*
Sylvester, J. J., 114
Synge, J. L., 80, *262*

T

Tada, T., *255*
Takahashi, H., 18, *262*
Takahashi, M., 247, 248, *263*
Takano, K., *243*
Talwani, P., 195–197, 205, 210, *257, 259, 262*
Tarakanov, R. Z., *240*
Teng, T. L., 40, 56, 157, 167, *244, 257, 262*
Thatcher, W., 20, 22, 156, 159, 189, *243, 262*
Thurber, C. H., 138, *250, 262*

Tien, K. Y., *266*
Timmel, K. E., 197, *262*
Tobin, D. G., 178, *262*
Tocher, D., 8, *233, 259*
Tokuhiro, I., 67, *259*
Tolmachoff, W. W., *234*
Tomblin, J. F., *233*
Tomkins, P. K., *240*
Tomoda, Y., *259*
Toppozada, T. R., *237*
Torrieri, D. J., 67, *262*
Trimble, A. B., 184, *256, 262*
Truscott, J. R., 2, *262*
Tsai, Y. B., 180, *251, 262*
Tsujiura, M., 161, 162, 179, 221, *253, 262, 263*
Tsumura, K., 156, 180, 191, 192, *245, 247, 261, 263*
Tucker, B. E., 19, 161, 190, *263*
Tudorache, G., *241*
Turcotte, T., 134, *234*

U

Ucer, S. B., 180, *238*
Udias, A., 147, 163, 217, *235, 263*
Uhrhammer, R. A., 17, 192, *234, 263*
Umana, J., *251*
Unger, J. D., 183, 185, *263*
Unger, W. L., *252*
Ursin, B., *235*
Usami, T., 7
Utsu, T., 207, 211, 213, 216, 217, *263*

V

Valdes, C., *252*
Van Hissenhoven, R., *256*
Van Loan, C., 122, *264*
Van Schaack, J. R., 27, 30, 38, 39, *239, 264*
Van Wormer, J. D., *258*
Varghese, T. G., 2, *264*
Vassiliou, M., *260*
Vered, M., *234*
Vere-Jones, D., 163, *264*
Vernon, F., *235*
Von Collin, R., *249*
Von Dollen, F. J., *252*
Vozoff, K., 106, *246*

W

Wadati, K., 153, 208, *264*
Wallace, R. E., 8, *264*
Walter, A. W., 168, *257, 264*
Wang, M. Y., 195, *264*
Wang, T. C., *259*
Wang, Z. Y., *240*
Ward, P. L., 168, 181, 182, 190, 223, *250, 251, 262, 264*
Ward, R. W., 168, *266*
Ward, S. N., 163, *264*
Watanabe, H., 60, 74, 169, 179, 189, *243, 249, 252, 264, 265*
Watanabe, K., *258*
Watanabe, S., 179, *265*
Weaver, C. S., 168, 238, *256, 264*
Weed, R. W., *259*
Wei, K. Y., *236*
Weichert, D. H., 2, *265*
Welsch, R. E., *238*
Wesson, R. L., 82, 84, 85, 169, 190, 202, 206, *235, 258, 265*
Westphal, W. H., 183, 184, *249, 265*
Wetmiller, R. J., 157, *245, 249, 250*
Whitcomb, J. H., 9, 157, 163, 210, 213, 232, *261, 265*
Wickens, A. J., 147, *265*
Widmann, R., *234*
Wiebols, G. A., 194, *252*
Wiggins, R. A., 106, 116, *265*
Wilkinson, J. H., 108, *265*
Williams, R., *238*
Willmore, P. L., 22, 46, 61, 169, *265*
Winkler, P. L., *260*
Wolfe, M. A., 122, *265*
Wood, H. O., 3, 8, *232*
Wood, R., 182, *265*
Woodruff, K. D., *259*
Woodward, R. S., 131, *266*
Wright, C., *237*
Wright, M. H., *242*
Wu, C., 218, *266*
Wu, F. T., 178, *266*
Wu, H. Y., *266*
Wu, K. T., 206, *266*
Wyss, M., 158, 201, 207, 211, 216, 217, *243, 248, 266*

**XYZ**

Xiao, Y. Y., 206, *266*
Yakusheva, V. N., *232*
Yamada, I., 180, *255*, *266*
Yamamoto, J., *252*
Yamashina, K., 203, *266*
Yang, C. J., *259*
Yang, J. P., 80, 82, 84, 85, *266*
Yang, M. Y., *264*
Yen, C. C., *236*
Yerkes, R. F., *250*
Yoshida, H., *245*
Young, C., 168, *266*
Young, G., 114, *239*
Yue, M. S., *266*
Zandt, G., 170, *246*, *266*
Zarayskiy, M. P., *232*
Zhao, Z. H., *250*
Zhelankina, T. S., *248*
Zheng, J. Z., *240*
Zverev, S. M., 181, *266*

# Subject Index*


A

Abuyama Seismological Observatory, 171, 189
Academia Sinica, Taiwan, 171
Acoustic wave, 83
Active fault, *see* Fault
Adak, Alaska, meq. network, 175, 221
Adak Canyon, Alaska, 1971 earthq., 213
Adak Island, Alaska, 1976 earthq., 210
Adelaide, Australia, meq. network, 173
Adelaide, University of, 173
Adirondacks, New York, 1971 earthq., 190
Adjoint system, 113
Adjustment vector
  for Geiger's method, 132–135, 137
  for minimization, 123, 125, 127–128
  for simultaneous inversion, 150, 152
Afghanistan, meq. survey, 178
Africa, meq. surveys, 178
Aftershocks, 3, 6, 9
  in earthq. prediction, 201, 204, 214, 217, 219, 221
  in selecting fault plane, 146
  studies of, 166, 188–192
AGC, *see* Automatic gain control
Agua Blanca fault, Mexico, 182
Agua Caliente Springs, Calif., 1973 earthq., 190
Ahuachapan geothermal area, El Salvador, 182
Air gun, 43, 213–214
Akita Geophysical Observatory, 171
Akita, Japan, 1970 earthq., 211
Alaska
  aftershock studies, 188, 192
  meq. networks, 175–176
  meq. surveys, 182
  seismic gaps, 200
  University of, 175
  velocity anomalies, 210, 213
Alaska Peninsula, Alaska, 175
Albuquerque Basin, New Mexico, 175
Alcoa, Tennessee, meq. survey, 185
Aleutian Islands, 84, 213, 221 (*see also* Alaska)
Alpine fault, New Zealand, 181
Alps, France/Italy, meq. survey, 181
Amchitka, Alaska, seismic network, 213
Amplifier, 23–27, 29, 33, 35–38, 40, 42, 44–45, 166, 226 (*see also* Amplifier step test)
Amplifier step test, 27, 29–30, 32–33, 35
Amplitude-frequency response, *see* Response, instrument
Amplitude ratio, 219–221, 229
Amplitude spectra, *see* Spectra
Anapa, USSR, meq. survey, 181
Anchored buoy OBS systems, 43–44
Ancona, Italy, meq. network, 174
Anderson Reservoir, Calif., 195
Antarctica, meq. surveys, 178
Antioch, Calif., 1965 earthq., 188
Anza, Calif., meq. survey, 182


* Many microearthquake networks are referred to by different names in the literature. For example, the word "microearthquake" is often used interchangeably with "earthquake" or "seismic," and the word "network" with "array," "observatory," or "station." We have used the following abbreviations: "Calif." for "California," "earthq." for "earthquake," "meq." for "microearthquake," and "U.S." for "United States."

Aomori, Japan, meq. network, 171
Argosystems, Inc., 41
Arizona, 176, 195
Arrays, *see* Seismic arrays
Arrival time
  error, 74, 138
  later phases, 129, 134–135, 137, 148, 168
  P-wave, *see* First P-arrival time
  residual, 74, 132–133, 149–150
  S-wave, *see* S-arrival time
Arthur's Pass, New Zealand, 1972 earthq., 211
Ashio, Japan, meq. survey, 180
Ashkhabad, USSR, 1948 earthq., 7, 188
Asia, 206
  induced seismicity, 195–197
  meq. networks, 171–173
  meq. surveys, 178–180
Assam, India, earthqs., 207
Atera fault, Japan, meq. survey, 180
Atlantic Ocean, meq. surveys, 186
Atsumi Peninsula, Japan, 1971 earthq., 189
Auburn, Calif., meq. survey, 183
Australia, 2, 173, 197
Australian National University, 173
Austria, induced seismicity, 197
Automatic calibration unit, 23, 27, 29–30, 32
Automatic earthquake detection, *see* Event detection
Automatic gain control, 6, 24–25, 30, 45, 226
Auxiliary plane, 140, 146
Azimuthal angle, 141
Azimuthal gap, 17, 135

B

Backus–Gilbert inversion, 111–112
Baja California, Mexico, 175, 182
Bear Valley, Calif.
  b-slope, precursory, 217
  focal depths, precursory, 218
  seismicity patterns, 206
  velocity anomalies, 210, 212
  1972 earthqs., 190, 206, 210, 212, 217
Beijing, China, meq. network, 171
Bell and Howell tape recorder, 31
Benham, nuclear explosion, 193
Bernard Price Institute of Geophysical Research, 5
Bisho zisin, 6
Blanco fracture zone, meq. survey, 187
Blue Mountain Lake, New York, 9, 210
Body-wave magnitude, defined, 155
Borgarfjordur, Iceland, 1974 earthq., 191
Borrego Mountain, Calif.
  seismicity patterns, 206
  velocity anomaly, 213
  1968 earthq., 189, 206, 213
Boso Peninsula, Japan, earthqs., 213
Boston College, 176
Botswana, meq. survey, 178
Boundary value problem, 82–89
Boxcar, nuclear explosion, 193
BPI (bits per inch), 48, 226
Brawley, Calif., 1975 swarm, 191
Briones Hills, Calif., 1977 swarm, 191, 220–221
British Columbia, *see* Canada
Broadband instrument, 19, 161, 190
Brune's source model, 20, 159, 161
b-slope, 4, 203, 215–218
Bucaramanga, Columbia, 185
Buena Vista Valley, Nevada, 184
Buffalo Valley, Nevada, 184

C

Calaveras fault, Calif., 201
Calibration, instrument, 27, 29–30, 32
California
  aftershock studies, 9, 188–192
  crust and mantle structure, 84, 169–170
  geothermal exploration, 168
  induced seismicity, 167, 195
  meq. networks, 175–176
  meq. surveys, 182–184, 187
  misc. precursors, 217–222
  seismicity patterns, 201–207
  University of, Berkeley, 8–9, 11, 165, 188–189, 191–192, 212, 217
  velocity anomalies, 209–210, 212–215
California Institute of Technology, 3, 8–9, 72–73, 176
Caltech, *see* California Institute of Technology
Caltech Earthquake Detection and Recording (CEDAR) system, 72–73
Canada, 2, 140
  aftershock studies, 191–192
  induced seismicity, 197

meq. networks, 40, 174
meq. surveys, 182
Canadian Department of Energy, Mines, and Resources, 174
Canal de las Ballenas, Mexico, 1975 earthq., 191
Cape Mendocino, Calif., 183
Caribbean area, meq. networks, 176–177
Carnegie Institution of Washington, 8
Carpathians, meq. network, 174
Carrizo Plains, Calif., 183
Cascade Range, Oregon, 176
Caucasus, USSR, meq. survey, 181
Center for Scientific Investigation and Higher Education, Mexico, 175
Center frequency, 24–25, 29–30, 39
Central America, 169
meq. networks, 174–175
meq. surveys, 182, 185
Central Basin fault, Philippine Sea, 187
Central California Meq. Network, 9–13
applications, 169–170, 175, 190, 192, 195, 203, 212, 214, 217
data processing, 46–50, 53, 58, 62, 70–74, 156
instrumentation, 19–20, 23–39
station distribution, 15–18
Centralia, Washington, 213
Central processing unit, 58, 89, 227
Ceres, South Africa, 1969 earthq., 189
Cerro Prieto, Mexico, 175
Characteristic equation, 108–109
Characteristic function, 63–68
China, 206
earthq. prediction, 209–211
induced seismicity, 195
meq. network, 171
China Lake, Calif., meq. survey, 183
Cholesky method, 121–122, 226
Chubu, Japan, meq. survey, 179
Chugoku-kinki, Japan, 1967 earthq., 211
Circum-Pacific seismic belt, 200, 212
CIRES, University of Colorado, 175
Clarence fault, New Zealand, 181
Clark Hill Reservoir, S. Carolina, 195
Clock correction, 17, 50
Coda, 67–68, 162
Coda amplitude, 157, 162
Coda magnitude, defined, 226
Coda wave, 159, 162–163, 226
Colombia, meq. survey, 185
Colorado, 167–168, 184
Colorado, University of, 175
Columbia and Geneva Coal Mines, Utah, 194
Columbia Basin, Washington, 1972–1974 earthq. swarm, 190
Columbia University, *see* Lamont–Doherty Geological Observatory
Compensation, 24, 30–31, 39, 226
Composite fault-plane solution, 147
Compression, 72, 139–141, 144–145
Compressional wave, 77, 229
Computer computations, 117–118
Condition number, 121–122, 137
Corner frequency, 20–23, 159, 161
Corona, Calif., explosions, 213
Corralitos, Calif., 1964 earthq., 188, 206
Correlation, waveform, 58, 212
Cosne d'Allier, France, 1977 earthq., 191
Coso geothermal area, Calif., 168, 183
Cost, meq. network, 58, 166, 223
Costa Rica, meq. network, 174
Costa Rica, University of, 174
Covariance matrix, 120–121
Coyote Lake, Calif., 1979 earthq., 192
Coyote Mountain, Calif., 1969 earthq., 189
CPU, *see* Central processing unit
Cramer's rule, 106, 116–117
Crillon Lake, Alaska, meq. survey, 182
Critical distance, 97–100
Crossover distance, 97
Crustal structure, 168–170 (*see also* Velocity structure)
Cutoff criterion for event recording, 55, 57, 68–69

D

Dale, New York, fluid injection, 167
Damped least squares, 120, 128
Danville, Calif., 1970 earthq. swarm, 189, 217
Data analysis methods, 129–163
Data processing procedures, 46–75
Datum Products Co., 31
Dead Sea region, 178–179, 203
Decomposition theorem
nonsquare matrix, 114–115
square matrix, 110–111

Delaware/New Jersey, 1973 earthq., 190
Delay-line, 5–6, 55–57
Delay time function, 95
Delta function, 37
Denali fault, Alaska, 182
Denver, Colorado, earthqs., 167
Derivatives, *see* Travel time derivatives
Determinant, 107–109, 113, 136, 228–229
Develocorder, 24–27, 31, 35, 157, 227
Digital event recorder, 41
Digital transmission, 40
Dilatancy model, 214–215
Dilatation, 72, 76, 139–141, 144–145
Direction angle, 83, 89, 91–92, 102–104, 137
Direction cosine, 78–79, 83–84, 88, 90–93, 102
Direction number, 79
Direct mode recording, 24–25, 31, 227
Direct path, *see* Ray path
Direct wave, 96–97, 100–104
Disaster Prevention Research Institute, Kyoto University, 171–172
Discriminator, 24–26, 30, 35–37, 39, 227
Dislocation, 20, 158
Displacement spectra, *see* Spectra
Distance, computing, 131
Dodaira Meq. Observatory, 171, 190
Dos Cuadras oil field, Calif., 42
Double-couple, 158
DPRI, *see* Disaster Prevention Research Institute, Kyoto University
Duration magnitude, *see* Magnitude
Duration, signal, *see* Signal duration
Dushanbe, USSR, meq. network, 173
Dynamic range, 5, 40, 61, 161
  definition, 19
  ocean-based system, 44–45
  USGS telemetry system, 38–39

E

Eagle Mountain, Calif., 213
Earthquake
  classification by magnitude, 4
  frequency-magnitude relation, 2–4, 6, 216
  intensity, 153
  local, defined, 54
  man-made, *see* Induced seismicity
  quantification of, 158–163
  regional, defined, 54
  teleseismic, defined, 54
Earthquake location, 5, 89, 112, 122
  formulation, 130–132
  real-time, 52, 57–58, 74–75
  solution, 132–139
Earthquake magnitude, *see* Magnitude
Earthquake mechanism, 139–148
Earthquake prediction, 6–7
  amplitude ratio, 219–221
  b-slope, 215–218
  foreshock activity, 206–207
  seismicity patterns, 199–207, 218
  source characteristics, 219–222
  velocity anomalies, 208–215
Earthquake Research Institute, Tokyo University, 7, 171–172
Earthquake statistics, 4, 163, 207
Earthquake swarm, *see* Swarm
East African Rift, meq. surveys, 178
Eastern Canada Telemetered Network, 174
East Pacific Rise, meq. surveys, 187
East Rand Proprietary Mines, South Africa, 194
Eguzon, France, 1977 earthq., 191
Eigenvalue, 108–111, 113–115
Eigenvector, 109–111, 114–115
Eikonal equation, 77–79, 83
Elastic rebound theory, 139, 158
Elastic wave propagation, *see* Wave propagation
El Salvador, meq. survey, 182
Elsinore fault, Calif., 183
Emosson Reservoir, Switzerland, 197
Epicenter, quick determination, 130 (*see also* Hypocenter parameters)
Equal-area net, *see* Equal-area projection
Equal-area projection, 141–146
Equation of characteristics, 78
Equation of motion, 76–77
Error
  arrival time, 74, 138, 215
  data processing, 61, 70–73
  first motion of P-wave, 146
  inverse problem, 115, 121
  overflow, 118
  roundoff, 118, 122, 136
  timing, 30
  underflow, 118
Eskdalemuir, Scotland, array, 2

ESSA (Environmental Science Service Administration, U.S.), 189
Ethiopia, meq. survey, 178
Ethiopia Rift, Ethiopia, 178
Etna, Italy, meq. survey, 181
Euclidean length, 113, 227
Euler's equation, 81, 85, 90
Europe
  earthq. prediction, 220
  induced seismicity, 194, 196–197
  meq. networks, 173–174
  meq. surveys, 181
Even-determined system, analysis of, 107–111, 116, 134
Event association, 69–70
Event detection, 2, 41, 45, 50, 56
  cutoff criterion, 55, 57, 68–69
  methods, 51–60, 63–70
  threshold, 55, 57, 59–60, 64–68
Event list, 47–48, 50, 73
Event processing, 2, 51, 60–70

F

Fairbanks, Alaska, 175
Fairview Peak, Nevada, 184
Fairweather fault, Alaska, 182
Fallon, Nevada, meq. survey, 184
Fast Fourier transform, 32, 227
Fault, 9–10, 139–140, 146, 158, 168, 170, 202–203, 205–206 (*see also* entries under specific faults)
Faulting, *see* Fault
Faultless, nuclear explosion, 193
Fault plane, 140, 142–143, 146
Fault-plane solution, 5, 89, 139, 220
  composite, 147
  computer methods, 147–148
  manual method, 141–146
  pitfalls, 146–147
  P-wave first motion, 140–148
FDM, *see* Frequency division multiplexing
Fermat's principle, 80
FFT, *see* Fast Fourier transform
Fiji Islands, 213
Fiji Plateau, meq. survey, 187
Finland, 2, 181
Fiordland, New Zealand, 181
First motion of P-wave, 5, 66
  convention, 71, 141, 227, 229
  earthq. prediction, 209, 220
  fault-plane solution, 140–148
First P-arrival time, 5
  automated determination, 63–70
  earthq. location, 129–139
  simultaneous inversion, 148–153
  weight, 67, 71, 74
First P-motion, *see* First motion of P-wave
Flathead Lake, Montana, 195
Floating-point number, 117–118
Fluid injection, 18, 167–168
FM, *see* Frequency modulation
Focal depth, 17–18, 158, 165
  determination, 130–139
  effect on magnitude, 154–155, 157
  temporal variations, 210, 218
Focal sphere, 70, 140–145, 147
Fontana, Calif., meq. survey, 183
Foreshocks, 201, 206–207, 219–222
Fort Tejon, Calif., 1857 earthq., 203
Fourier transform, 32–34, 37, 227
France
  aftershock studies, 191
  large aperture array, 60, 165, 191
  meq. network, 173
  meq. survey, 181
Frequency content of earthq. wave, 19 (*see also* Spectra)
Frequency division multiplexing, 24–25, 227, 230
Frequency-magnitude relation, 2–4, 6, 216
Frequency modulation, 24, 39, 42, 45, 51, 227
Frequency response, *see* Response, instrument
Friuli, Italy, 1976 earthq., 191, 207
Fukui (Hukui), Japan, 1948 earthq., 188
Fukui, Japan, meq. network, 171

G

Galapagos Islands, 187
Galapagos spreading center, 187
Galway Lake, Calif., 1975 earthq., 213
Garm, USSR, 7, 9
  meq. network, 173
  stress directions, 220
  velocity anomalies, 208–209, 211
Gauribidanur, India, array, 2
Gaussian elimination, 116–117
Gauss–Newton method, 127–128, 132, 150

Geiger's method, 130, 141
derivation, 132–134
generalization, 148–153
implementation, 134–139
pitfalls, 135–138, 152
Generalized inverse, *see* Inverse
Generalized inversion, *see* Inversion
Geophone, defined, 227
Geotech, *see* Teledyne Geotech
Geothermal exploration, 168
Germany, 40, 165
aftershock studies, 192
induced seismicity, 194
meq. network, 174
Geysers, The, Calif., 183
Gifu Prefecture, Japan
meq. network, 172
meq. surveys, 6, 179–180
velocity anomaly, 211
1969 earthq., 189, 211
Gisborne, New Zealand, 1966 earthq., 211
Global minimum, 123, 125, 137–138
Goat Mountain, Calif., 1975 earthqs., 213
Gobo, Japan, meq. survey, 179
GOES Satellite Time System, 32
Gorda Ridge, meq. survey, 187
Gordon-Pedder Reservoir, Tasmania, 197
Gradient vector, 124–126
Graefenberg, Germany, array, 165
Grangesberg Iron Ore Mine, Sweden, 194
Grass Valley, Nevada, meq. survey, 184
Greece, 192, 196
Gregory rift, Kenya, meq. survey, 178
Guatemala, 174, 182
Guatemala, 1976 earthq., 191
Guaymas Basin, Gulf of Mexico, 1974 earthq., 191
Gulf of California, Mexico, 187
Gulf of Calif., 1973 earthq., 190
Gutenberg–Richter relation
energy-magnitude, 160
frequency-magnitude, 2–4, 6, 216

H

Haast, New Zealand, meq. survey, 181
Hachijojima, Japan, 1972 earthqs., 190
Hachiman, Japan, meq. survey, 179
Hagfors Observatory, 174
Hagfors, Sweden, array, 2
Haicheng, China, 1975, earthquake
amplitude ratios, 219
foreshocks, 206
velocity anomaly, 211
Haines, Alaska, meq. survey, 182
Handley, nuclear explosion, 193
Hawaii
crust and mantle structure, 169–170
meq. network, 8, 170, 175
meq. survey, 184
velocity anomaly, 210
Hawaiian Ridge, meq. survey, 184
Hawaiian Seismic Network, 8, 170, 175
Hawaii Volcano Observatory, 175
Hebgen Lake, Montana, meq. survey, 184
Helena, Montana, meq. survey, 184
Helicorder, 24, 26–27, 31, 227
Helsinki, Finland, array, 2
Hengill-Hellisheidi, Iceland, 174
Hessian matrix, 124–127
Himalayas, 204
Hindu Kush, meq. survey, 178
Hirosaki Earthquake Observatory, 171
Hirosaki University, 171
Hiroshima, Japan, 172, 180
Hokkaido (*see also* Japan)
meq. network, 171
University of, 171
Hokuriku Meq. Observatory, 171
Hokushin Seismological Observatory, 171, 189
Hollister, Calif., 214
Hollister, Calif., 1974 earthq., 212
Honshu, *see* Japan
Hopei, China, meq. network, 171
Hot Springs area, Virginia, 185
Hsingfengkiang, China, 1962 earthq., 210
Hsingfengkiang Reservoir, China, 195
Hsintien, Taiwan, meq. survey, 180
Hydrophone, 41–44
HYPO71, 142–143, 147, 228
Hypocenter parameters
defined, 70
determination, 71–75, 130–139
simultaneous inversion, 148–153

I

Ibaraki, Japan, meq. network, 172
IBM, *see* International Business Machines Corporation

Iburi Province, Japan, 180
Iceland
  aftershock studies, 191
  meq. network, 170, 174
  meq. surveys, 181
  University of, 174
Idaho, 175, 177, 184, 194
Idaho National Engineering Laboratory, 175
Ilan, Taiwan, meq. survey, 180
*Ill conditioned, 117, 136–137, 228*
Imaichi, Japan, 1949 earthq., 188
Imperial Valley, Calif., 183, 191
Imperial Valley, Mexico/Calif., 1979 earthq., 192
Impulse response, 35
Inangahua, New Zealand, 1968 earthq., 211
Incident angle, 102
Inclination angle, 94
Index of refraction, 78, 80
India, 2
  Assam earthqs., 207
  induced seismicity, 196–197
Indian Ocean, meq. survey, 187
Induced seismicity, 5, 166, 193–197
INEL Meq. Network, 175
Information density matrix, 116, 119, 122
Initial value problem, 82–89
Institute for Seismic Investigations, Nicaragua, 175
Institute of Geological Sciences, Edinburgh, Scotland, 174
Institute of Geophysics, Milano, Italy, 174
Institute of Hydroelectricity, Bucharest, Romania, 174
Institute of Physics of the Earth, Moscow, USSR, 173
Institute of Physics of the Globe, University of Strasbourg, 173
Institute of Volcanology, Petropavlovsk-Kamchatsky, USSR, 8
Instrument response, *see* Response
Instrumentation systems, 15–45
Intensity, earthquake, 153
Interactive data processing, 62, 72–74
Intercept time, 95, 97–98
Intercept time function, 95
Intermountain seismic belt, Montana/Utah, 184
International Association of Seismology and Physics of the Earth's Interior, 72
International Business Machines Corporation, 89, 117, 228
International Seismological Center, 207
International Seismological Summary, 207
International Time Bureau, 229
Inter-Range Instrumentation Group, 24, 31, 228
Inuyama, seismic network, 189
Inverse
  *generalized, 118, 120*
  matrix, 106–107, 111, 115
  Moore–Penrose, 118, 120
  ordinary, 120
Inverse problem, 111, 115–122
Inversion, 125
  Backus–Gilbert, 111–112
  generalized, 105–122, 134, 137, 152
  seismic moment tensor, 163
  simultaneous, 148–153, 169–170, 214
  velocity structure, 138–139, 168–170
Iran, 178, 192, 211
Iraq, meq. survey, 178
IRIG, *see* Inter-Range Instrumentation Group
IRIG-C, 31, 228
IRIG-E, 31, 228
Ishimoto–Iida relation, 4
Israel, meq. surveys, 178–179
Italy, 174, 181, 191, 204, 206
Iteration, defined, 123
*Iteration step size, 127–128*
Iwate, Japan, meq. network, 172
Izu-Hanto-Oki, Japan, 1974 earthq., 191, 211
Izu-Oshima-Kinkai, Japan, 1978 earthq., 192, 221
Izu Peninsula, Japan
  seismic network, 192
  1974 earthq., 211
  1975–1977 swarm, 191

J

Jacobian matrix, 127, 133–134, 136–137, 150
Japan, 18, 60, 140, 153, 156
  aftershock studies, 188–192
  crust and mantle structure, 169–170
  development of meq. networks, 6–7
  earthq. prediction, 200–203, 207, 209, 211, 213

induced seismicity, 167, 195–196
meq. networks, 165, 171–173
meq. surveys, 179–180, 187
Japan Meteorological Agency, 73, 156, 165
Japan Trench, meq. survey, 187
Johannesburg, South Africa, 194, 213
Joint hypocenter determination, 138
Jordan, meq. survey, 179
Jordan Valley Rift, meq. survey, 178
Jorum, nuclear explosion, 193
Julian day, 31, 228–229
Jyvaskyla, Finland, array, 2

K

Kalapana, Hawaii, 1975 earthq., 207, 210
Kamchatka, USSR, 8, 200; 1971 earthq., 207
Kamikineusu, Japan, 213
Kamikochi, Japan, 1969 earthq., 189
Kamitakara Geophysical Observatory, 172
Kansas Geological Survey, 175
Kansas, meq. network, 18, 175
Kanto, Japan, 6, 171, 179, 213
Kanto–Tokai Meq. Network, 172
Kanuma, Japan, 1969 earthq., 189
Kaohsiung, Taiwan, meq. survey, 180
Kariba Reservoir, Zambia, 195
Karlsruhe, University of, 174
Katmai National Monument, Alaska, 182
Keilis–Borok algorithm, 205
Kenya, meq. surveys, 178
Kenya Rift, Kenya, meq. survey, 178
Kern County, Calif.
seismicity patterns, 202, 206
seismic spectra, 222
1952 earthq., 202, 206, 222
Khait, USSR, 1946 earthq., 7
Kii Peninsula, Japan, 6, 169, 179
Kinemetrics, Inc., 39
Kirgizia, USSR, 197
Kitagata, Uganda, meq. survey, 178
Kitakami Seismological Observatory, 172
Kitamino, Japan, 1961 earthq., 188
Kochi Earthquake Observatory, 172
Kochi, University of, 172
Kodiak Island, Alaska, 175
Koyna (Shivajisagar) Reservoir, India, 196
Kremasta Reservoir, Greece, 196
Kuriles, USSR, 8, 200
Kurobe Reservoir, Japan, 195
Kuusamo, Finland, meq. survey, 181
Kwangtung, China, 195, 211
Kyoto University, 171–172
Kyushu, *see* Japan

L

Lake Benmore, New Zealand, 196
Lake Hopatcong, New Jersey, 184
Lake Hughes, Calif., meq. survey, 183
Lake Jocassee, South Carolina, 197, 205, 210
Lake Keowee, South Carolina, 196
Lake Kitagata, Uganda, 178
Lake Mead, Arizona, 195
Lamont–Doherty Geological Observatory, 8–9, 173, 175–176, 222
Large Aperture Seismic Array (LASA), Montana, 2, 170
Lassen Peak, Calif., meq. survey, 183
L.D.G. Seismic Network, *see* France
Least squares method, 107, 116, 122
for instrument response, 33, 35, 37
in minimization, 113, 120, 127, 132, 138, 150 (*see also* Nonlinear least squares)
Leeward Islands, West Indies, 177
Levenberg–Marquardt method, 120, 128
Linear equation, defined, 122
Linear system, analysis of, 106–115
Livermore, Calif., 1980 earthq., 192
Local earthquake, defined, 54
Local magnitude, *see* Magnitude
Local minimum, 123
Local seismic network, *see* Microearthquake network
Location, earthquake, *see* Earthquake location
Long-period spectral level, 20, 159, 161
Long-term average, 54–55, 57, 59, 65, 68
Long Valley, Calif., meq. survey, 183
Los Angeles Basin, Calif., 56, 175
Los Angeles, Calif., 167
Lowland Valley array (LOWNET), Scotland, 70, 174

M

McKinley National Park, Alaska, 182
McMurdo Sound, Antartica, 178
McNaughton Reservoir, Canada, 197

Magnitude
  body-wave, defined, 155
  coda, defined, 226
  duration, 68, 157, 160–163, 226–228
  estimation of, 153–157
  local, 3, 20, 153–157, 161–162, 228
  Richter scale, 1–4, 153–158, 160–162
  surface-wave, 155, 160
Managua, Nicaragua, 1972 earthq., 190
Mangla Reservoir, Pakistan, 196
Manic 3 Reservoir, Canada, 197
Maniwaki, Canada, 1975 earthq., 191
Man-made earthquake, *see* Induced seismicity
Mantle structure, 168–170 (*see also* Velocity structure)
Marianas Islands, 213
Mark Products Inc., 27, 40
Marlborough, New Zealand, 180
Marmara Sea region, Turkey, 180
Marquardt method, *see* Levenberg–Marquardt method
Marysville, Montana, meq. survey, 184
Maryville, Tennessee, meq. survey, 185
Matsushiro, Japan, 167
  b-slope, precursory, 216–217
  meq. survey, 179
  velocity anomaly, 213
  1965–1967 swarm, 6–7, 188, 211, 221
  1970 earthq., 189
Matsushiro Seismological Observatory, 7, 217
Mendocino escarpment, meq. survey, 187
Mendocino fracture zone, 44
Menlo Park, Calif., 14–15, 23, 175–177
Mesa geothermal area, Calif., 183
Mexico (*see also* Gulf of California)
  aftershock studies, 190–192
  meq. network, 175
  meq. surveys, 182, 187
Micro-aftershocks, *see* Aftershocks
Microcomputer, 62–63, 73
Microearthquake
  definition, 1, 4
  first used, 6
  networks, list of, 171–177
  surveys, 165–166, 178–187
Microearthquake networks, 1
  applications, 164–197, 198–222
  classification, data from, 47–49
  cost, 58, 166, 223
  data analysis methods, 129–163
  data processing procedures, 46–75
  historical development, 1–9
  instrumentation systems, 15–45
  manufacturers, 39
  permanent, list of, 171–177
  shallow-water, 41–42
  signal characteristics, 53–54
  station distribution, 17–18, 224
  temporary, 40, 49, 51, 164, 166, 168
Microearthquake surveys at sea, 166, 186–187
Microearthquake surveys on land, 166
  Africa, 178
  Antarctica, 178
  Asia, 178–180
  Australia and New Zealand, 180–181
  Europe, 181
  North and Central America, 182–185
  South America, 185
Microprocessor, 45, 49, 56–57, 223
Microseismic noise, 19, 53
Mid-Atlantic Ridge, 181, 186
Mikawa district, Japan, 180
Mine tremors, 5, 167, 169, 194, 213
Minimization, *see* Optimization methods
Minimum in optimization, 123, 127–128
Minimum time path, 76–104, 138
Missouri, 18, 176, 185
Miura–Boso region, Japan, 180
Miyagi, Japan, 1962 earthq., 211
Moment-magnitude scale, 160–161
Moment, seismic, 20, 156–161, 228
Mono Lake, Calif., meq. survey, 183
Montana, 2, 177, 184, 195
Monticello Reservoir, S. Carolina, 210
Moore–Penrose generalized inverse, 118, 120
Mount Diablo, Calif., 217
Mt. Minakami, Japan, meq. survey, 179
Mt. Rainier, Washington, 185
Mt. St. Helens, Washington, 170
Mt. Tsukuba, Japan, meq. surveys, 179

N

Nagano, Japan, 1968 earthq., 211
Nagawado Reservoir, Japan, 196
Nagoya, Japan, meq. networks, 171–172

Nagoya, University of, 172
National Bureau of Standards, U.S., 31, 230
National Center for Earthquake Research, U.S., 12, 228
National Institute of Seismology, Guatemala, 174
National Research Center for Disaster Prevention, Japan, 172
NCER, *see* National Center for Earthquake Research
Nelson region, New Zealand, 181
Neo Valley fault, 179
Neo Valley, Japan, meq. surveys, 179
Netherland Antilles, meq. network, 176
Netherlands, 140
Networks, *see* Microearthquake networks, and Regional seismic networks
Nevada
  induced seismicity, 193
  meq. network, 175–176
  meq. surveys, 184
  University of, 175
Nevada seismic zone, 184
Nevada Test Site, 167, 212–213, 228
Newhall, Calif., 1976 earthq., 210
New Jersey, 184, 190
New Madrid, Missouri
  meq. network, 170, 176
  1811–1812 earthq., 18
New Madrid seismic zone, 18
New Mexico, 8, 175, 184–185, 228
New South Wales, Australia, 173
Newton method, 124–128
Newton–Raphson method, *see* Newton method
New York
  aftershock studies, 190
  induced seismicity, 167, 194
  velocity anomalies, 9, 210
New Zealand
  earthq. prediction, 201–202, 204, 211
  induced seismicity, 196
  meq. networks, 173
  meq. surveys, 180–181
New Zealand Seismic Network, 196
Nicaragua, 175, 182, 190
Niigata, Japan, 1964 earthq., 188
Noboribetsu hot spring, Japan, 180
Nodal plane, 71, 140–141, 143–147
Noise, 157
  cultural, 18–19, 53
  instrument, 27, 29–31, 33, 37–39
  microseismic, 19, 53
  reduction in borehole, 18, 41–42
  transient, 53–54, 64, 69, 74
Nonlinear equation, defined, 122
Nonlinear least squares, 120, 122, 126–128, 148, 169
Nonlinear optimization, 122–128, 132, 149
Nonsingular matrix, 111, 228
Normal axis, 143–145
Normal equations, 134, 136, 152
  by Cholesky method, 121–122, 226
  definition, 113
  for earthquake location, 133
Normal modes, 77
Norm of a vector, 121, 125, 228
NORSAR, Norway, array, 2, 170
North America
  aftershock studies, 188–191
  induced seismicity studies, 193–197
  meq. networks, 174–177
  meq. surveys, 182–185
Northeastern U.S. Seismic Network, 176
Northern Caribbean, meq. network, 176
North Island, New Zealand, 181
Norway, 2, 170
Novaya Zemlya, 210, 212
NTS, *see* Nevada Test Site
Nuclear detection, arrays for, 2, 165
Nuclear explosions, 146, 167, 193
Null axis, 145
Nurek Reservoir, USSR, 196

O

Oaxaca, Mexico, 1978 earthq., 192, 199
Objective function, 123–126, 132, 137, 150
OBS, *see* Ocean bottom seismograph
Observation Center for Earthquake Prediction, Tohoku University, 172
Ocean-based meq. systems, 41–45
Ocean bottom seismograph, 41–45, 57, 186–187
Office of Earthquake Studies, U.S. Geological Survey, 175–177, 228
Off-line event processing, 2, 57, 60, 62, 69, 72–74
Ogdensburg, New Jersey, 184
Okavango Delta, Botswana, 178

Oklahoma Geophysical Observatory, 176
Oklahoma, meq. network, 176
Oklahoma, University of, 176
Omega navigation system, 32
On-line data processing, 24–25, 51–52, 55, 57–60
On-line event detection, 2, 56–57, 60, 72
Open-file Reports, U.S. Geological Survey, 14
Optimization methods, 122–128
Ordinary inverse, 120
Oregon, meq. network, 170, 176
Origin time, *see* Hypocenter parameters
Oroville, Calif., 1975 earthq., 191, 210, 212
Osaka, Japan, meq. network, 171
Oscillomink, 25–26, 228
Oshima Island, Japan, 213
Overdetermined system, analysis of, 112–113, 116, 119, 134
Overflow error, 118
Owens Valley, Calif., meq. survey, 183

P

Pacific Ocean, meq. surveys, 187
Pakistan, 170, 173, 180, 196
Palmdale, Calif., 213; 1976–1977 swarm, 191
Parkfield, Calif., 217
  aftershocks, 9, 188
  seismicity patterns, 206
  velocity anomaly, 212
  waveform comparisons, 221–222
  1934 earthq., 221–222
  1966 earthq., 9, 188, 206, 212, 221–222
P-arrival, *see* First P-arrival time
Path length, 85–87, 92
Pattern recognition, 203–206
P-axis, 146
P-delay, 168, 210
Permanent meq. networks, 9, 164–166, 168, 170–177
Petatlan, Mexico, 1979 earthq., 192
Petropavlovsk–Kamchatsky, USSR, 8
Phase data or list, 47–48, 60–63, 69, 71, 73–74
Philippines, 220
Philippine Sea, meq. survey, 187
Pingtung, Taiwan, meq. survey, 180
Point Arena, Calif., 44
Point Mugu, Calif., 1973 earthq., 190, 210
Point process analysis, 163
Poisson's ratio, 208
Polarity
  first motion, 141–142, 144–145
  station, 50, 71–72, 146–147, 228–229
Polarization anomalies, 215
Polarization direction, 220
Pop-up OBS systems, 44–45
Portable seismograph, *see* Seismograph
P-phase, defined, 229
Precursor time, 202–203, 210–211
Precursory seismicity, 202–207
Precursory swarms, 202
P-residual, 208–214 (*see also* Arrival time residual)
P-residual method, 208–213
Primary wave, *see* P-wave
Projection
  equal-area, 141–146
  stereographic, 141–142
P/SV amplitude ratio, 219–221, 229
Puerto Rico, 176, 185
Puget Sound, Washington, 156, 177
Pukaki Meq. Network, 173
P-wave, defined, 77, 229
P-wave first motion, *see* First motion of P-wave

Q

*Q* (quality factor), 162–163, 229
Quarry blasts, 169, 210, 212–214
Quasi-Newton method, 126
Quebec, *see* Canada
Quetta, Pakistan, meq. survey, 180

R

Radiotelemetry, *see* Telemetry
Ramganga Reservoir, India, 197
Rangely, Colorado, 18, 168
Rank of matrix, 119–121, 137
Ray, defined, 79
Ray curvature, 94
Ray equation
  applications, 91–93
  derivations, 78–82
  numerical solutions, 82–89
Ray parameter, 94–95
Ray path, 79–103, 149, 151

Ray tracing, 153
earthq. location, 136, 138
fault-plane solution, 140–142, 147
methods, 76–104
Real-time earthquake location, *see* Earthquake location
Real-time processing, 64, 68
Record keeping, 49–50
Refracted path, *see* Ray path
Refracted wave, 95–100, 103–104
Regional earthquake, defined, 54
Regional seismic networks, 2, 5, 8–9, 165, 204
Reid's elastic rebound theory, 139, 158
Reno, Nevada, meq. survey, 184
Research Center for Earthquake Prediction, Hokkaido University, 171
Research Center for Earthquake Prediction, Nagoya University, 172
Reservoirs, meq. studies, 167, 195–197
Residual, 74, 126–128, 132–133, 135, 138, 149–150
Residual vector, 112–113, 126
Resolution matrix, 116, 119, 121
Response, instrument, 5, 19, 43, 155
effect of magnitude, 19–23
USGS system, 20–23, 25–27, 29, 32–38
Reykjanes Peninsula, Iceland, 181
Reykjanes Ridge, meq. survey, 186
Rhinegraben, meq. networks, 173–174
Richter magnitude, 1–4, 153–158, 160–162
Richter's method for computing distance, 131
Ridge regression, 120
Rise time, 30, 161
Rivera fracture zone, meq. survey, 187
Riverside County, Calif., 183
Rockbursts, *see* Mine tremors
Romania, 174, 191; 1977 earthq., 191
Roundoff error, 118, 122, 136
RRR triple junction, Indian Ocean, 187
Ruhr coal mining district, 194
Rupture length, 158, 160
Ruwenzori, Uganda, meq. survey, 178

S

St. Donat, Canada, 1978 earthq., 192
St. Elias, Alaska, 1979 earthquake
aftershocks, 192
b-slope, precursory, 217
seismic gap, 200–201
St. Lawrence Valley, Canada, 182
St. Louis University, 9, 170, 176
St. Lucia, West Indies, 185
St. Paul's fracture zone, 186
Sakashita, Japan, meq. survey, 179
Sakhalin Island, USSR, 156
Salton Sea geothermal area, Calif., meq. survey, 183
San Andreas fault, Calif., 23, 44, 148, 169, 183, 202–203, 207, 209, 212, 214, 217–218, 221
San Andreas Observatory, 217
San Bernardino, Calif., 183
San Fernando, Calif., 1971 earthquake
aftershocks, 190
seismicity patterns, 201–202, 206
velocity anomaly, 9, 210, 213
San Francisco, Calif., 1906 earthq., 139
San Jacinto fault, Calif., 182
San Jacinto Valley, Calif., 183
San Luis Valley, Colorado, 184
San Miguel fault, Mexico, 182
Sanriku, Japan, 187
Santa Barbara, Calif., 145
meq. network, 42, 144
1968 Channel swarm, 189
1978 earthq., 192
Santa Rosa, Calif., 1969 earthq., 206
S-arrival time, 130, 215 (*see also* Arrival time, later phases)
Scan list, 50–52, 62
Schlegeis Reservoir, Austria, 197
Schmidt net, 142–143
Scotland, U.K., 2, 70, 174
Secondary wave, *see* S-wave
Seddon, New Zealand, 1966 earthq., 211
Seismic arrays, 2, 165, (*see also* Microearthquake networks, and Regional seismic networks
Seismic cycle, 8, 200
Seismic efficiency, 160
Seismic energy, 160–162
Seismic gap, 8, 199–201, 203, 206
Seismicity patterns, 199–207
Seismic moment, 20, 156–161, 228
Seismic moment tensor inversion, 163
Seismic networks, *see* Microearthquake networks, and Regional seismic networks

Seismic ray tracing, *see* Ray tracing
Seismic source parameters, *see* Source parameters
Seismic spectra, *see* Spectra
Seismic velocity, temporal variations of, 208–215
Seismic wave propagation, *see* Wave propagation
Seismograph
  broadband, 19, 161, 190
  portable, 3, 6, 8–9, 40–41, 165–167, 178–185, 188–197
  smoked paper, 166, 178–185, 190, 195, 197
  telemetered, *see* Telemetry
  ultrasensitive, 6, 179
  Wiechert, 5
  Wood–Anderson, 3, 8, 154–156, 162
Seismographic Stations, University of Calif., *see* California, University of
Seismological Laboratory, Caltech, *see* California Institute of Technology
Seismological Observatory, DSIR, New Zealand, 173
Seismometer, 229
  manufacturers, 39–40
  release test, 27, 29–30, 32–33, 35
  USGS telemetry system, 24–27, 36–37
Seismometry, principles of, 40
Sempaya, Uganda, meq. survey, 178
Seward Peninsula, Alaska, 175
Seymore Canyon, Alaska, earthqs., 213
Shallow-water meq. network, 41–42
Shear phase, *see* S-phase
Shear wave, *see* S-wave
Shikoku, *see* Japan
Shimabara Peninsula, Japan, 179
Shimane, Japan, meq. survey, 180
Shimane, Japan, 1978 earthq., 203
Shiraki Meq. Observatory, 172
Short-term average, 54–55, 57–58, 60, 65, 68
Shumagin Islands, Alaska, 175
Siemens Corp., 228
Signal characteristics, 53–54
Signal duration, 60–61, 68, 72, 156–157, 162–163
Signal-to-noise ratio, 23, 29–30, 38–39, 41–42, 56, 74
Simultaneous inversion, *see* Inversion
Single couple, defined, 140
Singular matrix, 107, 120, 229
Singular value, 114, 119–121, 137
Singular value decomposition, 114, 118–119, 121–122
Singular vector, 120
Sizuoka, Japan, meq. survey, 180
Slip, 9, 158–159
Slip vector, 146
Slowness, 85–86, 91–92, 151
Smoked paper seismograph, *see* Seismograph
Snake River, Idaho, meq. survey, 184
Snell's law, 94, 96–98, 101–102
Socorro, New Mexico, 8, 184–185
Songpan-Pingwu, China, 1976 earthq., 211
Sonobuoy–hydrophone systems, 41–43, 190
Sonoma County, Calif., 183
Source characteristics, 219–222
Source dimension, 159, 161
Source parameters, 158–159, 161–163
South Africa, 2
  aftershock study, 189
  development of meq. network, 5–6
  induced seismicity, 167, 194
  velocity anomaly, 213
South America, meq. surveys, 185
South Australia, meq. network, 173
South Carolina
  induced seismicity, 195–197
  seismicity patterns, 205
  velocity anomalies, 210
Southeastern U.S. Seismic Network, 176
Southern Alaska Meq. Network, 176, 192
Southern California Seismic Network, 3, 5, 8–9, 57, 72, 154, 170, 176, 192, 213
Southern California, University of, 175, 192
Southern Great Basin Meq. Network, 176
South Island, New Zealand, 173, 180–181, 196
Soviet Union, *see* USSR
Spectra, 19–23, 159, 161–162, 221
Spectral level, long-period, 20, 159, 161
S-phase, defined, 229
S–P interval time, 130, 135, 208, 229
Sprengnether Instrument Co., 39
S-residual, 208 (*see also* Arrival time residual)
Stanley, Idaho, meq. survey, 184
Star Mine, Idaho, 194
State Seismological Bureau, China, 171

Station
coordinates, 50, 131, 135, 141
distribution, 17–18, 165, 218, 224
polarity, 50, 71–72, 146–147, 228–229
Statistics, earthquake, 4, 163
Steepest descent, 125, 128
Stepwise multiple regression, 137
Stereographic projection, 141–142
Sterling Mine, New Jersey, 184
Stone Canyon, Calif., 1972 earthq., 210, 218
Stone Canyon Observatory, 212
Strain energy, 159–160
Strasbourg, University of, 173
Stress axes, 146, 220–221
Stress drop, 20, 159, 161
Stromboli, Italy, meq. survey, 181
Sulphur Springs, West Indies, 185
Sunbeam, Idaho, meq. survey, 184
Surface-wave magnitude, *see* Magnitude
SVD, *see* Singular value decomposition
Swabian Jura, Germany, 1978 earthq., 192
Swarm, 6–7, 9, 188–191, 202, 207, 211, 217, 219–221, 227
S-wave, defined, 77, 229
Sweden, 2, 174, 194
Swedish Seismographic Network, 194
Swiss Alps, 174, 181
Swiss Seismological Service, 174
Switzerland, 3, 174, 181, 197
Syowa Station, Antarctica, 178

T

Tabas-E-Golshan, Iran, 1978 earthq., 192
Tadzhik SSR, USSR
induced seismicity, 196
Institute of Seismic Construction and Seismology, 173
meq. networks, 173
meq. survey, 7
Taiwan, 171, 180
Takayama Seismological Observatory, 172
Take-off angle
computing, 89–104
direct wave, 92, 104
fault-plane solution, 141, 146
refracted wave, 103–104
Talbingo Reservoir, Australia, 197
Tanzania, meq. survey, 178
Tarbela, Pakistan, array, 170, 173
Tasmania, Australia, 173, 197
Tasmania, University of, 173
Tateyama, Japan, 213
Tau($p$) method, 95
$T$-axis, 146
Taylor expansion, 124
Teheran region, Iran, 178, 211
Teledyne Geotech, 39, 157, 228
Telemetered buoy OBS systems, 44, 186–187
Telemetry, 5–6, 8, 15–19, 23–26, 30, 41, 44, 60, 73, 164, 167
Teleseismic earthquake, defined, 54
Temporary meq. networks, 40, 49, 51, 164, 166, 168
Tennessee, meq. survey, 185
Tennessee, 1973 earthq., 191
Terra Technology Corp., 41
Thessaloniki, Greece, 1978 earthq., 192
Threshold level for event detection, 55, 57, 59–60, 64–66, 68
Tibet, China, 204
Time code, 24–25, 30–31, 51–52, 228
Time code generator, 31, 229
Time-term analysis, 169
Timing resolution, 5–6, 23
Timing systems, 17, 31–32
Tjednes Peninsula, Iceland, 181
Tochigi Prefecture, Japan, 180
Tohoku, Japan, meq. network, 172
Tohoku, University of, 171–172
Tokachi-Oki, Japan, 1968 earthq., 189
Toktogul Reservoir, USSR, 197
Tokushima Seismological Observatory, 172
Tokyo, Japan, 3, 18
Tokyo, University of, 7, 171–173
Tonga Islands, 212–213
Tottori Meq. Observatory, 172
Transient noise or signal, 53–54, 64, 69, 74
Transpose of a matrix, defined, 109
Transverse Ranges, Calif., 169
Travel time, 80, 87–88, 122
computing, 89–104
direct wave, 96–97, 100, 102
earthq. location, 131–138
refracted wave, 96–100
simultaneous inversion, 149–153
Travel time derivatives
computing, 89–104
direct wave, 92, 104

earthq. location, 133–137
refracted wave, 104
simultaneous inversion, 151–153
Triggered recording, 5–6, 40–41, 45, 51–52, 55–57
Tripartite array, 179–182, 187–189, 193–194, 221, 229
Truckee, Calif., 1966 earthq., 189
Tsukechi, Japan, meq. survey, 179
Tsukuba, Japan, 213 (*see also* Mt. Tsukuba)
Turkey, meq. survey, 180
Turkmenia, USSR, 7

U

Uganda, meq. surveys, 178
uhf, *see* Ultrahigh frequency
Ultrahigh frequency, 32, 229
Ultra-microearthquake, defined, 4
Unalaska Island, Alaska, 175
Underdetermined system, analysis of, 111–112, 116
Underflow error, 118
United Kingdom, 2, 174
United States, 2, 23, 39–40, 140, 166
aftershock studies, 9, 188–192
crust and mantle structure, 168–170
development of meq. network, 8–9
earthq. prediction, 200–222
induced seismicity, 193–197
meq. networks, 175–177
meq. surveys, 182–185
Universal Time Coordinated, 31, 229–230
Urakawa Seismological Observatory, 189
USC, *see* Southern California, University of
U.S. Geological Survey, 9–10, 14, 19, 167, 175–177, 223, 228 (*see also* Central California Meq. Network)
USGS, *see* U.S. Geological Survey
USGS Alaska Seismic Network, *see* Southern Alaska Meq. Network
USGS Central California Meq. Network, *see* Central California Meq. Network
USSR, 2, 9, 140
aftershock studies, 188
development of meq. network, 7–8
earthq. prediction, 7–8, 209, 211
induced seismicity, 196–197
meq. networks, 173
meq. survey, 181
Utah, 177, 184, 194, 213
Utah, University of, 177
UTC, *see* Universal Time Coordinated
Utsu's formula, 216

V

Variable metric method, 126
Variance, 115–116, 121
VCO, *see* Voltage-controlled oscillator
Vector norm, *see* Norm of a vector
Velocity anomalies, 9, 198–199, 208
alternative interpretation, 214–215
negative results, 209, 212–213
positive results, 209–211
Velocity structure, 69–70
earthq. location, 82, 89, 136
inversion, 95, 138–139, 168–170
models, 84, 90–104, 147, 218
simultaneous inversion, 148–153
Very high frequency, 24, 230
vhf, *see* Very high frequency
Vibroseismic techniques, 214
Virginia, meq. survey, 185
Virginia Polytechnic Institute, 176
Virginia seismic zone, Virginia, 185
Virgin Islands, 176, 185
Voice-grade telephone circuit, 23–24, 230
Volcanoes, 170, 182–183, 185
Voltage-controlled oscillator, 23–27, 29, 35–37, 39, 230
$V_P$ (or $V_S$) anomaly method, 208
Vrancea, Romania, meq. network, 174

W

Wachi, Japan, 1968 earthq., 189
Wadati diagram, 208, 214–215
Wadati method, 208–209, 211, 213–214
Wakayama, Japan, 156, 173, 179, 189
Wakayama Meq. Observatory, 173
Wappingers Falls Quarry, New York, 194
Warramunga, Australia, array, 2
Wasatch Front, Utah, 177, 213
Washington
aftershock studies, 190
meq. networks, 175, 177, 213
meq. surveys, 185
University of, 9, 175, 177
velocity anomaly, 213

Watsonville, Calif., 1964 earthq., 206
Wave equation, 77–78
Waveform
  comparison, 221–222
  correlation, 58, 212
  data, 47–48, 63
Wave front, defined, 79
Wave potential, 77–78
Wave propagation, 76–77, 79, 215
Wellington Meq. Network, 173
Western Canada Telemetered Network, 174
West Indies, 176–177, 185
West Indies, University of, 177
Weston Observatory, Boston College, 176
White Sands Missile Range, New Mexico, 228
Whittier fault, Calif., 183
Wiechert seismograph, *see* Seismograph
Windward Islands, West Indies, 177
Windy Island, Alaska, 1971 earthq., 210
Witwatersrand, South Africa, 5, 169
Wood–Anderson instrument or seismograph, 3, 8, 154–156, 162
World-Wide Standardized Seismograph Network, 5, 220, 230
Wulff net, 142
WWSSN, *see* World-Wide Standardized Seismograph Network
WWV, 31, 230
WWVB, 24, 31, 50, 230
Wyoming, 170, 177, 184–185, 191

Y

Yellowknife, Canada, array, 2
Yellowstone National Park, Wyoming
  meq. network, 170, 177
  meq. surveys, 184–185
  1975 earthq., 191
Yongshan-Daguan, China, 1974 earthq., 211

Z

Zambia, induced seismicity, 195
Zurich, Switzerland, 3